ADVANCED ELECTRIC PROPULSION RESEARCH

prepared for

NATIONAL AERONAUTICS AND SPACE ADMINISTRATION

GRANT NGR06-002-032

SPACE PROPULSION PROGRAM

ENERGY CONVERSION PROGRAM

COLLEGE OF ENGINEERING

COLORADO STATE UNIVERSITY

FORT COLLINS, COLORADO

MER66 67WRM-1

INTERIM REPORT

ADVANCED ELECTRIC PROPULSION RESEARCH

Prepared for

NATIONAL AERONAUTICS AND SPACE ADMINISTRATION

June 1966

Grant NGR06-002-032

Technical Management
NASA Headquarters
Washington, D.C.
Nuclear Electric Systems
Dr. George Pfannebecker
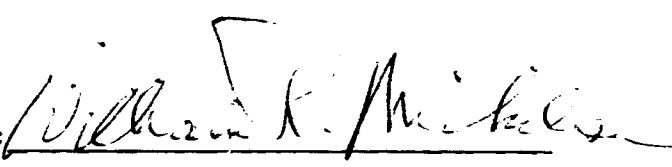
ADVANCED ELECTRIC PROPULSION RESEARCH

First Semi-Annual Report

NASA Research Grant NGR06-002-032

submitted to

Dr. George Pfannebecker, grant monitor
Electric Thruster Systems
Nuclear-Electric Systems
Office of Advanced Research and Technology
National Aeronautics and Space Administration
Washington, D.C.

prepared by:

William R. Mickelsen, principal investigator
Professor of Mechanical Engineering and
Professor of Electrical Engineering
Colorado State University
Fort Collins, Colorado

June 30, 1966

CONTENTS

SUMMARY

The grant contract was officially approved on April 1, 1966, but had been anticipated prior to that date. Initial work was an analysis of colloid-particle electrostatic thrusters. Results of this analysis indicated that colloid thrusters may be the only known concept that could provide acceptable performance in the lower range of specific impulse. Although definite conclusions could not be made, the analysis also indicated that charge-exchange particle erosion could be a very serious problem in colloid thrusters.

The field of electric propulsion was surveyed with emphasis on application of existing electric thruster systems to satellite propulsion, planetary-orbiter-landers, lunar-supply, and manned-interplanetary missions. Thrusters for satellite propulsion appear to have adequate performance, but great gains in simplicity and precision control can still be made. Existing thrusters are fairly adequate for planetary-orbiter-lander missions, but could not perform lunar-supply or manned-interplanetary missions. Advanced concepts in electric thrusters appear to be required if electric propulsion is to achieve its full promise of superior performance.

Radioisotope heating of contact ionizers has been analyzed, and the scheme does not appear to be practical for primary propulsion because of limited availability of suitable radioisotopes. The scheme could have practical application to satellite propulsion.

Research work presently in progress includes the analysis of plasma discharges, a lunar-supply mission study, the analysis of mission gains by using spent tankage as propellant, the analysis of aluminum colloid-particle formation by vapor condensation, and colloid formation by chemical reaction.

Future research will include experimental investigation of colloid thruster concepts, and of concepts where the electric thruster is directly integrated with the power-generation sub-system.

COLLOID-PARTICLE ELECTROSTATIC THRUSTORS

by William R. Mickelsen*

Colorado State University
Fort Collins, Colorado

*Professor of Mechanical Engineering and Professor
of Electrical Engineering

ABSTRACT

Electric rocket lunar ferries will require specific impulses in the range of 1000 to 3000 seconds. Existing electric thrustors have poor efficiency in this range of specific impulse, but colloid-particle thrustors have promise of high efficiency throughout the range of interest. Additional features of colloid-particle thrustors include the promises of high exhaust-jet power density, and adequate durability.

Three colloid-particle thrustor concepts have received the most attention: liquid sprays, condensation from vapor, and pre-formed particles. Of these three, the liquid-spray type has the most developed status. Liquid-spray thrustors have been operated at a specific impulse of 450 seconds with an efficiency of 75% and an exhaust power density of 1 kw/m^2. Durability has not been proven experimentally, and an approximate analysis made herein indicates that durability may be a severe problem.

A recent theoretical analysis has shown that the maximum particle formation efficiency that can be expected from condensation-colloid thrustors is less than 50%. Experiments done so far with pre-formed particles indicate that particle agglomeration is a serious problem.

INTRODUCTION

Electrostatic thrustors are in a fairly advanced state of development at present. Thrustor modules of kilowatt size have been operated for thousands of hours at high efficiencies above 4000 seconds specific impulse. Small thrustors have been test flown in space, and thrustor modules of several-hundred-kilowatt size are being tested in vacuum facilities.

Electron-bombardment thrustors using mercury or cesium propellant are in a state of development very near to flight qualification. However, these thrustors have poor efficiency in the specific impulse range below 4000 seconds, and also are limited in exhaust-jet power density because of charge-exchange ion erosion of the accel electrode.

The present paper contains a discussion of specific impulse requirements for lunar ferry missions. The relative performances of ion thrustors and colloid-particle thrustors in this range of specific impulse are discussed. Three types of colloid-particle thrustors have received the most attention, and the status of each of these is summarized.

SPECIFIC IMPULSE FOR LUNAR SUPPLY MISSIONS

The future performance of electric spacecraft for lunar supply missions has been discussed and analyzed in a number of papers[1-5]. If lightweight electric power and propulsion systems can be developed, then electric space-craft will be ideally suited to carrying great payloads to the moon.

Multiple round trips by the same electric power and propulsion system could provide a cost effectiveness[6] superior to nuclear or chemical rockets as illustrated in Figure 1. The number of round trips is a function of the durability of the whole electric spacecraft, and of the duration of each round trip. Thrust-to-mass ratio F/M of the spacecraft determines the dura-tion of each round trip. There is an optimum power-to-mass ratio for each mission and specific mass of the power and propulsion system. Since power level of an optimized spacecraft design is a particular constant value, then specific impulse is related to round-trip time. This chain of relation-ships is shown by the following equations for the case of constant F/M

trajectories:

$$I = \frac{v_{j,eff}}{g_c} = \frac{2P_{j,eff}}{Fg_c} = \frac{2(P_{j,eff}/M_o)}{g_c(F/M_o)} = \frac{2(P_{j,eff}/M_o)}{g_c(4L^*/t^2)} = \frac{2(P_{j,eff}/M_o)t}{g_c\ v^*} \quad (1)$$

Where $P_{j,eff}$ is effective jet-power, $v_{j,eff}$ is effective jet velocity, and $L^* = v^*t/2$ is the characteristic length of the mission as defined by Zola[7]. Characteristic velocity v^* is approximately constant for the lunar round-trip trajectory, so that specific impulse is approximately proportional to round-trip time for a given $P_{j,eff}/M_o$.

Variation of specific impulse with round-trip time is shown in Figure 2 for a range of effective specific mass α^*_{ps} of the power and propulsion system. This parameter[8] includes the effect of all component specific masses, all component efficiencies, payload loss due to non-optimum specific impulse program, and payload loss due to non-optimum $P_{j,eff}/M_o$. Trajectory and mission parameters for these lunar round trips were calculated by methods described elsewhere[2,9]. Specific impulse during other portions of the trip can be determined from the relation:

$$\frac{P_{j,eff}}{M_o} = \frac{1}{2} \frac{F_o}{M_o}\ I_o\ g_c = \frac{1}{2} \frac{F}{M} \frac{M}{M_o}\ I\ g_c \quad (2)$$

Since F/M is constant, then $(I/I_o) = (M_o/M)$ so that specific impulse increases throughout the constant F/M trajectories.

From inspection of Figure 2, it is evident that specific impulse in the range of 1000 to 3000 seconds is of interest for lunar supply missions. These values are approximately correct for constant thrust trajectories as well as constant F/M trajectories. If non-optimum specific impulse is used, then appreciable payload capacity will be lost[10]. For this important reason,

electric thrustors should be capable of efficient operation at specific impulse as low as 1000 seconds.

IMPORTANCE OF THRUSTOR EFFICIENCY

An exact definition of electric thrustor efficiency has been derived and discussed previously[10]. Thrustor efficiency has a direct effect on payload capacity, but this effect depends on the difficulty of the mission. Fast trips, long distances, and strong gravity fields are measures of mission difficulty. Optimized payload fractions are high for easy missions, and low for difficult ones. Payload fraction decreases with thrustor efficiency[10] as shown in Figure 3. The relations shown in Figure 3 are for the idealized case of Irving-Blum trajectories and independence of thrustor efficiency from specific impulse. Thrustor efficiency has the most severe effect on the more difficult missions.

Effect of thrustor efficiency on mission performance can also be represented by the effective specific mass α^*_{ps} of the power and propulsion system[8]. To illustrate this representation, efficiencies of exisiting electric thrustors are shown in Figure 4 for the specific impulse range of interest for lunar ferry missions. Effective specific mass of power and propulsion systems using these thrustors are shown in Figure 5. From this figure it is evident that the high mission performance of lightweight power-plants can be realized only at specific impulses above 4000 seconds if existing thrustors are used. Degradation of performance is especially severe in the specific impulse range of interest for lunar ferry missions.

Efficiency of electron-bombardment thrustors can be approximated by the expression:

$$\eta = \eta_U \frac{1}{1 + \frac{ev/ion}{\Phi_{net}}} \tag{3}$$

where η_U is utilization efficiency, ev/ion is the power consumed in generating each ion, and Φ_{net} is the accelerating voltage. Typical electron-bombardment thrustors have a power loss of about 400-500 ev/ion. As specific impulse is decreased, Φ_{net} decreases according to the relation:

$$\Phi = \frac{1}{2} \frac{m}{q} g_c^2 I^2 \tag{4}$$

and this explains the severe decrease in efficiency suffered by ion thrustors at low specific impulse.

Colloid-particle thrustors have a very much greater particle mass than ions. Therefore, the net accelerating potential must be greater. For example, if a colloid-particle thrustor has a net accelerating voltage of 100,000 volts and a power loss of as much as 1000 ev/ion, then the power efficiency will be nearly 100%. If a high utilization efficiency can be achieved also, then the colloid-particle thrustor would be markedly superior to ion thrustors in the specific impulse range below 4000 seconds.

EXHAUST POWER DENSITY

Size and mass of electrostatic thrustors are largely determined by the exhaust-jet power density. Both of these thrustor characterisitics can be a severe problem, particularly below 4000 seconds specific impulse. For example, the best Kaufman thrustor reported to date[11] has a specific mass of 0.61 kg/kwj and an exhaust power density of 270 kwj/m^2 at a specific impulse

of 9000 seconds. With a 2 mm accel length, the ideal power density for mercury propellant is about 100 kwj/m^2 at a specific impulse of 4000 seconds. Because of electrode blockage and insulator support structure, the actual area will be at least twice the jet area, so that power density for the Kaufman thrustor is estimated as 50 kwj/m^2 at 4000 seconds. Thrustor mass scales approximately linearly with power density, and total power is constant, so that the specific mass is estimated as 3 kg/Kwj at 4000 seconds specific impulse. In the specific impulse range of interest for lunar ferry missions, the Kaufman thrustor clearly would be very heavy and very large.

Colloid-particle thrustors offer promise of much higher exhaust power density as illustrated in Figure 6. The left-hand portion of the colloid thrustor curve was determined by assuming a fixed accel length of 1 cm and space-charge limited current. The right-hand portion of the colloid-thrustor curve was determined by assuming that the Cranberg breakdown relation would limit the current density[10], i.e., accel length would have to be increased for specific impulses above 2500 seconds.

Comparison of the 100,000 amu/e and the mercury propellant exhaust-power-density shows clearly the superior promise of colloid particle thrustors in the lower range of specific impulse. Whether this promise can be achieved depends on whether charge-exchange particle erosion of the accel electrode will limit the current density.

DURABILITY

Lifetime of ion thrustors is limited by accel electrode durability. Neutral atoms from incomplete ionization have charge exchange collisions with ions, and the new ions formed in these collisions fall into the accel electrode, causing sputtering. Durability of accel electrodes in ion thrustors

is given by the expression:

$$\mathcal{L}_+ = K_+ \frac{(1-f_+)}{f_+} \frac{1}{j_+^2 \sigma_+ Y_+ V_+} \tag{5}$$

where K_+ is a constant, f_+ is the ratio of neutral atom efflux to total flow, j_+ is ion current, σ_+ is the charge-exchange cross section, Y_+ is the sputtering yield, and V_+ is the volume from whence charge-exchange ions will impinge on the accel electrode.

If colloid-particle thrustors also have a charge-exchange process, then an expression similar to equation (5) can be written, and the ratio of colloid thrustor durability to ion thrustor durability would be:

$$\frac{\mathcal{L}_c}{\mathcal{L}_+} = \frac{K_c}{K_+} \frac{f_+}{(1-f_+)} \frac{(1-f_c)}{f_c} \frac{j_+^2}{j_c^2} \frac{\sigma_+}{\sigma_c} \frac{Y_+}{Y_c} \frac{V_+}{V_c} \tag{6}$$

The constants K depend on the accel electrode thickness and the allowable volume of electrode sputtered away during the thrustor life, so it may be assumed that $K \sim L^3$, where L is accel length. Using Childs' Law and assuming that the cross-sectional area of each accelerator beam is proportional to L^2, then:

$$\left(\frac{K_c}{K_+}\right)\left(\frac{j_+}{j_c}\right)^2\left(\frac{V_+}{V_c}\right) = \left(\frac{L_c^3}{L_+^3}\right)\left(\frac{m_c}{m_+} \frac{\phi_+^3}{\phi_c^3} \frac{L_c^4}{L_+^4}\right)\left(\frac{L_+^3}{L_c^3}\right) = \frac{m_c}{m_+} \frac{\phi_c}{\phi_+} \frac{(\phi_+/L_+)^4}{(\phi_c/L_c)^4}$$

$$= \left(\frac{m_c}{m_+}\right)^2 \left(\frac{I_c}{I_+}\right)^2 \frac{(\phi_+/L_+)^4}{(\phi_c/L_c)^4} \tag{7}$$

Electric field strength ϕ/L and specific impulse I may be assumed to be the same for both thrustors, so the durability ratio reduces to:

$$\frac{\mathcal{L}_c}{\mathcal{L}_+} = \left(\frac{m_c}{m_+}\right)^2 \frac{\sigma_+}{\sigma_c} \frac{Y_+}{Y_c} \frac{f_+}{(1-f_+)} \frac{(1-f_c)}{f_c} \tag{8}$$

Sputtering yield from ion impact increases to several sputtered atoms per incident ion at some incident-ion energy, then decreases again. If this trend holds for colloid particles, then the yield Y_c can be expected to be:

$$Y_c = Y_o \frac{m_c}{m_a} \qquad (9)$$

where $Y_o = Y_+$ and m_a is the mass of each atom in the colloid particle. Using equation (9) in equation (8):

$$\frac{\mathcal{I}_c}{\mathcal{I}_+} = \frac{m_a}{m_+} \frac{m_c}{m_+} \frac{\sigma_+}{\sigma_c} \frac{f_+}{1-f_+} \frac{1-f_c}{f_c} \qquad (10)$$

Whether this simplification can be used for colloid-particle sputtering of electrodes remains to be seen. For example, experiments with micrometeoroids have shown that the crater volume V_{cr} is related to particle energy by:

$$\frac{1}{2} m_c v_c^2 = E_{cr} V_{cr} \qquad (11)$$

where $m_c v_c^2/2$ is kinetic energy of the particle and $E_{cr} = 4 \times 10^9$ joules/m^3 is the energy per unit crater volume[12]. Noting that the yield Y_c per incident colloid particle is given by $\rho_e V_{cr}/m_e$, where ρ_e is electrode-material density and m_e is electrode-atom mass, then:

$$Y = \frac{\rho_e \, q \phi_c}{m_e E_{cr}} \qquad (12)$$

A 10,000 amu colloid particle requires 5000 volts net accelerating voltage for $v/g_c = 1000$ seconds, and if molybdenum electrodes were used, then $Y = 14,300$ sputtered atoms per incident colloid particle. There are about 100 atoms in each 10,000 amu colloid particle, so that about 140 electrode atoms would be sputtered for each atom in the incident colloid particle. A model

used to account for cratering is that an explosion occurs because of the great energy per unit volume resulting from micrometeoroid impacts. If a similar mechanism occurs for colloid-particle impacts, then it is clear that sputtering erosion would be much higher than predicted by equation (10).

Charge-exchange cross-section for Hg on Hg^+ is 6×10^{-19} m^2. Although data is not available for colloid charge-exchange collisions, a reasonable assumption might be that the charge-exchange cross-section for colloid particles is merely the projected frontal area πr^2. In this case the colloid-particle charge-exchange cross-section is given by:

$$\sigma_c = \pi^{1/3} \left(\frac{3m_c}{4\rho_c} \right)^{2/3} \tag{13}$$

For example, if the density $\rho_c = 1$ gm/cc for a 10,000 amu colloid particle, then $\sigma_c = 154 \times 10^{-19}$ m^2 (this corresponds to a particle diameter of 44 angstroms).

Neutral atom fraction is usually small, and if $m \doteq m_+$, then equation (10) is approximately:

$$\frac{\mathcal{L}_c}{\mathcal{L}_+} \doteq \frac{m_+}{m_+} \quad \frac{\sigma_+}{\sigma_c} \quad \frac{f_+}{f_c} \tag{14}$$

If the preceding values for charge-exchange cross-section are used, then $\sigma_+ / \sigma_c = .04$, and if 10,000 amu colloids are compared with mercury, then:

$$\frac{\mathcal{L}_c}{\mathcal{L}_+} = 2 \frac{f_+}{f_c} \tag{15}$$

If colloid neutral efflux can be less than the neutral atom efflux from ion thrustors, then colloid-thrustor durability can be greater than ion-thrustor durability. However, it is important to note here that equal field strengths

were assumed in arriving at equation (8), so that at the same specific

impulse, the exhaust-jet power density would be the same for both thrustors.

If colloid thrustors are to fulfill their promise of higher power density,

the results of this analysis suggest that the neutral colloid efflux must be

much smaller than the 10% efflux commonly encountered in ion thrustors.

These remarks must be tempered with the observation that the analysis made

herein is approximate at best, and that much additional information is needed

on colloid-particle impact before an accurate analysis can be made. In any

event, it is clear that colloid thrustor durability should be examined in

greater detail, both analytically and theoretically.

PRE-FORMED COLLOID-PARTICLE EXPERIMENTS

Pre-formed colloid-particle thrustors have been investigated experimen-

tally in an electron-bombardment discharge and extraction system[13]. Results

of this investigation indicated that considerable agglomeration of particles

had occurred. Mass-to-charge ratio of the resulting particles were much

too high for use colloid-particle thrustors, because exceedingly high voltages

would be required to obtain a specific impulse of even 1000 seconds.

Research on the feasibility of pre-formed particles is continuing at

the NASA Lewis Research Center under the direction of H. R. Kaufman. Another

research investigation is proceeding at Stanford University under the direc-

tion of Professor H. Seifert. Results of these two investigations have not

been published as yet.

Whether the agglomeration problem can be solved remains to be seen. One

possible solution is ultra-sonic vibration to break the agglomerate apart

before charging.

CHARGING OF COLLOID PARTICLES

Particles can be charged by contact with surfaces. In the presence of a strong local electric field, the particle will become polarized and the charge adjacent to the surface may flow into the surface. The charged particle then accelerates away, leaving the charge behind in the surface.

Another method of charging is by electron bombardment. A typical coefficient for secondary-electron emission is shown in the upper portion of Figure 7. After the primary electrons reach a threshold energy, secondary electron emission increases with primary energy. If the primary electrons pass on through the particle (particle size is about 100 angstroms) then the net charge on the particle is shown by the solid line in the lower part of Figure 7. If the primary electron stays in the particle, then the net charge is as shown by the broken line. The real case probably lies somewhere between these two lines. Experiments are needed to verify this simple theory.

COLLOID-PARTICLE GENERATION BY CONDENSATION

Colloidal droplets can be formed by condensation from the vapor state by either heterogeneous or homogeneous condensation. Condensation onto positive ions has been investigated by Cox[14] and Harrison, but the feasibility of this method of colloid-particle formation is still unresolved.

Homogeneous condensation from supersaturated vapor has been investigated extensively by Norgren[15, 16, 17] and Goldin. Condensation was accomplished in a condensation-shock region in a supersonic nozzle. Charging was done by electron attachment in a corona discharge. Accelerated particles were analyzed with a quadrupole mass spectrometer. Spectrum of mass/charge were very narrow, and the spread in mass/charge would cause less than 1% loss in

efficiency. Mean size of the particles could be controlled by changing the stagnation temperature of the flowing vapor. Thrust was measured, so that some feasibility has been proven.

Although extensive experiments have been performed with the homogeneous-condensation colloid-thrustor, no determination has been made as yet of the propellant utilization efficiency. Of particular importance is the fraction of total vapor flow that is converted into colloid particles. A recent theoretical analysis by Goldin[18] and Kvitek has treated the homogeneous condensation process with equilibrium, continuum thermodynamics. This analysis predicts that less than 50% of the vapor propellant flow can be condensed into colloid particles. If the analysis is correct and if the uncondensed propellant cannot be recovered, then the homogeneous-condensation colloid-particle thrustor does not appear attractive.

LIQUID-SPRAY COLLOID THRUSTORS

Considerable research has been done to establish the feasibility of electrostatic spraying of liquids to obtain charged colloid particles. This research has been concentrated on liquid flowing from needles in the presence of strong electric field. Polarization of the droplet as it leaves the tip affords the means of charging as in the surface contact method. Polarization is best accomplished in liquids with fairly low electric conductivity, but charge transfer to the needle tip is slowed by low conductivity. Because of these contradictory factors, a limit of 1 microampere to the propellant flow in each needle has been predicted, which would in turn limit the power density of this thrustor[10].

Basic mechanisms involved in the droplet formation and charging processes have been examined by Professor C. Hendricks[19] and his associates at the

University of Illinois for a number of years. Much has been discovered in this fine research program, but more remains to be done before an adequate body of information is available for the completely rational design of liquid-spray thrustors.

Laboratory versions of liquid-spray thrustors have been developed by E. Cohen[20] at TRW Systems. Propellant flow from each needle has been increased to as much as 7 microamperes, and a 36-needle array has been operated for 100 hours with glycerol-H_2SO_4 propellant. Accelerating voltage was 5000 volts, and mean mass/charge was 50,000 amu/e, which corresponds to $\bar{v}/g_c$ = 440 seconds. Mass/charge spectrum of the spray was fairly broad, resulting in a thrustor efficiency of η = 75%. This development is a definite step forward in colloid-particle thrustor research, and represents the first laboratory colloid-particle thrustor having a respectable efficiency.

The 36-needle thrustor had a needle-array of 3.8 cm and a total current of 250 microamperes. With a 5000 volt net accelerating voltage, the exhaust power density was about 1 kw/m^2, which is much too low for practical application in primary propulsion for spacecraft. Research is continuing on this laboratory thrustor, and satisfactory operation at 100,000 volt accelerating voltages is expected in the future. However, it is clear that greater needle current and/or closer needle spacing will be necessary to provide adequately high exhaust-jet power density.

A research program on liquid-spray colloid thrustors is also being conducted by R. E. Hunter at the U.S. Air Force Aero Propulsion Laboratory. Mass/charge distribution efficiencies as high as 81% have been obtained[21] with glycerol-NaI, and with a mean mass/charge of 20,000 amu/e, from single needles. An electrodeless thrustor concept[22] is also under investigation in which needles are arranged geometrically with positive and negative d.c. voltages. Positively

and negatively charged particles issuing from adjacent needles would eliminate the need for an accel electrode and a neutralizer. Preliminary experiments have indicated that this concept may have promise.

OTHER RESEARCH

An alternate version of the needle configuration is that of a spinning cup with a sharp lip. Liquid drops are drawn from the lip by a strong electric field. This work is being done by D. Gignoux at Cosmic, Inc. Information on the status of this research was not available for inclusion in this paper.

Chemical reaction as a means for colloid particle formation is being investigated at Thiokol Chemical Corp., Reaction Motors Division under the direction of Dr. W. G. Courtney. Information on this research was not available for inclusion in this survey, but a paper[23] will be given in the near future.

Pre-formed particle colloid-thrustors are being investigated by S. P. Harris and M. Farber at the Maremont Corporation. A paper[24] on this research will be given in the near future.

CONCLUDING REMARKS

In many theoretical respects, the colloid-particle thrustor has promise of performance superior to ion thrustors in the specific impulse range below 4000 seconds. To date, this promise has not been fulfilled even by laboratory thrustors.

Liquid-spray thrustors have been developed by E. Cohen to an efficiency of 75%, but the exhaust-jet power density is still much too low. Other researches do not appear to be at the laboratory thrustor state as yet.

An approximate analysis made herein suggests that durability of the accel electrode may be a serious problem. The validity of this suggestion will be established when future research provides more knowledge about colloid-particle impact.

Because of theoretical promise of superior performance, research on colloid-particle thrustors should go forward.

REFERENCES

1. Stuhlinger, E.: Lunar Ferry with Electric Propulsion System. Japanese Rocket Society Annual Meeting, Tokyo. May, 1959.

2. London, Howard S.: A Study of Earth-Satellite to Moon-Satellite Transfers Using Nonchemical Propulsion Systems. Res. Dept. R-1388-1, United Aircraft Corp., May 21, 1959.

3. Fimple, W. R. and Edelbaum, T. N.: Applications of SNAP-50 Classpowerplants to Selected Unmanned Electric Propulsion Missions. AIAA Paper, 64-494, 1964.

4. Brown, Harold and Nicoll, Harry E., Jr.: Electrical Propulsion Capabilities for Lunar Exploration. AIAA Journal, February, 1963.

5. Larson, J. W.: Economics of Electrical Propulsion for Earth-Orbit to Lunar-Orbit Cargo Transfer. AIAA Paper No. 65-415, July, 1965.

6. Mickelsen, W. R. and MacKay, J.: Inter-planetary Flight with Electric Propulsion. Astronautics and Aeronautics, January, 1965.

7. Zola, Charles L.: Trajectory Methods in Mission Analysis for Low-Thrust Vehicles. AIAA Paper No. 64-51, January, 1964.

8. Mickelsen, W. R.: Effect of Thrustor Characteristics on Electric Space-Craft Missions. AIAA Paper, No. 64-676, September, 1964.

9. Sauer, C. G., Jr. and Melbourne, W. G.: Optimum Earth-to-Mars Round-trip Trajectories Utilizing a Low-Thrust Power-Limited Propulsion System. TR 33-376, Jet Prop. Lab., C.I.T., March 29, 1963.

10. Mickelsen, W. R. and Kaufman, H. R.: Status of Electrostatic Thrustors for Space Propulsion. NASA TN D-2172, May, 1964.

11. Reader, Paul D.: Experimental Performance of A 50-Centimeter Diameter Electron-Bombardment Ion Rocket. AIAA Paper No. 64-689, August, 1964

12. Mark, H., Goldberg, G. and Mirtich, M. J.: Determination of Cratering Energy Densities for Metal Targets by Means of Reflectivity Measurements. AIAA Journal, May, 1964.

13. Singer, S.; Kim, N. G.; and Farber, M.: An Experimental Study of Colloidal Propulsion Using Sub-Micron Solid Particles. AIAA Paper No. 63-052, 1963.

14. Cox, A. Lucile and Harrison, S.: The Controlled-Growth Colloidal Ion Source. AIAA Paper No. 63-049, 1963.

15. Norgren, C. T.: Onboard Colloidal Particle Generator for Electrostatic Engines. ARS Paper No. 2380-62, 1962.

16. Goldin, D. S. and Norgren, C. T.: Thrust Measurements of Colloidal Particles as an Indication of Particle Size and Thrustor Operation. AIAA Paper, No. 63-050, 1963.

17. Norgren, C. T. and Goldin, D. S.: Experimental Analysis of the Exhaust Beam From a Colloidal Thrustor. AIAA Paper No. 64-674, August, 1964.

18. Goldin, D. S. and Kvitek, G. L.: An Analysis of Particle-Formation Efficiency In a Colloid Thrustor. AIAA Paper No. 66-253, March, 1966.

19. Hendricks, C. D., Jr. and Pfeiffer, R. J.: Parametric Studies of Electrohydrodynamic Spraying. AIAA Paper No. 66-252, March, 1966.

20. Cohen, E.; Somol, C. J.; and Gordon, D. A.: A 100-kv, 10-w Heavy-Particle Thrustor. AIAA Paper No. 65-377, July, 1965.

21. Hunter, R. E. and Wineland, S. H.: Charged Colloid Generation Research. Paper presented at Space Electronics Symposium, Los Angeles, California, May, 1965.

22. Hunter, R. E. and Wineland, S. H.: Exploration of the Feasibility of an Electrodeless Colloid Thrustor Concept. Sixth International Symposium on Space Technology and Science, Tokyo, Japan, November, 1965.

23. Courtney, W. G. and Budnik, C.: Colloid Propulsion Using Chemically-Formed Particles. AIAA Paper No. 66-253, March, 1966.

24. Harris, S. P. and Farber, M.: Development of a Solid Charged Colloidal Particle Thruster. AIAA Paper No. 66-255, March, 1966.

electric rocket durability: 400 days

$\$_{SM}$: $/Kg of payload onto surface of Moon

$\$_{OE}$: $/Kg boosted into Earth parking orbit

cost
effectiveness

$\dfrac{\$_{SM}}{\$_{OE}}$

round trips

Specific weight, Kg/Kwj

chemical
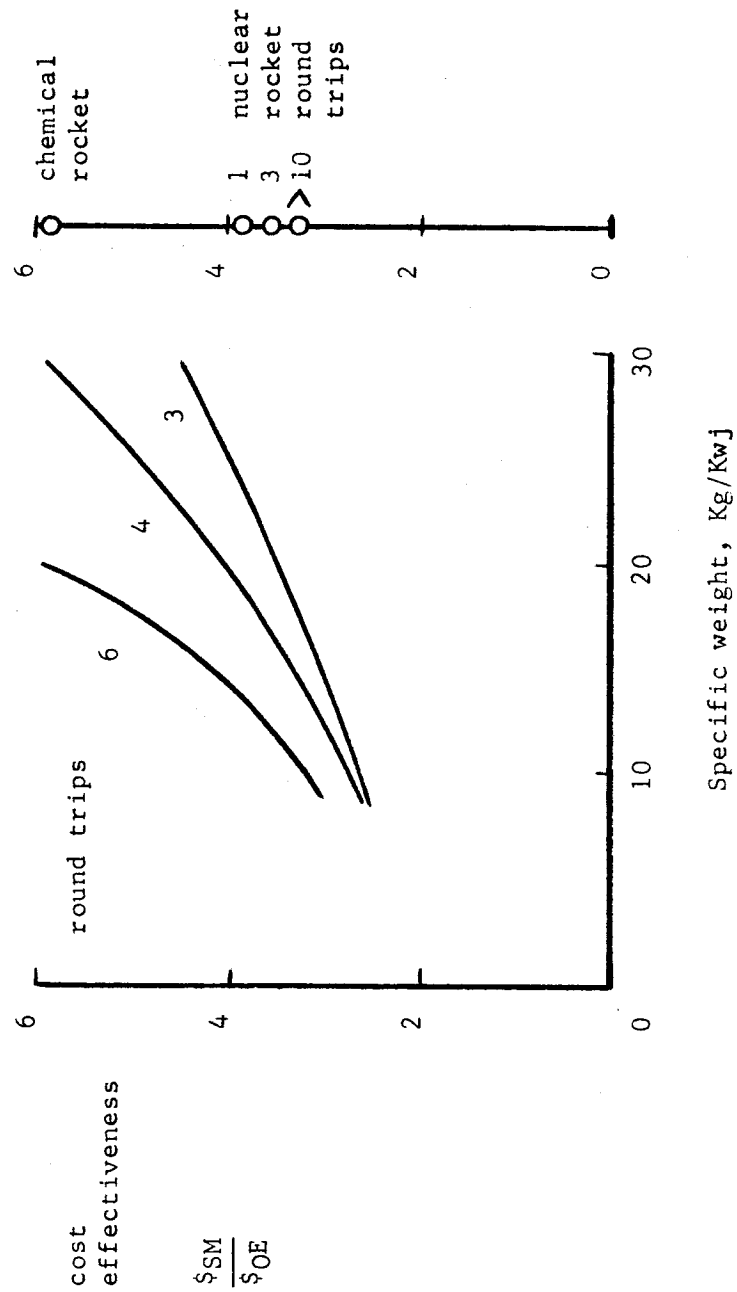rocket

1   nuclear
3   rocket
>10 round
    trips

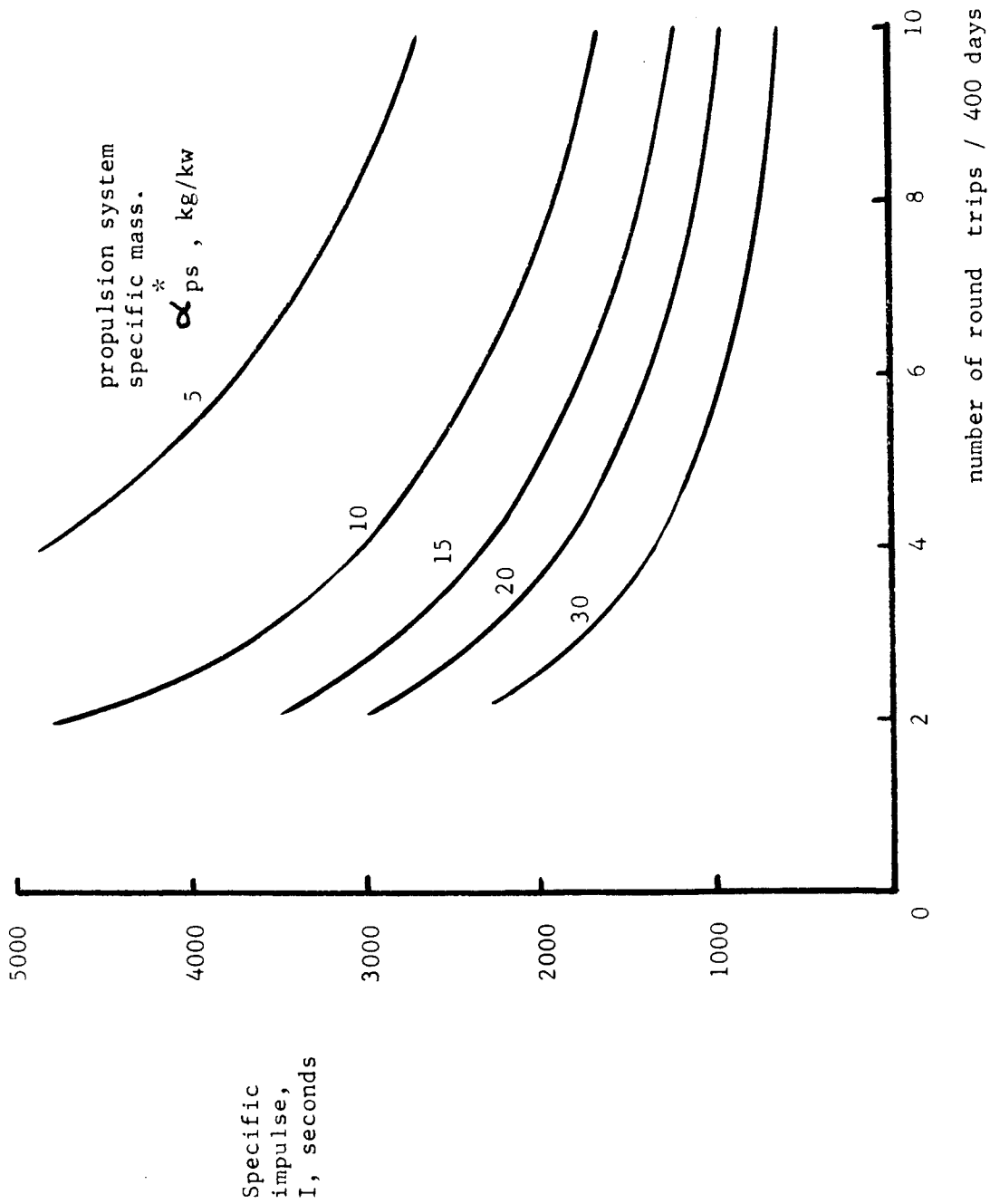FIG. 1 - Cost effectiveness of electric lunar ferries.

Figure 2 - Specific impulse requirements for lunar ferries
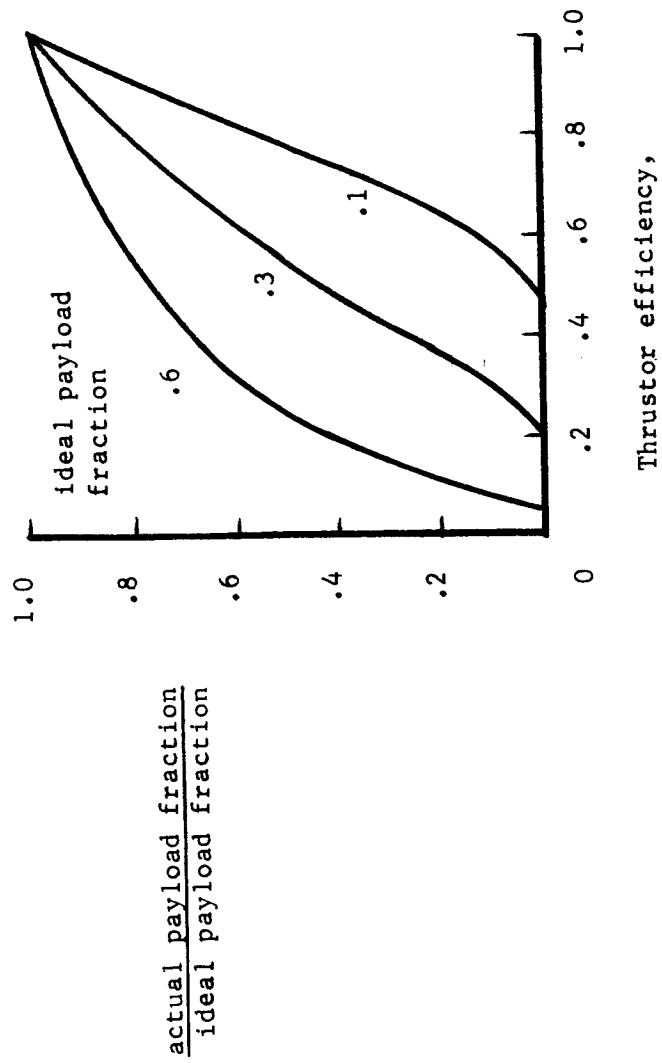Propulsion system durability, 400 days.

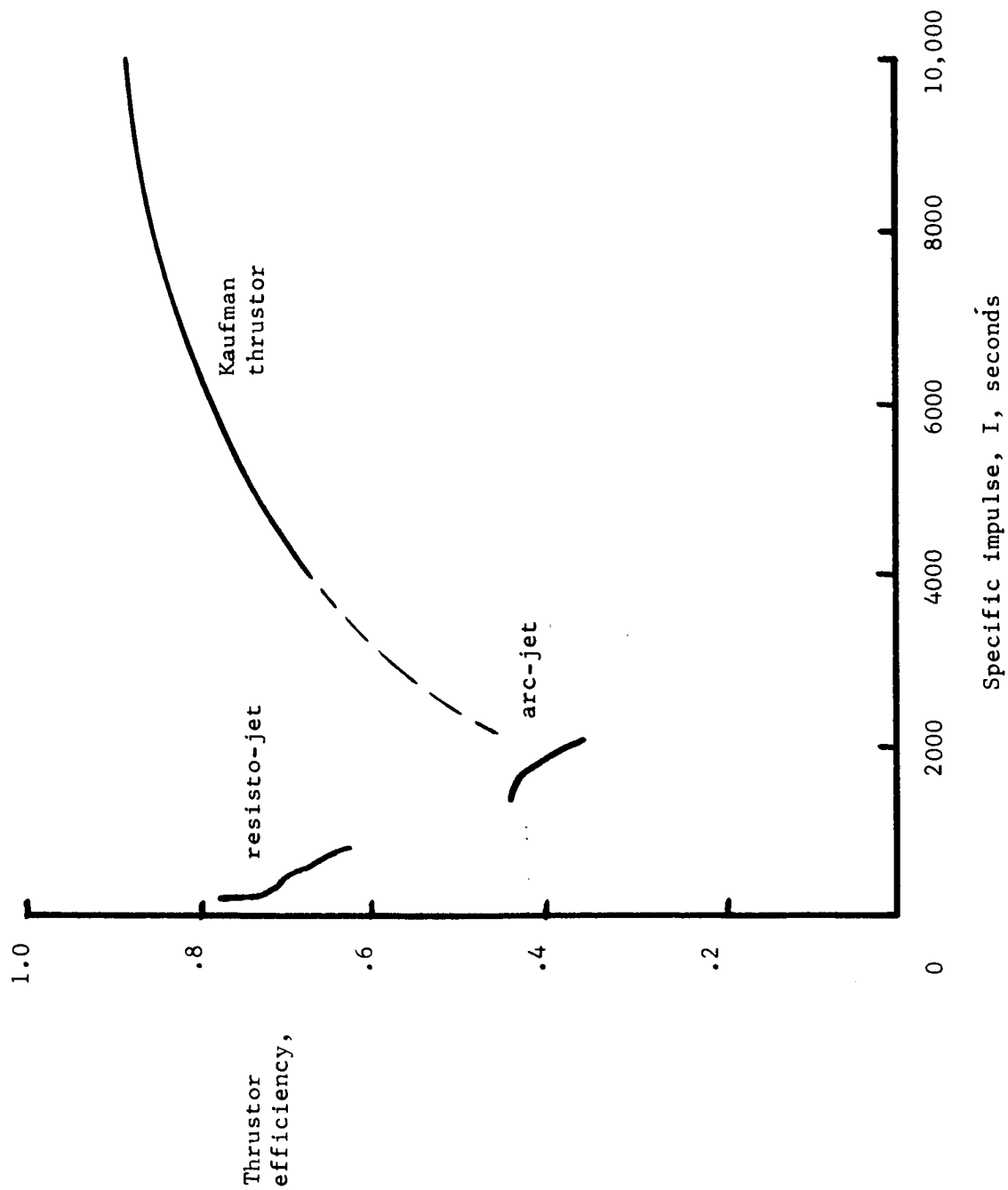FIG. 3 - Effect of thrustor efficiency on payload

FIG. 4 - Efficiencies of existing thrustors.

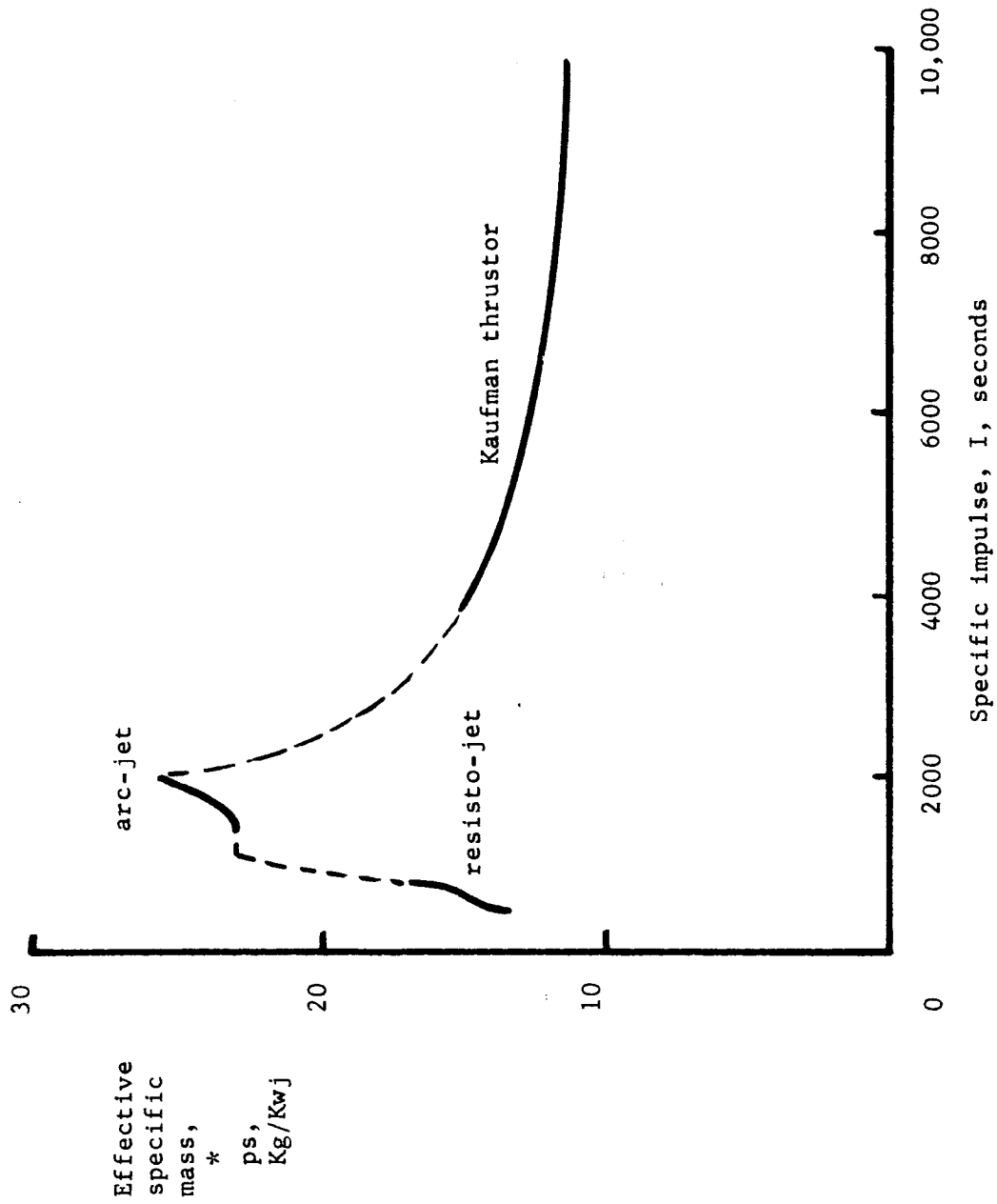FIG. 5 - Effective specific mass of propulsion systems with existing thrustors and $\alpha = 10$ Kg/Kw when $\eta = 100\%$.
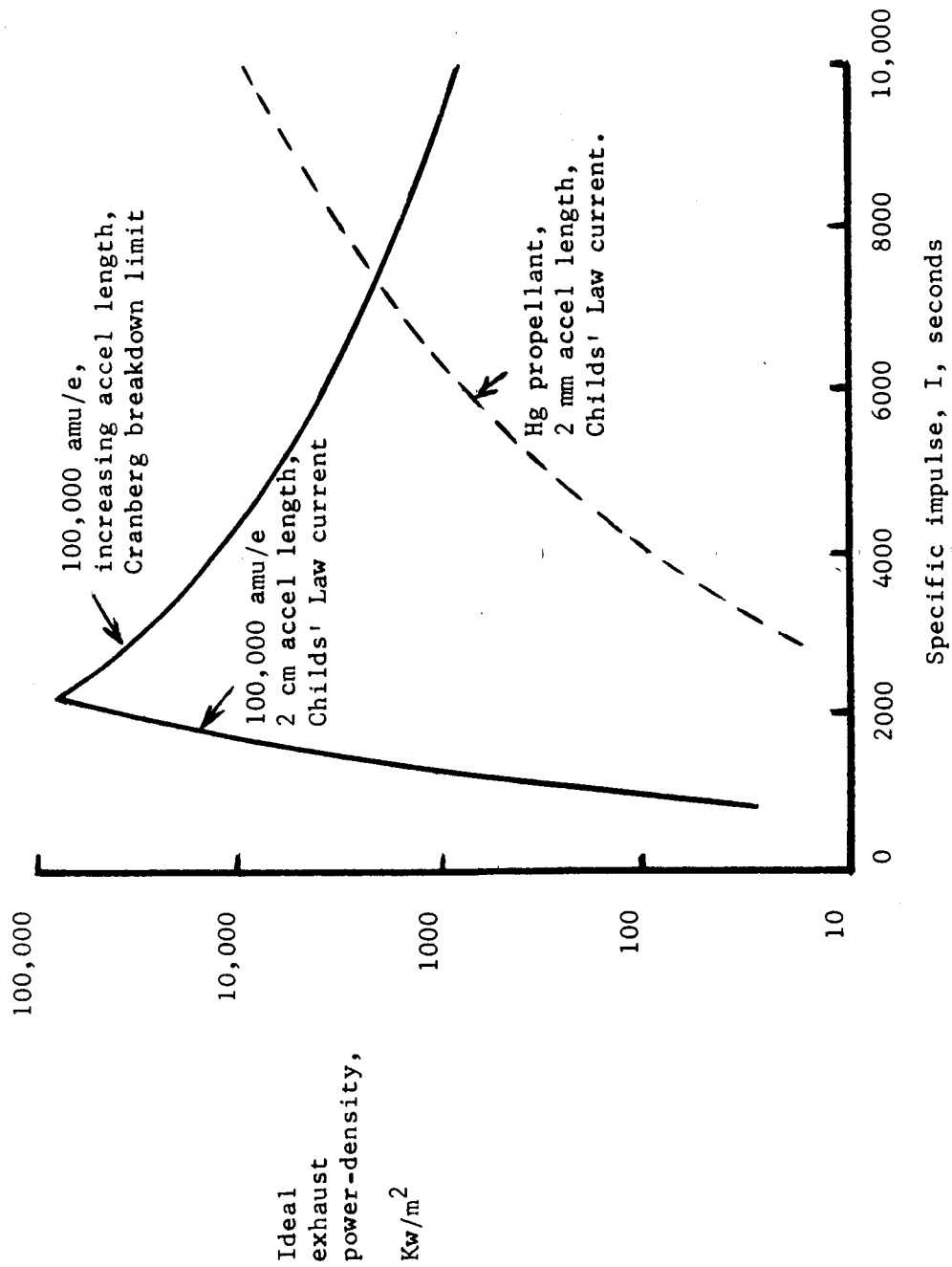
FIG. 6 - Ideal exhaust-jet power density.

Secondary
electron
coefficient

Net electronic
charge after
collision

primary electron
passes through

primary electron
stays in particle

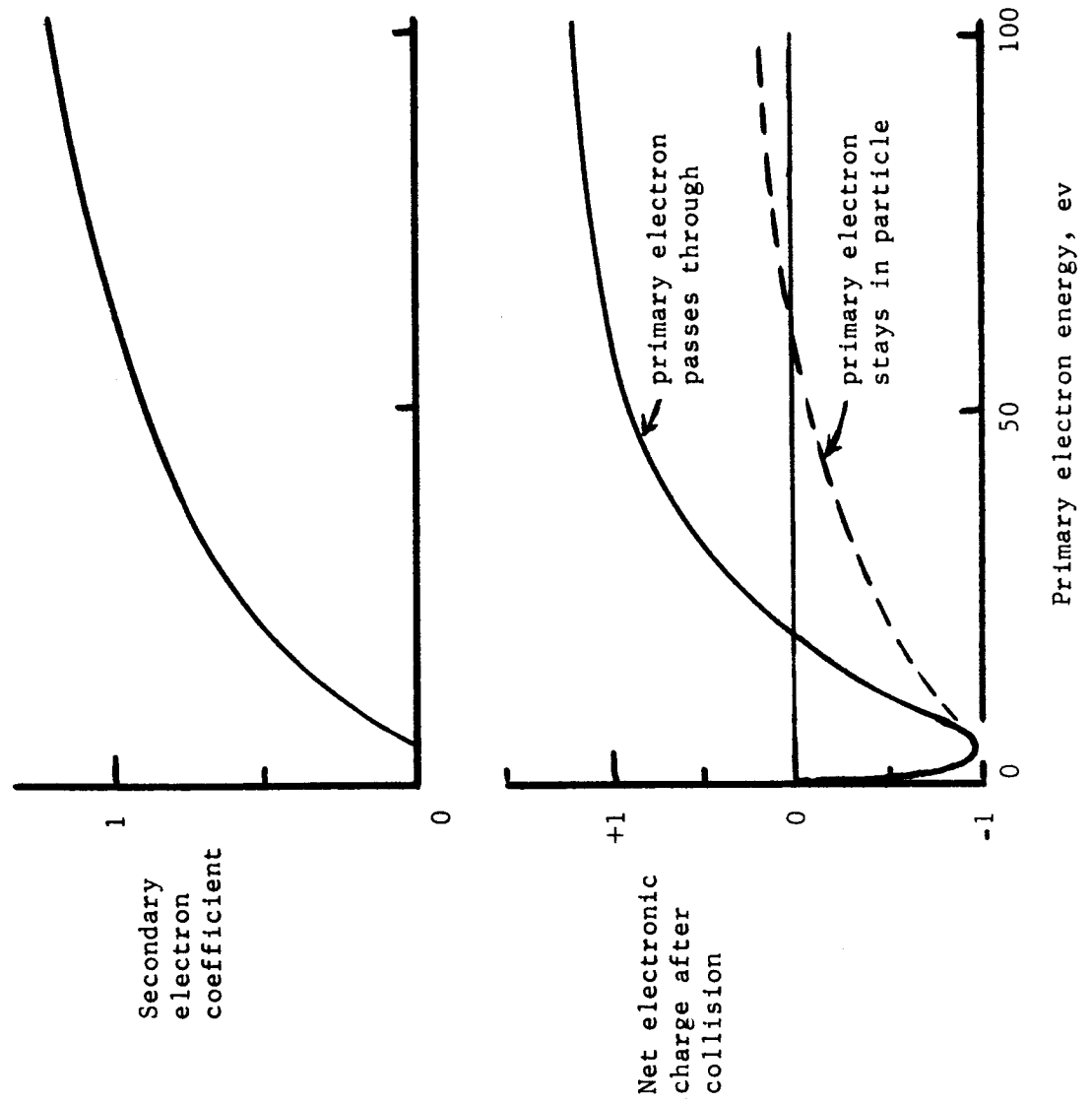Primary electron energy, ev

Figure 7 - Possible mechanisms for charging
colloid particles.

FUTURE TRENDS IN ELECTRIC PROPULSION

by

WILLIAM R. MICKELSEN
Colorado State University
Ft. Collins, Colorado

AIAA SECOND

PROPULSION JOINT SPECIALISTS MEETING

FUTURE TRENDS IN ELECTRIC PROPULSION*

by

William R. Mickelsen**

Colorado State University
Ft. Collins, Colorado

INTRODUCTION

Electric propulsion has repeatedly been predicted to have superior payload
capacity or faster trip times than chemical rockets or nuclear rockets, with
the proviso that the electric propulsion system mass must be small. This is
tantamount to saying that electric propulsion will be practical if the energy
storage and power generation, power conversion, and electric thruster systems
can be made much lighter in weight than any similar equipment has ever been
made before.

In about 1957, the work of Ernst Stuhlinger struck the imagination of many,
and much research was begun on electric propulsion. Of the total system, sub-
systems such as the energy source (nuclear reactor), the power generation
(Rankine system), the power conversion (generators and electronics), seemed to
be within reach of existing technology. Because of this viewpoint, much re-
search emphasis has been given to the thruster itself. As a result, the
electric thruster is nearly a flight-ready component in the over-all electric
propulsion system, but the rest of the system is far from a flight-qualified
status.

There is little doubt that the power-conditioning sub-system can be vastly
improved over the present status. In contrast, improvement of the power-gener-
ation system does not appear to be straightforward. Rankine power-generation
systems are notably subject to forced-outage rates that are unthinkable for

manned space missions. Not only is very advanced reliability required, but in addition, high reactor temperatures, nuclear radiation, corrosive liquid metals, micrometeoroid punctures, and radiative heat-transfer all place very stringent requirements on the power-generation system. Many of these problems are being solved*, and the Rankine system still survives as a serious contender for primary power. Thermionic diode power systems have been pursued assiduously by the research dilletante since well before 1957, but the low out-put voltage per cell and the extreme radiation environment of in-pile systems have been serious deterrents to the early success of the thermionic scheme. Some of these problems are being solved**, and practical thermionic power systems may be developed in the future.

SOLAR-ELECTRIC PROPULSION

Into this power-generation breach has come the lowly solar cell. Even with its few tenths of a volt output per cell, its high weight, and its sensitivity to over-temperature, the solar-cell power generation system stands today fully flight-qualified and adaptable to electric propulsion. Another paper[1] at this symposium has detailed the virtues and applications of solar-electric-propulsion systems. With chemical-rocket boost beyond Earth escape, the solar-electric-propulsion system offers highly significant payload-capacity advantage over all-chemical propulsion systems. This superiority is illustrated in Figure 1.

Design studies have been reported[2,3] which show clearly that solar-electric propulsion systems could provide much greater payloads for the forthcoming Mars-orbiter-lander missions. An example of such a design[2] is shown in Figure 2. Solar panels designed for Saturn 1B packaging would provide 48 kilowatts of electric power to the electric propulsion system. This low-voltage d.c.

---

*"Dynamic Liquid-Metal Plants Practical" by John F. Judge. Missiles and Rockets, p. 22, May 9, 1966.

**"Heat pipe transfers energy for conversion to electricity". IEEE Spectrum, p. 148, April, 1966.

power would be converted to high-voltage power for ion thrusters in an inverter-power-conversion sub-system, and further adjustment to various voltages would be done in a power-conditioning sub-system. Automatic control of the thruster power and propellent would be a part of these sub-systems. Power-conversion, power-conditioning, and controls components would be mounted on thermal radiation panels to provide for heat rejection of electrical losses.

Solar-cell power decreases as the spacecraft moves towards Mars so that a modular design is used in which thrusters can be switched off on schedule. Thruster system reliability is enhanced by redundancy in this modular design. A constant specific impulse would be used with an optimum thrust-vectoring program. Improvements in solar-cells and panel designs are expected to result in solar-panels of 50 lb/kwe specific weight. All other components of the electric propulsion system design study are state-of-the-art. Components and weights are listed[2] in Table I.

A performance comparison[2] with an all-chemical propulsion system is made in Table II. This comparison shows that a substantial cost savings could be gained by using the solar-electric propulsion system.

Three ion-thruster types are possible candidates for the electric propulsion system that is illustrated in Figure 2: the mercury-discharge thruster[4], the cesium-discharge thruster[5], and the contact-ionization thruster.[6,7] Both of the discharge-type thrusters have been endurance tested for thousands of hours, and the mercury-discharge thruster has been flown in space,[8] so there is no doubt of flight-qualification for these two. Lifetime of the contact-ionization thruster at high-performance conditions is still open to question, and its efficiency is too low at the specific impulse required so it cannot be considered for the Mars-orbiter-lander mission in the present paper.

Efficiencies of the three thruster types in life-tests[5,6,7,9] are shown in Figure 3. All of these thrusters have been life-tested in runs of 2000-4000 hours, which approach the 6000 hours required for 250-day Mars-orbiter missions. Optimum specific impulse for this mission is about 2000-3000 sec.,

but because of poor thruster efficiency in this range, the design study has been forced to 4000 sec. Contact-ionization thrusters have poor efficiency at low specific impulse because thermal radiation power loss from the ionizer is nearly constant, but jet power decreases as specific impulse is decreased. Mercury-discharge and cesium-discharge thrusters have the same basic design originated by Harold R. Kaufman at NASA Lewis. Power consumed in ionizing each atom of cesium propellant is less than that for mercury propellant. However, the net accelerating voltage is less for cesium than for mercury; at the same exhaust velocity, the voltages have the same ratio as the ion mass. Even with these power relationships, the cesium-discharge thruster has an efficiency advantage of about 10% at a specific impulse of 4000 seconds.

Cesium-discharge and mercury-discharge thrusters are compared in Table III with respect to their relative performances in the Mars-orbiter-lander mission. With its higher efficiency, the cesium-discharge thruster will provide a higher jet power. However, the cesium-discharge thruster has a lower exhaust-jet power density, so it must be larger than the mercury-discharge thruster. As noted previously, cesium ions require less accelerating voltage at the same exhaust velocity as mercury ions. Ion current density is limited because of charge-exchange ion erosion of the accelerator electrode, so that for a given durability L, the allowable current density j is:

$$j = (K \frac{\eta_U}{1-\eta_U} \frac{1}{\sigma VYL})^{\frac{1}{2}} \tag{1}$$

where K is a factor that depends on electrode design, and where the propellant utilization efficiency η_U is the ratio of ion mass flow to total mass flow. Assuming that the lower sputtering yield Y of cesium ions is offset by the larger charge-exchange cross-section σ of cesium and that the volume V for charge-exchange collisions is the same, then the ratio of allowable current densities for the two thrusters becomes:

$$\frac{j_{Hg}}{j_{Cs}} = \frac{\left[\eta_U/(1-\eta_U) \right]_{Hg}^{\frac{1}{2}}}{\left[\eta_U/(1-\eta_U) \right]_{Cs}^{\frac{1}{2}}} \tag{2}$$

Effective jet power density is[10]:

$$P_{j,eff} = \frac{1}{2} F v_{j,eff} = \frac{1}{2} \dot{m}_{tot} v_{j,eff}^2 \tag{3}$$

Since $v_{j,eff} = g_c I$, and $m_{tot} = m_+/\eta_U$, then:

$$P_{j,eff} = \frac{1}{2} \frac{\dot{m}_+}{\eta_U} I^2 g_c^2 = \frac{1}{2} g_c^2 I^2 \frac{m}{e} \frac{jA}{\eta_U} \tag{4}$$

where m is ion mass, e is electronic charge, and A is exhaust area.
Equations (2) and (4) can be combined to obtain a ratio of exhaust areas:

$$\frac{A_{Cs}}{A_{Hg}} = \frac{m_{Hg}}{m_{Cs}} \frac{\left[\eta_U (1-\eta_U) \right]_{Cs}^{\frac{1}{2}}}{\left[\eta_U (1-\eta_U) \right]_{Hg}^{\frac{1}{2}}} \tag{5}$$

This expression provides a comparison of thruster sizes for the same specific impulse and effective jet power. Mercury-discharge thrusters[4] have a utilization efficiency of about 85%, and cesium-discharge thrusters[5] have about 92%. With these operating conditions, the area ratio would be $A_{Cs}/A_{Hg} = 1.2$.

Both thrusters have about the same weight per unit exhaust area, so that by comparison with Table I, the cesium-thruster weight for the 48kw system would be 210 lb. In addition, cesium is of lower density than mercury so that cesium tankage will be higher by the ratio of spherical tank areas, which is $A_{tankCs}/A_{tankHg} = (\rho_{Hg}/\rho_{Cs})^{2/3} = (13.6/1.88)^{2/3} = 3.75$ and this results in a cesium reservoir weight of 390 lb. Other components of the thruster system should be about the same for the mercury and cesium systems. (see Table I.) Total weight of the cesium-discharge thruster system would be 774 lb., and this results in an effective specific mass of 61 lb./kwj for the cesium-discharge thruster as shown in Table III. If effective jet power of the cesium-discharge thruster were reduced to 23kwj, then weight savings in the solar panels, power conversion-conditioning-controls, and thruster system would be 390 lb., 40 lb., and 50 lb. respectively, thereby bringing the two propulsion systems within 165 lb. of each other when designed with the same degree of conservatism. This weight difference would change the scientific payload listed in Table II only

slightly, so cesium-discharge and mercury-discharge thrusters are competitive for this mission.

In comparing the two thrusters in Table III, use has been made of performance parameters defined in a previous paper[10]. Effective specific mass of the thruster includes mass increases in other components caused by thruster inefficiency. Consideration of this parameter in Table III clearly shows that the thruster is responsible for about one-half of the total propulsion system mass. Further effort to improve electric thrusters is certainly warranted.

Serious consideration of the potential performance benefits of solar-electric-propulsion leads to the first future-trend statement of this paper:

I. Solar-electric propulsion with Kaufman-type cesium or mercury-ion thrusters can provide very substantial payload increases for un-manned vehicles in the exploration of the solar system. There can be no doubt that these payload increases would lead to significant cost reductions in the national space program.

ELECTRIC PROPULSION FOR SATELLITES

The first coming-of-age of the space program is the practical, economic use of satellites. Weather monitoring, world communications, precision mapping, and military missions are all imminently profitable enterprises. A key factor in the success of these systems is precision attitude and position control. Cold-gas jets and chemical rockets have use in this propulsion function only for short-term test flights of about a year in duration. Economically realistic systems should have lifetimes of the order of trans-oceanic cables; for such durations electric propulsion appears to be the only practical solution.

Solar-electric propulsion is a fairly good first-generation system type for this function. Solar cell arrays are fully flight-qualified, and miniature

ion engines have had adequate feasibility demonstration in the laboratory[11,12,13]. All that remains is the development of complete systems to a fully operational status. A reasonable question remains whether the development of solar-electric satellite-propulsion systems is justifiable. The need for sun-facing orientation of solar arrays, the long-term degradation of solar cells in Van Allen belts, and energy storage in Earth shadow are all shortcomings of solar-electric ion thruster systems.

Radioisotope-heated gas jets[12,14,15] and ion thrusters powered with radioisotope-thermoelectric-generators have distinct advantages over solar-electric thrust systems because of their independence from sun-orientation, degradation, and dark-side periods. Sensitivity of some instruments to minute flux of nuclear radiation has prevented consideration of radioisotope propulsion systems for certain scientific missions. Aside from these few cases, radio-isotope power is very promising for micro- and milli- pound thrust propulsion systems.

Development of radioisotope-heated gas-jets in the milli-pound thrust range is underway at present. A radioisotope type has been selected, a thruster design has been prepared, and materials compatibility tests are underway[16]. Heat shielding has been a problem, but reduction of heat loss to a tolerable level appears to be certain. Propellant mass is acceptably low for operational life of a year or two, but will become too high for decade missions requiring a 10% duty cycle as shown in Figure 4. Some propulsion functions have duty cycles of about 1%, and for these, the resistojet system is competitive with the ion thruster system. Propellant flow must be controlled with a valve and electronic control system, and valve failure rate may be a serious problem for economically practical missions which must be of the order of a decade. Precision of impulse-bit may be acceptable for milli-pound thrust levels in this thruster type, but the thrust level is too high for micro-pound impulse-bit requirements. The "light touch" of micro-thrust impulse-bits can be supplied

only by electrostatic ion thrusters.

Because of their much higher specific impulse, electrostatic thrusters have only a minute flow rate at micropound thrust levels. Propellant can flow continuously and still only a few tens of grams would be needed for a decade of operation. With valveless operation the electrostatic ion thruster system will have adequate reliability. Electric power for the ion thruster could be provided by a radioisotope thermoelectric generator. Ion thrusters require d.c. power at several thousand volts, so that an inverter-transformer-rectifier system would be required[11,13]. Additional complexity of this conversion equipment will certainly add much weight to the propulsion system, and certainly will decrease reliability of the system. Thrust vectoring can be done with great precision in cesium contact-ionization thrusters with simple electrostatic deflectors. Alignment of the thrust vector of position-control thrusters could virtually eliminate unwanted couples, thereby reducing the attitude-control requirements.

Three electric thrusters having thrust levels in the milli-pound range have been tested in the laboratory sufficiently to ensure future flight-qualification status. These are compared in Table IV. All have a fraction of a milli-pound thrust. Because of the low duty cycle of attitude and position control, it is desirable in many applications to turn off all power to the thruster during thrust-off periods. With this mode of operation, approximately 45,000 thermal cycles are required each year[13].

Thermal-cycling tests have been done for the mercury-discharge thruster[17] and for the cesium-contact thruster[13]. A cathode for the mercury-discharge thruster has been heat-cycled 418,000 times before failure, and the porous-tungsten ionizer in the cesium-contact thruster has been heat-cycled 85,000 times without any indication of incipient failure.

Mercury-discharge and cesium-contact thrusters listed in Table IV operate at specific impulses of 4000 and 5000 seconds respectively, while the ammonia-

resistojet[18] has a specific impulse of only 120 seconds. As a result, power requirements are less for the resistojet, but propellant and tankage weights are much greater for the resistojet. Electric thruster systems are compared with chemical-rocket systems in Figure 4. Chemical-rocket tankage is assumed to be 10%. Milli-pound thrust chemical rockets could be superior to the resistojet if a specific impulse higher than 100 seconds can be obtained. Ion-engine systems with solar-cell power are clearly superior to any other propulsion system for long mission times. It must be noted that this superiority exists only if solar-cell power is acceptable.

Micro-pound-thrust chemical rockets have not been developed as yet, and it appears that attainment of satisfactory specific impulse may be difficult for a number of reasons. For instance, the extremely small size of micro-pound-thrust chemical rockets forces nozzle flow into the slip-flow and transition-flow regimes[19]. Since resisto-jets have about the same specific impulse, then losses due to slip flow will occur in these electric thrusters also. From these considerations it can be concluded that ion thrusters are the only satisfactory means for providing micro-pound thrust levels.

A lower practical limit of thrust level for mercury-discharge thrusters is about 100 micro-pounds[17], and this may be true for cesium-discharge thrusters also. Contact-ionization thrusters with cesium propellant can be designed and operated in the micro-pound thrust range, as shown by the thruster performance data[11,13,20] in Table V. Although warm-up time for the ionizer is fairly long, precision impulse-bits can be produced by the cesium-contact thruster. This precision is achieved by merely switching the accelerator voltage on and off, and since capacitance of the thruster is negligible, the thrust program is very nearly a square wave. In addition to this high precision, the accelerator voltage control system is relatively simple. An example of a 10 micro-pound cesium contact-ionization thruster system is shown in Figure 5.

Assessment of the various propulsion systems suitable for satellite attitude and position control has led to the second future-trend statement of

this paper:

II. The choice of electric thruster systems for attitude and position control of satellites will depend on factors such as the thrust level, duty cycle, impulse bit precision, and thrust vector alignment requirements for each particular mission. Some missions of ten year duration and duty cycles of about 1% will be done with resistojets. For duty cycles of about 10% and satellite operational life of ten years, electrostatic thruster systems are superior to all other types of propulsion. Cesium-contact ion thrusters probably will be used for all satellite missions requiring micro-pound thrust levels and high-precision impulse bits.

ELECTRIC ROCKETS FOR PRIMARY PROPULSION

Lightweight electric propulsion systems could be used in the exploration of the complete solar system, in lunar ferry missions, and in manned Mars round-trip missions[21]. For example, a 220 kwj system with a specific weight of 33 lb/kwj could perform nearly all of the missions listed in Tables VI and VII. The outer-planet lander missions in Table VII would require a Saturn V booster, and a 1700 kwj electric propulsion system which conceivably could be a cluster of 220 kwj systems.

In contrast, neither nuclear-rocket spacecraft or chemical-rocket spacecraft could perform all of the unmanned exploration missions listed in Tables VI and VII. Furthermore, because of the lower size limit of nuclear-rocket engines, the Saturn V would be used for all the orbiter and lander missions with nuclear rockets. Saturn V boosters would be needed for three of the orbiter missions with chemical-rocket spacecraft, and all of the lander missions.

The potential advantages of electric propulsion for lunar ferry and for manned Mars round trips[21] are shown in Table VIII. The lunar ferry vehicle would be all electric, but boost to hyperbolic velocity from Earth would be necessary to take full advantage at the 33 lb/kwj electric propulsion system

in manned Mars missions. Electric propulsion payloads with nuclear-rocket hyperbolic boost[21] are shown in Figure 6.

The preceding comparisons of propulsion systems show that great savings in booster costs are possible if a lightweight electric propulsion system can be developed. In considering the possibility of a sufficiently lightweight system, it must be assumed at present that an electric powerplant can be developed with a specific weight of about 20 lb/kwe. With this future power-plant as a basis, existing electric thruster systems can be examined for their potential performance.

Power conditioning and control systems for ion engines have been success-fully operated in actual space flight[8]. However, such systems have specific weights of more than 30 lb/kwe, and so are not practical for primary propulsion. Design studies have been made that predict specific weights of 17 lb/kwe for 1-kw thrusters[22], 5 lb/kwe for the 48-kw solar electric system[2] discussed previously, and 10 lb/kwe for 300-kw nuclear-electric systems[23]. Radiation shielding mass is included in the design study for nuclear-electric systems. For the purposes of the thruster comparison being made here, a specific mass of 10 lb/kwe and an efficiency of 92% will be assumed for the power-conditioning and controls system.

There are three thruster types at present that have had performance testing for durations comparable to those required for interplanetary missions; these are the cesium-discharge[5], the mercury-discharge[4,9,24], and the cesium-contact[6,7] thrusters. Efficiencies of these thrusters are shown in Figure 3. Each of the three thrusters has a fundamental limitation in ion current density that is due to charge-exchange ion erosion of the accel electrode. This limitation is expressed by the equation for accel electrode lifetime L:

$$L = K_1 V_e n_e \frac{1-f}{f} \frac{1}{j^2} \frac{1}{\sigma V_i Y} \tag{6}$$

where K_1 is a constant, V_e is the electrode volume that can be allowed to n_e is the number density of atoms in the electrode, f is the fraction of

total propellant that emerges as neutral atoms, j is the local ion current density, σ is the charge-exchange cross-section, V_i is the volume from which the eroding charge exchange ions originate, and Y is the average yield of sputtered atoms per incident charge-exchange ion. By using equation (6) together with published data, an estimate of allowable current-density can be prepared, as shown in Figure 7 for the cesium contact-ionization thruster. On this basis, it appears that the allowable ion currents for the three thrusters are as listed in Table IX.

Weights of the thrusters are also listed in Table IX. From the design study of the solar-electric spacecraft discussed previously[2], an estimate has been included in Table IX of the weight of thruster mounting structure, vectoring mechanism, cabling, and miscellaneous accessories. Tankage for electric propulsion systems is a matter of some contention. In the present analysis, the tank described in the solar-electric design study[2] has been accepted as being a minimum weight design for the acceleration conditions in chemical-rocket boost phases. This design results in a tankage of 6.5% for mercury. Using the previously derived tankage weight ratio of 3.75, based on the ratio of mercury and cesium densities, the cesium tankage is 24.4%. In addition to these weight penalties, the thruster must be charged with the weights of additional power conditioning and powerplant that are needed to supply the thruster losses. A complete expression for effective specific weight α^* of the thruster is[10]:

$$\alpha_{th}^* = \alpha_{th} + \left(\frac{\alpha_{pp}}{\eta_c} + \alpha_c \right) \frac{1-\eta_{th}}{\eta_{th}} + \frac{M_{tank}}{P_{j,eff}} + \frac{\Delta M_{pay}}{P_{j,eff}} \qquad (7)$$

where α_{th} is the physical weight of the thruster divided by the effective jet power of the thruster, α_{pp} is the specific weight of the powerplant, α_c is the weight of the power conditioning and controls divided by the electric power output from this sub-system, η_c is the efficiency of the power conditioning and controls sub-system, η_{th} is thruster efficiency, M_{tank} is the weight of the propellant tank, $P_{j,eff}$ is effective jet power, and ΔM_{pay} is the payload

loss due to a non-ideal specific impulse program.

Existing thrusters are not capable of operating with a variable specific impulse which is required for an ideal Irving-Blum trajectory. The payload loss term in equation (7) can amount to as much as 10 lb/kwj for planetary orbiter missions with constant specific impulse programs[10], and since existing thrusters can only be operated at constant specific impulse, this payload loss is unavoidable with existing thruster concepts. However, this payload loss is not included in the present comparison of thrusters.

Tankage weight was estimated by assuming that propellant weight M_{pr} will be equal to propulsion system weight M_{ps}. In other words, $M_{tank} = kM_{pr} = kM_{ps} = k\alpha_{ps}Pj,eff$. A propulsion-system specific weight α_{ps} of 33 lb/kwj was assumed.

A comparison of cesium-discharge, mercury-discharge, and cesium-contact ion thrusters is shown in Figure 8. These effective specific weights were calculated from equation (7), and from the other information described in the preceding paragraphs. Noting that the powerplant was assumed to have a specific weight of 20 lb/kwe, it is clear that existing electric thrusters would at least double the propulsion-system specific mass for specific impulses of 7000 to 8000 seconds. At specific impulses below 7000 seconds, the effective specific mass of existing thrusters would become much too high.

It should be noted here that the cesium-contact ion thruster has not been tested for the durability required for interplanetary missions. There also is some question whether the cesium-discharge thruster can be scaled to larger size, because of sensitivity to changes in thermal balances.

As discussed in a previous paper[10], planetary orbiter and lander missions will require specific impulses in the range of 7000 to 14,000 seconds when a constant specific-impulse program is used. From inspection of Figure 8, it appears that existing thrusters would be acceptable for application to such missions. However, such application would result in large payload loss in

some missions because of the constant specific impulse program. Ideal Irving-Blum trajectories have specific impulse as low as 2000 to 4000 seconds, so that existing thrusters clearly cannot be used for ideal performance missions.

Manned Mars round-trips will require specific impulses below 6000 seconds, and lunar ferries will require specific impulses in the 1000 to 3000 seconds range[25]. The effective specific weights shown in Figure 8 clearly show that existing electric thrusters are inadequate for manned Mars round-trip missions, and for lunar ferry missions.

The discussion in this section has led to the third future-trend statement of this paper:

III. Existing electric thrusters could be used for planetary orbiter and lander missions in the future, but considerable payload loss would result in a number of these missions because of non-ideal thruster performance. Existing electric thrusters are not adequate for manned interplanetary flight, or for lunar ferry missions.

ADVANCED CONCEPTS IN ELECTRIC PROPULSION

New electric thruster concepts are needed to provide high performance in the specific impulse range of 1000 to 7000 seconds. Some improvements of existing thruster types can be expected as a result of continued research and development. However, these improvements will probably provide only minor increases in efficiency and moderate decreases in specific weight.

A mercury-discharge thruster of the basic Kaufman-type, but with a mercury-pool cathode is presently being developed[26]. In the specific impulse range of 4000-5000 seconds this thruster has about the same efficiency as the cesium-discharge thruster with an auto-cathode, which is shown in Figure 3. The mercury-pool thruster has an effective jet power of about 3 kwj at a specific impulse of 5000 seconds, and has an anode diameter of 20 cm. Because of high

exhaust-jet power density this thruster has a lower effective specific mass, as illustrated in Figure 9. Ion current density in the mercury-pool thruster is 32 amp/m^2, which is the same as the cesium-discharge thruster current density. The cesium-discharge thruster has been life-tested for 3000 hours and based on this test the durability is predicted at more than 20,000 hours[5]. From the previous discussion in the present paper, it was concluded that the mercury-discharge and cesium-discharge thrusters should have the same allowable current density when the neutral-atom fraction is the same in both thrusters. Neutral-atom fraction in the cesium-discharge thruster was 8%, while the mercury-pool thruster data is for operation at 20% neutral-atom fraction. From equation (6) it can be seen that the durability of the mercury-pool thruster should be: $L = 20,000 \left[(1 - .2)/.2 \right] / \left[(1 - .08)/.08 \right] = 7000$ hr. Whether such a durability can be achieved with a current density of 32 amp/m^2 in the mercury-pool thruster remains to be verified by future tests.

If future development insures adequate durability of the mercury-pool thruster, then performance would be better than that of existing thrusters. However, an effective specific mass of 20 lb/kwj would still cause appreciable payload loss, so that greater improvement is desirable.

A new concept, the cesium plasma-separator thruster, is described in another paper[27]. There is some experimental evidence that this concept might be developed to the status of a high-performance thruster. For example, the theoretical performance predictions can be used to obtain hypothetical effective specific mass as shown in Figure 10. If such performance could be obtained in a long-life thruster, then electric propulsion systems would become much more attractive in the specific impulse range above 5000 seconds. It is important to note that an 8 lb/kwj penalty must be assigned to the cesium-plasma-separator thruster. If mercury propellant could be used, this penalty would be reduced to 2 lb/kwj, and the hypothetical performance of the plasma-separator thruster would be even more attractive.

Another possible future development is the MPD (magnetoplasmadynamic) thruster[28]. Proponents of this concept point out that the MPD thruster would have much higher exhaust-jet power density than the electrostatic ion thrusters. If a high thruster efficiency could be attained, then the MPD thruster might have excellent performance in the specific impulse range of 2000 to 7000 seconds where existing electrostatic thrusters have such poor performance. In addition, it appears that MPD thrusters would have a good compatibility with low-voltage power generation systems. Since power conversion and power conditioning sub-systems for electrostatic thrusters have such high specific weights, this potential feature of MPD thrusters should add much incentive to further research efforts. However, the basic mechanisms involved in the operation of the MPD thruster are not well understood as yet. Furthermore, experimental measurements of performance are still suspect. Efficiencies that have been measured with some degree of confidence are not nearly as high as those of existing ion thrusters. Finally, research has not progressed far enough as yet to provide even approximate estimates of durability. For these reasons, the MPD thruster cannot be considered as a future thruster type until further research provides a more firm basis for a prognosis.

Colloid-particle electrostatic thrusters are another possible future development. Acceleration of charged colloid particles instead of atomic ions offers a possiblity of significant improvements in efficiency, as illustrated by the following approximate expression for efficiency of electrostatic thrusters:

$$\eta_{th} = \eta_U \frac{1}{1+(ev/ion)/\phi_{net}} \tag{8}$$

where η_U is the fraction of total propellant flow that is charged and accelerated, and ev/ion is the energy consumed in generating and charging each charged particle. Since the net accelerating voltage ϕ_{net} is directly proportional to the particle mass/charge ratio, then it is evident that the

high voltage acceleration of colloid-particle thrusters could lead to high efficiency[25] if the propellant utilization efficiency η_u remained near 100%, and if the ev/ion remained about the same as in ion thrusters. Durability of colloid thrusters has been discussed elsewhere[25], and it appears that further basic information is required before durability problems can be defined.

Electrostatic spraying of a liquid propellant is used in one type of colloid thruster[29]. Polarization of droplets leaving a hollow needle tip is accomplished in the presence of a strong electric field. Droplets leaving the tip have an electrostatic charge and are accelerated electro-statically as in conventional ion thrusters. A 36-needle array has been operated for 100 hours with glycerol-H_2SO_4 propellant. Total exhaust current was 252 micro-amperes, and the accelerating voltage was 5000 volts. Average mass/charge was 50,000 amu/e, so that specific impulse was about 440 seconds. Even if the voltage were increased to 50,000 volts, the jet power would be only 13 watts, which is much too low to be of interest for primary propulsion since the thruster needle array is 3.8 cm in diameter. Much higher power densities will be necessary before this thruster concept can become competitive with existing ion thrusters.

Colloid particles have been generated by homogeneous condensation from the vapor state in condensation regions of supersonic nozzles[30]. Particles of sufficiently small and uniform size can be formed and charged by this method. A recent analysis[31] has predicted a maximum utilization efficiency of 50%, and on these grounds alone, the statement has been made "these results raise serious doubts regarding the potential usefulness of a number of colloid thrustor concepts". In making this statement it seems that one of the primary advantages of colloid-particle thrusters has been overlooked: the possiblity of using a wide variety of materials for propellant.

In principle, the colloid-particle thrusters can use any liquid or solid material as propellant. For example, bio-wastes in manned missions could be utilized as propellant[32]. A summary of biowastes from a seven-person crew on

a 450-day mission is shown in Table X[33,34]. With an open-cycle system, bio-wastes amount to a total of 49,300 lb. In comparison, an estimated[33] weight of a closed-cycle life-support system for a seven-person crew is about 16,000 lb. Whether a reliable, flight-qualified closed-cycle system could be made with such a weight is still open to question.

Future developments in electric propulsion[35] promise a gross starting weight in Earth-satellite parking orbit of about 500,000 lb. for this mission as shown in Figure 11. Hyperbolic boost with an 850 sec.-specific-impulse nuclear rocket would require a Δv of about 11,000 ft./sec. Assuming a tankage of 10% and an engine mass fraction of 4% for the nuclear rocket, the electric spacecraft starting weight after hyperbolic boost would be about 300,000 lb. Of this, about 136,000 lb. would be payload, leaving about 164,000 lb. to be divided between the propulsion system and the propellant. Total jet power for this hypothetical mission is 4 megawatts, so the propulsion system would weigh 58,000 lb., leaving 106,000 lb. for propellant.

For the particular mission under consideration, biowaste from an open-cycle life-support system could provide about 50% of the propellant requirement. This savings in propellant would reduce the electric spacecraft weight to about 250,000 lb., and the starting weight in Earth-satellite parking orbit to about 420,000 lb. In other words, two Saturn V boosters could launch the manned Mars mission instead of the three boosters required when biowaste is not used as propellant. Attractive features of biowaste propellant that are deserving of further analysis are: (1) reduction in booster requirements, and hence, reduction in mission costs, (2) greatly improved reliability by using an open-cycle instead of a closed-cycle life-support system, (3) use of the greater water supply for radiation shielding, and (4) physiological and psychological advantages of having fresh water continuously available to the crew throughout the mission.

Further study of improvements in mission performance will establish the

relative advantages of biowaste propellant, and from the results of this study will form the rationale for research on biowaste-propellant electric thrusters.

Another promising source of propellant for colloid-particle electric rockets is that of upper-stage tankage. Aluminum alloys are expected to be used for high-energy chemical rocket upper-stage tankage because of good fracture resistance at cryogenic temperatures[36]. Aluminum has a low melting point, so it could be vaporized easily. One method of generating colloid particles is by homogeneous nucleation from the vapor state. Propellant utilization efficiency could be low without seriously affecting mission per- formance, because the aluminum propellant would be "free" since the tankage is normally abandoned in the parking orbit. The Saturn V upper stage has an empty weight of 25,700 lb., and with two such boosters required to launch the space- craft, there would be 40,000 - 50,000 lb. of aluminum for electric-rocket propellant. In addition, the nuclear rocket used for hyperbolic boost would have a tank weight of 16,500 lb.

Aluminum tankage is clearly a valid source of propellant, and the use of aluminum as propellant in electric rockets appears possible in principle. Because of promise of great gains in mission performance, studies are being made of payload gains, and research is underway on aluminum-colloid-particle thrusters.

In summarizing the discussion in this section, the fourth future-trend statement of this paper can be made:

IV. Future developments in existing electric thruster types will provide a reasonably good performance for planetary orbiter and lander missions. New concepts in ion thrusters will be developed that could provide excellent performance for planetary orbiter and lander missions, and possibly fairly good performance for manned interplanetary missions. To gain the full potential of electric propulsion, advanced concepts will be required. Conception and

feasibility demonstration of these advanced concepts will require a sustained
research effort.

FUTURE TRENDS IN ELECTRIC PROPULSION RESEARCH

Electric propulsion systems for satellite propulsion are being developed
to a flight-qualified status. This trend to flight hardware will increase in
the future to meet the demand for precision attitude and position control of
satellites in a wide variety of economically practical satellite applications.
Because of the low power levels required, radioisotope energy sources are
ideally suited for satellite propulsion systems. Future research efforts will
be directed toward the conception and feasibility demonstration of new
radioisotope-electric propulsion concepts having greater reliability and
simplicity of control.

Electric propulsion systems that are presently considered for primary
propulsion have a number of fundamental deterrents to high performance:

1. high weight, inefficiency, and complexity of equipment for conversion
   of power from the power-generation sub-system, and conditioning of
   that power for input to the thruster

2. poor efficiency in the 2000 - 7000 sec. specific impulse range

3. high weight and large size of the thruster in the 2000 - 7000 sec.
   specific impulse range

4. inability of the system to operate with a variable specific impulse
   program

5. restriction to the use of particular propellants such as cesium or
   mercury

When the electric propulsion system is viewed as a whole, these deterrents
to high performance are not surprising. All propulsion systems operate on the
principle that energy is transferred from a prime source of energy to the
propellant mass, with the objective of imparting a momentum change to the

propellant mass in order to produce thrust. As a consequence of the laws of motion of bodies in gravitational fields, there is an optimum ratio of energy-to-momentum of exhaust mass which will provide the best performance of each space-rocket transportation system. In this sense, the electric propulsion system is an energy/momentum transducer. To accomplish this function at present, a large number of poorly matched sub-systems are used. Each sub-system and mis-matched interface inevitably will add to the weight and unreliability of the total system.

If electric propulsion is ever to attain its full potential in primary space propulsion, it will not be with systems where the power generation, power conversion, power conditioning, propellant supply, and thruster are treated as separate entities during research and development, and then patched together with electrical and fluid conductors to make a semblance of a flight-qualified system.

Future research in primary electric propulsion will be directed towards concepts where the thruster is directly connected to the power-generation sub-system, or where the thruster is physically integrated into the power-generation device. Fundamental limitations of electric power generation must be recognized and accepted as immutable. For example, the voltage outputs of each cell in solar-electric, thermoelectric, and thermionic powerplants are limited to a fraction of volt, and series connections of these cells can be carried only so far. Thrusters intended for integration with these power-generation sub-systems must be capable of multi-specific-impulse operation with voltages of the order of 100 volts.

If satisfactory performance with low-voltage powerplants is not attainable, then an alternative is the use of high-voltage powerplants. Nuclear-fission turboelectric powerplants have the fundamental capability of providing fairly high voltage through rotating electric generators. Direct connection of electric thrusters to rotating generators is possible in principle, but it is clear that

.hruster power requirements must contain only a few voltage levels. Integration of high-voltage thrusters with the power-generation sub-system must depend on the conception and feasibility demonstration of high-voltage direct energy conversion concepts. Future research in electric propulsion will include concepts in high-voltage, direct energy/momentum conversion.

REFERENCES

1. Stearns, J.W., and Kerrisk, D.J.: Solar Electric Propulsion Systems - Engineering and Applications. Paper presented at AIAA Second Joint Specialists Meeting, Colorado Springs, Colorado. June 13-17, 1966.

2. Molitor, J.H., Berman, D., Seliger, R.L., and Olson, R.N.: Design of a Solar-Electric Propulsion System for Interplanetary Spacecraft. AIAA Paper No. 66-214. March, 1966.

3. Ritchie, D., Toms, R., and Menetrey, W.: Potentials of Solar Power Electric Propulsion. AIAA Paper No. 66-210. March, 1966.

4. Reader, P.D.: Durability Tests of Mercury Electron-Bombardment Ion Thrusters. AIAA Paper No. 66-231. March, 1966.

5. Sohl, G., Speiser, R.C., and Wolters, J.A.: Life Testing of Electron-Bombardment Cesium Ion Engines. AIAA Paper No. 66-233. March, 1966.

6. Zimmerman, R.L., Garvin, H.L., McKee, W.E., and Kami, S.: Development of Multistrip Cesium Contact Thrustors. AIAA Paper No. 66-235. March, 1966.

7. James, E.L., Worlock, R.M., Ernstene, M.P., and Forrester, A.T.: Surface Ionization Engine Development. AIAA Paper No. 66-236. March, 1966.

8. Cybulski, J., Shellhammer, D.M., Lovell, R.R., Domino, E.J., and Kotnik, J.T.: Results from Sert I Ion Rocket Flight Test. NASA TN D-2178. March, 1965.

9. Kaufman, H.R.: Private Communication. NASA Lewis Research Center. April 7, 1966.

10. Mickelsen, W.R.: Performance Parameters for Electric-Propulsion Systems. Journal of Spacecraft and Rockets. February, 1966.

11. Worlock, R.M., Caplinger, E., and Eilenberg, S.L.: Characteristics of Micropound Range Ion Thrustors. AIAA Paper No. 66-212. March, 1966.

12. Goodman, M.: Advanced Low-Thrust Propulsion Systems for Station Keeping and Stability Control of the NASA Manned Orbital Research Laboratory (MORL): Resistojets and Radioisotope Thrustors. AIAA Paper No. 66-226. March, 1966.

13. Anderson, J.R., and Thompson, S.A.: Development and Long-Life Performance of Ion Engines for Satellite Control. AIAA Paper No. 66-234. March, 1966.

14. Leventhal, E.L., and Berganini, D.F.: Snapoodle Demonstration Design Study. IEEE/AIAA National Aerospace Electronics Conference, Dayton, Ohio. May 10-12, 1965.

15. Romero, J.B.: Radioisotope Propulsion. Journal of Spacecraft and Rockets. Sept. - Oct., 1964.

16. Bromberg, M.: private communication. General Electric Company. March, 1966.

17. Kerslake, W.R., Wasserbauer, J.F., and Margosian, P.M.: A Mercury Electron-Bombardment Ion Thrustor Suitable for Spacecraft Station Keeping and Attitude Control. AIAA Paper No. 66-247. March, 1966.

18. Cybulski, R.J., John, R.R., and Malenda, J.: A Low Power Resistojet Propulsion System for Spacecraft Control. AIAA Paper No. 66-227. March, 1966.

19. Jonath, A.D.: Gasdynamic Problems in Low-Pressure Microthrust Engines. AIAA Bulletin, p. 232, May, 1965. Astronautics Acta. Sept. - Oct. 1965.

20. Lockwood, D.L.: unpublished data on NASA Lewis micro-pound ion thruster. NASA Lewis Research Center. April 18, 1966.

21. Mickelsen, W.R., and MacKay, J.S.: Interplanetary Flight with Electric Propulsion. Astronautics and Aeronautics. January, 1965.

22. King, H.J., Pinckney, K.R., Knauer, W., Molitor, J.H., Muldoon, W.J., and Kover. O.G.: The Development and Testing of a Light Weight Flight Ion Engine System. AIAA Paper No. 66-216. March, 1966.

23. Ramirez, P.Jr., and Tollefson, D.: Design and Analysis of Power Conditioning for Ion Propulsion Systems. AIAA Paper No. 66-215. March, 1966.

24. Reader, P.D.: Experimental Performance of a 50-Centimeter Diameter Electron-Bombardment Ion Rocket. AIAA Paper No. 64-689. August, 1964.

25. Mickelsen, W.R.: Colloid-Particle Electrostatic Thrustors. Paper presented at DGRR Sonnenberg Symposium on Electric Propulsion, West Germany. February 24, 1966.

26. Molitor, J.H.: private communication. Hughes Research Laboratories. April 20, 1966.

27. Free, B.A., and Mickelsen, W.R.: Plasma Separator Ion Thruster Development. Paper presented at AIAA Second Joint Specialists Meeting, Colorado Springs, Colorado, June 13-17, 1966.

28. Bennett, S., John, R.R., Enos, G., and Tuchman, A.: Experimental Investigation of the MPD Arcjet. AIAA Paper No. 66-239. March, 1966.

29. Cohen, E., Somol, C.J., and Gordon, D.A.: A 100-kv, 10-w Heavy-Particle Thrustor. AIAA Paper No. 65-377, July, 1965.

30. Norgren, C.T., and Goldin, D.S.: Experimental Analysis of the Exhaust Beam from a Colloidal Thrustor. AIAA Paper No. 64-674, August, 1964.

31. Goldin, D.S., and Kvitek, G.L.: An Analysis of Particle-Formation Efficiency in a Colloid Thrustor. AIAA Paper No. 66-253, March, 1966.

32. Roth, J.R.: An Open Cycle Life Support System for Manned Interplanetary Spacecraft. Paper presented at AIAA and AAS Stepping Stones to Mars Meeting. Baltimore, Maryland. March, 1966.

33. Meyers, J.R.: Combined Photosynthetic Regenerative Systems. NASA SP70, 1963.

34. Sanders, H.C.: The Effects of Man on the Weight of a Manned Space Vehicle. Advances in the Astronautical Sciences, Vol. II. Western Periodicals Co. 1963.

35. MacKay, J.S.: Preliminary Analysis of Manned Mars Mission Using Electric Propulsion

36. Johnsen, I.A., and Smith, G.: private communication. NASA Lewis Research Center. April 22, 1966.

Component	Weight, lb.
solar panels	2400
conversion, conditioning, controls	240
thruster	180
tanks for 1600 lb. propellant	104
propellant feed system	33
structure	80
cabling	51
thruster vectoring	10
total propulsion system	3098

TABLE I.

Component weights of 48-kilowatt solar-electric propulsion system with mercury-discharge thruster for Mars-orbiter-lander vehicle launched with Saturn 1B booster.

spacecraft propulsion system	all-chemical	solar-electric
Earth-Mars trips time, days	190	250
approach velocity at Mars, Km/sec	4.3	1.8
Mars-orbiter vehicle weight, lbs.	1850	3600
scientific payload in orbiter, lb.	470	1743
total program cost (ten units) $million	195	376
total program cost/lb. scientific payload, $/lb.	42,000	21,000

TABLE II.

Cost-effectiveness of solar-electric and all-chemical propulsion systems for Mars-orbiter-lander spacecraft with Saturn 1B booster.

	mercury-discharge thruster				cesium-discharge thruster			
	weight lb.	efficiency	output power	effective specific mass	weight lb.	efficiency	output power	effective specific mass
solar-cell power source	2400	--	48 kwe	50 lb/kwe	2400	--	48 kwe	50 lb/kwe
conversion conditioning, controls	240	93%	45 kwe	10 lb/kwe	240	93%	45 kwe	10 lb/kwe
thruster feed, tankage	458	52%	23 kwj	73 lb/kwj	774	62%	28 kwj	61 lb/kwj
TOTALS	3098	--	23 kwj	133 lb/kwj	3413	--	28 kwj	121 lb/kwj

TABLE III

Comparison of mercury-discharge and cesium-discharge ion thrusters for solar-electric spacecraft propulsion system at specific impulse of 4000 seconds.

thruster type	mercury-discharge (ref. 17)	cesium-contact (ref. 13)	ammonia resistojet (ref. 18)
thrust, milli-pound	.65	.56	.55
thermal tests, number of cycles	418,000	85,000	--
warm-up time, min.	0.16	0.3	--
power required, watts	144	125	9
*solar-panel weight, lb.	14.4	12.5	0.9
thruster-system weight, lb.	**7.2	**6.8	5.0
propellant and tankage for 10 yr. with 10% duty, lb.	3.3	3.0	***182
total weight of 10 yr. system, lb.	24.9	22.3	188
system weight/thrust, lb/milli-pound	38	29	340

* 100 lb/kwe
** assuming 0.05 lb/watt for power conditioning, batteries, and controls.
*** with 25% tankage

TABLE IV

Comparison of electric thruster systems in the milli-pound range for satellite attitude and position control.

thruster type	cesium-contact (ref. 11)	cesium-contact (ref. 13)	cesium-contact (ref. 20
thrust, lb.	24	10	10
warm-up time, min.	15	-	60
power required, watts	25	15	18
*solar-panel weight, lb.	2.5	1.5	1.8
thruster-system weight,lb.	< 7	3	6
propellant and tankage for 10 yr., 10% duty, lb.	0.1	0.3	0.2
total weight of 10 yr. system, lb.	< 9.6	4.8	8.0
system weight/thrust lb/ -lb.	< 0.40	0.48	0.80

*at 100 lb/kwe

TABLE V

Performance of micro-pound ion thruster systems for satellite attitude and position control.

mission	trip time, days			
	Electric spacecraft with Saturn 1B booster	Nuclear rocket with Saturn V booster	Chemical rocket spacecraft	
			Saturn 1B booster	Saturn V booster
Mercury, 300 n.m	165	60	-	65
Venus, 300 n.m.	130	30	55	-
Mars, 300 n.m.	170	80	125	-
Jupiter, Ganymede	590	250	500	-
Jupiter, 41,000 n.m.	1100	no mission	-	no mission
Saturn, Titan	850	600	1100	-
Saturn, outer ring	1000	900	-	1200
Uranus, Titania	1270	2000	-	2000
Uranus, 14,000 n.m.	1490	2000	-	no mission
Neptune, Triton	1850	no mission	-	no mission
Neptune, 13,000 n.m.	2170	no mission	-	no mission
Pluto, 170 n.m.	2160	no mission	-	no mission

TABLE VI

Comparison of propulsion systems for 2000 lb. planetary orbiters[21].
Electric propulsion system, 33 lb/kwj; jet power, 220 kwj; constant thrust.
Nuclear rocket specific impulse, 800 sec; engine mass fraction, 0.04; tankage
0.10. Chemical rocket specific impulse, 430 sec.; engine mass fraction, 0.02;
tankage, 0.05.

| mission | trip time, days | | Nuclear rocket with Saturn V booster | Chemical rocket with Saturn V booster |
| | Electric spacecraft | | | |
	220 kwj Saturn 1B booster	1700 kwj Saturn V booster		
Mercury	410	-	75	no mission
Venus	280	-	30	40
Mars	260	-	90	120
Ganymede	-	550	250	300
Titan	-	780	700	850
Titania	-	1200	2000	2000
Triton	-	1740	no mission	no mission
Pluto	-	2030	no mission	no mission

TABLE VII

Comparison of propulsion systems for 10,000 lb. landers[21]. Electric propulsion system, 33 lb/kwj; constant thrust. Nuclear rocket specific impulse, 800 sec; engine mass fraction, 0.04. Chemical rocket specific impulse, 430 sec; engine mass fraction, 0.02; tankage, 0.05.

2.32

mission	number of Saturn V boosters		
	Electric spacecraft	Nuclear Rocket	Chemical Rocket
Lunar ferry (4,000,000 lb. in 6 yrs.)	35	56	100
450 day manned Mars round-trip; 25,000 ft/sec. Earth re-entry	5	14	123
420 day manned Mars round-trip, 37,000 ft/sec. Earth re-entry	3	4	9

TABLE VIII

Comparison of propulsion systems for lunar ferry and manned Mars round-trip missions. Electric propulsion system, 33 lb/kwj; jet power, 1700 kwj; constant thrust; optimum hyperbolic boost with nuclear rocket. Nuclear rocket specific impulse, 800 sec.; engine mass fraction, 0.04; tankage, 0.10. Chemical rocket specific impulse, 430 sec.; engine mass fraction, 0.02; tankage, 0.05.

thruster type	cesium-discharge (ref. 5)	mercury-discharge (ref. 9)	mercury-discharge (ref. 9)	cesium-contact (ref. 6)
nominal size of thruster, cm.	12.7 cm. anode diam.	15 cm. anode diam.	50 cm. anode diam.	8.46 x 13.6 cm.
design specific impulse, sec.	5000	5000	9000	9000
jet power at design, kwj	0.7	0.8	22.0	1.0
ion current for 10,000 hr. life, amp.	0.4	0.27	2.2	0.2
thruster weight, lb.	4.7	6.6	43	19.3
structure, vectoring, cabling, etc. weight, lb.	5	5	5	5
tankage, %	24.4	6.5	6.5	24.4
tankage, lb/kwj	8.0	2.1	2.1	8.0

TABLE IX

Characteristics of existing ion thrusters for 10,000 hour durability.

biowaste	weight, lb.
water	17,600
dry solids	4,170
gas	6,800
wash-water	6,260
used clothes	3,110
miscellaneous	320
storage containers	14,000
total	49,300

TABLE X

Summary of open-cycle biowastes for seven-person crew on 450-day Mars round-trip.

Specific mass of propulsion system, lb/kwj
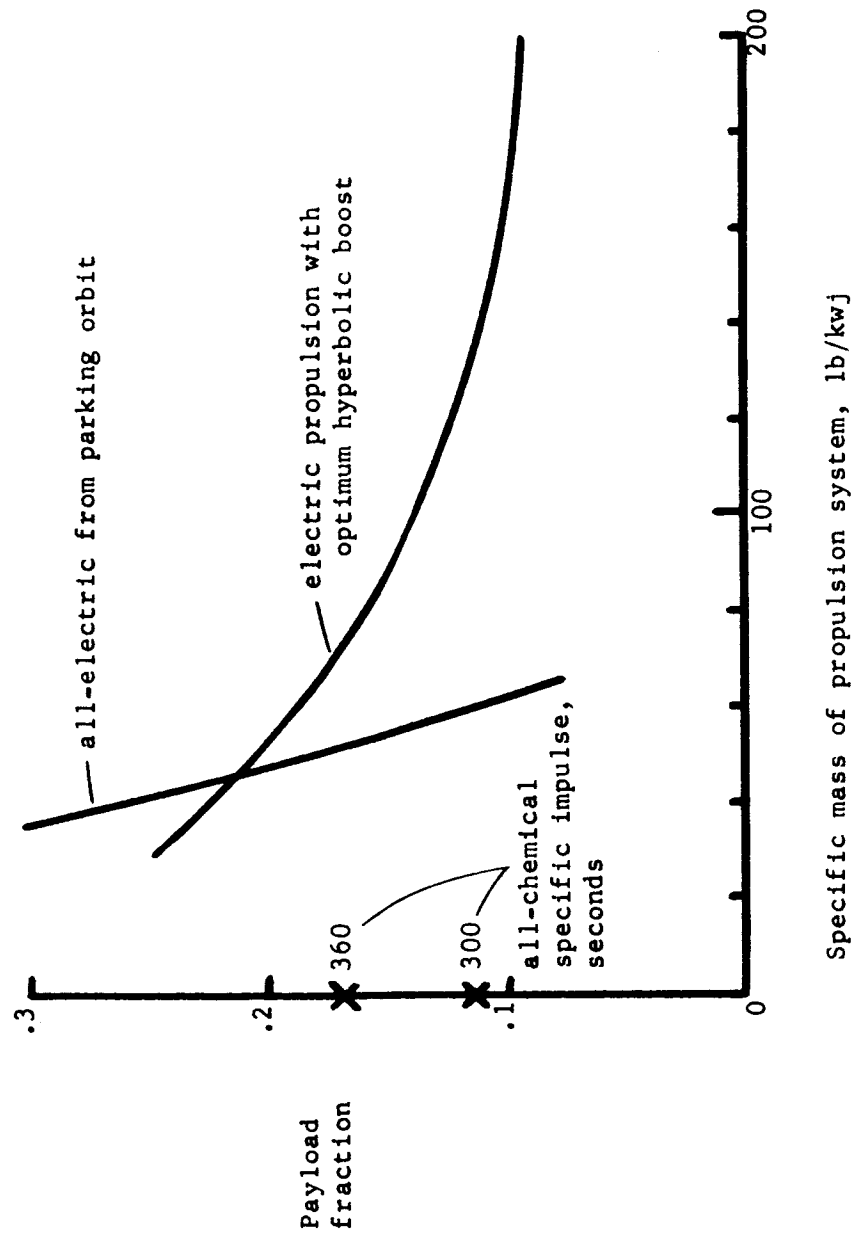
Fig. 1 - Effect of hyperbolic boost on performance of electric
spacecraft for 250-day Mars-orbiter mission with ideal thrust
program. Chemical rocket tankage, 5% of propellant weight;
chemical rocket engine, 1% of total vehicle weight.

Fig. 4 - Solar-electric spacecraft for Mars-orbiter-lander mission. (courtesy of JPL and Hughes Research Laboratories)
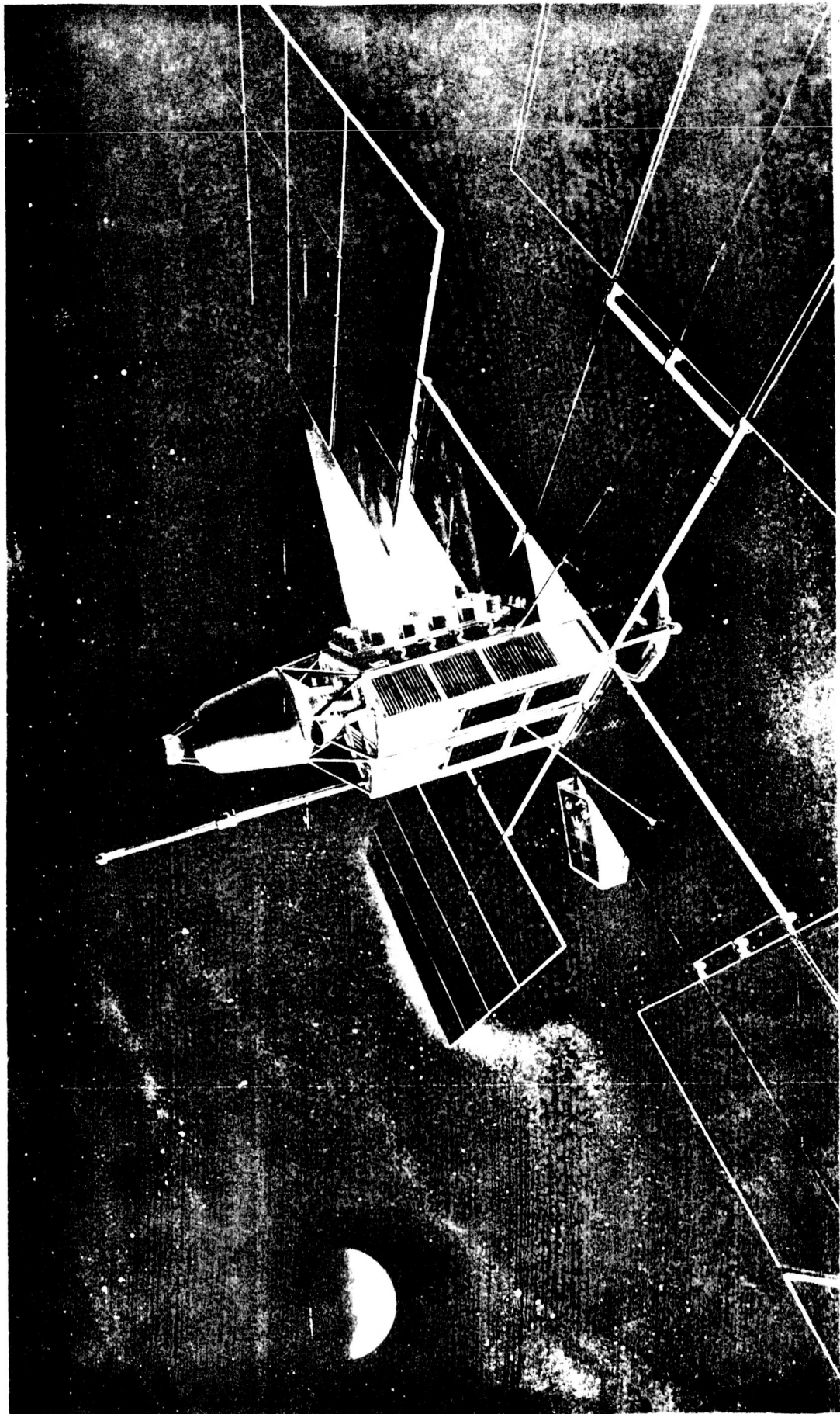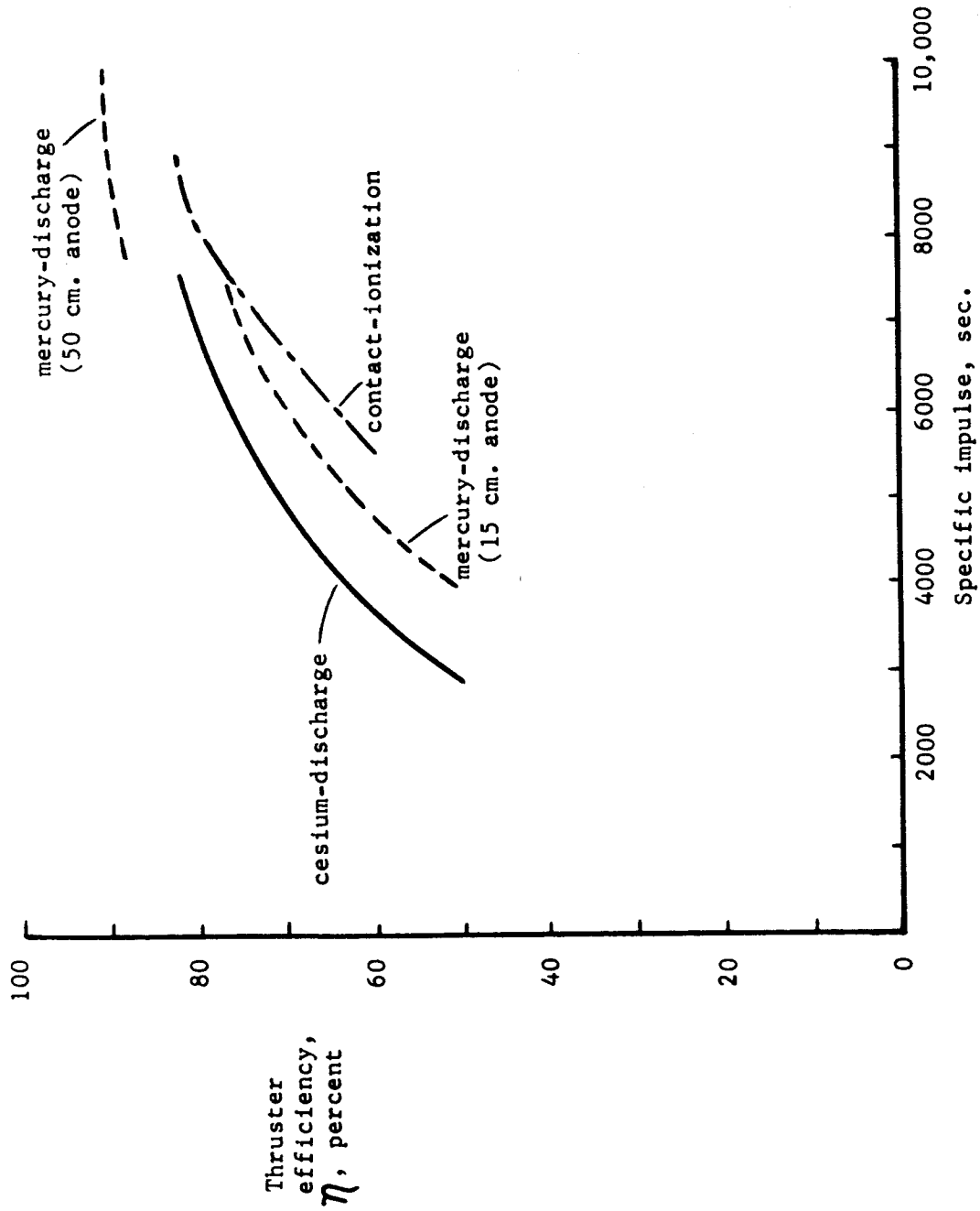
Figure 3 - Efficiencies of ion thrusters of 1-kw module size at operating conditions for 1 yr. durability.

Propulsion
system
specific weight,
$\dfrac{\text{lb weight}}{\text{millipound thrust}}$
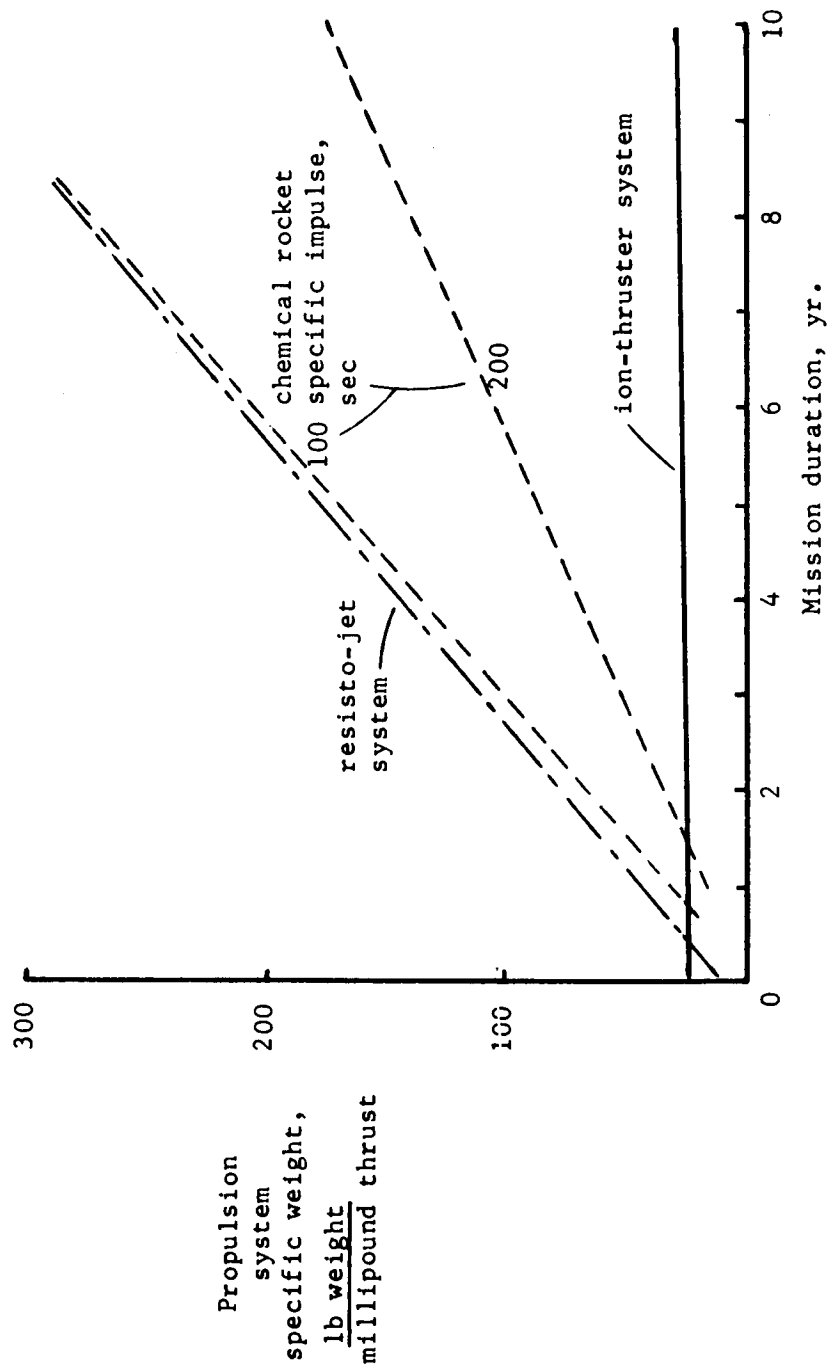
(a) 10% duty cycle

Figure 4. - Comparison of milli-pound-thrust propulsion systems
for satellite attitude and position control. Duty cycle, 10%;
chemical rocket tankage, 10%; other parameters from Table IV.
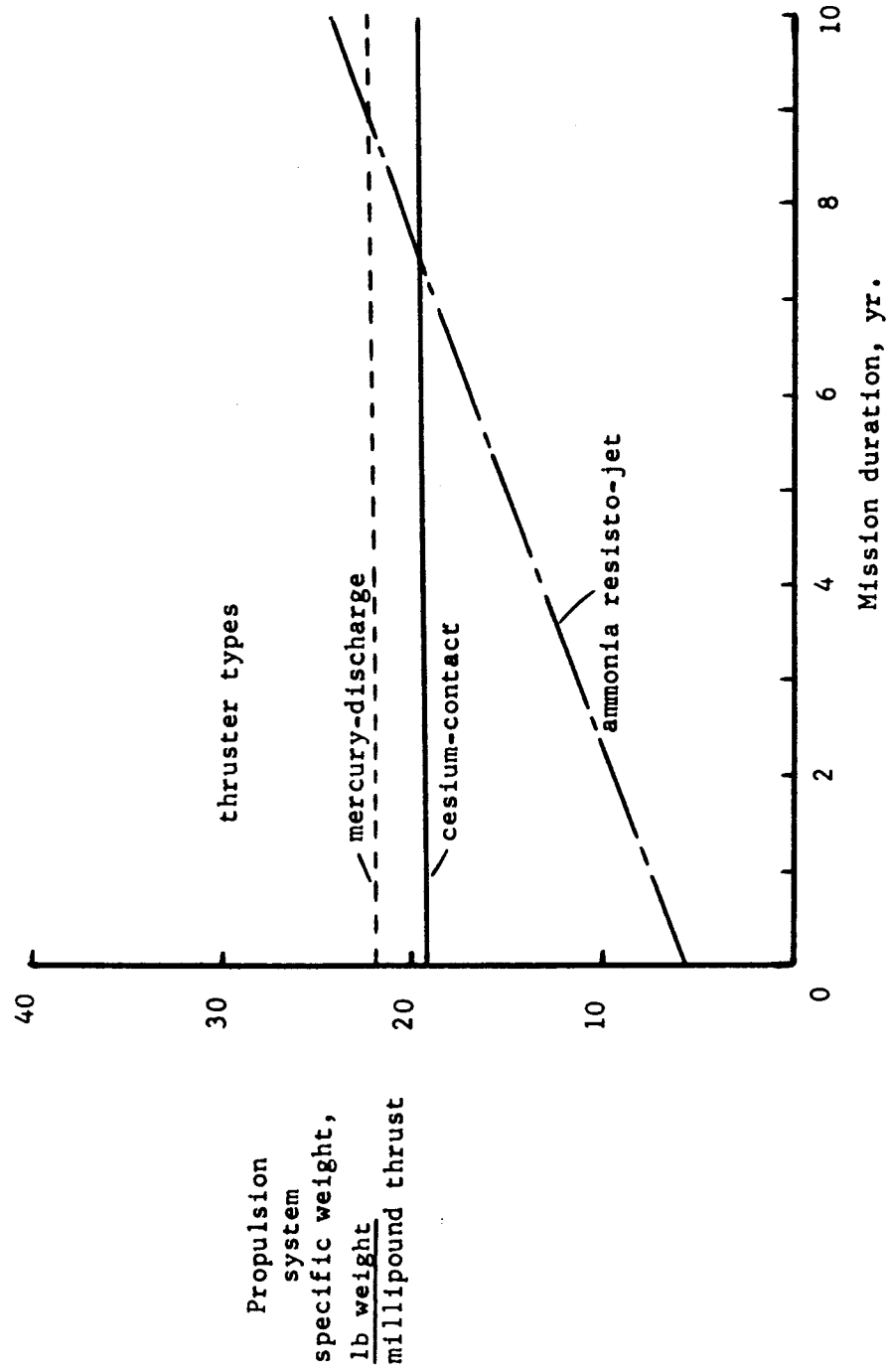
(b) 1% duty cycle

Figure 4. - (con't)

Figure 5. - Ten-micropound cesium contact-ionization thruster system. (courtesy of Hughes Research Laboratories).

HEAT SHIELDS

HIGH VOLTAGE INSULATOR

FOCUS ELECTRODE

IONIZER

SEGMENTED ACCEL

NEUTRALIZER

POWER CONDITIONING MODULE

ONE-SHOT VALVE

HERMETIC SEAL

CESIUM IN POROUS METAL

VAPORIZER HEATER
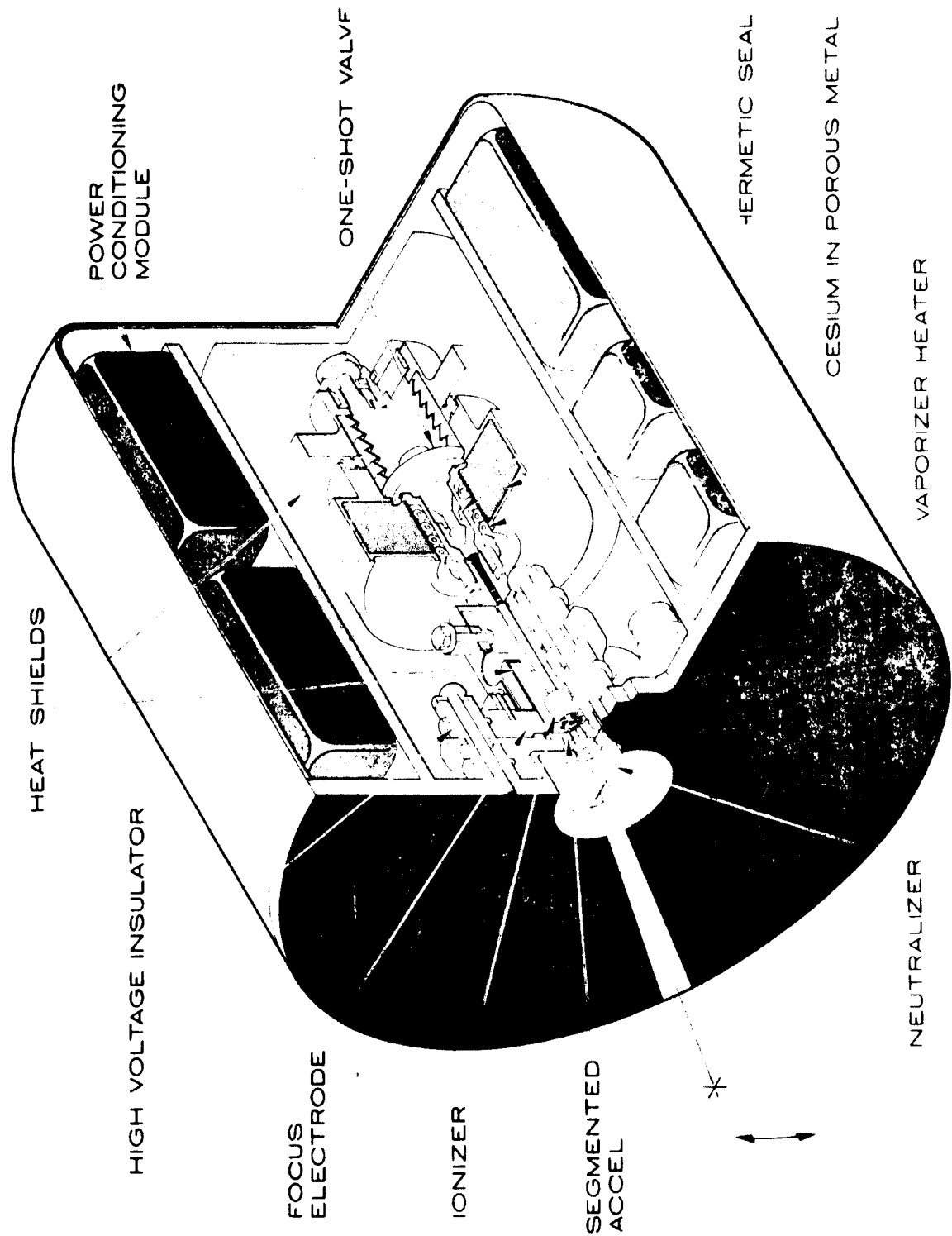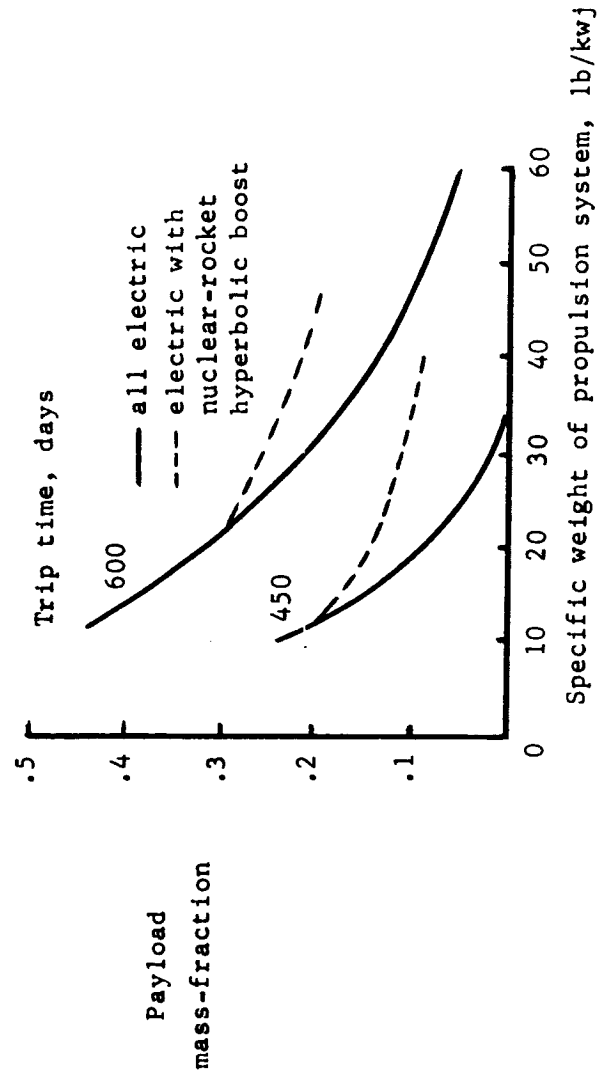
Figure 6. - Effect of hyperbolic boost on electric-propulsion mission performance.
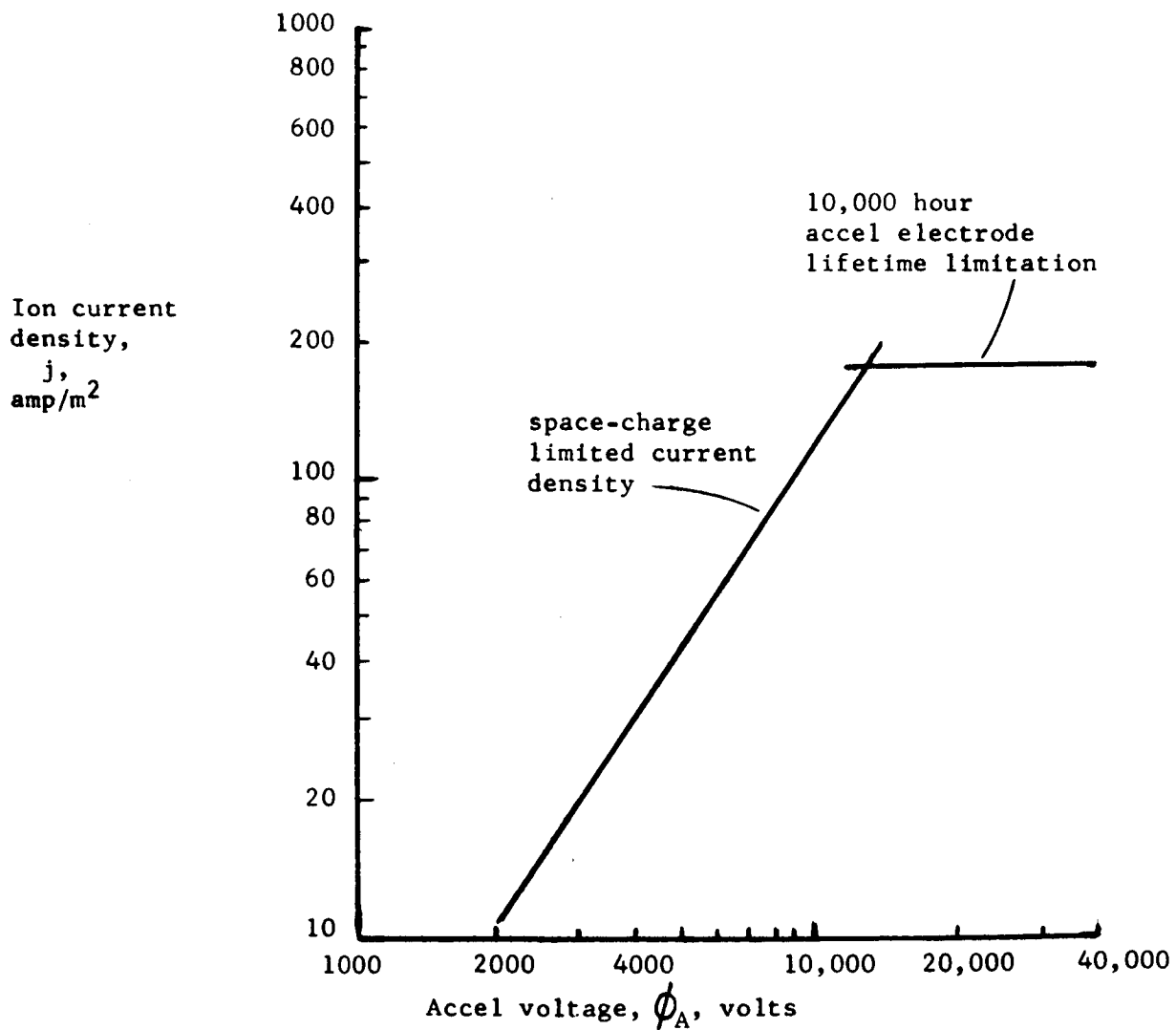
Figure 7. - Current density limitations for cesium contact-ionization thruster (reference 6), assuming 80% dense copper accel electrodes.
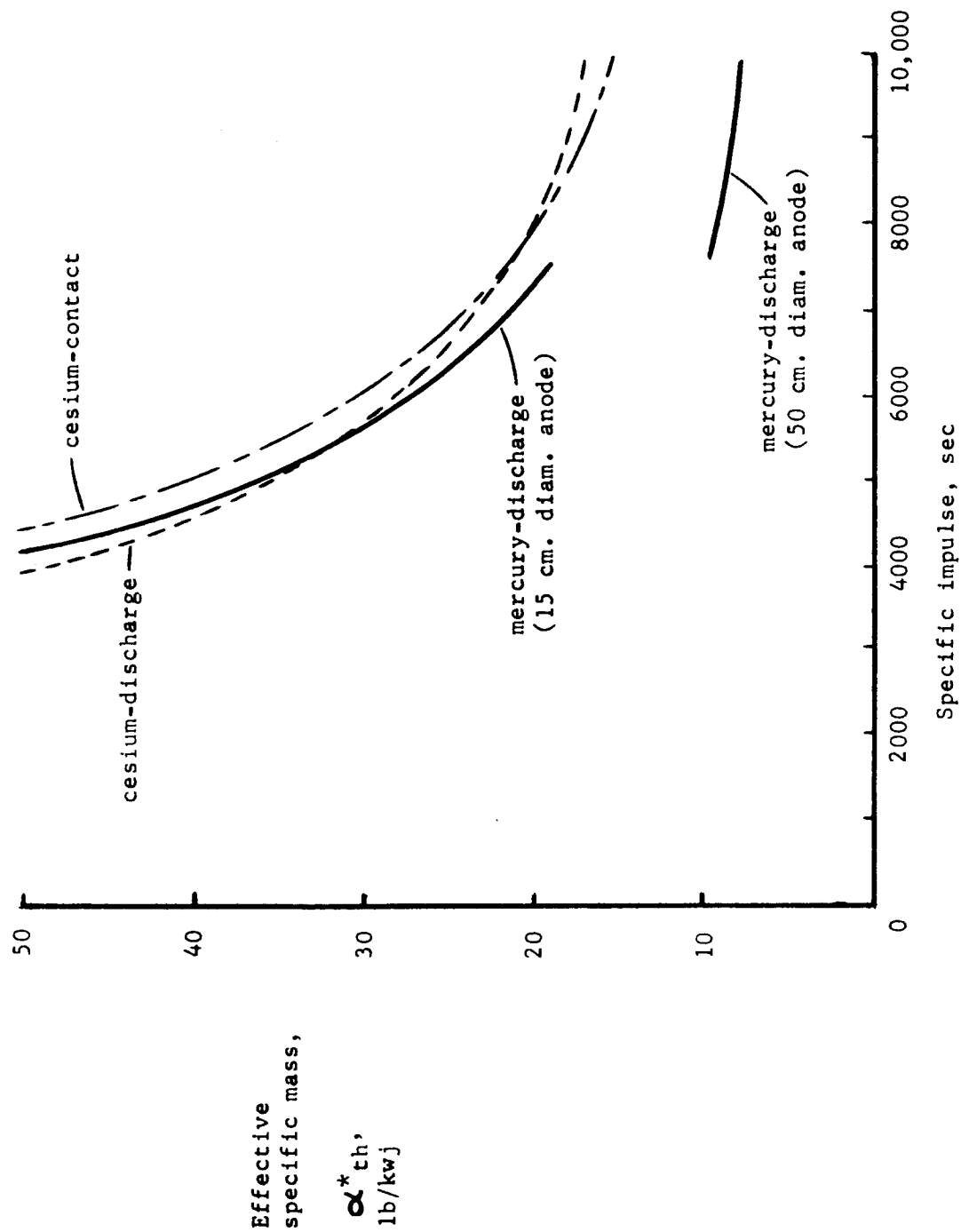
Figure 8. - Comparison of existing electric thrusters for primary propulsion. Powerplant α_{pp} = 20 lb/kwe; power conditioning and controls α = 10 lb/kwe, η_c = 92%; mercury tankage, 0.065; cesium tankage, 0.24.
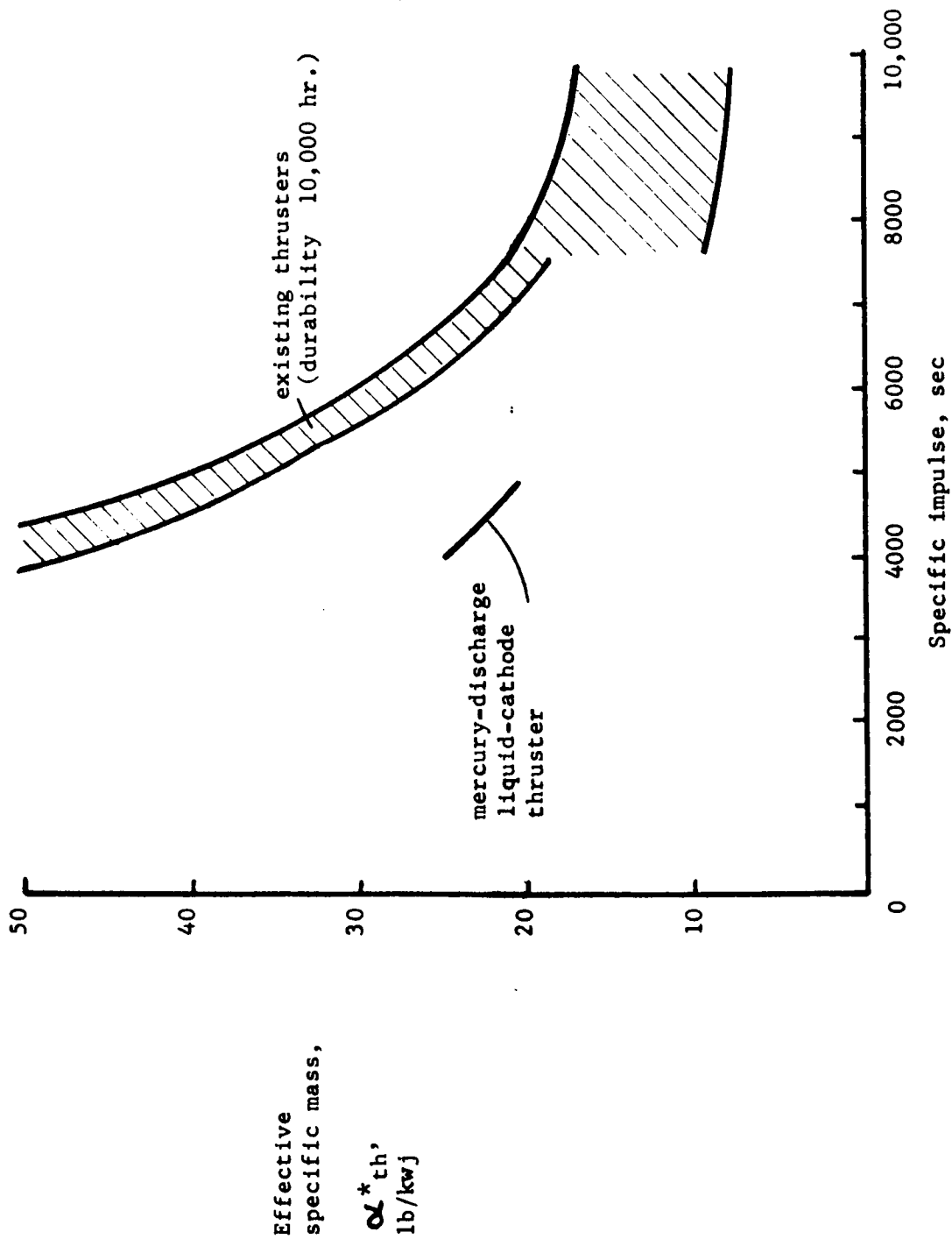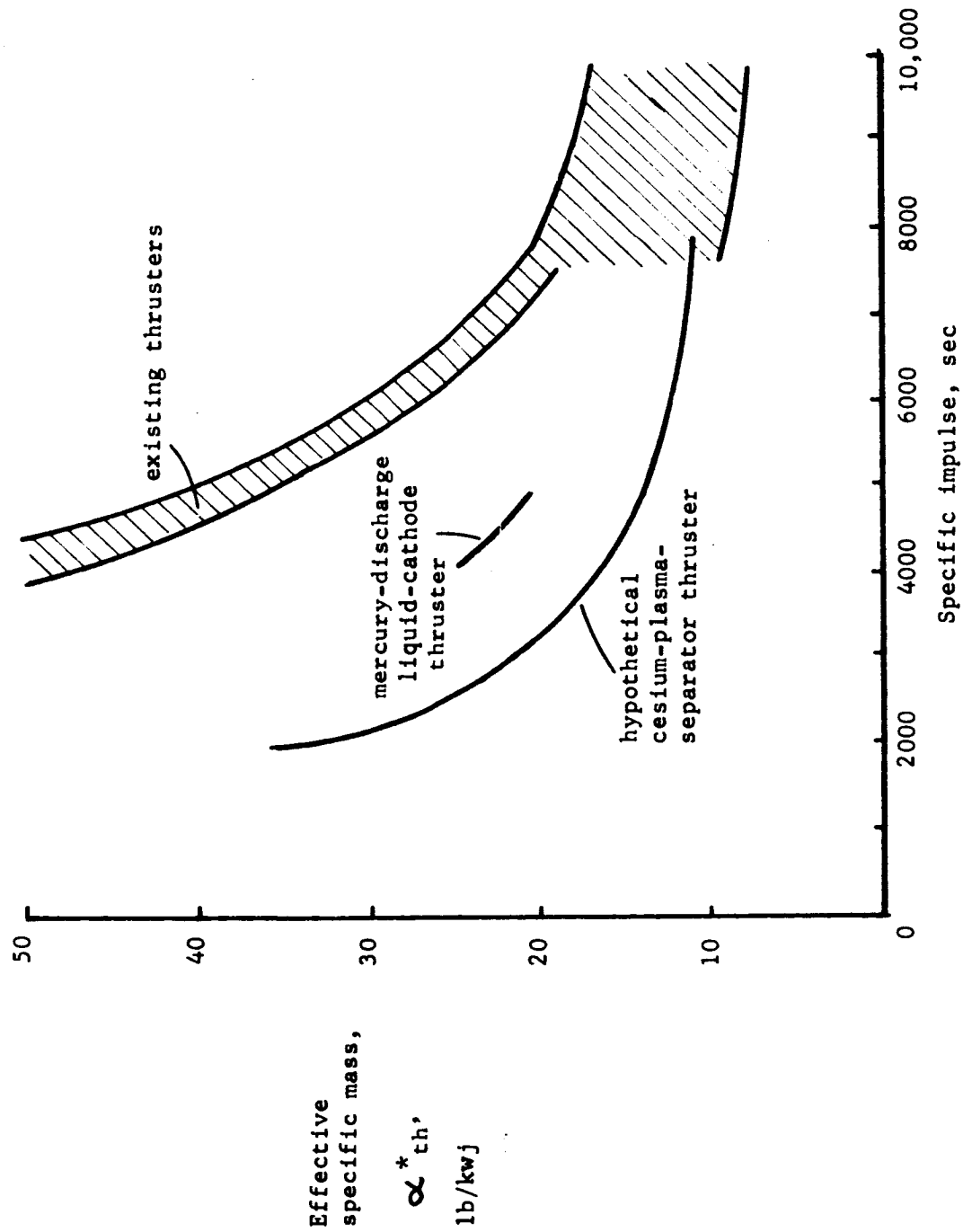
Figure 9. - Performance of mercury-discharge thruster with liquid-pool cathode. Powerplant α_{pp} = 20 lb/kwe; power conditioning and controls α_c = 10 lb/kwe, η_c = 92%; mercury tankage, 0.065; cesium tankage, 0.24.
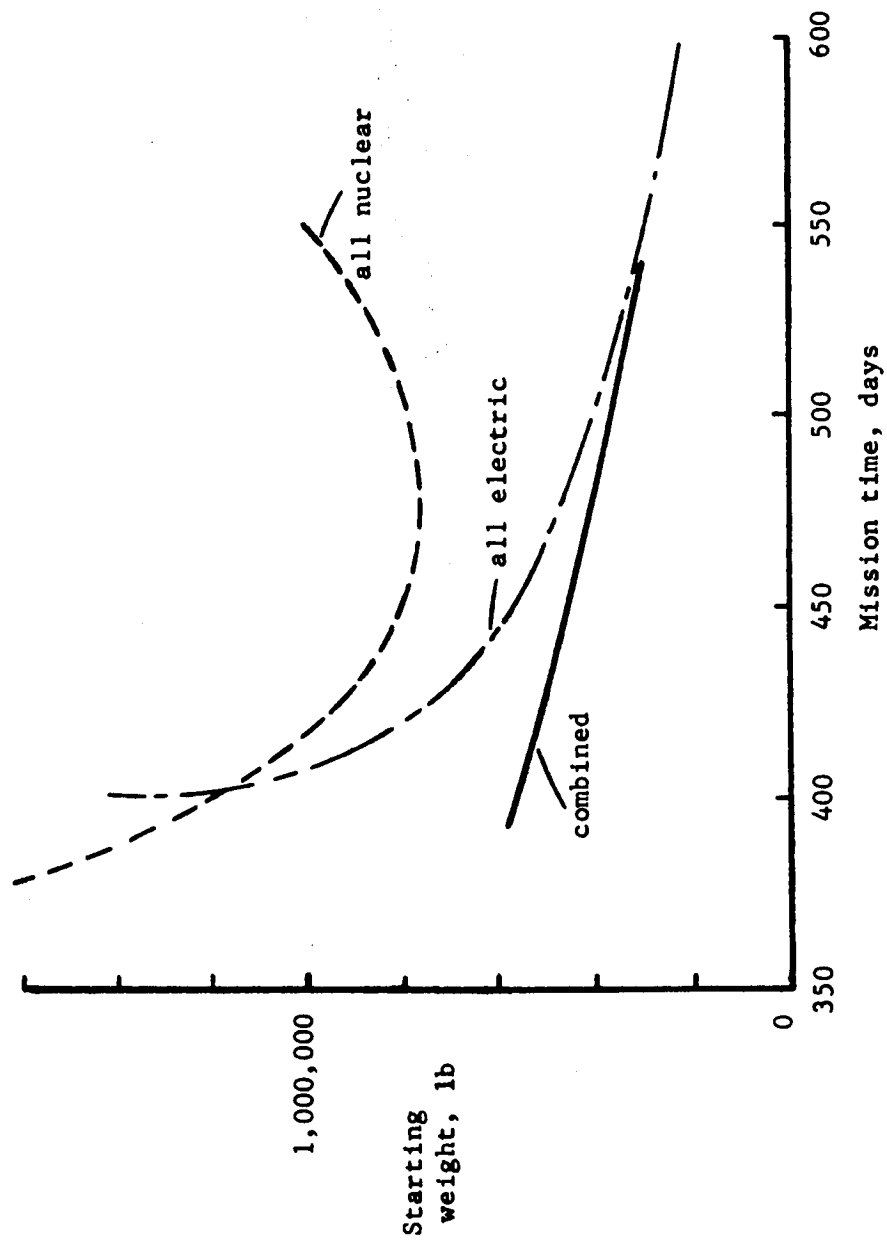
2.45

Figure 10. - Hypothetical performance of cesium-plasma-separator thruster. Powerplant α_{pp} = 20 lb/kwe; power conditioning and controls α_c = 10 lb/kwe, η_c = 92%; mercury tankage, 0.065; cesium tankage, 0.24.

Figure 11.- Spacecraft initial weight for 7-person Mars round trip[34]. Starting orbit, 1.1 Earth radius. Wait time at Mars, 40 days. Propulsion-system specific weight, 14 lb/kwj. Earth re-entry, 52,000 ft/sec.

RADIOISOTOPE HEATING OF CONTACT IONIZERS

by W.R. Mickelsen

The use of radioisotopes for heating ionizers in contact-ionization thrusters has been suggested at least as early as March, 1963.* More recently, the subject has been raised again, with the intent of improving the performance of the contact-ionization thruster with respect to the mercury-discharge and cesium-discharge thrusters. Feasibility and possible gains in performance can be assessed on simple and fundamental grounds as described in the following analysis.

Required power levels are of first importance because radioisotope production is limited. Annual production rates of most radioisotopes is related directly to nuclear-electric power generation, since most radioisotopes are fission products. Electric-spacecraft effective jet power $P_{j,eff}$ is directly related to three basic parameters, the spacecraft starting mass M_o, the electric-propulsion-system effective specific mass α_{ps}^*, and the electric-propulsion-system mass-fraction M_{ps}/M_o:

$$P_{j,eff} = M_o \ (1/\alpha_{ps}^*) \ (M_{ps}/M_o) \qquad (1)$$

Effective specific mass α_{ps}^* has been defined by Mickelsen[1].

Melbourne[2] has shown that the propulsion-system mass-fraction M_{ps}/M_o is approximately constant for nearly all missions of interest. This constancy can be shown by use of a parameter β which is defined as:
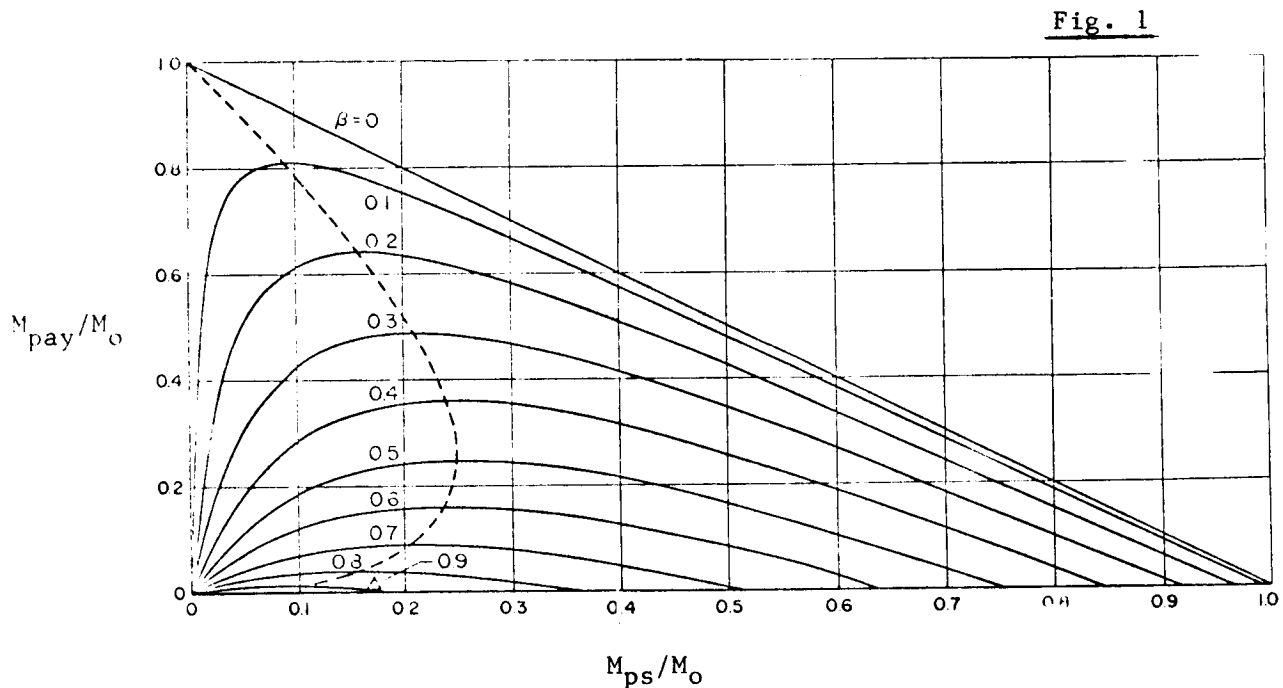
$$\beta^2 \equiv (\alpha_{ps}^*/2) \int_o^\tau (F/M)^2 \ dt \qquad (2)$$

The definite integral of the square of the instantaneous thrust/mass ratio is a measure of trajectory difficulty, and its value also depends on the thrust program. Melbourne showed that payload fraction M_{pay}/M_o is related to β and M_{ps}/M_o as follows:

$$M_{pay}/M_o = (M_{ps}/M_o)\left[\frac{1}{\beta^2 + (M_{ps}/M_o)} - 1\right]$$ (3)

This equation is represented by the following figure:

Fig. 1

From inspection of this figure. it is evident that the propulsion-system mass-fraction M_{ps}/M_o will have optimum values of 0.2 to 0.25 for all missions where the payload fraction M_{pay}/M_o has values between 0.1 and 0.5. The relationships shown in the figure above are fundamental to all electric-propulsion missions, irregardless of the type of thrust program, whether hyperbolic boost is used or not, etc. Because of the fundamental nature of these relationships,

it can be said that the propulsion-system mass-fraction is universaliy about 0.2.

Electric-spacecraft starting mass M_o will depend on the type of booster, and on whether hyperbolic boost is used. For example, Saturn V and Saturn V/ Centaur payloads are shown in the following figures as function of hyperbolic velocity with respect to Earth (ie, boost beyond escape):
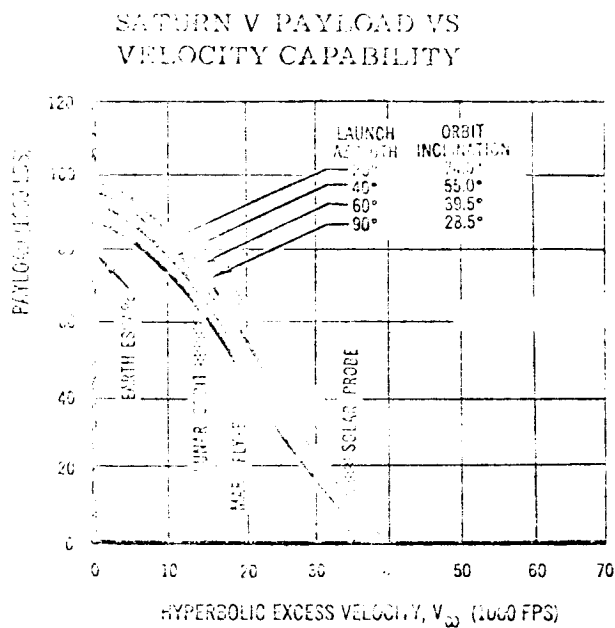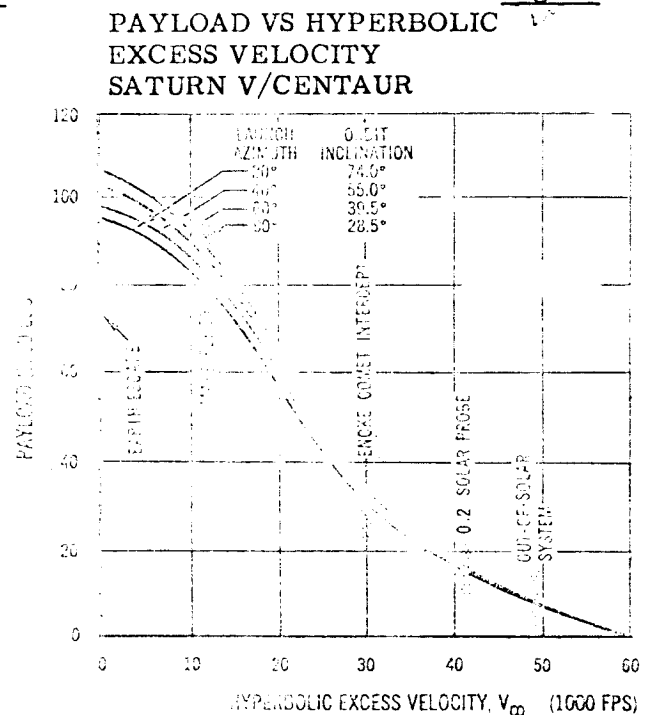
Fig. 2

SATURN V PAYLOAD VS VELOCITY CAPABILITY

Fig. 3

PAYLOAD VS HYPERBOLIC EXCESS VELOCITY SATURN V/CENTAUR

From inspection of these figures it appears that electric spacecraft starting mass could be from 20,000 lb. to 100,000 lb.

In addition to this wide range of possible starting mass M_o, mission analysis has shown that α_{ps}^* can be in the range from 20 lb/kwj to 120 lb/kwj and still be of interest. From these considerations it appears that electric spacecraft launched with Saturn V-class boosters might have anywhere from 160 to 5.000 kwj. (the notation kwj denotes kilowatts of effective jet power).

Contact-ionization thrusters are operated at the highest current density j commensurate with the required durability of accel electrodes which are eroded by charge-exchange-ions. The best performance of "flight-type" contact-ionization thrusters reported to date[3] is a current density of j 170 amp/m^2. To obtain this current density in the Hughes multi-strip thruster, and accel voltage of ϕ_A = 13,000 volts is needed. Operation in the specific-impulse range-of-interest requires a very wide range of the ratio ϕ_A/ϕ_{net}, where ϕ_{net} is the net acceleration voltage. This is illustrated by the following figure:

Fig. 4

Hughes multi-strip thruster with
j = 170 amp/m^2
ϕ_A = 13,000 volts

Specific impulse, I, sec.
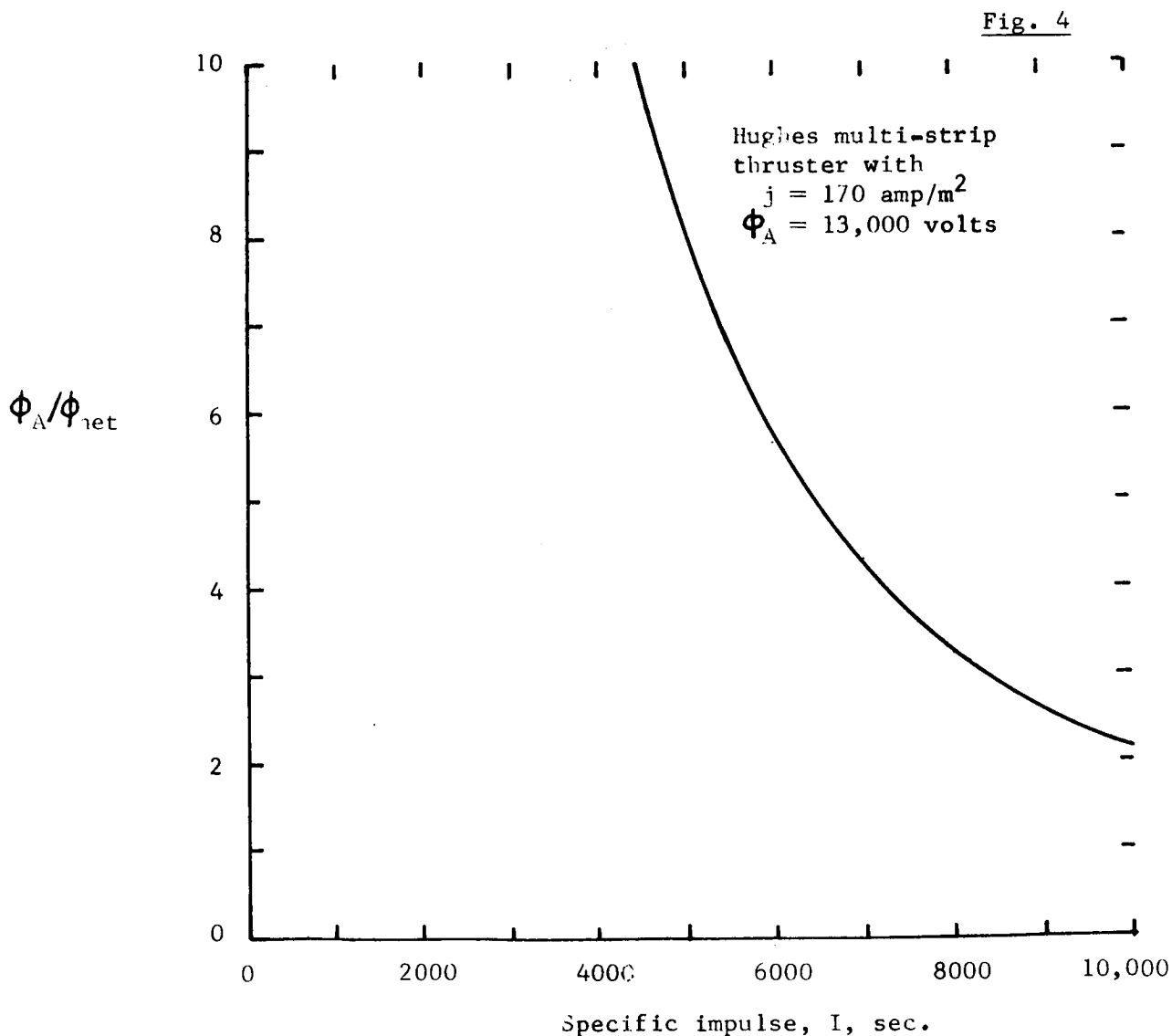
Operation at such high values of ϕ_A/ϕ_{net} is questionable, but it is assumed here that such high values will be found to be feasible. In this way, current density j may be held constant throughout the specific-impulse range-of-interest in order to obtain the highest power-density possible.

Power density $P_{j,eff}/A$ is given by:

$$P_{j,eff}/A = j\,\phi_{net} \tag{4}$$

so that if j is constant, then $P_{j,eff}/A$ is directly proportional to ϕ_{net}. When j is held constant, then ionizer temperature is also constant. Therefore, the heat loss from the ionizer must also be constant. At $j = 170$ amp/m^2, the heat loss per unit ionizer area in the Hughes multi-strip thruster[4] is $\dot{Q}/A = 150$ kw/m^2. With this information, the ratio of heat loss $\dot{Q}$ to jet power $P_{j,eff}$ can be written:

$$\dot{Q}/P_{j,eff} = (\dot{Q}/A) / (P_{j,eff}/A) = 150,000/(170\,\phi_{net})$$
$$= 870/\phi_{net} \tag{5}$$

Net accelerating voltage ϕ_{net} is related to specific impulse, so $\dot{Q}$ can be calculated for various jet-power levels over a range of specific impulse, as shown in the following figure: (the notation kwt denotes kilowatts of thermal power).

Fig. 5
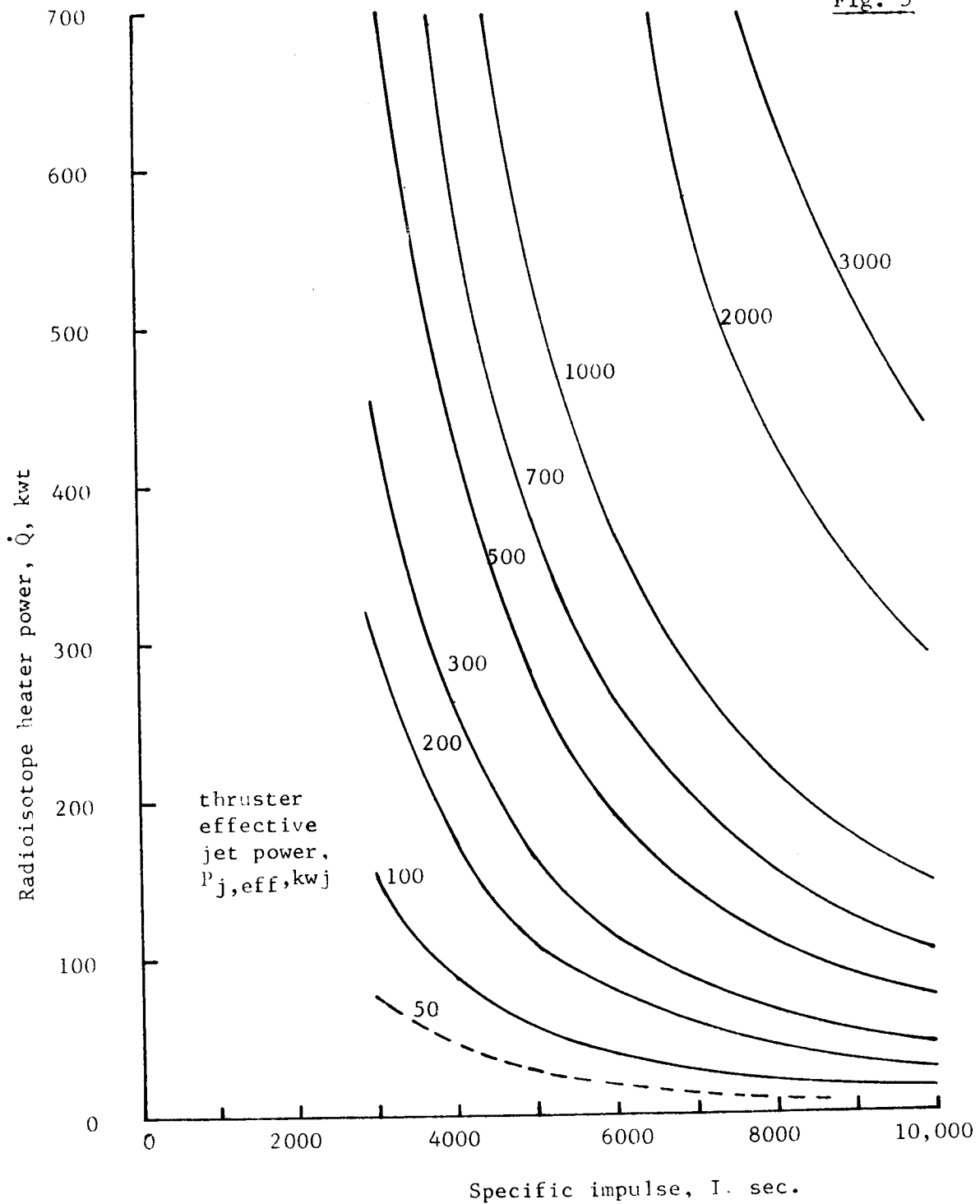
This figure represents the radioisotope-heater power level required for various jet-power levels. Use of radioisotope-heating at low specific impulse will depend on the amount of radioisotope that is available for use in electric propulsion systems.

Radioisotope properties and availability are reported in a number of papers, and some of these [5,6,7] are referenced here. The following table summarizes information about those radioisotopes that have appreciable production rates and that are relatively free from radiation:

TABLE 1

radioisotope	emission	ref.	availability, kwt			sp. vol. cc/kwt	sp. wt. lb/kwt	half-life years
			1967	1970	1980			
Pm - 147 (Pm$_2$O$_3$)	β^- to 0.223Mev	5		9.4	94	1000	12.3	2.6
		6	11			550	8.2	2.7
		7	17	25	111	670	8.2	2.6
Cm-242 (Cm$_2$O$_3$)	α^{++} at 6.1Mev	5		1.8	50	0.86	0.0184	0.44
		6				0.87	0.0225	0.45
Cm-244 (Cm$_2$O$_3$)	α^{++}	5						
		6				37	0.96	18
Po-210 (metal)	α^{++} at 5.3Mev	5				0.76	0.0157	0.38
		6				0.83	0.0164	0.38
		7	140*	140*		0.83	0.017	0.38
Pu-238 (PuO$_2$)	α^{++} at 5.5Mev	5		29	53	108	4.6	90
		6				256	5.7	89
		7	13	26	73	200	5.1	89.6

* produced by neutron irradiation of bismuth, and production is estimated on basis of using bismuth coolant in private and public reactors.

If the values in this table are correct, then it appears that the quantity of radioisotope available for electric propulsion will be severely limited. For example, the 1980 production of Pu - 238 will be about 60 kwt, and if 1/3 of this production could be given to electric propulsion then only 20 kwt would be available for radioisotope heating of the ionizer in contact-ionization thrusters. Since Po - 210 is produced by neutron irradiation of bismuth, the annual production rate is uncertain because bismuth would have to be used in great quantities as a reactor coolant in order to achieve the production figures listed in the table. About one inch of lead shielding [6] would be required to reduce Pm - 147 radiation to 10 milli-roengten at one meter from a one kilowatt source. This amount of shielding should pose no great problem in launch operations. Shielding is not required for Pu - 238.

3.8

From these considerations it appears that Pm - 147 and Pu - 238 are possible candidates for radioisotope heating of contact ionizers, and the Po - 210 might be a candidate if firm values for annual production rate were known.

Decay rate is an important consideration when half-life is of the order of mission time. Thermal power as a function of time is shown in the next figure.


Fig. 6

Time, days
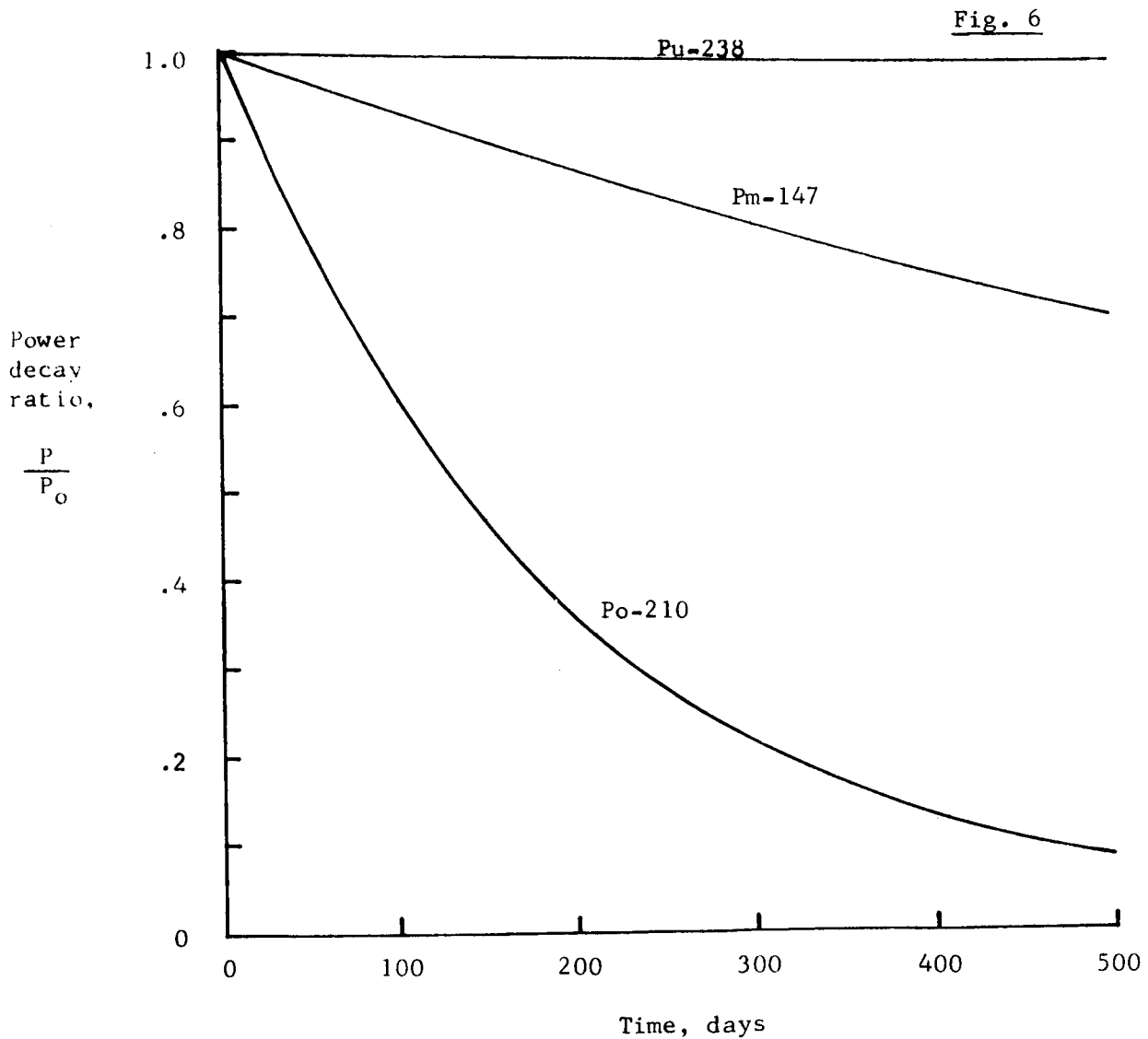
If the ionizer heating power is primarily due to radiation heat transfer, then the significant parameter is $(P/P_o)^{\frac{1}{4}}$. In real ion thrusters, there is considerable ionizer heat loss due to conduction, so the value of $(P/P_o)^{\frac{1}{4}}$ is an optimistic measure of performance. However this parameter is plotted in the following figure to represent the most optimistic performance obtainable from the three radioisotopes in contact ionizer heater applications. Actual decreases in ionizer temperature will be greater than suggested by the parameter $(P/P_o)^{\frac{1}{4}}$.

Fig. 7
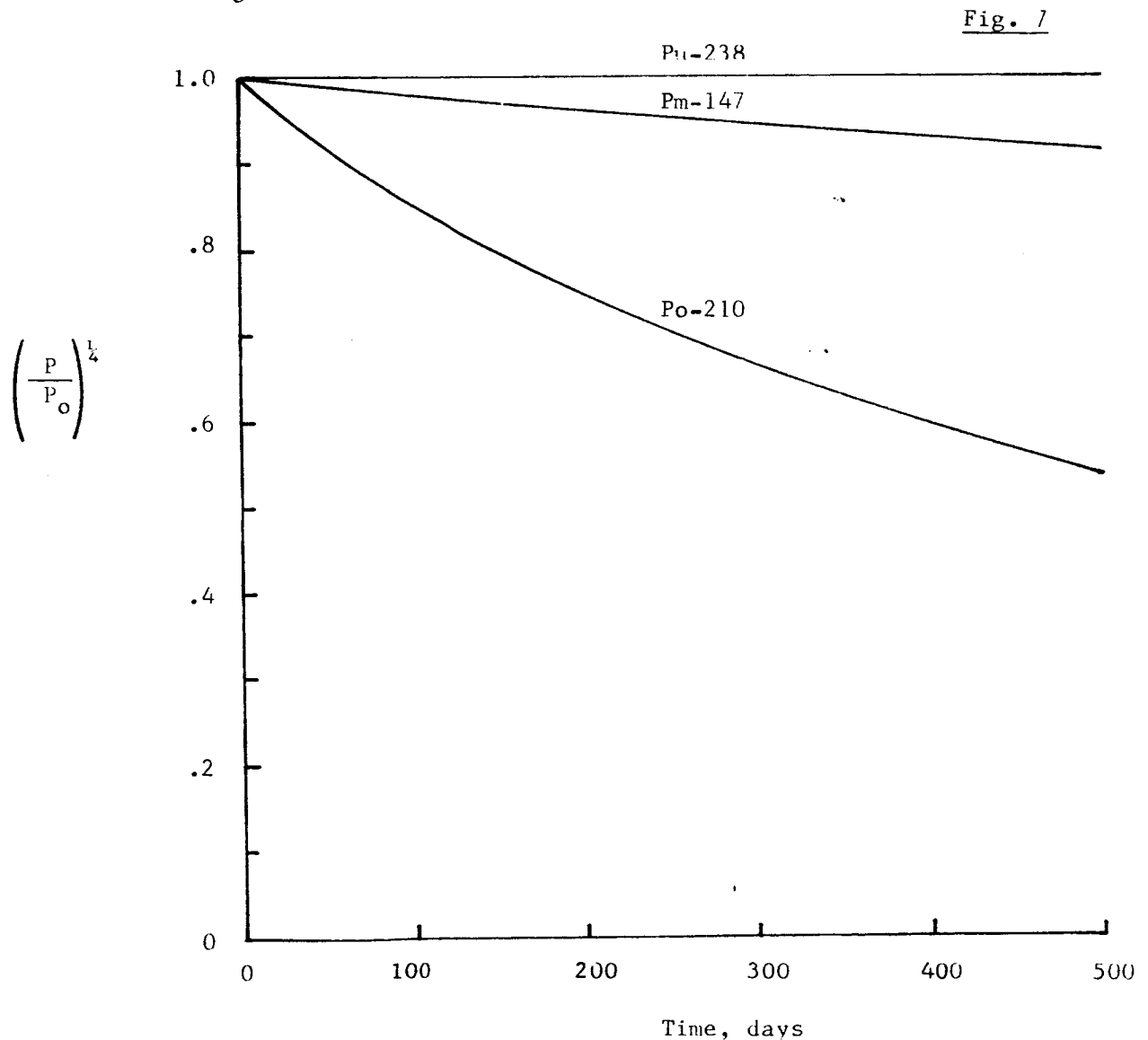
Allowable variation in ionizer temperature will depend on a number of factors and considerations. The most obvious of these is that the ionizer temperature must not be allowed to fall below the critical value for contact ionization. Ionizer temperature may be higher than the critical value, but the neutral atom fraction will be higher also, as illustrated in the following figure which is for a typical porous tungsten ionizer.[8]

Fig. 8

Ionizer temperature, °K
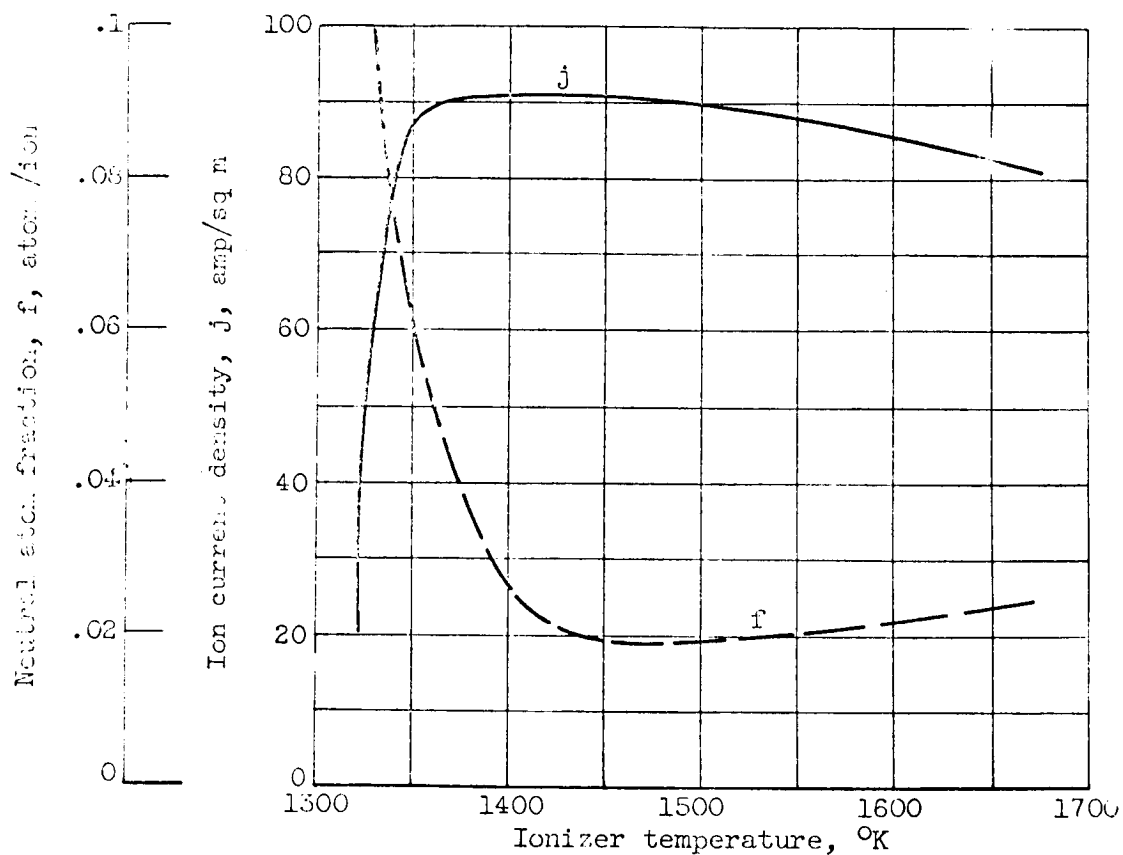
From inspection of this figure it appears that a temperature change of 200°K would be acceptable. This amounts to a temperature change of about 15%. With reference to the preceding figure, it appears that Pu - 238 would certainly provide less than 15% temperature change over reasonable mission times, and that Pm - 147 might be acceptable on this basis if most of the ionizer

heat loss were thermal radiation. However, a Po - 210 system would require some means of maintaining a fairly constant temperature for most missions. For example, a mechanical shutter arrangement is used in radioisotope-thermo-electric powerplants to obtain power-flattening. If Po - 210 were used for ionizer heating, then the weights of the shutters, mechanism, and controls would have to be charged against the thruster, thereby increasing the thruster effective specific weight. For these reasons, Po - 210 is not considered as a possible radioisotope for ionizer heating in the present analysis.

Effective specific weight[1] of contact-ionization thrusters with radio-isotope heating of the ionizer can be estimated from the information presented so far. An expression for thruster effective specific weight α_{th}^{*} can be written as[3]:

$$\alpha_{th}^{*} = \alpha_{th} + \alpha_r \ (\dot{Q}/P_{j,eff}) + (\alpha_c + \alpha_{pp}/\eta_c) \ (1-\eta_{th})/\eta_{th}$$
$$+ M_{tank} /P_{j,eff}$$

(6)

where the following definitions are used:

α_{th} physical specific weight of thruster, lb/kwj

α_r specific weight of radioisotope, lb/kwt

α_c physical specific weight of power conversion, power conditioning, and controls, lb/kwe

α_{pp} specific weight of powerplant

η_c efficiency of power conversion, conditioning, and controls subsystem

η_{th} thruster efficiency

M_{tank} weight of propellant tanks

The Hughes multi-strip thruster can be used for purposes of comparison with other existing thrusters. This thruster has a weight for a given ionizer area[4], and assuming that the electric heaters would weigh no more than the

radioisotope container, and that the heat shielding would be the same as for the all-electric design, then the physical specific weight is:

$$\alpha_{th} = (24.3 \times 1000)/(0.0115 \times 170 \times \phi_{net}) = 12,400/\phi_{net} \qquad (7)$$

Specific weights of radioisotopes are listed in Table 1. Pu - 238 has a lower specific weight than Pm - 147, so Pu - 238 is used for the present analysis in order to be the most favorable towards the radioisotope-ionizer-heating concept. The ratio $\dot{Q}/P_{j,eff}$ is given by equation (5). Some other system parameters must be assumed: $\alpha_c = 10$ lb/kwe, $\eta_c = .92$, and $\alpha_{pp} = 20$ lb/kwe (these are the same as used in a previous comparison[3] of existing thrusters).

With radioisotope heating of the ionizer, the only remaining thruster losses are the vaporizer heating, the neutralizer power, and the accelerator drain currents. These losses will vary with thruster module size. For example, the NASA-Lewis mercury-discharge thruster has such losses amounting to about 5% for a 15-cm anode size and about 1% for a 50-cm anode size at design operating conditions of 5000 and 9000 seconds specific impulse respectively. These losses are equivalent to about 190 ev/ion for the 15-cm thruster and 100 ev/ion for the 50-cm thruster. Since the 50-cm mercury-discharge thruster represents the best performance to date, the neutralizer and vaporizer powers of 100 ev/ion will be assumed here. This assumption results in an expression for thruster efficiency as follows:
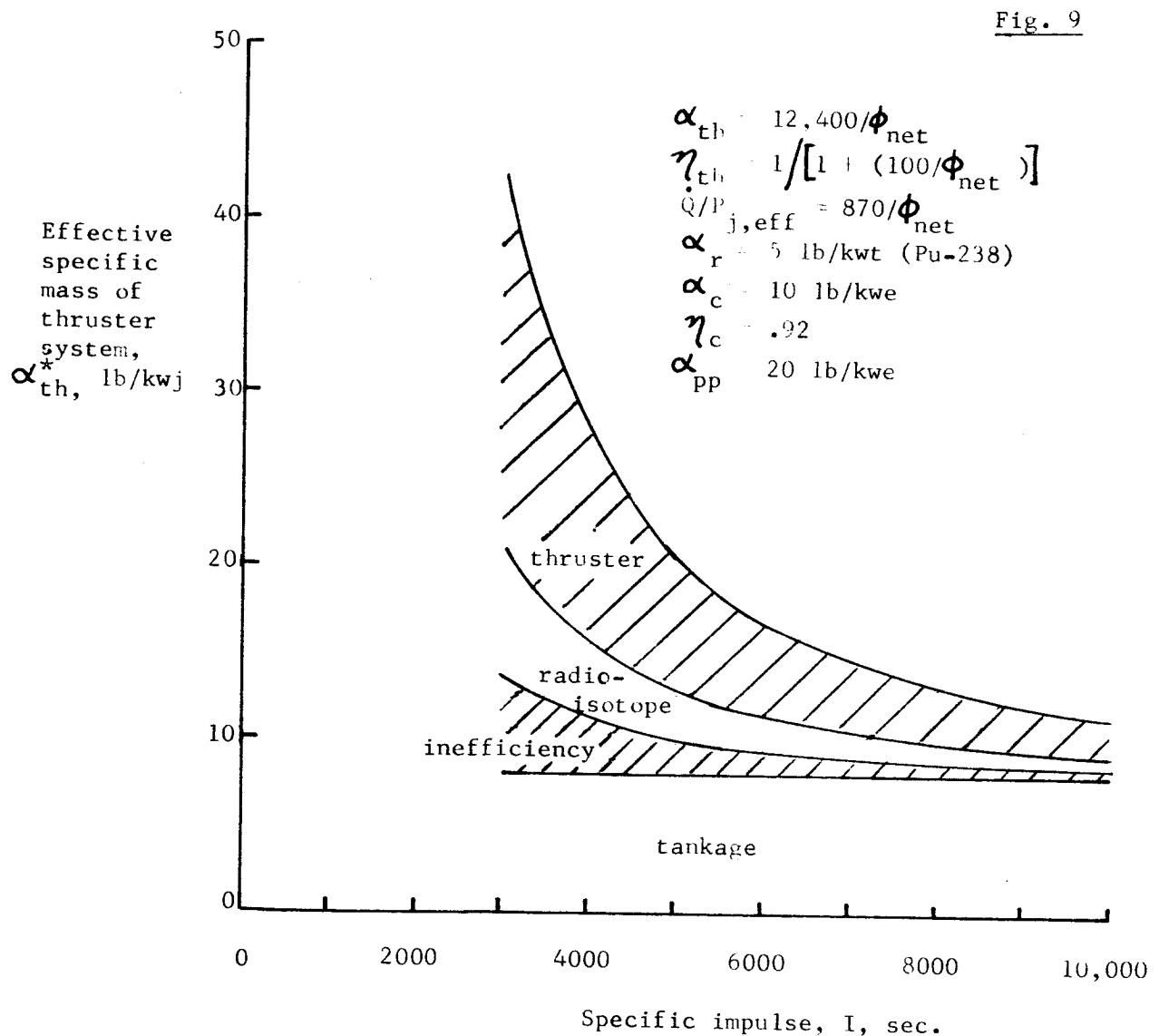
$$\eta_{th} = \frac{1}{1 + (100/\phi_{net})} \qquad (8)$$

Propellant utilization efficiency has been assumed to be 100%, but would be somewhat less if a plasma-bridge neutralizer were used.

Tankage has been discussed in a previous analysis[3], where a 24% tankage for cesium was calculated by comparison with a flight-qualified mercury tank

design[9]. Future advances in tank design such as frozen cesium may decrease

this tankage fraction, but until such advances are shown to be feasible, the

24% tankage represents the best state-of-the-art. In the previous analysis[3],

a tankage penalty of $M_{tank}/P_{j,eff} = 8$ lb kwj was found for cesium-propellant
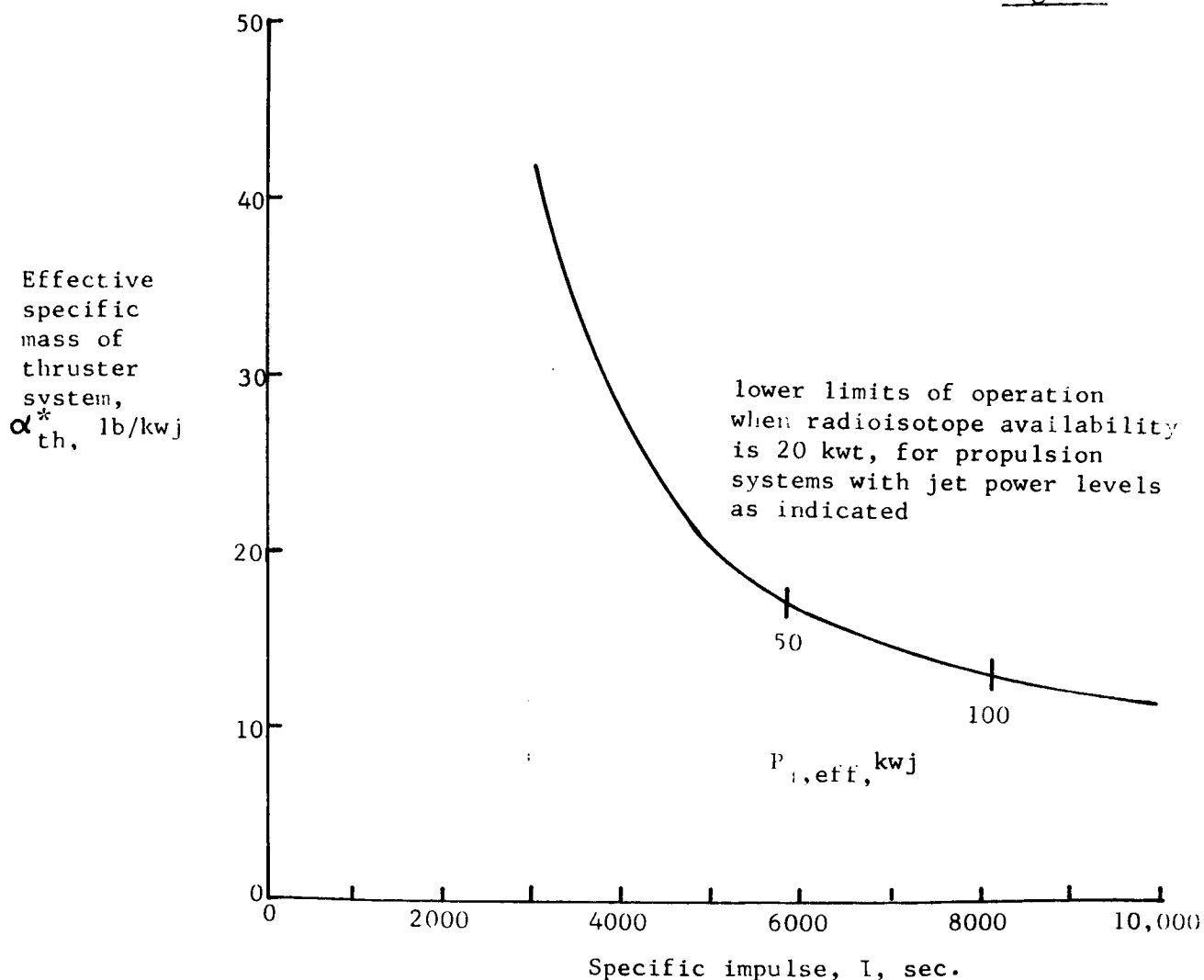
thrusters, and this same value is used here.

Effective specific weight of a contact-ionization thruster with radio-

isotope-ionizer heating can be estimated from the discussion so far. An

estimate such as this is shown in the following figure.

Fig. 9

$\alpha_{th} \quad 12,400/\phi_{net}$

$\eta_{th} \quad 1/[1 + (100/\phi_{net})]$

$\dot{Q}/P_{j,eff} = 870/\phi_{net}$

$\alpha_r \quad 5$ lb/kwt (Pu-238)

$\alpha_c \quad 10$ lb/kwe

$\eta_c \quad .92$

$\alpha_{pp} \quad 20$ lb/kwe

Effective specific mass of thruster system, α^*_{th}, lb/kwj

thruster

radio-isotope

inefficiency

tankage

Specific impulse, I, sec.

If lighter weight tankage can be devised, then the total values of α_{th}^* could be reduced accordingly. It must be noted here that the additional penalty associated with non-ideal thrust program is not included in these calculations. This penalty can amount to 5 or 10 lb/kwj for many missions[1].
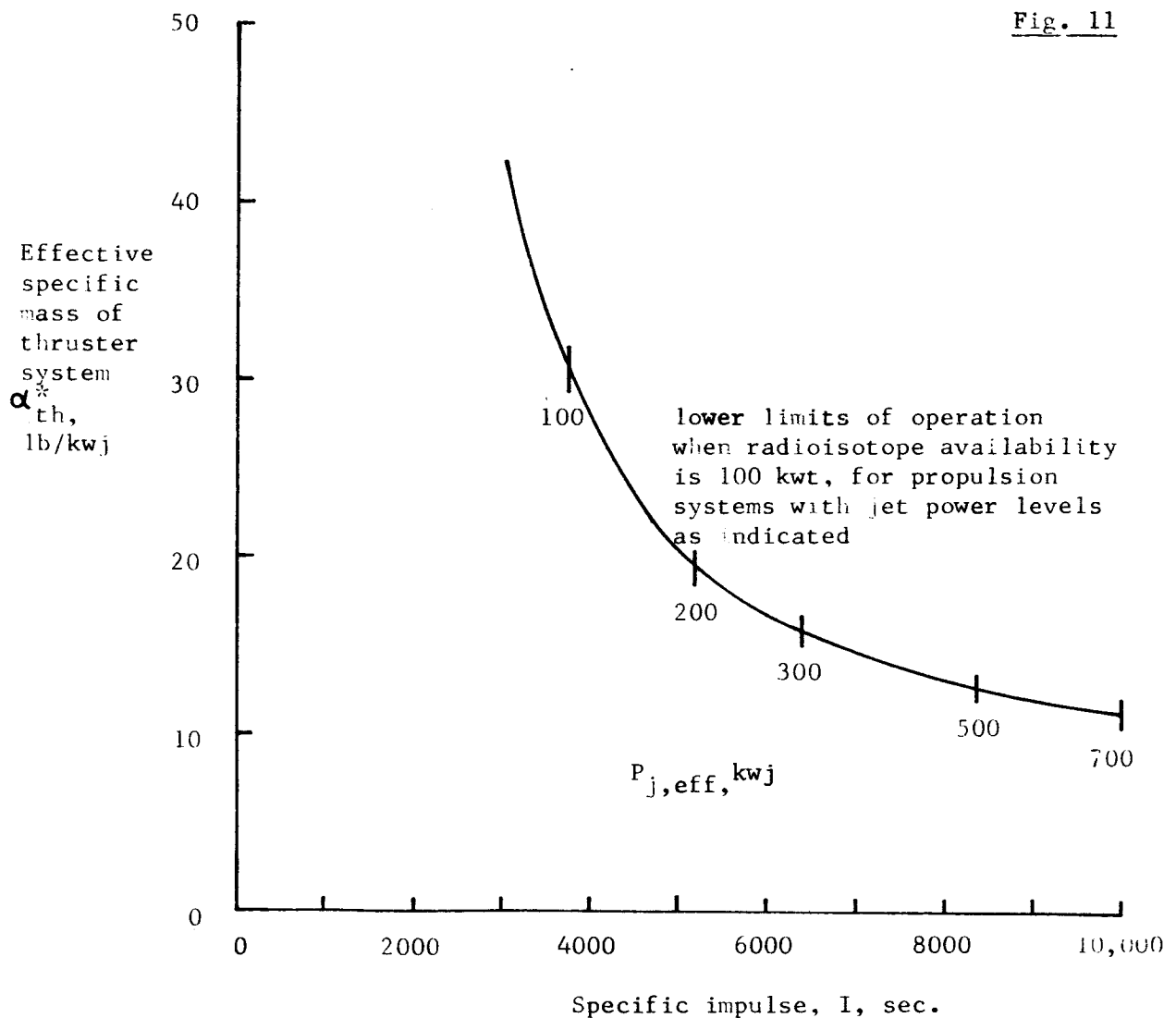
The preceding figure was composed without regard to radioisotope availability. As discussed previously, 1/3 of the 1980 annual production of Pu-238 might be assigned to electric propulsion, which would amount to 20 kwt. This limitation in availability would result in the restrictions in the operating range of the radioisotope-heated contact-ioniztion thruster as indicated in the following figure. This figure was constructed from the information shown in Figures 5 and 9.

Fig. 10

Effective specific mass of thruster system, $\alpha_{th,}^*$ lb/kwj

lower limits of operation when radioisotope availability is 20 kwt, for propulsion systems with jet power levels as indicated

50

100

$P_{j,eff,}$ kwj

Specific impulse, I, sec.

From inspection of this figure it is clear that radioisotope heating of contact thruster ionizers would be limited to electric propulsion systems having power levels in the lowest portion of the range of interest for Saturn-V-class boosted electric spacecraft.

If radioisotope availability were increased by a factor of five to 100 kwt, then the restrictions in operating range would be as shown in the next figure.

Fig. 11

Effective specific mass of thruster system α_{th}^*, lb/kwj

lower limits of operation when radioisotope availability is 100 kwt, for propulsion systems with jet power levels as indicated

$P_{j,eff}$, kwj

Specific impulse, I, sec.

Availability of radioisotopes may be different from these discussed

here. In this event, the lower limits of operation would change, and

could be incorporated quite simply onto figures such as the preceding.

The general format of calculations could be the same as used herein.

The final portion of assessment of the radioisotope-heated contact-

ionization thruster is that of comparison with existing and hypothetical

future thrusters. This comparison can be done with the aid of a previous[3]

analysis, and is shown in the following figure.

Fig. 12

Specific impulse, I, seconds
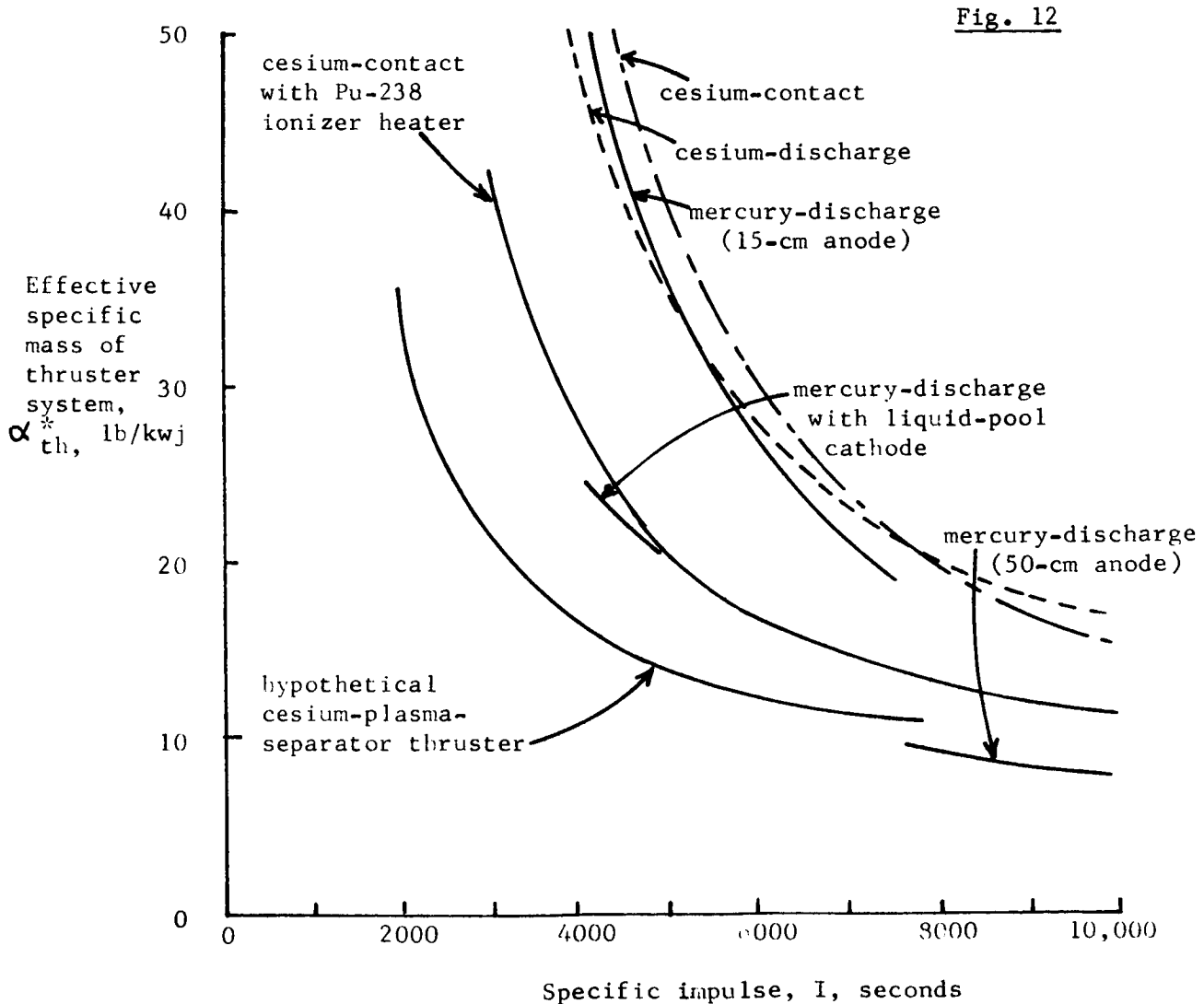
On the basis of this comparison, the cesium-contact thruster with a Pu-238 ionizer heater appears to offer performance gains over existing thrusters. It should be noted here that a neutralizer and vaporizer power loss of 100 ev/ion has been charged against the radioisotope-heated contact thruster. If this loss could be reduced, then the performance would be somewhat better. A rough estimate of possible savings in inefficiency loss can be made by inspection of **Figure** 9.

The disquieting feature of the radioisotope-heated contact thruster is the limitation of operating range due to radioisotope availability. If boosters smaller than the Saturn-V class could be used for electric spacecraft missions, these limitations would be eased somewhat. For example, solar-electric spacecraft boosted with the Saturn 1B/Centaur might be a possible application. However, such applications would be short-range, and the question of whether the costs of development of a radioisotope-heated contact thruster system would be worthwhile is cogent to the future of the overall electric propulsion program. If this application is considered seriously, then a more exact and comprehensive systems study could be done along the lines of the analysis described here.

This analysis has been confined to consideration of primary electric propulsion. Application of radioisotope heaters to contact-ionization thrusters for satellite attitude and position control is certainly feasible with regard to radioisotope availability. The potential advantage of elimination of electric heaters is attractive, and would do much to reduce the complexity of currently proposed electrostatic thrusters for satellite propulsion.

References

1. Mickelsen, W.R.: Performance Parameters for Electric Propulsion Systems. Journal of Spacecraft and Rockets. February, 1966.

2. Melbourne, W.G.: Interplanetary Trajectories and Payload Capabilities of Advanced Electric Propulsion Vehicles. Jet Propulsion Laboratory Technical Report No. 32 - 68. March, 1961.

3. Mickelsen, W.R.: Future Trends in Electric Propulsion. AIAA Paper No. 66-595. June, 1966.

4. Zimmerman, R.L., Garvin, H.L., McKee, W.E., and Kami, S.: Development of Multistrip Cesium Contact Thrusters. AIAA Paper No. 66-235. March, 1966.

5. Division of Isotopes Development: Present and Potential Annual Availability of Isotopic Power Fuels. U.S. Atomic Energy Commission. April, 1962.

6. Rohrmann, C.A., and Sayre, E.D.: Radioisotopic Space Power-Prospects and Limitations. AIAA Paper No. 64-453. September, 1964.

7. Streb, A.J.: Radioisotope Power Systems for Manned Space Stations. AIAA Paper No. 64-711. September, 1964.

8. Mickelsen, W.R., and Kaufman, H.R.: Status of Electrostatic Thrusters for Space Propulsion. NASA TN D-2172. May, 1964.

9. Molitor, J.H., Berman, D., Seliger, R.L., and Olson, R.N.: Design of a Solar-Electric Propulsion System for Interplanetary Spacecraft. AIAA Paper No. 66-214. March, 1966.

THE EFFICIENCY OF ELECTRICAL DISCHARGES
FOR ELECTRIC PROPULSION

by K.W. Arnold

1. Introduction

Stuhlinger[1] has given a concise account of the history of electric

propulsion beginning with the pioneer work of Goddard in 1906 and cul-

minating with the establishment of the experimental and theoretical re-

search program in 1957 at the Lewis Flight Laboratory of NACA.

In a number of respects, the growth of electrical propulsion has been

dictated by the understanding of the mechanisms of electrical discharges

in gases. Quantitative understanding of discharges might be said to date

from the work of Townsend in the early 1900's[2], and in particular with the

discovery of interelectrode multiplication processes. Further development

of the field followed von Engel and Steenbeck's publication in 1932[3] and

Seeliger's in 1934[4] in Europe, and the work of Loeb[5] in California. However

the resurgence in interest which began during World War II has been main-

tained to the present because of the promises of plasma physics and its

engineering aspects (e.g. magnetohydrodynamics).

The dependence of electric propulsion programs on the continued study of

the fundamentals of electric discharges is axiomatic because of the very

nature of the propulsion mechanism. The need to optimise the formation and

acceleration of charged particles in electric propulsion devices is impor-

tant because, as Mickelsen[6] has pointed out, the practicality of such de-

vices depends strongly on their mass. For these reasons, this review of

electrical discharges for electric propulsion is concerned both with the

fundamental processes of gaseous electronics and with their efficiency (in

the broadest sense). The first aim of this review is to establish the

important mechanisms for each electric propulsion concept and to evaluate the concepts in such a way that quick and meaningful comparison may be made between each of them.

Equally important are the ideas which may develop from a fresh look at current work. This is closely tied in with the ability to compare concepts and to estimate their potential. Thus the second aim of the review is to provoke thought about the existing ideas and hopefully to improve on them.

Because the fundamentals of gaseous electronics are so basic in electric-propulsion, the review will begin with a short resumé of those processes which are important in the study. The aim in this section of the report will be to establish both the important physical mechanisms and also the magnitudes of the effects. (Deviations from the general behavior will be discussed as necessary during later sections). The particular concepts will then be treated separately, some in this report and others in the final report. The latter will also contain a discussion of the concepts en masse and an evaluation of their efficiency. Finally, both this and the final report will discuss the findings of the period covered.

2. Fundamental Processes

2.1 Introduction

An important parameter in electric propulsion is the thrust f per unit terrestrial weight of fuel expended in unit time, W, called the specific impulse I_{sp} in seconds. For a gas of molecular weight M escaping through a nozzle with velocity v, $I_{sp} = \frac{f}{W} = \frac{RT}{M}$ vg_o where R is the gas constant and g_o is the acceleration due to gravity at the earth's surface. For air at room temperature flowing with molecular velocity ($\sim 2 \times 10^2$ m/sec), I_{sp} is about 100 sec. However, with accelerated ions, v might become 10^4 m/sec or more[7], and specific impulses $(=\frac{v}{g_o})$ on the order of 10^3 to 10^4 sec. can be obtained. In addition, colloidal thrustors with I_{sp} = 1000 to 3000 sec. have considerable interest for lunar supply missions[8], so that the charging (ionization) of both atomic and macro particles must be considered in this section. Ionization mechanisms will be covered only briefly, for the purpose of describing the physical processes involved, and determining the relative efficiency (cross-section) for each mechanism.

2.2 Ionization by electron impact

When a primary electron approaches an atom it may by virtue of its electric field interact with one of the bound electrons nearest to its path. If the force exerted by the 'primary' electron on the bound one is sufficiently large and acts for a sufficiently long time, a 'secondary' electron may be ejected from the atom. The approaching primary electron will displace atomic electrons with respect to the nucleus and the atom becomes an induced electric dipole. The degree of polarization is larger for heavier atoms, an effect related to the screening of the nucleus by the electron cloud (Madelung number), and it follows that the exchange of momentum, the ionization potential, and the probability of ionization will depend on the polarizability of the atom.

It is apparent from energy considerations that ionization by electron impact can occur only if the initial kinetic energy of the electron exceeds eV_i, where e is the electronic charge and V_i is the ionization potential of the atom. Thus the curve of ionization efficiency s_e (the number of ion pairs produced by one incident electron per cm of path at 1 torr and $0°C$) as a function of electron energy rises sharply from zero at $V = V_i$. However, for large electron energies ($E \sim 100ev$ or so) the ionization efficiency decreases because the electron interacts with the atomic electron cloud for a shorter and shorter period. Figure 1 shows the dependence of s_e on E for a number of gases, and in particular illustrates that s_e max. occurs for $E = 50$ to 150ev.

In some cases ionization of pre-excited atoms or molecules may occur (so called stepwise ionization): in this event ionization can occur for $V > V_i - V_{exc}$ and cross-sections may be large compared to the normal process.

2.3 Ionization by Positive Ions and Atoms

If positive ions and atoms of sufficient velocity collide with gas molecules, ionization as well as excitation can take place. For all ions or atoms moving in their own gas, the critical energy for ionization is $2V_i$ (because from the collision kinetics only a half of the incident kinetic energy can be transferred), and a representative curve for ionization efficiency s_i versus kinetic energy E is shown in figure 2. (the curves for ionization by impact with neutral atoms are quantitatively similar).

The absolute values of efficiency as well as its gradient with respect to particle energy is much smaller for this process than for electron impact. Ions as well as atoms of low energy are inefficient in ionizing the gas because of their large mass and low relative speed. The ion spends a relatively long time in the neighborhood of the atom with which it collides so that there is a good
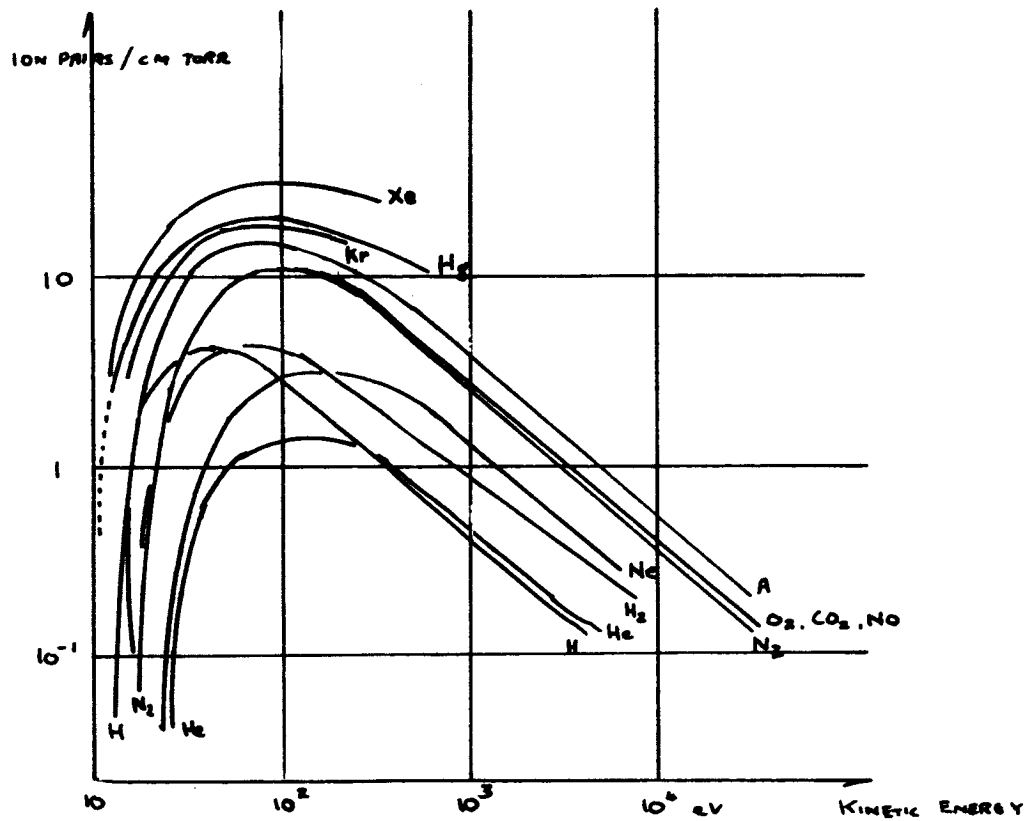
Fig. 1

Fig. 1.   Ionization efficiency s_e as a function of the
electron energy for various gases at 1 torr and
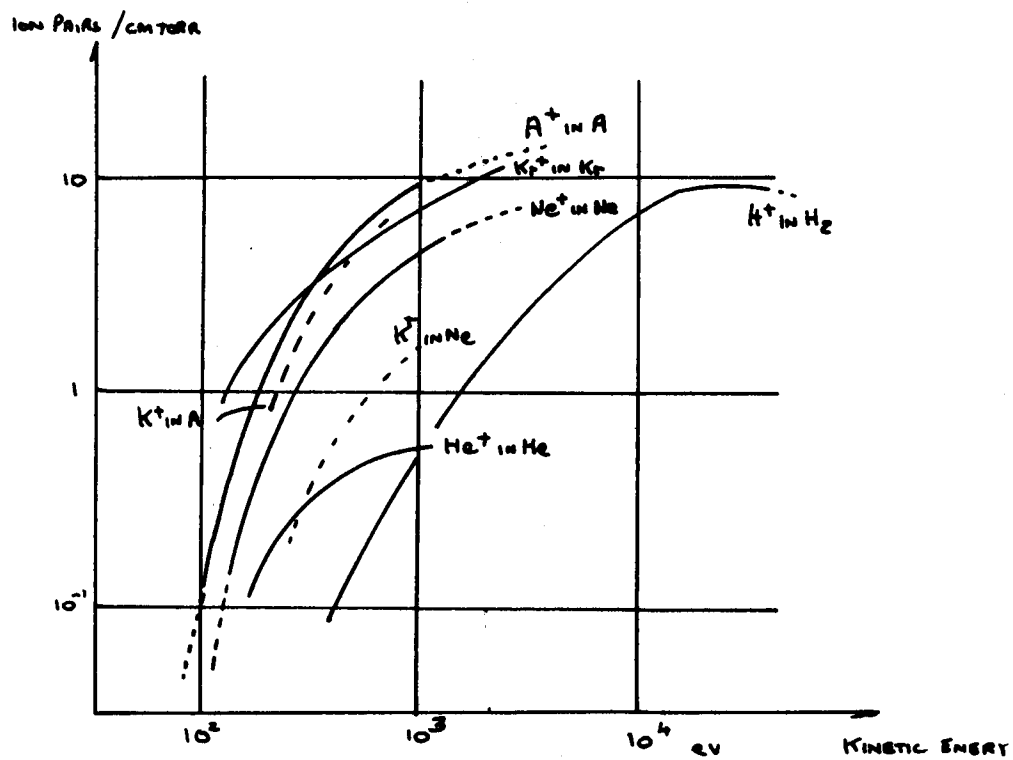0°C.

Fig. 2

Fig. 2.   Ionization efficiency s_i of ions as a function of
their kinetic energy at 1 torr and 0°C.

chance that the electrons adjust their positions but remain in the atom while momentum between the ion and the atom are exchanged.

2.4 Photo ionization

Light quanta passing through a gas may under certain circumstances ionize and excite the atoms. In the case where the energy $h\nu$ of the quanta (h being Planck's constant and ν the frequency associated with the radiation) is of the order of the ionization energy eV_i , the probability of ionization expressed by the absorption coefficienct μ is a sharp function of the photon energy. For $h\nu < eV_i$, $\mu = 0$ unless some of the gas atoms are already excited. As $h\nu$ increases , μ typically follows the behavior shown in figure 3.

The differences between this process and those described in sections 2.2 and 2.3 are note worthy. A photon ionizes or excites an atom with a maximum probability at a certain critical energy of the order of 0.1 or 1 ev above the minimum energy, and following the collision only two particles (one ion and an electron) are available to meet the energy and momentum requirements. Hence, the conditions for photo ionization are substantially more stringent.

For $h\nu \gg eV_i$ the electron ejected from the atom is no longer in the valence shell, but comes rather from the inner shells, K, L, etc. The excess photon energy can appear as kinetic energy of the ejected electron, or can be used to increase temporarily the potential energy of the atom. Figure 4 shows the dependence of μ on photon wavelength down to 10^{-1} Å for four gases: the sharp discontinuities occur at the critical energies associated with the inner atomic shells.

2.5 Thermal Ionization

Although ionization energies are modest (eV_i is usually from 3 to 25 electron volts) they are considerably in excess of thermal energies. However, if
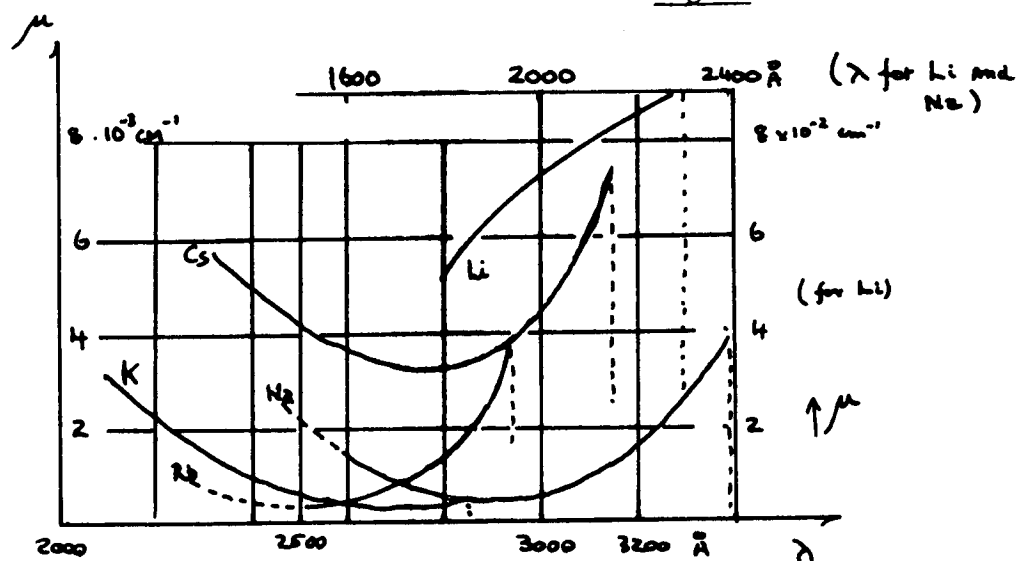
Fig. 3. Absorption coefficient μ in cm^{-1} at 1 torr and 0°C. for alkali vapors as a function of wavelength λ. The dashed lines indicate the ionization limit.
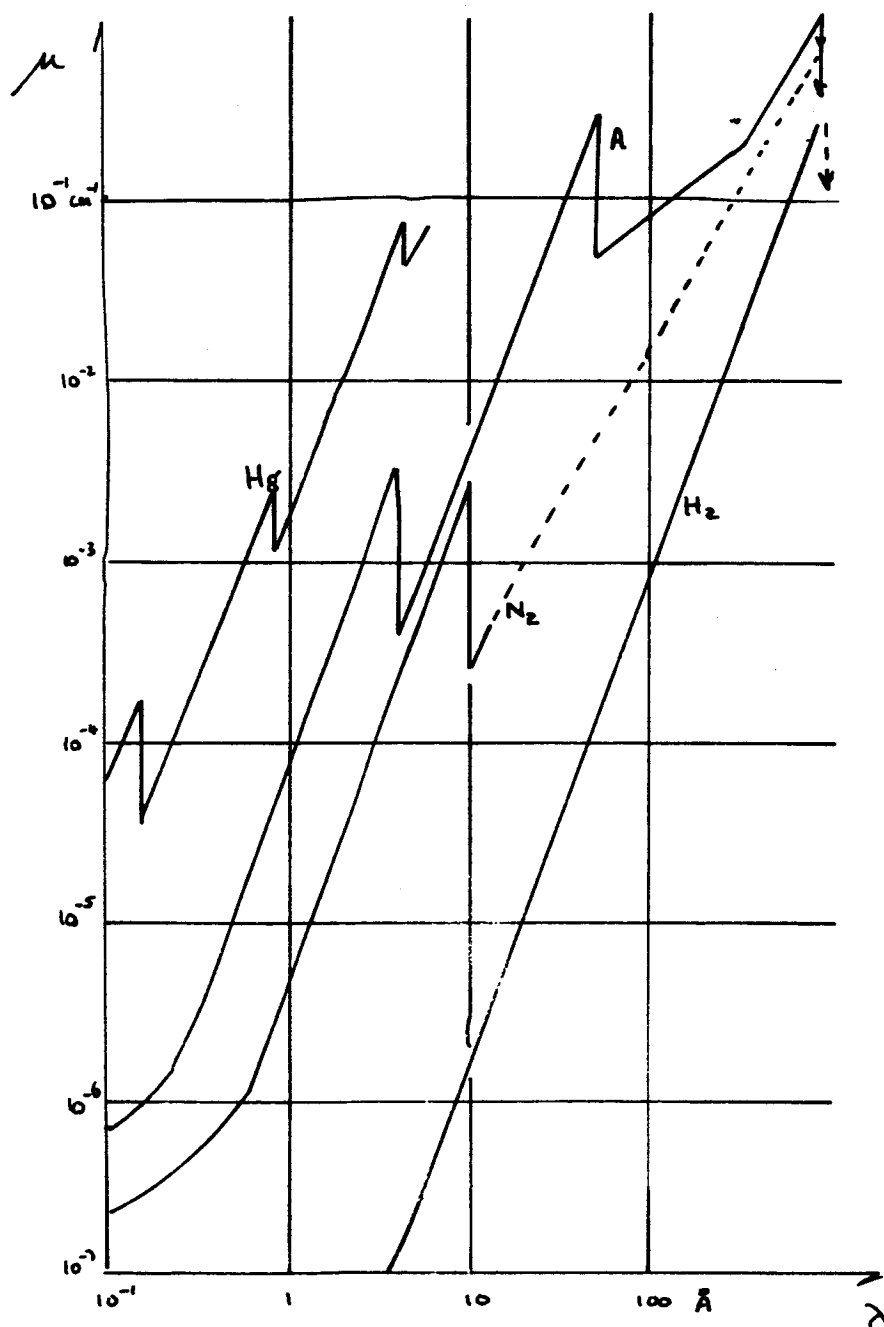
Fig. 4.

Fig. 4. Absorption coefficient μ in cm^{-1} at 1 torr
and 0°C. as a function of wavelength λ.
The discontinuities are due to the removal
of the K, L,.... electron.

the gas density is sufficiently low, the rate of recombination may be low enough so that a considerable degree of ionization can still be obtained. Using the methods of statistical mechanics it is possible to determine the degree of ionization in a gas in thermal equilibrium, a derivation due to Saha and Lindemann[9]. The simple form of the equation is:

$$\frac{n_+ n_-}{n_o} = \left\{\frac{2\pi m_- kT}{h^2}\right\}^{\frac{3}{2}} \exp\left\{\frac{-eV_i}{kT}\right\}$$

where n_+, n_-, and n_o are the number densities of positive ions, electrons and neutrals respectively, m_- is the mass of the electron and k is Boltzmann's constant. The accompanying table, figure 5, gives the degree of ionization n_+/n_o for hydrogen and cesium plasmas of interest, and points out the heavy dependence of this process on the magnitude of V_i since it occurs exponentially.

The Saha equation is widely used (for want of another tool) in circumstances where thermal equilibrium is not achieved. However, the danger of this maneuver seems to be apparent rather than real.

2.n Shock Waves

While somewhat less than fundamental, in comparison with the other topics in this section, the shock wave can produce the high temperatures necessary for ionization. In normal shock tubes a compressed gas expands on the rupturing of a diaphragm and pushes an initially rarefied gas ahead of it. The ratio between the temperature T_2 behind the shock in the driven gas and T_1 the initial temperature is given by[10]:

$$\frac{T_2}{T_1} = \frac{\gamma_1(\gamma_2-1)}{2\gamma_2} \cdot \left\{\frac{\gamma_2+1}{\gamma_1-1}\right\}^2 \cdot \frac{m_2}{m_1}$$

where γ_1, γ_2, m_1, m_2 are the specific heat ratios and the masses of the driver gas and driven gas respectively. For hydrogen as a driver gas, and argon as

Fig.

Hydrogen: $V_i = 13.6$ V

System	Temperature, °K	Density n, cm⁻³	Ionization ratio r_i n_+/n_0
Hottest furnace	3,000	10^{10}	10^{-13}
best vacuum			
Solar surface	6,000	10^{16}	$5 \cdot 10^{-4}$
Solar atmosphere	10,000	10^{14}	10^{7}
Hot confined plasma	$2 \cdot 5 \times 10^{5}$	10^{14}	10^{12}
Solar corona	10^{6}	10^{10}	10^{12}
Hot gaseous nebula	10^{4}	10^{3}	
Cold interstellar gas	10^{2}	10^{2}	10^{-580}
	Caesium, $V_i = 3.9$ V		
Vacuum furnace	3,000	10^{13}	20
Vacuum furnace	2,000	10^{12}	$0 \cdot 14$
Solar surface	6,000	10^{16}	40

Fig. 6 Degree of Ionization from the One-level Saha Equation.

the driven , then T_2/T_1 may be so large that hydrogen at 1000°K could produce argon at 2.5×10^5 °K , which would be fully ionized at atmospheric densities.

2.7 Thermionic and Field Emission of Positive Ions

When a metal is heated to sufficiently high temperature it can be shown by means of a mass spectograph that besides neutral atoms positive ions are evaporated. Singly charged ions of W, Mo, Ta, Cu, Ag, Fe, Ni have been found at temperatures near the melting point , with a current density j+ following an equation of the type

$$ J^+ = C T^2 \exp \left\{ - e \phi^+/kT \right\} $$

where ϕ^+ is the work function for positive ions (which is larger than ϕ for electrons). ϕ^+ is 6.5 and 6.1 electron volts for W and Mo respectively, and C is on the order of 10^{-1} A/cm^2°K^2. At 2800°K about 1 in 4×10^3 evaporated W atom is ionized.

It is not necessary that only atomic ions are emitted. Experiments by Drowart[11], who heated carbon to 4100°K and performed mass spectrometric analysis of emitted particles indicate that the molecular populations are in the ratio:

$$ C_1: C_2: C_3: C_4 = 1:2.8 : 4.5: 0.35 $$

and it is likely that ionic populations will follow similar ratios.

Larger currents of positive ions are emitted from heated salts of K and Na, and halide negative ions from oxide cathodes and from lithium aluminum silicate: Kunsman anodes can also give j+ of 10 ma/cm^2 or so at dull red heat in vacuum. Similar positive ion emitters were used by Franklin[12] in an experiment to produce a steady state plasma.

Field emission of positive ions is by no means an important process. Field strengths in excess of 10^{10} v/m are required[13] and the emitted ions

originate from absorbed gases rather than the anode material.

2.8 Secondary emission of positive ions

When neutral unexcited atoms of a gas of ionization potential V_i impinge upon a metal surface of work function ϕ and if $\phi > V_i$, electrons are liberated from the atoms and enter the metal lattice while the positive ion returns to gas. This is a well known process for C_s on W in contact ion engines.

It can be shown that the number of positive ions leaving the surface divided by the number of neutrals,

$$\frac{n+}{n_o} = \exp \left\{ -\left(\frac{V_i - \phi)}{kT}\right) \right\} : \quad \text{for W at } 1200°K \text{ and } C_s \text{ vapor}$$

this ratio is 500:1 . This emission mechanism is used in surface ionization detectors for the measurement of atomic beam intensities.

Positive ions are also emitted as a result of negative ion impingement on a neutral surface, but the ratio of positive ions to incident negatives is very small even at incident energies approaching 1Mev.[14]

2.9 Ion Products by Charge Transfer

In the single charge transfer process one electron and very little kinetic energy is transferred from the target atom to the projectile ion:

$$X^+ + Y \longrightarrow X + Y^+ + \Delta E$$
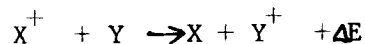
The process $X^+ + X \longrightarrow X + X^+$ with zero energy defect, is known as symmetrical resonance charge transfer; its cross-section may be larger than gas kinetic and falls with increasing impact velocity. Furthermore, charge transfer processes are most strongly pronounced for ions moving in their own gas.[15]

Figure 6 shows the charge transfer neutralization cross section Q_{+o} as a function of energy E in various gases. This cross-section is much larger than for Q_{oi}, the ionization processes, for the same kinetic energy, so that the tendency of the charge transfer process is to reduce the number of energetic ions in a beam or discharge. This is particularly important at high gas pressures,
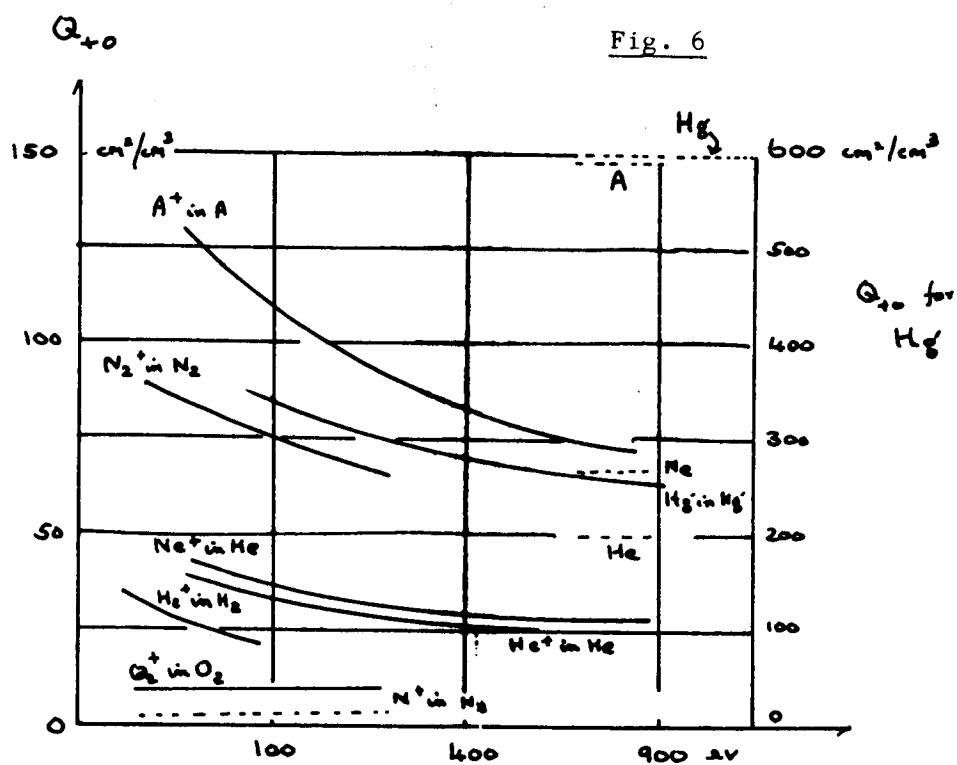
Fig. 6

Q_{+0}

Fig. 6. Charge transfer neutralization cross-section Q_{+0} as a function of energy for various gases at 1 torr and 0°C. The dotted lines are the classical cross-section values.

for example, in the cathode region of a vapor arc discharge.

2.10 The formation of negative ions

When an electron collides with a neutral gas atom or molecule it may become attached and form a negative ion. This process depends on the energy of the electrons and on the nature of the gas. For example, 0^-, 0_2^-, NO_2^-, NO_3^-, OH^-, H^-, Li^-, CH^-, C^- and negative halogen ions are readily formed but N^-, N_2^-, or negative rare gas ions are not. In the attachment

$$X + e + \text{kinetic energy} \rightarrow X^- + (Ea + \text{kinetic energy})$$
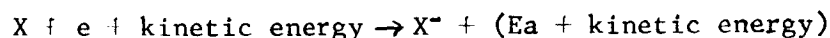
where Ea is the attachment energy, which can be calculated for simple cases by the Hartree-Fock method.[16] The sum (Ea + kinetic energy) must appear as a radiated photon. Figure 7 gives values for some of the more interesting elements.

Figure 7

Substance	Ea (in electric volts)
F	4.1
Cl	3.8
Br	3.6
I	3.2
O	1.5
C	0.9
Li	0.5
H	0.7
O_2	0.5

When an electron becomes attached to a molecule, the molecule may become dissociated if the energy of the incoming electron is sufficiently large; so called dissociative attachment. This will be discussed at greater length in the next subsection.

2.11 Problems of Macromolecules

The problems discussed in this section stem from the necessity to charge the macromolecule before it can be accelerated in a suitable field and give thrust. Mickelsen[8] has pointed out that the efficiency of a colloid particle thruster is approximately:

$$\eta = \eta_u \frac{1}{1 + \frac{ev/ion}{V}}$$

where η_u is the utilization efficiency, ev/ion is the work done in generating each colloidal ion, and V is the accelerating voltage. Then with large accelerating voltages and $\eta_u \rightarrow 1, \eta$ would tend to 100% even if power losses of as much as 1000 ev/ion were experienced in the charging of this colloid.

A method of charging is by electron bombardment and Mickelsen has given a simple theory in his paper[8] . However, as the electron bombardment energy is increased, it may exceed the fragmentation energy of the colloid, which suffers a catastrophic disintegration. This is illustrated for an analogous case, the dissociation of the H_2 molecule in figure 8.

Collisions between electrons and molecules (or electrons and colloids) will in general raise the latter into higher states of rotations and vibrations. If the electron energy is sufficiently large, electronic excitations will occur, which can lead to the emission of light or to dissociation ; however, transfer of the excitation energy to other particles is also possible.[17] In figure 8 in electron colliding with an H_2 molecule can excite it to a higher state H_2^* , the transition time is order 10^{-12} sec. from the Franck-Condon hypothesis, and takes place therefore at constant r (r is the interatomic distance). It follows then that the majority of transitions take place between the two vertical lines on figure 8.
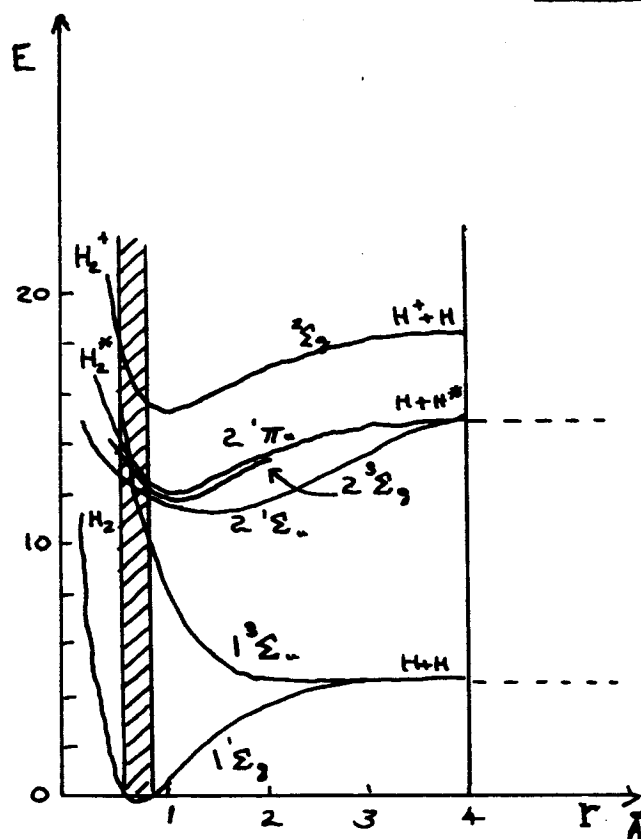
Fig. 8

Fig. 8.   Potential energy E as a function of
interatomic distance r (in Å) of a
hydrogen molecule in various states.
The shaded area is the Franck-Condon
range.

This illustrates the difference between a thermal and an electron collision leading to dissociation : by heating the gas absorption of vibrational and rotational quanta increases gradually the amplitude of vibration until in the case of hydrogen at E = 4.5 ev the two atoms are no longer bound. When electrons of E $>$ 8.8ev hit the molecule H_2 it can be excited into the repulsive $1^3\Sigma_u$ state, forming two H atoms with about 2.1ev kinetic energy each.

The relaxation processes of colloidal particles are somewhat similar to this, while at the same time being modified as though the particle were part of a solid lattice. Molecular spectra have been analyzed extensively by Herzberg[18], and some work has been done by H.P. Broida[19] on the lattice, but the nature of the energy curves for intermediate (colloidal) particles is somewhat more complex. This accounts for the variety of methods for colloid charging which have already been tried.[6]

When the colloid is charged, the maximum charge it can assume is determined by the mechanical strength of the particle, and the ratio of loss of charge by field emission, etc. The former occurs when the electrical pressure on the outside of the colloid is equal to the yield strength of the particular particle, while the latter might be expected to occur for field strengths on the order of 10^9 v/ m, or less if microscopic projections are present on the particle. Leakage currents of microamperes might generally be anticipated at that effective field strength. The charge losses due to gas kinetic interactions may be small if the mean free path is long enough.

3. Discharge Mechanisms

3.1 Introduction

Some discharge mechanisms of interest to the electric propulsion program will be discussed in this section. Since this is an interim report additional analysis of these and other mechanisms will be given in the final report. The order of presentation at this stage in the investigation does not reflect the relative importance or complexity of the discharges.

3.2 The Vacuum Arc Thruster

(a) Introduction

A recent paper by A.S. Gilmour, on the feasibility of the vacuum arc thruster[21], has suggested the use of a low power arc discharge in a station keeping satellite. He defines the vacuum arc as a low-power (as low as 10 watts) electrical discharge established in vacuum between a cathode and an anode when the cathode material is evaporated and ionized to the extent that it provides a high conductivity path between the electrodes. The cathode consumption rate is given at 2×10^{-4} gm/coulomb (an average value), and the emitted plasma is reported by Gilmour to have an average velocity of about 2×10^4 m/s, quoting earlier results.[22,23,24] The von Engel-Robson theory of the cold cathode arc[25] is considered to explain adequately the cathode processes.

In an experimental program Gilmour measured with a calorimeter the total power in the plasma beam at the same time computing the rate of loss of mass of the cathodic material. In some cases an axial magnetic field of 500 gauss was also used, although it is not clear from the paper whether the sole purpose for this was to direct the beam or to control the cathode spot as well[26]. Representative of Gilmour's results seem to be the quoted values (for OFHC copper ?) of a cathode evaporation rate of $5 \cdot 3 \times 10^{-3}$ gm/sec, at a beam power

of 430 watts. Assuming that the calorimeter measures only the kinetic energy of the beam, the power P is given by:

$$P = \frac{dE}{dt} = \frac{d}{dt}\left\{\tfrac{1}{2}\,mv^2\right\}$$

where $E = \tfrac{1}{2}\,mv^2$ is the kinetic energy of the beam with usual notation.

Since v is constant with respect to time,

$$P = \frac{\dot{m}v^2}{2}$$

But the thrust $F = \dot{m}v$, so that

$$F = \sqrt{2\dot{m}P}$$

$$= 6.8 \times 10^{-2} \text{ newtons}$$

and the specific impulse $= \dfrac{F}{9.8\dot{m}} = $ <u>1300 sec.</u>

If the particle beam consists of atoms of copper, the evaporation rate and beam power combine to give an average beam velocity of 1.28×10^4 m/sec. in good agreement with Tanberg's result of 1.6×10^4 m/sec.[22]

Superficially it appears from this paper that the vacuum arc thruster is more than feasible, it is also efficient. Taking 2×10^{-4} gm/coulomb for the material evaporated, the arc current for $5\cdot3 \times 10^{-3}$ gm/sec is about 26 amps. Arc voltages for such a current might be commonly about 20 volts, giving a power input of 520 watts, and a power in the beam of 430 watts (actually Gilmour states in this case that the efficiency was 25% implying an arc voltage of $>$ 65 volts, which seems unlikely). However, such high beam powers seem somewhat unlikely from the energy balance of the arc discharge: old[27] and[28] newer calorimetric measurements have shown that some 45% of the input energy to a copper arc enters the cathode, and about 37% to the anode, the remainder being lost by radiation, diffusion, etc.

(b) The Vacuum Arc Discharge

The low current arc (i $<10^2$ amps) normally belongs to one of two categories,

which are determined by the nature of the cathode spot. It appears that the relevant factor is whether thermionic emission or intense evaporation of electrons sets in first when the spot temperature is raised. Refractory metals support a relatively large stationary cathode spot having current density $j_c \sim 10^2$ amp/cm^2 (thermionic emission), whilst low boiling point metals (Cu, Fe, Hg, etc.) exhibit a small, mobile spot with $j_c = 10^6$ or 10^7 amps/cm^2 (or more)[29,30].

Interpreting the observations of Seeliger and Schmick[30], von Engel and Arnold[31,34] have suggested that even refractory metals below a certain critical pressure P_c should exhibit the latter kind of cathode spot with the high current density. The transition from thermionic to vapor mode in carbon occurs as the pressure **is lowered** to about 70 torr, but occurs for tungsten at a somewhat lower pressure, depending on the electrode geometry[26]. However, from space environmental considerations it may be assumed that Gilmour's arcs are of the vapor type, similar to arcs with a mercury cathode.

The electron emission mechanism at such an arc cathode is still undetermined, although the von Engel-Robson theory[25] seems by far the most likely. This suggests that the electrons are emitted from the cathode because of the impingement there of excited particles, where the energy relationship $eV_{exc} > e\phi$ holds. It follows that the minimum arcing voltage for a vacuum arc can be as small as the first electronically excited level above the work function of the cathode. The high vapor density close to the cathode spot is probably responsible for the loss of fast ions by charge transfer, and certainly accounts for the excited particle flux on the cathode. The mechanism of evaporation of the cathode material has also been thought to be caused by this flux[31,34,35] because cathode temperatures are too low to account for evaporation by classical theory[36]. Thus a simplified picture of the cathode region of a vacuum arc discharge might be similar to that in figure 9. Excitation of the cathode vapor is caused by electrons which have

Fig. 9

GAS

CATHODE

SOME HEAT FLUX
INTO CATHODE
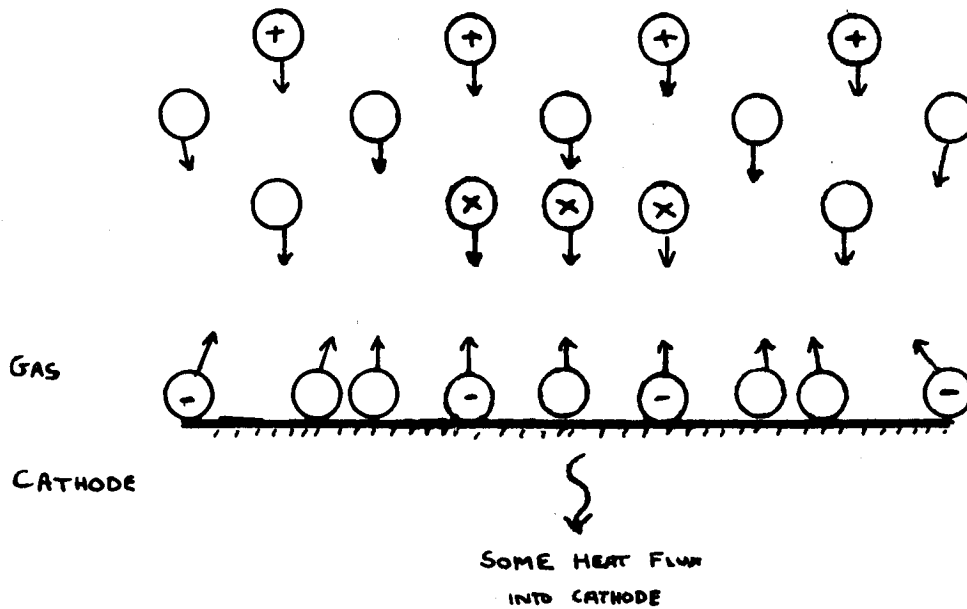
LEGEND : (+) POSITIVE IONS

O NEUTRALS (SOME FROM CHARGE TRANSFER)

(-) ELECTRONS RELEASED FROM CATHODE

(X) EXCITED PARTICLES

O NEUTRALS ABLATED FROM CATHODE SURFACE

Fig. 9. Particle flux at the cathode of a vapor arc.

been accelerated to a few electron volts energy close to the cathode.

Nothing in this picture suggests a mechanism for the continuous for-
mation of a beam of neutral cathode particles, or a plasma beam, in the
cathode region, although a "magnetic pinch" might suffice[37]. In an attempt
to determine the mechanism, Arnold and von Engel measured the velocity dis-
tribution, rather than the average velocity, of the particles in the beam
emitted from a copper arc cathode in vacuum[31,34,38]. For convenience refer-
ence (34) has been reproduced as Appendix A in this section, and the results
showed that the average velocity of the particles was only 4×10^4 cm/sec,
nearly two orders of magnitude lower than Tanberg. It becomes now a question
not of finding the origin of the fast particle beam, but of determining where
the other results might be in error.

A literature search has shown a wide variation in measured vapor jet ve-
locities, with those of Tanberg, Kobel, and Easton et. al. at the high extreme.
Noske and Schmidt[39] measured 2×10^5 cm/sec in vacuum for an Hg arc; Wienecke[40]
measured 10^6 cm/sec for a carbon arc (at one atmosphere); Haynes[41] found a ve-
locity of 2×10^5 cm/sec for a Hg cathode, but the velocity decreased as dis-
tance from the cathode increased. Kobel's[23] value of about 2×10^6 cm/sec is
reduced by two orders of magnitude when Froome's data for the current density
is used in the computation instead of the value that Kobel assumed. Other ex-
perimentors have been Schuster and Hensalech[42], who found v for spark vapor in
air to be 4×10^4 cm/sec; Mohler[42] who by Doppler shift found $v = 3.7 \times 10^4$ cm/sec,
Lawrence and Dunnington[44], with $v = 2 \times 10^5$ cm/sec for zinc using Kerr cells,
and Hermoch[45].

In comparing their results with other published data, Arnold and von Engel[38]
divided the latter into one of two categories, depending on whether the measure-

ments of force were made continuously by reaction techniques, or whether the production of the vapor jet employed large, instantaneous currents. In the first case, it is true of Tanberg's experiment (and others) that the measurements of the mass transported per unit time, $\dot{m}$, was made by condensation on a vane, and assume no losses through reflexion. Yet it is known that a number of heavy aggregates do deliver momentum to the vane, and then rebound, so that besides the momentum change measured being artificially high, the true value of $\dot{m}$ should be much larger than that recorded. Even Tanberg's data show that substantially more material leaves the cathode than is condensed on the vane.[22]

Experiments similar to Tanberg's have been performed at the ERA Laboratories in England: the instability of the arc and strong fluctuation of the vapor and globules emitted meant that the deflection of the vane varied with time so erratically that observations of the average deflection were hardly possible.[46]

In the second case the use of instantaneous current pulses to cause the vapor jets give results which agree with measurements on shock waves[47], where the velocity is given by $\left\{\frac{kT_e}{m}\right\}^{\frac{1}{2}}$, T_e being the electron temperature. This is hardly surprising, but it does appear that the results are not representative of a steady discharge emitting a constant stream of vapor.

(c) Discussion

By using a radioactive cathode in their experiment Arnold and von Engel showed conclusively that the number of Cu particles with directed velocities of 10^5 cm/sec or more were negligible compared to those at lower velocities. Yet Gilmour's data seems at first sight to agree with Tanberg at a value of about 10^6 cm/sec for $\bar{v}$. It appears that the answer may lie in the use by Gilmour of a calorimeter to measure the beam power, and in the assumption that the

energy collected by the calorimeter is all kinetic.

Disregarding the "blackbody" radiation flux received from the cathode it is clear that a fraction of the species incident on the calorimeter will be excited, or even charged. Since the immediate cathode region is the place where electron excitation would be most likely, the time taken for the flight to the calorimeter would normally be such that most excited particles could have decayed. However, some of the emitted photons would be collected by the calorimeter, and some excited states (particularly metastables) will still have substantially potential energy when they hit the surface. The spectrum of copper is complex[48], so that the particulars of the metastable states will be investigated at a later date.

It can be anticipated that the potential energy carried by a metastable would be about 3ev., and that the variety of photons from the excited gas absorbed by the calorimeter might have the same average energy. For ions impinging on the calorimeter, the potential energy given up is $(eV_i - e\phi)$, while for electrons it is simply $e\phi$: these values for copper would be 2.2ev and 4.5ev respectively. These energies are substantially greater than the kinetic energy of a Cu atom, having a velocity of 4×10^4 cm/sec: this is merely 5×10^{-2}ev.

Another source of potential energy deliverable to the calorimeter is the neutral particles themselves. The evaporation energy of copper is about 10ev per atom (found from Trouton's rule), which is the average energy expended in removing a copper atom from the cathode. When the neutral particles hit the calorimeter, some of them may condense onto the calorimeter surface and release potential energy to the calorimeter lattice by becoming adsorbed or absorbed. The surface energy levels probably occur in steps of about 1 or 2 electron volts[49] at temperatures below the sticking temperature of the deposit (which for copper on a metal target is probably 350°C[50]) The two-dimensional motion of the deposit

on the surface (so-called 'Rutscheffckt') helps in the adsorbing of atoms in the beam onto the surface.

It is not possible to tell from Gilmour's paper what precautions were taken to eliminate the energy (other than kinetic) flux to the calorimeter: this will be investigated during the next period. At the present, when it seems that no precautions were in fact taken, the possibilities for transference of potential energy to the calorimeter by one or more of the mechanisms detailed above are so strong that no reliance can be placed on the values for the kinetic energy of the beam given in Gilmour's paper. If the true kinetic energy of the beam were found to be about 1 watt, rather than about 400 watts, this would correspond to a beam velocity of 4×10^4 cm/sec, and a specific impulse of about 40 sec.

(d) Conclusions

It can be concluded from this analysis that the calorimetric techniques of Gilmour need to be explored in greater detail before the true kinetic energy of the beam can be determined. The possible potential energy flux associated with the beam far outweighs the expected kinetic energy in the author's opinion, and the agreement with the measurements of Tanberg, the erroneous results of Kobel and the pulsed arc results of Easton et. al. is superficial.

It was suggested by Wehner[51] that a doppler shift experiment be performed to try to determine (again) whether fast particles do emanate from arc cathodes. Such an experiment is feasible, and is being planned. The results will be given in a subsequent report. Until this or other experiments, using calorimeters or otherwise, properly demonstrate the existence of the fast particle flux, it is suggested that the low current vacuum arc thruster in the form that Gilmour has described be considered impractical.

3.3 The Kaufman Electron Bombardment Ion Source

This section is concerned with an analysis of the early Kaufman discharge[52], the electron bombardment ion source. Figure 10 is taken from his paper.

Neutral particles (in Kaufman's case mercury) enter the chamber through an orifice on the left of the figure, and impinge on a distributor, whose function is to break up the directed flow into the chamber. Electrons from the thermionic filament ionize the mercury vapor in the volume of the ionization chamber on their way to the walls of the chamber, which are positively charged with respect to the filament. Ions which are formed are extracted from the body of the chamber by a screen grid and acceleration grid to the right of the figure. The distributor, filament, and screen grid are maintained at the same negative potential with respective to the walls, so that electrons should not be attracted to either end of the chamber.

From section 2.2, and from reference 9, it can be seen that the electron energy for maximum ionization cross-section in Hg occurs at about 80ev and has a value of 20 ion pairs/cm torr. To increase the electron path length, and hence the ionization probability, an axial magnetic field of about 10 gauss was added to the apparatus. This has the effect of reducing the diffusion coefficient perpendicular to H, being proportioned to $\frac{1}{H^2}$ [53,54].

Under operation, the ion chamber is filled with a plasma, with an expected density of 10^{11} to 10^{13} per cubic centimeter. (If the neutral particle temperature is a few hundred °K this can be approximated to a pressure of about 10^{-3} torr) At these particle densities, the mean free path for ionization even at optimum energy is order 1 metre, so that the reason for the magnetic field is clear. At the same time, the Debye shielding distance λ_D is small compared to the physical

Fig. 10

Accelerator

Screen

Anode

Magnetic
field

Distributor

Filament

Propellant

Ionization
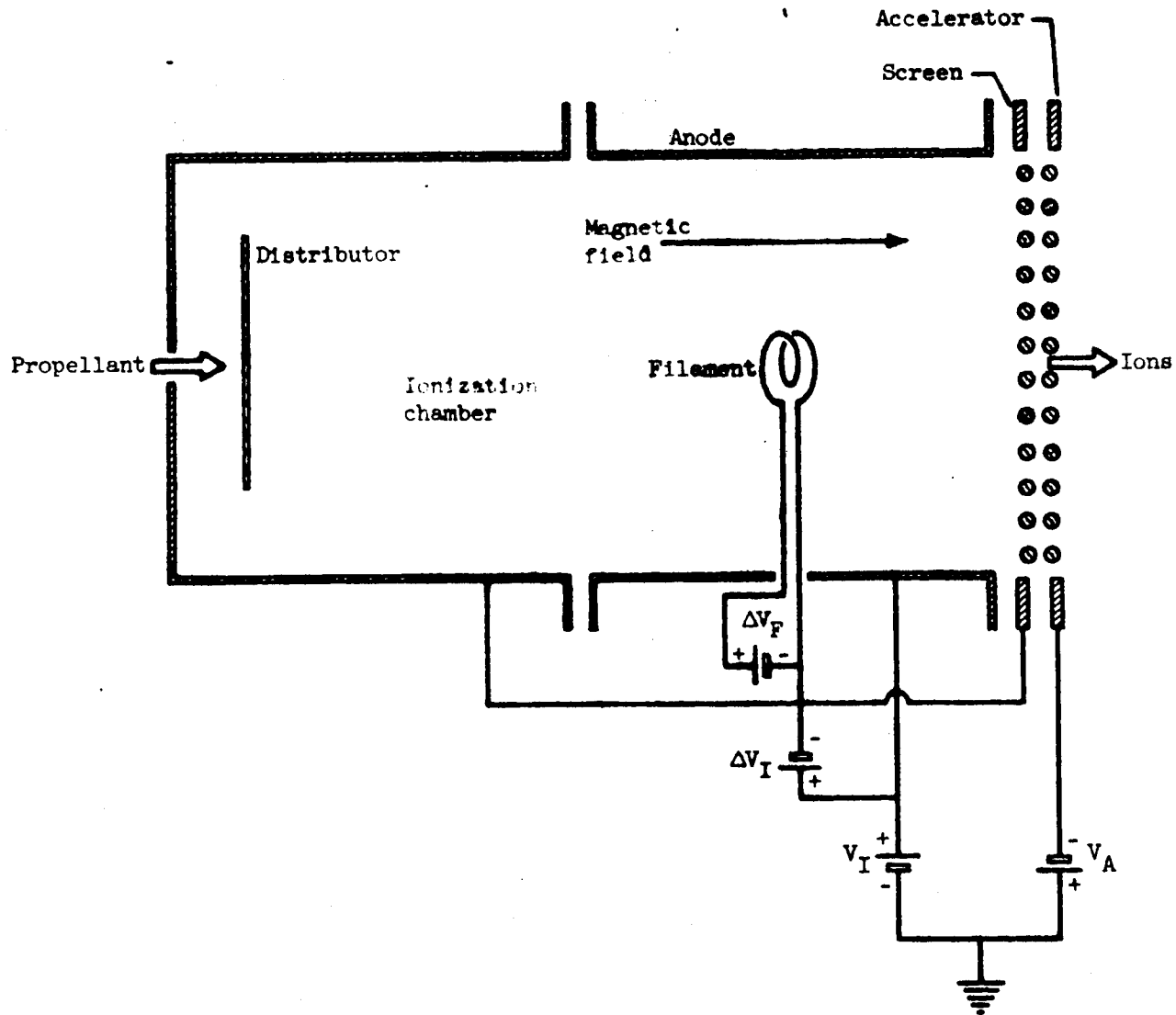chamber

Ions

ΔV_F

ΔV_I

V_I

V_A

Fig. 10. Schematic diagram of Kaufman's ion engine.

size of the ionization chamber, so that the general requirement for plasma equations is satisfied. (The potential in the region surrounding any chosen ion or electron in the plasma falls as $\frac{q}{r} \exp\left\{-\frac{r}{\lambda_D}\right\}$[53], so that approximately the field of the particle can be regarded as effectively screened off at distances beyond λ_D. λ_D is given by $\sqrt{\frac{kT}{8\pi n e^2}}$, with the usual notation.

The other requirement of the plasma is that the electron density is the same as the ion density over most of the volume.

Electrons emitted from the filament fall through the potential difference of the sheath surrounding the filament. The average electron will lose enough energy in a few mean free paths that it reaches the bulk electron temperature, estimated by Kaufman to be about 5ev for the mercury plasma. The number of ions produced per electron is $N+ = \frac{\sigma_i}{\sigma_o}$ X (total number of collisions) where σ_i and σ_o are the cross-sections for ionization and collision respectively; this must include ion pairs produced by subsequent collision between ambient atoms and daughter electrons. Production of ions by other processes are considered to be negligible.

The principal loss mechanisms would appear to be recombinations in the plasma itself, and diffusion of ions to the walls of the chamber. The rate of recombination can be estimated for Kaufman's plasma: it is given by

$$-\frac{dn}{dt} = \rho n^2$$ where n is the density of ions and electrons and ρ is the recombination coefficient ($=$ about 2×10^{-10} cm^3/sec for Hg vapor at 3×10^{-1} torr). For $n = 10^{13}/cc$ and a pressure of say 10^{-3} torr,

$$\frac{-dn}{dt} \sim 10^{-11} \times 10^{26} = 10^{15}$$ per cc and second.

To determine whether this is allowable or not, an estimate needs to be made of the volume ionization.

This is given by:

$$n_i \text{ (number of ion pairs/unit volume)} = \sigma_i \, v_e \, N_i \, N_e$$

$$\simeq 4 \times 10^{-16} \times 3 \times 10^8 \times 10^{26}$$

$$= 10^{17} \text{ or so}$$

Thus volume recombination is a small part of the loss.

The number of ions diffusing to the walls across the plasma sheath can be estimated as follows. Let V = total volume of discharge and A be the wall area. Then $\frac{1}{4} N_i \bar{v}_i$ A is the number diffusing to the walls, where $\bar{v}_i$ is the mean ion random velocity. If $\underline{\text{this}}$ is the principal mechanism of loss $\frac{1}{4} N_i \bar{v}_i$ A should be approximately equal to $10^{17}V$. With Kaufman's engine, $A \sim 100 \, \pi \text{ cm}^2$ and $V \sim 300\pi \text{ cm}^3$. Assuming $\bar{v}_i \sim 4 \times 10^4 \text{ cm/sec}$, $\frac{1}{4} N_i \bar{v}_i$ A = $\frac{1}{4} \times 10^{13} \times 4 \times 10^4 \times 100 \, \pi$

$$= 100 \, \pi \times 10^{17} \sim 10^{17}V$$

This appears to account qualitatively for the fact that in the Kaufman engine, the energy expended per ion was about 500 ev. However, more discussion will be given in a subsequent report.

3.4 Electron Bombardment Thrustors Using Liquid Mercury Cathodes

This is a development of a Kaufman thrustor being currently considered at Hughes Research Laboratories[55]. Analysis of this discharge is only superficial so far, so that no report will be given at this time.

4. Conclusions and Future Work

So far under this grant, three discharges have been investigated. The latter two - the Kaufman discharge and the thrustor with the liquid mercury cathode - have much in common, and it is expected that the major inefficiency in both discharges occurs because of recombination at the walls of the ionization chamber. This has been established for the Kaufman discharge, and will be considered also for the thrustor with the liquid mercury cathode.

The investigation of the vacuum arc thrustor led to the conclusion that Gilmour's calorimetric determination of the beam power needed to be checked to ensure that measurements made were of the beam kinetic energy. It appears unlikely that the beam of particles has a velocity in excess of 10^5 cm/sec, and the agreement between Gilmour's measurements and Tanberg's is coincidental. Unless other evidence is forthcoming, the feasibility of the vacuum arc thrustor is in doubt.

Work on the Kaufman and Kaufman-like discharges will be continued, together with some investigation of other interesting discharges. These will include the plasma-separator ion engine of General Electric Co., Cincinnati, and the work of La Rocca at General Electric Co., Philadelphia.

REFERENCES

1. E. Stuhlinger: Ion Propulsion for Space Flight. McGraw-Hill (1964)

2. J.S. Townsend: Electricity in Gases, Clarendon Press, Oxford (1915)

    : Handbuch d. Radiol. 1 Akad. Verlag. Leipzig (1920)

    : Motions of Electrons in Gases. Clarendon Press, Oxford (1925)

3. A. von Engel and M. Steenbeck: Elektrische Gasentladungen. Vols. 1,2. Springer, Berlin. (1932-34)

4. R. Seeliger: Physik der Gasentladungen. Barth, Leipzig. (1934)

5. L.B. Loeb: Fundamental Processes. Wiley, New York. (1939)

6. W.R. Mickelsen: Future Trends in Electric Propulsion. AIAA Paper No. 66-595.

7. A. von Engel: Nature. 183 573 (1959)

8. W.R. Mickelsen: Colloid-Particle Electrostatic Thrustors. DGRR Sonnenberg Symposium on Electric Propulsion, Braunschweig, West Germany. (1966)

9. A. von Engel: Ionized Gases. 2nd Edition. Clarendon Press. Oxford (1965)

10. W.B. Thompson: Introduction to Plasma Physics. 2nd Edition. Pergamon (1964)

11. J. Drowart et al: J. Chem. Phys. 31 1131 (1959)

12. R.N. Franklin: D. Phil. Thesis. Oxford University (1960)

13. E.W. Müller: Phys. Rev. 102 734 (1936)

14. A.S. Denholm: Can. J. Phys. 36 476 (1958)

15. J.B. Hasted: Physics of Atomic Collisions. Butterworths (1964)

16. H.S.W. Massie: Negative Ions. Cambridge Monographs (1956)

17. K.W. Arnold and A. von Engel: Proc. Phys. Soc. 79 1098 (1962)

18. G. Herzberg: Spectra of Diatomic Molecules. Van Nostrand (1959)

19. H.P. Broida and M. Peyron: J. Chem. Phys. 32 1068 (1960)

20. D. Alpert, D.A. Lee, E.M. Lyman, and H.E. Tomaschke: Proc. 1st Symposium on Insulation of High Voltages in Vacuum. 1 1 (1964)

21. A.S. Gilmour, Jr.: Concerning the Feasibility of the Vacuum Arc Thrustor. AIAA Paper No. 66-202.

22. R. Tanberg: Phys. Rev. 35 1080 (1930)

23. E. Kobel: Phys. Rev. 36 1636 (1930)

24. E.C. Easton, F.B. Lucas, and F. Creedy: Trans. Amer. Inst. Elec. Engrs. 53 1454 (1934)

25. A. von Engel and A.E. Robson: Proc. Roy. Soc. A 242 217 (1957)

26. H. Wroe: Brit. J. App. Phys. 9 488 (1958)

27. R. Seeliger: Hand. d. Exp. Phys. 13 Akad. Verlag. Leipzig (1924)

28. W. Rieder: Z.f. Phys. 146 629 (1956)

29. K.P. Froome: Nature. 179 267 (1957)

30. A.E. Robson: D. Phil. Thesis. Oxford University (1956)

31. K.W. Arnold: D. Phil. Thesis. Oxford University (1961)

32. A. von Engel and K.W. Arnold: Proc. 5th Int. Conf. on Ionization Phenomona in Gases. Munich (1961) Vol. 1   858   (1961)

33. K.W. Arnold and A. von Engel: Proc. Phys. Soc. 79   1098   (1962)

34. K.W. Arnold and A. von Engel: Proc. 6th Int. Conf. on Ionization Phenomona in Gases. Paris (1963) Vol. 2 129 (1963)

35. A. von Engel and K.W. Arnold: Nature. 187   1101   (1960)

36. J.M. Somerville: The Electric Arc. Methuen (1959)

37. L.A. King: E.R.A. Laboratories. Leatherhead, England. private communication.

38. A. von Engel and K.W. Arnold: Phys. Rev. 125   803   (1962)

39. H. Nöske and E. Schmidt: Z. f. Naturf. 7a   667   (1952)

40. R. Wienecke: Z. f.Phys. 150   231   (1958)

    ibid   151   159   (1958)

41. J.R. Haynes: Phys. Rev. 36   706   (1930)

42. A. Schuster and G. Hemsalech: Proc. Roy. Soc. 64   331   (1899)

43. J.F. Mohler: Astrophys. J. 15   125   (1902)

44. E.O. Lawrence and F.G. Dunnington: Phys. Rev. 35   396 (1930)

45. V. Hermoch: Czech. J. Phys. 9 221 (1959)

46. A. von Engel: Clarendon Laboratory, Oxford. Private communication.

47. A. von Engel, M. Sakuntala, and R.G. Fowler: Phys. Rev. 118   1459   (1960)

48. A.G. Shenstone: Phil. Trans. 241   297   (1948)

49. O. Knacke and I.N. Stranski: Prog. in Metal Physics 6 181 (1956)

50. S. Wexler: Rev. Mod. Phys. 30   402   (1958)

51 G.K. Wehner: private communication.

52. H.R. Kaufman: NASA TN D585 (1961)

53. G. Francis: Ionization Phenomena in Gases. Butterworths (1964)

54. R.J. Bickerton and A. von Engel: Proc. Phys. Soc. B69   468   (1956)

55. H.J. King, W.O. Eckhardt, W. Ward, and R.C. Knechtli: AIAA Paper No.66-232.

EMISSION PROCESSES AT THE CATHODES OF
VACUUM ARCS

by

K. W. ARNOLD* AND A. H. VON ENGEL

The Clarendon Laboratory University of Oxford, Oxford, England

Abstract: The rotating drum method was used to measure the
velocity distribution in the vapor jet which emerges from the
cathode region in a magnetically stabilized vacuum arc discharge
between cooled copper electrodes. Part of the cathode was made
of radioactive copper, and the number distribution of radioactive
atoms deposited on the drum as a function of their velocity per-
pendicular to its surface was measured by a Geiger-Müller coun-
ter. An average velocity $\bar{v}$ of about 4×10^4 cm/sec was found for
the atomic beam.
    Consideration of the mechanisms by which copper vapor might
be evaporated from the cathode spot of the arc show that the tem-
perature of the spot is too low to account for the copious emission
observed.   A new evaporation mechanism is suggested by which
ablation of the cathode is caused by the impact there of excited vapor
atoms. Experimental evidence is given to support the conception
of the importance of excited atoms in the cathode ablation process.

1. Introduction

Whereas earliest work[1,2] indicated that vapor emitted from
the cathode of an arc or spark between metal electrodes in air had
an average speed $\bar{v}$ of the order of 10^4 cm/sec, Tanberg[3] found
$\bar{v} \approx 10^6$ cm/sec for copper evaporated from the cathode of a 10-
20 amp d. c. arc discharge in vacuum. In his experiment, copper
cathode vapor impinged on a Pyrex plate acting as a pendulum:
from the deflection the average rate of momentum transferred to
the plate could be determined, and knowing the rate of change of
mass of the plate, $\bar{v}$ could be calculated. In a separate experi-
ment, the same value of $\bar{v}$ was measured when the cathode itself
was suspended as a pendulum. Other measurements[4] with neu-
tral vapor jets emanating from arc cathodes have supported partly
the lower and partly the higher values of $\bar{v}$.

It appeared that a first step in the study of vapor emission
from arc cathodes would be an experiment to clarify these con-
flicting results. In fact, a measurement of the velocity distribu-
tion of vapor atoms from the cathode region, rather than $\bar{v}$. Thus
part of this paper describes such an experiment for a copper arc
discharge in vacuum, and the conclusions which can be made con-
cerning the earlier work. The rest of the paper relates to the
mechanism by which material may be evaporated from an arc
cathode, and to the importance of electronically excited states
of neutral species in this process.

2. Measurement of the Velocity Distribution

Figure 1 shows the experimental apparatus. A steady arc
discharge of about 30 amp d. c. was maintained between a vertical
copper cathode and a hollow copper anode, both water-cooled. The
ambient pressure p in the arc chamber was always $< 10^{-5}$ torr,
so that copper vapor from the cathode region could pass through
the anode and a collimating slit to a velocity selector in a secon-
dary chamber, where p was the same. The selector consisted
of a cylindrical drum, 15 cm in diameter and 5 cm wide, which
could be rotated up to 3000 rpm from outside the secondary cham-
ber. An axial slit in the drum periphery allowed copper vapor to
be deposited at different positions on aluminum foil attached to
the inside of the drum: thus the velocity spectrum of the vapor
could be derived if the copper deposit was suitably detected.

To increase the sensitivity of detection, a sample of 1 gm.
of copper, irradiated to give 76 mc of Cu^{64}, was inserted in
the cathode tip. The motion of the cathode spot was restricted
primarily to this area by application of an axial magnetic field
of 10^3 gauss, produced by a cylindrical magnet. Thus, when
the aluminum foil was removed from the drum at the completion
of an experiment, the number distribution of radioactive copper
particles deposited could be measured as a function of their posi-
tion on the foil by counting the emission from a section of the de-
posit with a Geiger-Müller tube.

Cu^{64} emits electrons and positions of about 0.6 Mev, as well
as γ-rays, and has a half-life of 12.8 hours. Counts were taken
both when a 0.5 cm thick aluminum plate with a narrow slit was
interposed between the tube window and the foil, and when this
plate was replaced by a similar one without a slit. The second
count enabled allowance to be made for background radiation
which originates from a section of deposit larger than the area
of the slit.

3. Experimental Results and Discussion

The number distribution of copper atoms as a function of
their velocity v in a direction perpendicular to the drum surface
is shown in Fig. 2, which is derived from the results of several
experiments. The distribution (which seems to be non-Maxwellian)
has a weak maximum at about 3×10^3 cm/sec, and an average ve-
locity $\bar{v}$ about 4×10^4 cm/sec, for particles with v between 10^3
cm/sec and infinity: larger experimental errors prevented mean-
ingful measurements of v much below 10^3 cm/sec.

There are apparently no appreciable numbers of atoms with
velocities between 10^5 and 10^6 cm/sec, which contradicts Tan-
berg's findings. Careful evaluation of his experiments, however,
suggests that no account had been taken of large aggregates which
transferred momentum to the plate but failed to stick there: thus
the measured rate of change of mass, m, of the plate would be
too small, as well as the momentum change being larger for ag-
gregates which rebound. Tanberg's own figures show that, within
the range i = 14 - 18 amps, five times more copper came off the
cathode than was deposited on the plate, a factor too large to be
explained away by solid angle considerations. Similar arguments
can be advanced in connection with the deflected cathode experi-
ment, for which m was measured in a separate experiment of
which no details were given. These views are supported by the
fact that, in our experiment, aggregates were observed to pass
through the collimating slit and rebound from the drum.

The other experiments[4], based for instance on light emis-
sion or probe currents, also gave higher average velocities than
we have measured. However, these correspond to values ex-
pected from shock wave measurements[5,6]: both the results and
the experimental method used (superimposition of large current
pulses on an auxiliary discharge) suggest that such high average
velocities are not representative of those in a steady discharge.

4. The Mechanism of Evaporation

The extent of electrode erosion during arcing depends on
the electrode material and geometry, the nature and density of
the ambient gas, etc. The dense vapor cloud associated with a

* Present Address: Ion Physics Corporation, Burlington, Mass.,
  U. S. A.

11) I. Langmuir, Phys. Rev., 8, 149 (1916).

12) G. K. Wehner, Advances in Electronics, 7, 239 (1955).

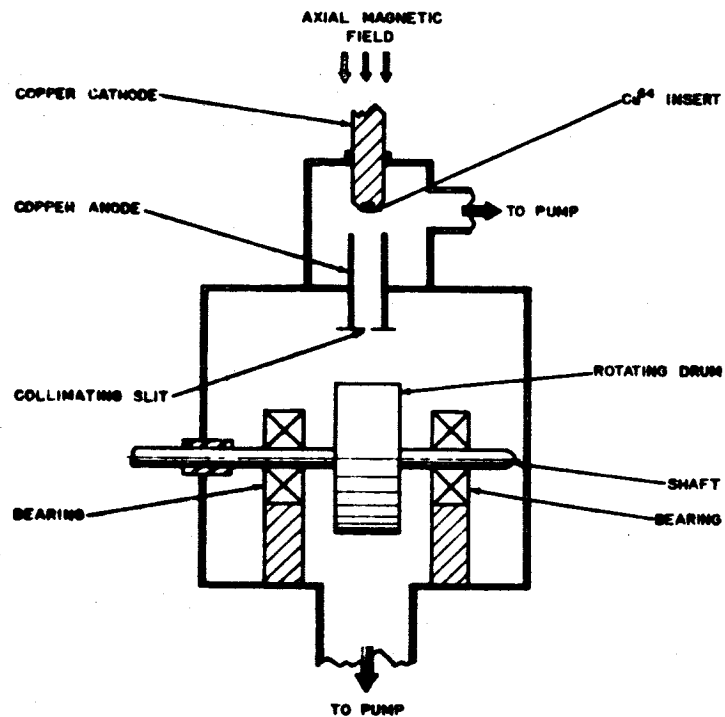13) A. von Engel and K. W. Arnold, Proc. Phys. Soc., 79, 1098 (1962).

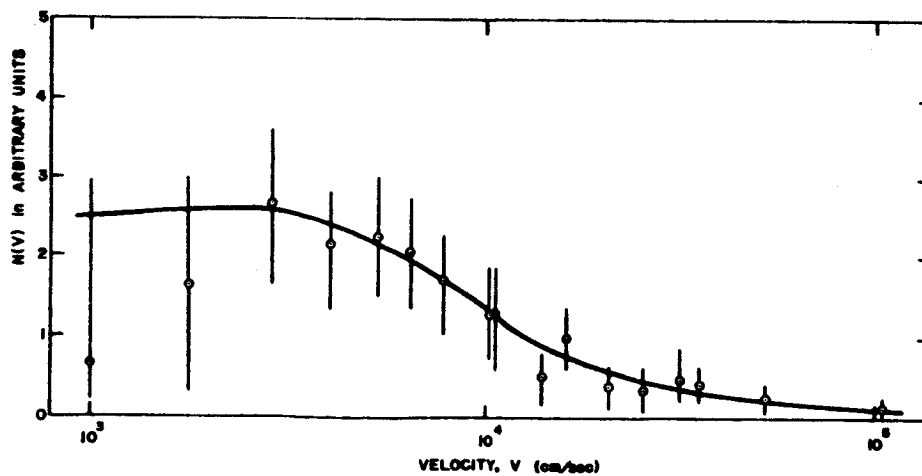Figure 1   The experimental apparatus

Figure 2   N(v) as a function of v

·130·

cold cathode spot was originally assumed to be caused by a "boiling-off" of vapor from the cathode because of its high temperature, even though this was too low to support thermionic emission of electrons[7].

It has been demonstrated, however[8], that the cold-cathode spot temperature is also too low to account for the rate of evaporation, Q, of cathode material. Furthermore, measured values of Q are the difference of two much larger quantities, viz. the true evaporation rate minus the rate at which material is back-scattered in the dense vapor and returns to the cathode. Thus, a new model is needed to account for the heavy rate of loss of cathode material when the cathode temperature may be less than 2000°K.

It has been shown by Volmer[9] that the theory of coupled oscillators cannot explain the processes of "classical" evaporation of material from a matrix at temperature T, but that a step-wise process must be invoked. On his hypothesis, an atom moves in a first step from its "half-crystal" position (where its binding energy equals the evaporation energy) to the surface, where it is less strongly bound and only adsorbed. The atom then migrates along the surface for a longer or shorter interval and subsequently evaporates.

Quantitative formulation of these ideas gives good agreement with experimental observations of evaporation rates from a hot matrix, but still does not fit with anticipated values of Q for a cold-cathode arc. However, the concept of stepwise evaporation does point to a new mechanism which may account for the loss of material from a cathode spot: this new mechanism can be termed "stepwise ablation."

5. Stepwise Ablation

A cathode spot experiences a large energy influx from the gas in the form of unexcited and excited neutral particles, ions and quanta. It is suggested that the electronically excited species ablate the cathode by a stepwise process, in which atoms adsorbed on a crystal surface may receive enough energy from impinging excited species to cause them to evaporate, and atoms in the half-crystal position to move to a step on the crystal surface, etc. It is known that atoms in higher electronically excited states can re-lease electrons from a cathode[10] but both lower and higher states may contribute to stepwise ablation. One may deduce that more energy is needed to remove an electron from an atom in an adsorbed layer than from a strongly bound lattice atom, so that low energy excited states might ablate the loosely bound crystal atoms while high energy states remove electrons from more strongly bound atoms. Calculations[9] show that an atom needs to absorb about 1 ev to move from one crystal position to the next of higher energy.

The question arises whether species other than electronic-ally excited atoms or molecules can ablate a cathode surface. In the case of positive ions this is unlikely since ion energies are too low to cause sputtering; furthermore, the approach of an ion disturbs the electron cloud in the metal matrix so that the trans-fer of ionization energy may be a relatively long process. Kinetic energy of all species will probably be communicated directly to the lattice[11]. The essential quality of an excited vapor atom is that, carrying a relatively large amount of potential energy, it can still approach close to the cathode before it communicates its energy. It is feasible that this energy is available to move crystal atoms to higher potential states or to remove them com-pletely. Wehner[12] has, in fact, observed in sputtering experi-ments that metastable particles can ablate atoms from a crystal surface.

Since there are large numbers of vapor particles impinging on or near the cathode spot, it can be seen that the ablation proc-ess is not similar to normal evaporation from a heated metal. One might imagine that, in an ideal situation, all impinging excited atoms give energy to the production of vapor by stepwise ablation,

which would be "evaporation" which had no relationship to lattice temperature. Thus, stepwise ablation may explain both the high rate of cathode vapor production, and the low conduction heat loss to the cathode[8].

6. Measurement of the Cathode Ablation Rate

An experiment was devised to illustrate the effect of the pres-ence of excited vapor atoms on the ablation of an arc cathode. It is known[13] that carbon electrodes in air support either a thermi-onic or vapor (cold-cathode) arc discharge depending on the am-bient pressure p: below a critical pressure p_c (~50 torr) the dis-charge is of the latter type. It is also thought[13] that the reason why the discharge changes as p is raised is because excited par-ticles close to the cathode are then quenched. Thus a measure-ment of the cathode ablation rate Q for both a cold-cathode and a thermionic carbon arc discharge in air at $p \sim p_c$ should show that Q is greater for the cold-cathode discharge

The experimental apparatus for this measurement comprised a pair of carbon electrodes on small copper holders which could be screwed into water-cooled blocks. A glass vacuum vessel sur-rounded the electrodes so that an arc discharge could be main-tained between them in air at a constant pressure p, measured with a mercury manometer, McLeod or Pirani gauge. Electrodes were weighed before and after arcing for a known time with a known current (~5 amps d.c.), and Q determined in gms/coulomb. In a series of experiments, p was varied from 760 to 10^{-2} torr.

Figure 3 shows Q as a function of p. It can be seen that, when $p > p_c$ the cathode gained slightly in weight during arcing, because of material from the anode which impinged on it. With $p < p_c$ the rate of loss of cathode material was about 10^{-5} gms/coulomb, and the inside of the vacuum vessel was heavily coated with ablated carbon. For $p \sim 760$ torr, the loss of cathode material is caused by chemical action between the electrode and the ambient gas (formation of CO, CO_2 and CN, etc.).

Absolute values of Q depend upon the electrode geometry. It was not the purpose of the experiment to measure these accu-rately, but to detect the change in Q at the critical pressure. Because Q is so much greater for $p < p_c$, when excited particles are present to bombard the cathode, the observations do appear to support the role assigned to such particles by the concept of stepwise ablation of the cathode. This concept is applicable to all low current d.c. arc discharges having a cold-cathode, and not merely to a carbon arc discharge.

References

1) A. Schuster and G. Hemsalech, Proc. Roy. Soc. A64, 331 (1899).

2) J. F. Mohler, Astrophys. J., 15, 125 (1902).

3) R. Tanberg, Phys. Rev., 35, 1080 (1930).

4) E. O. Lawrence and F. G. Dunnington, Phys. Rev., 35, 396 (1930).
   J. R. Haynes, Phys. Rev., 36, 706 (1930).
   E. Kobel, Phys. Rev., 36, 1636 (1930).
   H. Nöske and E. Schmidt, Z. Naturforsch, 7A, 667 (1952).
   R. Wienecke, Z. Physik, 150, 231 (1958); 151, 159 (1958).
   V. Hermoch, Czech. J. Phys., 9, 221 (1959).

5) M. Sakuntala, A. von Engel and R. G. Fowler, Phys. Rev., 118, 1459 (1960).

6) P. F. Little, Proc. Vth International Conference on Ionization Phenomena (North-Holland Publishing Co., Amsterdam, 1962), Vol. 2, p. 1440.

7) A. von Engel and M. Steenbeck, "Electrische Gasentladungen," 1 and 2.

8) A. von Engel and K. W. Arnold, Nature, 187, 1101 (1960).

9) O. Knacke and I. N. Stranski, "Prog. in Metal Physics," 6, 181 (1956).

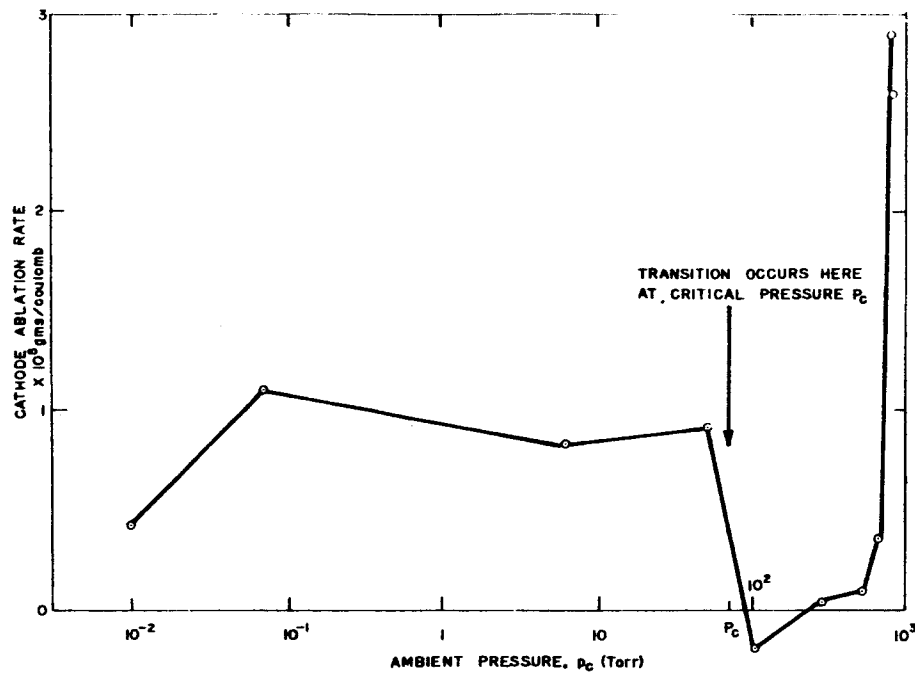10) A. von Engel and A. E. Robson, Proc. Roy. Soc., A242, 217 (1957).

Figure 3   Q as a function of ambient pressure p

DISCUSSION

Question by C. KENTY (U.S.A.) :

What contribution to the momentum (given to the quartz plate in Tanberg's experiment, or in your experiment) do neutralized ions make. Ions that have received energy in the cathode fall, strike the cathode and come off as neutral particles with a fraction of their energy as ions. For example A^+ ions on W rebound with about half their energy, see the work of Compton and Van Vorhis.

Answer by K. W. ARNOLD (U.S.A.) :

Both for our experiment and those of Tanberg, it can be expected that positive ions make many collisions in the dense vapor close to the cathode region. The pressure in this region may be 1 to 10 atmosphere, so that it is unlikely that ions would rebound as in sputtering experiments.

LUNAR-SUPPLY MISSION STUDY

by T.D. Fehr and W.R. Mickelsen

Although there has been much work done on low-thrust cis-lunar missions, there appears to be some aspects of this class of missions which need to be explored further. In particular, various combinations of high-thrust/low-thrust propulsion may provide great gains in payload capacity. It is the purpose of this analysis to explore unique mission profiles for lunar-supply which involve electric propulsion. The results of the analysis are expected to be of great assistance in defining the requirements for electric propulsion systems.

This analysis will cover six general mission profiles with some of the many possible variations of these included. The general profiles are:

1. Various increments of chemical boost in the near-earth phase, then electric propulsion to a lunar satellite orbit, followed by chemical deorbit and soft landing.

2. Various increments of chemical boost in the near-earth phase, then electric propulsion for approach to the moon, followed by chemical propulsion from approach to perilune and then to soft landing.

3. Various increments of chemical boost in the near-earth phase, then electric propulsion to sub-satellite velocity above the Moon, followed by chemical soft-landing.

4. Various increments of chemical boost in the near-earth phase, then electric propulsion to lunar fly-by, followed by chemical propulsion for retro to perilune and to soft landing.

5. Round trips composed of the combinations of the profiles listed above.

6. Round trips as in five using an atmospheric braking upon return to earth.

The general purpose of the study is to determine the optimum profile or profiles, the potential paylo capability, and the requirements that relate to the electric propulsion systems.

In all facets of the analysis, the Saturn V has been assumed as the launch vehicle. The data for the performance of the Saturn V has been obtained from the "Saturn V - Payload Planner's Guide" as published by Douglas Aircraft Company, Inc., Santa Monica, California. Further information as to the capabilities of the Saturn V is being furnished by the Missile and Space Systems Division, Douglas Aircraft Company, Inc.

A seventh mission profile was initially considered for its potential in lunar supply. The hover capability of electric spacecraft was investigated for its possible application in a fixed point docking station for the lunar lander. The radius above the moon, the propulsion-system specific mass α, and the specific impulse can be related to find hover requirements. The gravitational field near a body of the solar system is nearly a central gravitational field and can be described according to Newton as:

$$f = \frac{\gamma M_o M^*}{r^2} \tag{1}$$

where M^* is the mass of the planet or body, γ is the universal gravitational constant, and r is the distance between the masses as measured from the center of the bodies. Assuming uniform density, γ is equal to 6.67×10^{-11} newton-m^2/kg^2. The acceleration due to gravity can be expressed as

$$g = \frac{f}{m_o} = \frac{6.67 \times 10^{-11} M^*}{r^2} \tag{2}$$

For electric spacecraft, the power is defined as:

$$P = \tfrac{1}{2} F v_j \tag{3}$$

where F is the thrust and v_j is the exhaust or jet velocity. For hover, the thrust is just equal to the gravitational attraction; therefore, $F = M_o g_m$ where g_m is the gravitational acceleration of the moon at a point.

The jet velocity can be expressed as:

$$v_j = \frac{2\,P}{M_o g_m} \tag{4}$$

The expression $\frac{P}{M_o}$ can be expressed as a function of the Melbourne parameter β .[1]

$$\frac{P}{M_o} = \frac{\beta(1-\beta)}{\alpha} \tag{5}$$

The term $\beta(1-\beta)$ is the propulsion system mass fraction M_{ps}/M_o as optimized by Melbourne[2]. The optimization shows values of M_{ps}/M_o ideally in the range of .2 to .25. The value of .2 was chosen as a fairly representative value for $\beta(1-\beta)$ in equation 5:

$$\frac{P}{M_o} = \frac{0.2}{\alpha} \tag{6}$$

Using equation (6) in equation(4):

$$v_j = \frac{0.4}{\alpha g_m} \tag{7}$$

Since $v_{ex} = g_o I_{sp}$ and $g_m = 6.67 \times 10^{-11} \times M*/r^2$ where $M* = 7.35 \times 10^{22}$ kg, then the following relation can be written:

$$I_{sp} = 8.32 \times 10^{-12} \times r^2/\alpha \tag{8}$$

where r is in meters and α in kg/kwj . Assuming values for α and I_{sp} yields the altitude of the point of hover as illustrated in figure 1.

The specific impulse of interest for lunar missions will be shown later to be in the range of 1000 to 3000 seconds. Consideration of figure 1 shows the altitude of hover to be beyond 10,000 kilometers and much greater for realizable or even optimistic values of the specific mass α.

A second profile of the study to date is that of all-electric propulsion with constant I_{sp} from 300 n.m. circular orbit at earth to 50 n.m. circular orbit at the moon. The analysis utilizes the Zola characteristic length[3,4] as

the medium of comparison. The Zola characteristic length was chosen because of its potential for less complicated usage in later studies involving chemical propulsion phases in an effort to improve the payload capacity of the system. A comparison will be made with an analysis for a similar mission using the equations of Melbourne to obtain a check of the validity and a method of comparison of the two techniques. It is important to note that the results of this portion are only a rough approximation. It is hoped that a simple modification of the Zola-characteristic-length method can be found, which will provide acceptable accuracy.

The characteristic length can be obtained from an escape-trajectory correlation by Sauer and Melbourne[5] and the Stephenson[6] correction for London's[7] trajectories. The Sauer-Melbourne correlation for escape trajectories relates J and time T by the relation:

$$J = K'/T^{0.913} \tag{9}$$

where the constant K' contains gravitational field parameters for the particular central body and initial orbit radius. The quantity J is defined by Melbourne[2] as follows:

$$J = \int_0^T (F/M)^2 \, dt \tag{10}$$

In a gross approximation, escape trajectories from Earth and from Moon can be merely added to obtain a total J for the Earth-Moon transfer:

$$J = J_{01} + J_{23} = K'_E/T_{01}^{0.913} + K'_m/T_{23}^{0.913} \tag{11}$$

where the subscripts E and M refer to Earth and Moon respectively.

London[7] has found that a simple correction to the transfer time provides fairly accurate results:

$$J_{03} = K'_E/(0.92 \, T_{01})^{0.913} + K'_M/(0.92 \, T_{23})^{0.913} \tag{12}$$

Noting that:

$$T_{03} = T_{01} + T_{23} \tag{13}$$

and that for a fixed transit time T_{03}, then $dT_{03} = 0$ and $dT_{01} = -dT_{23}$. For maximum final mass fraction, $dJ_{03} = 0$, so:

$$dJ_{03} = dJ_{01} + dJ_{23} = 0 \tag{14}$$

From equations 13 and 14:

$$\frac{dJ_{01}}{dT_{01}} = \frac{dJ_{23}}{dT_{23}} \tag{15}$$

and from equation 9, the equation 15 can be used to obtain a relationship between T_{23} and T_{01}:

$$\frac{T_{23}}{T_{01}} = \left(\frac{K_M}{K_E}\right)^{0.523} \tag{16}$$

where the K_M and K_E include the factor 0.92 of equation 12. The preceding relations can be combined to obtain:

$$J_{03} = \left[1 + (K_M/K_E)^{0.523}\right]^{1.913} K_E T_{03}^{-0.913} \tag{17}$$

For the particular mission where electric propulsion starts from a 300 n.m. circular orbit about Earth and ends with a 50 n.m. circular orbit about Moon, equation 17 becomes:

$$J_{03} = 587/T_{03}^{0.913} \qquad (T_{03} \text{ in days}) \tag{18}$$

If it is assumed that the variable thrust and constant F/M solutions are very similar as is suggested by the nature of the Lunar mission[5], the Zola characteristic length can be expressed as:

$$L = (JT^3/12)^{\frac{1}{2}} \tag{19}$$

This is really only true for variable thrust programs and an analysis of the validity of assuming that the variable and constant F/M solutions are nearly equal will be examined later. Substitution of equation 18 in 19 and changing

to T in days yields

$$L = (1.775 \times 10^8) \, T^{1.044} \text{ meters} \tag{20}$$

where T is in days. The characteristic length is plotted as a function of time of flight in figure 2.

The electric velocity increment necessary for the mission can be found using the following equation from Zola[3]:

$$\Delta V_e = 2v_j \ln \left[\frac{v_j + \frac{L}{T}}{v_j - \frac{L}{T}} \right] \tag{21}$$

where v_j is the jet velocity and dependent on the specific impulse, L is the characteristic length, and T is the time of flight in seconds. These values have been calculated as a function of specific impulse for selected periods of time. The results are presented graphically in figure 3. Using the values of ΔV_e as calculated, the final mass fraction is determined from the relation

$$\frac{M_f}{M_o} = e^{-\Delta V_e/v_j} \tag{22}$$

The information displayed in figure 3 can be used to construct the curves of constant specific impulse shown in figure 4 as final mass fraction M_f/M_o against trip time. In this same figure 4, curves of constant α can be constructed by following the method outlined here:

1. For a particular value of M_f/M_o, β is calculated from the equation

$$\beta = 1 - M_f/M_o \tag{23}$$

2. For the particular time and specific impulse corresponding to the value of M_f/M_o chosen, F/M_o is calculated from

$$F/M_o = L/T^2 \left[\frac{1}{\left(\frac{\frac{L}{v_j T} + 1}{2} \right)^2} \right] \tag{24}$$

3. Since $P = \frac{1}{2} F v_j$, then P/M_o can be calculated from

$$P/M_o = \frac{1}{2} v_j \, F/M_o \tag{25}$$

4. Since $M_{ps}/M_o = \beta(1-\beta)$ and $P = M_{ps}/\alpha$, P/M_o can also be expressed as

$$P/M_o = \beta(1-\beta)/\alpha \tag{26}$$

5. Using equations 25 and 26, one can find an expression for α given as

$$\alpha = \frac{\beta(1-\beta)}{P/M_o} \tag{27}$$

6. Using the values for β and P/M_o, α can be determined and plotted on figure 4.

The final mass fraction M_f/M_o can be utilized with the Saturn V data to find the payload as a function of trip time. The final mass M_f can be found using $M_o = 220,000$ pounds at 300 n.m.[8], and since P/M_o is known, then P can be determined. With these quantities and α, it is possible to determine the payload into lunar satellite orbit.

$$M_{pay} = M_f - M_{ps}$$

$$M_{pay} = M_f - (\alpha)(P)(2.205 \text{ lbs/kg}) \tag{28}$$

The values of payload into lunar orbit are shown as a function of the specific mass (α) with specific impulse and time of flight as parameters in figure 5.

As a check on the validity of the previous results, the Sauer and Melbourne[5] relationships as modified by Stephenson's[6] correction for London's[7] trajectories can be used to determine the characteristic length for the all-propulsion, constant-F/M mode. As demonstrated previously, J_{03} can be expressed as:

$$J_{03} = 587/T_{03}^{.913} \qquad (T_{03} \text{ in days}) \tag{29}$$

Sauer and Melbourne show that a_0 can be expressed as a function of time:

$$a_0 = f(T_{03}) \tag{30}$$

Since J is defined as the integral of $(a^2 \, dt)$ and a is a constant, J_{03} can be expressed as:

$$J_{03} = a_0^2 \, T_{03} \tag{31}$$

Using equation 31 to find a_0 yields:

$$a_0 = (J_{03}/T_{03})^{\frac{1}{2}} \tag{32}$$

Since J_{03} is a function of time, a_0 can be expressed as a function of time as required by equation 30. Substituting equation 18 into equation 32 produces the desired result:

$$a_0 = .0824/T_{03}^{.9565} \qquad (T_{03} \text{ in days}) \tag{33}$$

Melbourne defines the parameter β :

$$\beta = (\alpha J_{03}/2)^{\frac{1}{2}} \tag{34}$$

Further use is made of equation 26 where:

$$P/M_0 = \beta(1 - \beta)/\alpha$$

to allow the solution of equation 3 for v_j :

$$v_j = \frac{2 \, P/M_0}{F/M_0} = \frac{2 \, P/M_0}{a_0} \tag{35}$$

Since the Sauer and Melbourne relations as derived and modified previously are for a constant F/M, all-propulsion mission, the appropriate expression can be selected from Zola's paper to determine the Zola characteristic length.

$$F/M = a = 4L/T^2 \tag{36}$$

This can be rewritten as:

$$L = aT^2/4 \tag{37}$$

Applying equation 32 in equation 36 yields

$$(J/T)^{\frac{1}{2}} \quad 4L/T^2 \tag{38}$$

Equation 38 can be rewritten as

$$L = \frac{1}{4} \sqrt{JT^3} = \sqrt{JT^3/16} \tag{39}$$

Since J is a function of time as expressed in equation 29, the Zola character-istic length is a function of time only. This function is plotted in figure 6 and compared to the approximate result as specified by equation 20.

Analysis of figure 6 shows good correlation of the approximate to the Sauer and Melbourne solution. A correction factor can be determined for the approximate solution. Using equations 19 and 39, a ratio of the characteristic lengths can be determined:

$$\frac{L_{app}}{L_{sm}} = \frac{\sqrt{JT^3/12}}{\sqrt{JT^3/16}} = 2/\sqrt{3} \tag{40}$$

where the subscript app refers to approximate and the subscript sm refers to Sauer and Melbourne. This ratio can be used to find the corrected value of the characteristic length:

$$L_{corrected} = \sqrt{3}/2 \; L_{app} = .866 \; L_{app} \tag{41}$$

Further analysis will be done to compare the characteristic length method with the modified Sauer-Melbourne correlation method.

Preliminary work has been completed on both the near-earth phase and the all-electric round trip capability but is not sufficiently developed for inclu-sion at this time. One significant portion of the all-electric round trip per-formance is included to show the desirability of specific impulses in the range of 1000 to 3000 seconds as previously suggested in reference 9. The analysis is based on equations 3,5,18, and related expressions. Analysis is completed for one way trips and the return trip time was calculated from:

$$T_{47} \quad T_{03} \left(\frac{M_{ps}}{M_0} \right)^{1.043} \tag{42}$$

Summing the times and plotting the range of specific impulses with α as a parameter yields figure 7. It is evident from figure 7 that for reasonable trip times and specific masses, the specific impulse is in the 1000 to 3000 second range.

Analysis of the near-earth phase is in progress and nearing completion. The procedure is to evaluate the effect of chemical boost to higher circular orbits from the 300 n.m. orbit before beginning electric propulsion to determine the effect this maneuver will have on the payload into lunar orbit as well as the requirements of the electric propulsion system. The mechanics will be based upon the use of the ratio of final to initial circular orbit radii to find the equivalent time of flight required if performed electrically[10]. This time can be used in the Zola relations to find the reduction in the total electric ΔV required and this value used to determine the final mass fraction and payloads into lunar orbit.

Future plans call for analysis of the effects of various modes of chemical propulsion in the near-moon phase following electric propulsion to near the moon in modes varying from sub-satellite to fly-bys. There is also intention of adding some analysis of utilizing an atmospheric braking phase upon return to earth in round-trip configurations.

REFERENCES

1. Mickelsen, W.R.: Mission Analysis - Electric Propulsion Systems and Missions. Lecture Notes. 1963-64.

2. Melbourne, W.G.: Interplanetary Trajectories and Payload Capabilities of Advanced Propulsion Vehicles. NASA JPL Technical Report No. 32-68. March, 1961.

3. Zola, C.L.: Trajectory Methods in Mission Analysis for Low-Thrust Vehicles. AIAA Paper No. 64-51. January, 1964.

4. Zola, C.L.: A Method of Approximating Propellant Requirements of Low-Thrust Trajectories. NASA TN D-3400. April, 1966.

5. Sauer, C.G. and Melbourne, W.G.: Optimum Earth-to-Mars Roundtrip Trajectories Utilizing a Low Thrust Power-Limited Propulsion System. JPL TN No. 32-376. March, 1963.

6. Stephenson, R.R.: The Electrically Propelled Lunar Logistic Vehicle. AIAA Paper No. 64-497. July, 1964.

7. London, H.S.: A Study of Earth-Satellite to Moon-Satellite Transfers using Nonchemical Propulsion Systems. United Aircraft Corporation Report. R-1383-1. May, 1964.

8. Saturn V- Payload Planner's Guide. Douglas Missile and Space Systems Division. Douglas Report. SM-47274. November, 1965.

9. Mickelsen,W.R.: Colloid-Particle Electrostatic Thrustors. Paper presented at DGRR Sonnenberg Symposium on Electric Propulsion, West Germany. Feb. 24, 1966.

10.Moeckel, W.E.: Trajectories with Constant Tangential Thrust in Central Gravitational Fields. NASA TR R-53. 1959.
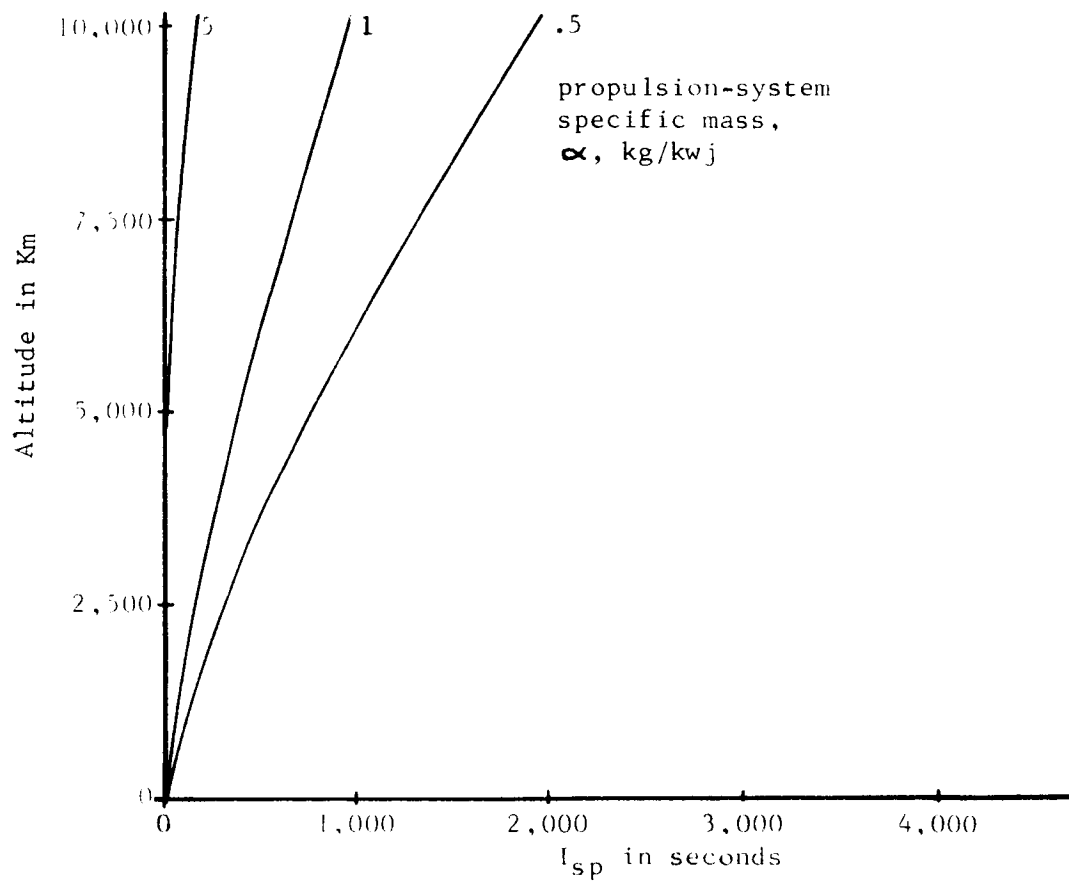
Fig. 1. Hover capability of electric propulsion systems at the moon.
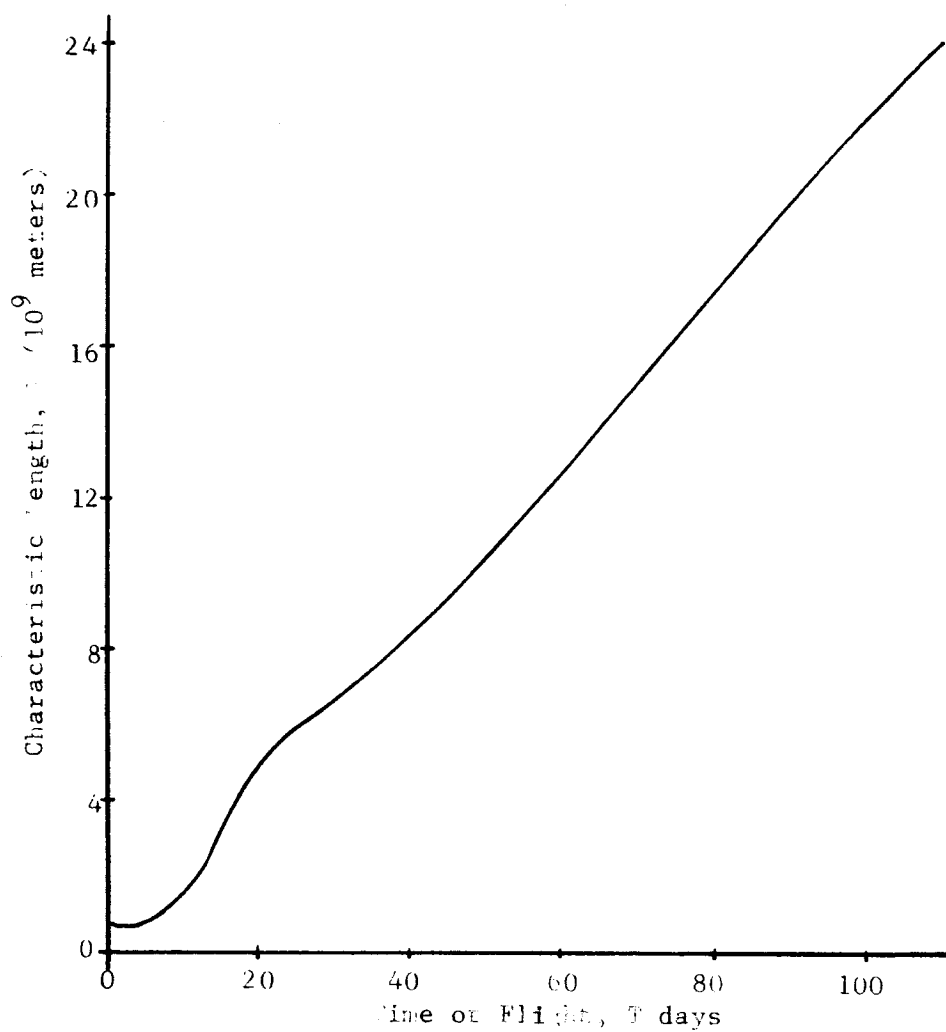
Fig. 2. Zola characteristic length as a function of the one-way trip time for a lunar supply mission.
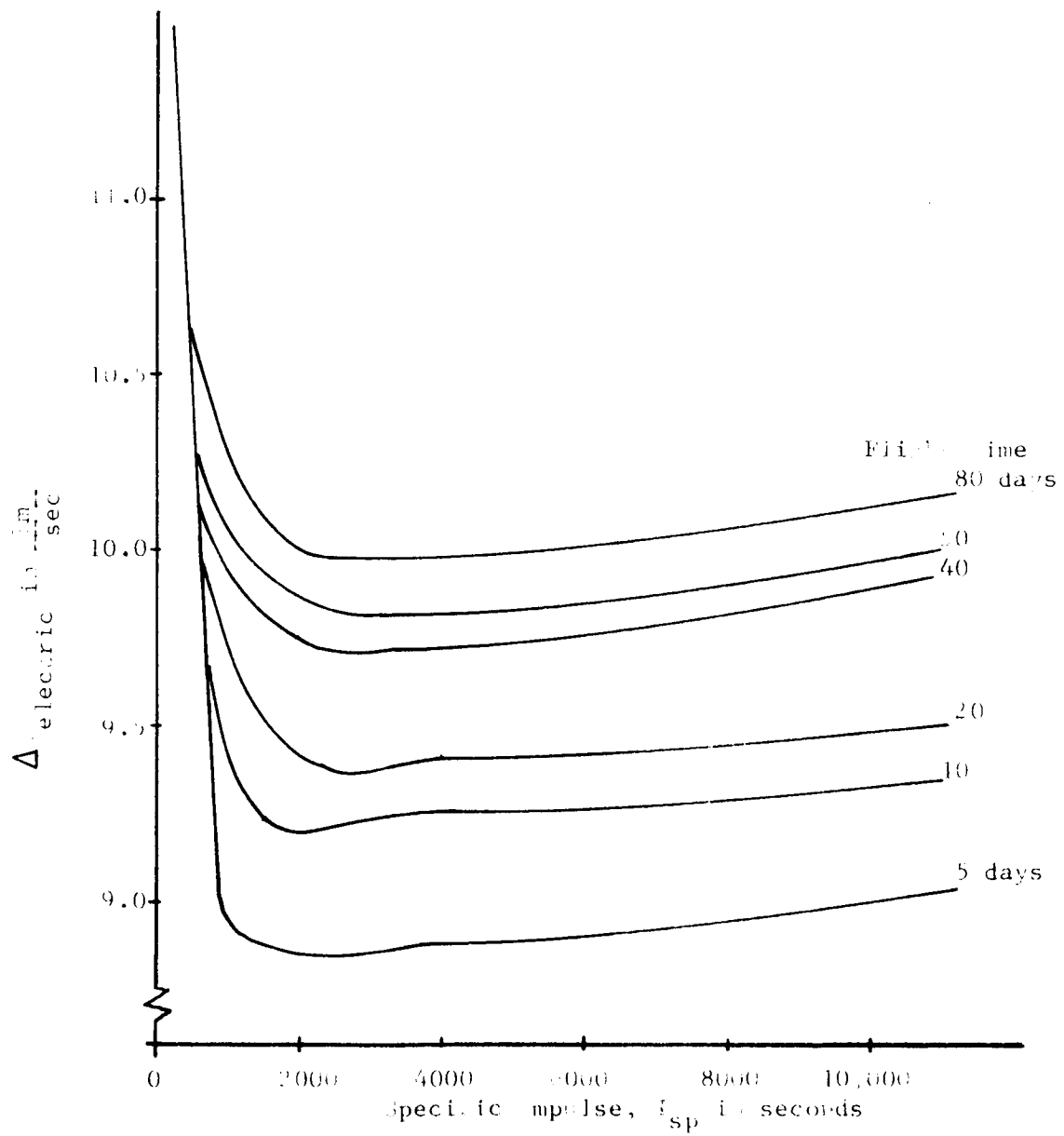
Fig. 3. Required electric Δv for the all electric propulsion transfer of various flight times to lunar orbit from 100 n.m. orbit at earth.
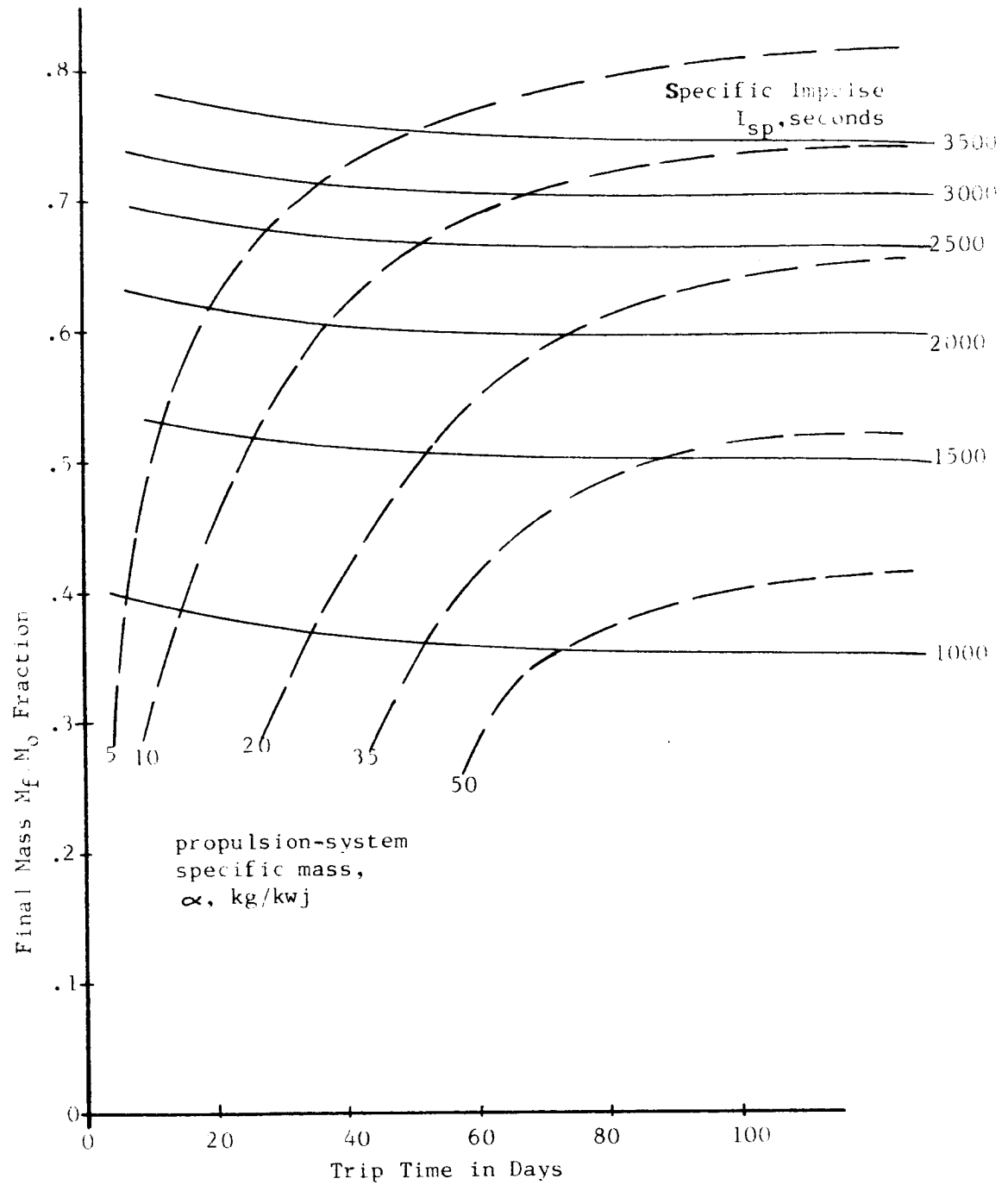
Fig. 4. Final Mass Fraction capability for all electric
constant thrust transfer to lunar orbit, assum-
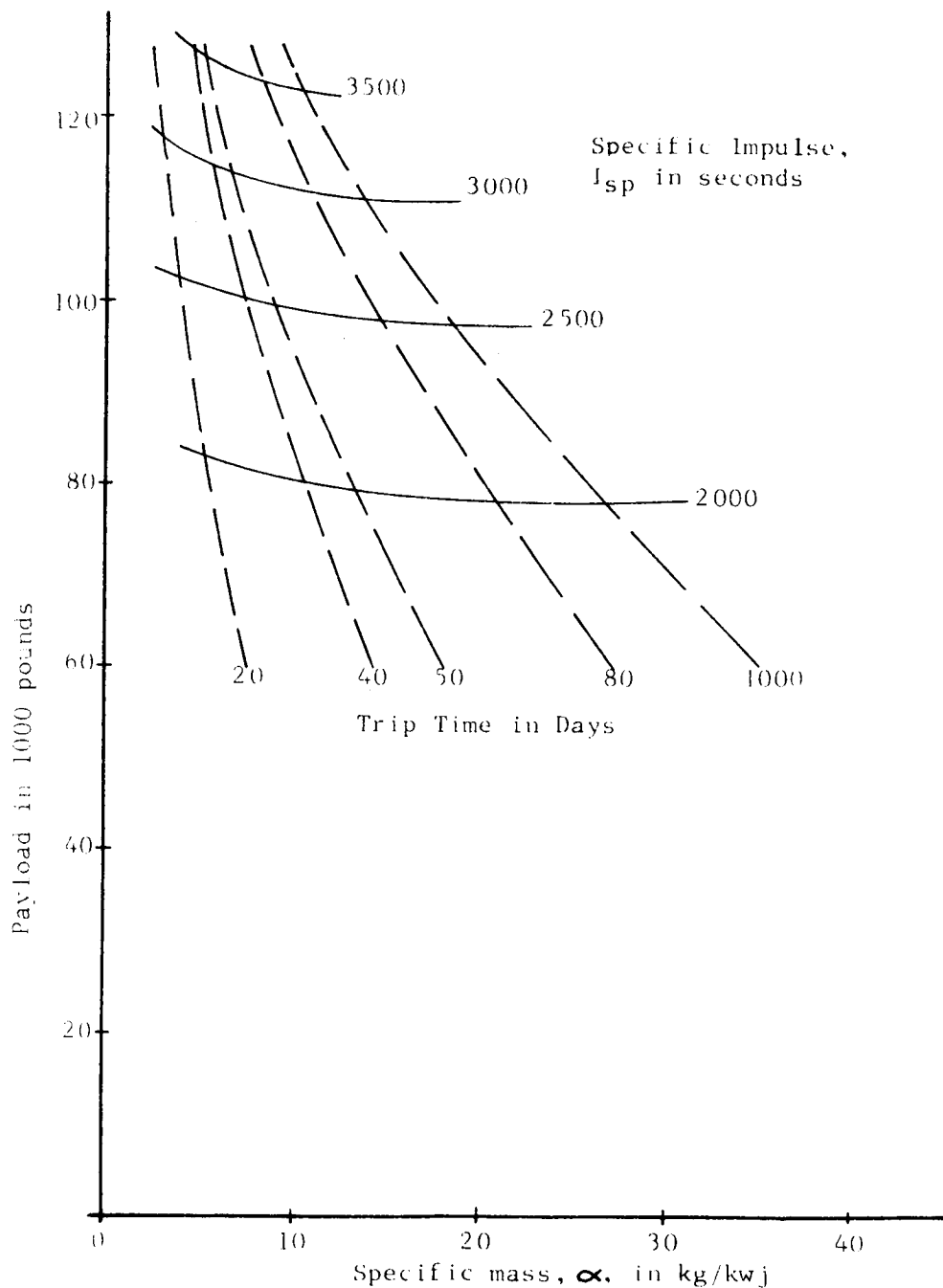ing an invariant characteristic length L(T).

Fig. 5. Payload capacity into lunar orbit for the all-
electric constant-thrust transfer, assuming an
invariant characteristic length L(T).
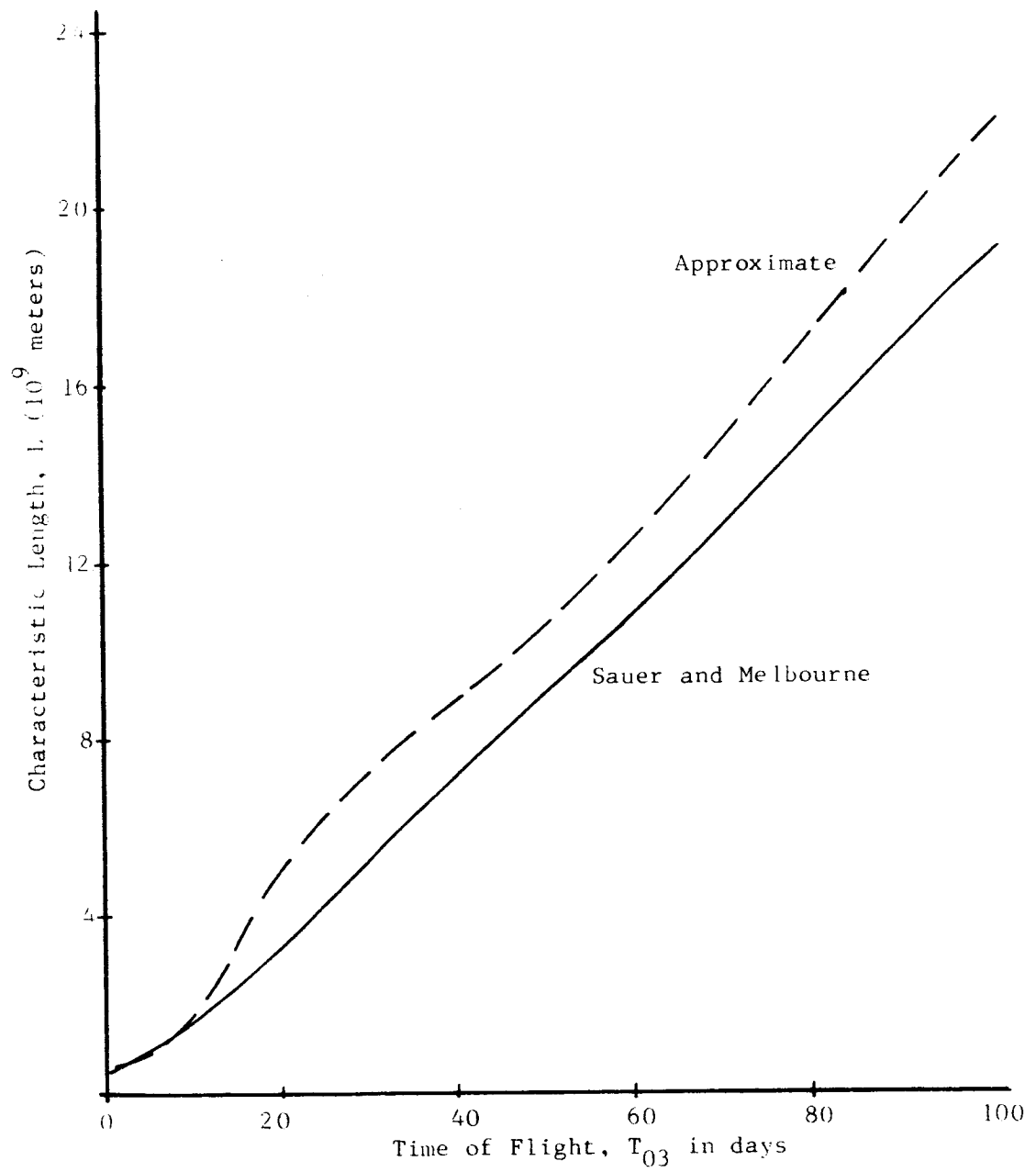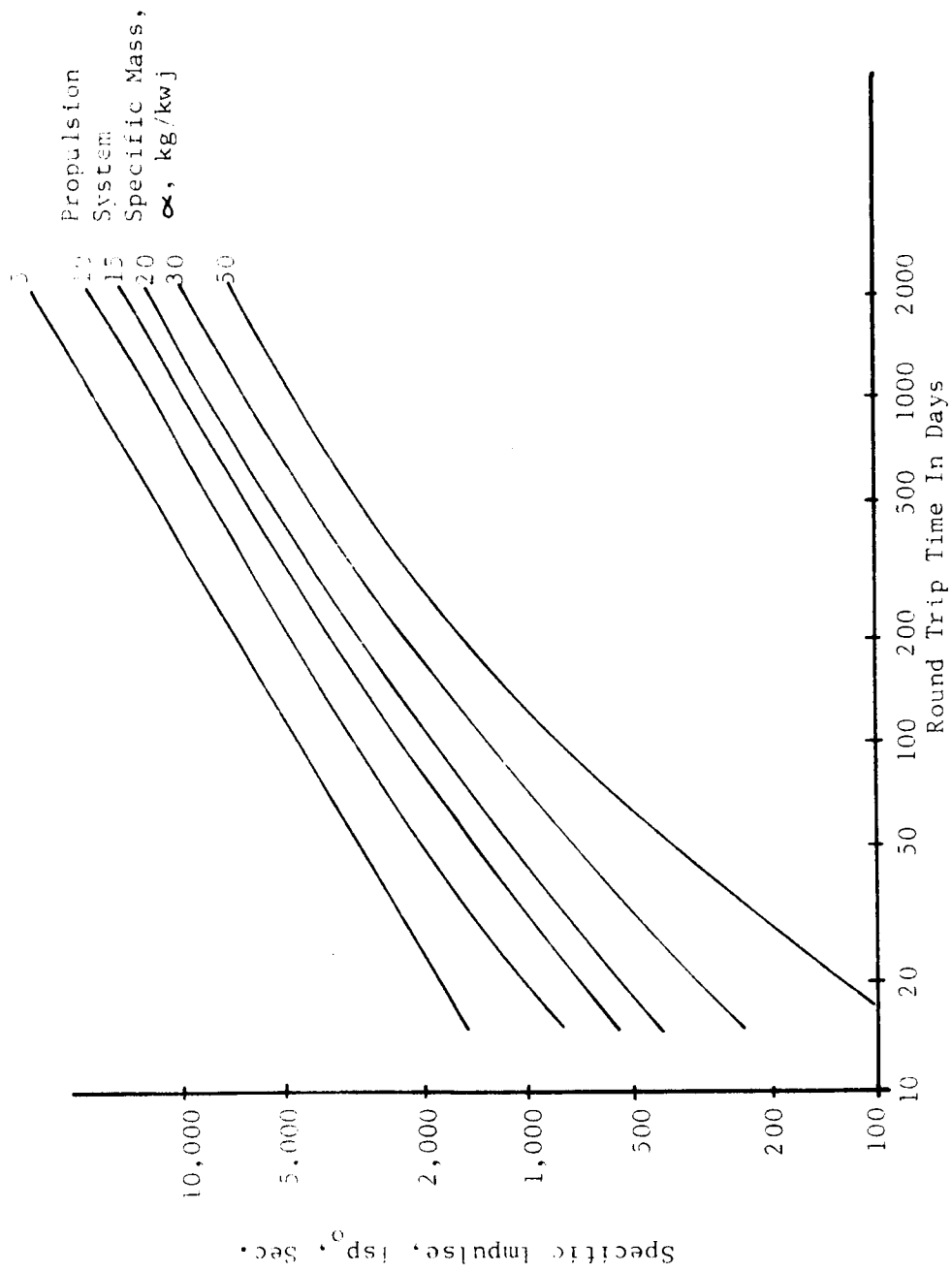
Fig. 6. Comparison of the Zola characteristic lengths for the two techniques.

Fig. 7. Specific Impulse as a function of Round Trip Time for the lunar supply mission.

PROPELLANT FROM SPENT TANKAGE

by W.R. Mickelsen

Spent tankage has been suggested as a possible source of propellant for electric spacecraft[1]. Chemical rocket propellant tanks are expected to be made of aluminum because of the superior fracture resistance of aluminum at cryogenic temperatures[2]. Aluminum melts at 932°K, which is a reasonably moderate temperature for conversion of spent tankage to the vapor state. Aluminum vapor could then be fed into electric thrusters as propellant.

Before investigating the feasibility of aluminum vapor as propellant in electric thrusters, it is necessary to evaluate the improvement in mission performance that would result from the utilization of spent booster tankage. Fortunately a precise evaluation of performance gains can be made in a simple, closed-form analysis which is described in this section.

Payload mass fraction M_{pay}/M_o for electric spacecraft is given by the expression derived by Melbourne[3]:

$$L \equiv \frac{M_{pay}}{M_o} = \frac{1}{1 + \dfrac{M_o}{2P_{j,eff}} J} - \frac{M_{ps}}{M_o} \tag{1}$$

In this expression the following definitions are used:

M_{pay} — mass of payload delivered at terminus of electric-propulsion phase

M_o — total mass of electric spacecraft at beginning of electric propulsion phase, including spent-tankage used as propellant

$P_{j,eff}$ = effective jet power, ie, $P_{j,eff} = F^2/(2\dot{m}_{tot})$, where F is thrust and $\dot{m}_{tot}$ is total rate of propellant consumption

J — $\int_o^{\mathcal{T}} (F/M)\, dt$, where $\mathcal{T}$ is the propulsion duration, and M is instantaneous mass of the electric spacecraft

M_{ps} mass of electric propulsion system

If spent tankage from upper stages of chemical boosters were used for electric-thruster propellant, then the parameter for evaluating mission performance is the payload mass fraction based on electric spacecraft mass not including the spent tankage mass M_{st}. That is, the chemical booster would launch an electric spacecraft of mass $M_o - M_{st}$, and the spent booster tankage would be added to make a total spacecraft starting mass of M_o. This payload fraction L_{st} is defined by:

$$L_{st} = \frac{M_{pay}}{M_o - M_{st}} \tag{2}$$

where M_{st} is the mass of spent tankage which is salvaged for electric-propulsion propellant. By combining equations (1) and (2), the following expression for payload fraction can be written:

$$L_{st} = \frac{1}{\frac{M_o - M_{st}}{M_o} + \frac{M_o - M_{st}}{M_{ps}} \frac{\alpha_{ps}}{2} J} - \frac{M_{ps}}{M_o - M_{st}} \tag{3}$$

where α_{ps} is the propulsion-system specific mass.

Spent tankage mass fraction F can be defined as:

$$F = \frac{M_{st}}{M_o} \tag{4}$$

Propulsion-system mass fraction S can be defined as:

$$S = \frac{M_{ps}}{M_o - M_{st}} \qquad \frac{M_{ps}}{M_o} \frac{1}{1 - F} \tag{5}$$

These mass fractions can be used to simplify equation (3) as follows:

$$L_{st} \qquad \frac{1}{1 - F + \frac{1}{S} \frac{\alpha_{ps}}{2} J} - S \tag{6}$$

This equation can be further simplified by using the Melbourne[3] parameter β:

$$\beta^2 = \frac{\alpha_{ps}}{2} J \tag{7}$$

which results in:

$$L_{st} = \frac{1}{1 - F + \frac{\beta^2}{S}} - S \tag{8}$$

Mass fraction F and the parameter β are fixed by the mission and by the propulsion system specific mass. Propulsion-system mass fraction S can be varied to obtain maximum payload by setting $dL_{st}/dS = 0$ as follows:

$$\frac{dL_{st}}{dS} = \frac{\beta^2/S^2}{(1 - F + \beta^2/S)^2} - 1 = 0 \tag{9}$$

Solving for optimum S:

$$S_{opt} = \frac{\beta(1 - \beta)}{1 - F} \tag{10}$$

and using this expression for S_{opt} in equation (8):

$$L_{st} = \frac{1}{1 - F}(1 - \beta)^2 \tag{11}$$

Maximum payload mass fraction L when spent tankage is not used is derived by Melbourne[3] with the relult:

$$L_{max} = (1 - \beta)^2 \tag{12}$$

The gain in mission performance can be expressed as the ratio of payload mass fractions:

$$\frac{L_{st}}{L} = \frac{1}{1 - F} \tag{13}$$

Melbourne[3] has also shown that when payload is maximized, then the propellant mass fraction M_{pr}/M_o is:

$$\frac{M_{pr}}{M_o} = \beta \qquad (14)$$

Now, it is clear that for maximum payload gain, F should be as near unity as possible in equation (13). However F cannot exceed the propellant mass fraction given by equation (14). Therefore, the maximum payload gain is expressed by:

$$\left(\frac{L_{st}}{L}\right)_{max} = \frac{1}{1 - \beta} \qquad (15)$$

Payload mass-fraction gains calculated from equation (13) are shown in Figure 1.

Fig 1.

Spent-tankage-propellant mass fraction, F
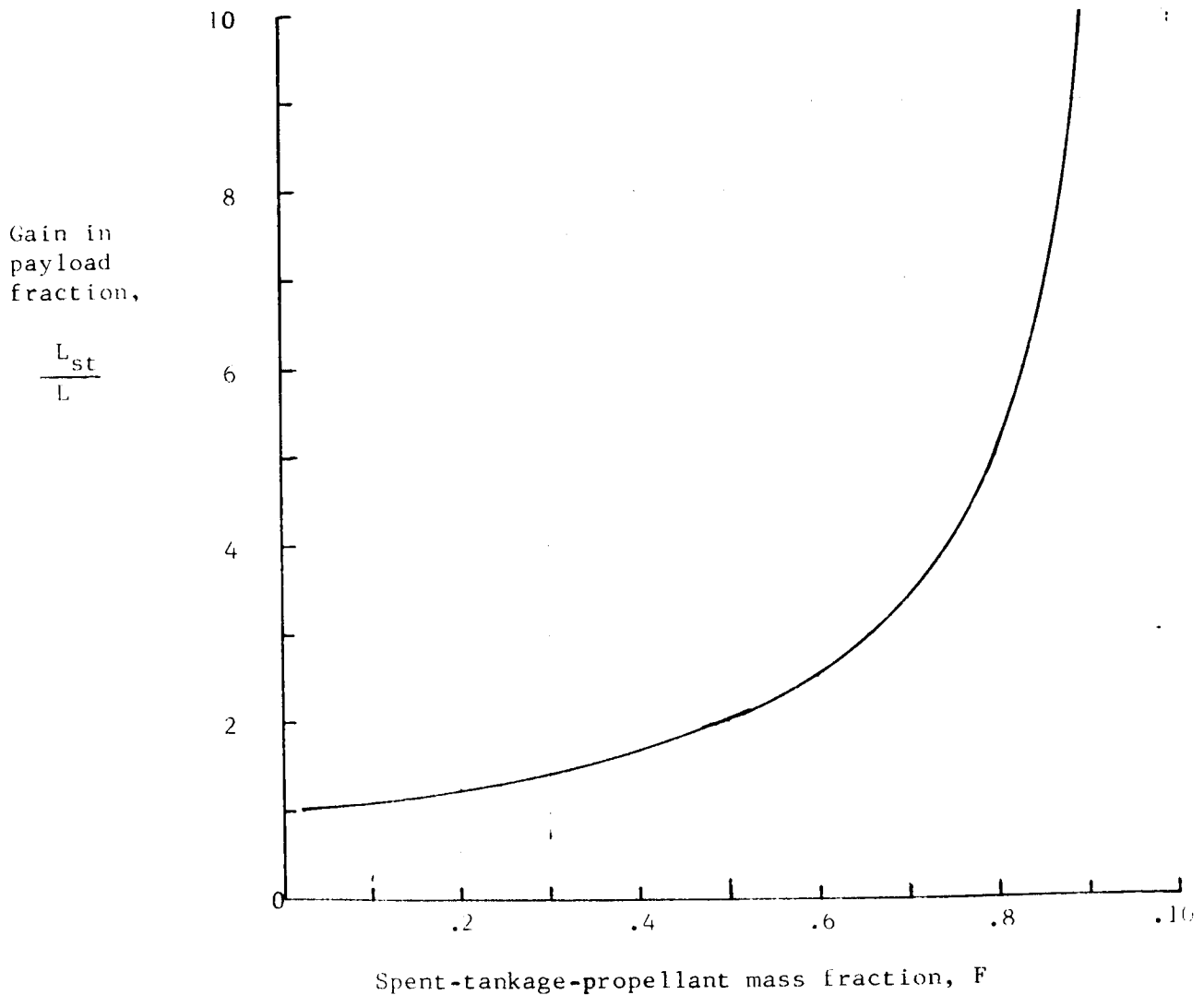
From inspection of Figure 1 it is evident that the greatest gains in payload fraction will occur at the highest values of F, which correspond to the highest values of β. In essence, the observation can be made that payload gains will be the greatest for the more difficult missions (ie, those with the highest values of β).

Dependence on mission difficulty can be illustrated further by noting that equation (11) can be rewritten with the aid of equation (14) for F_{max}:

$$L_{st\ max} = 1 - \beta \qquad (16)$$

This expression is plotted in Figure 2. Together with equation (12) for L.

Fig. 2
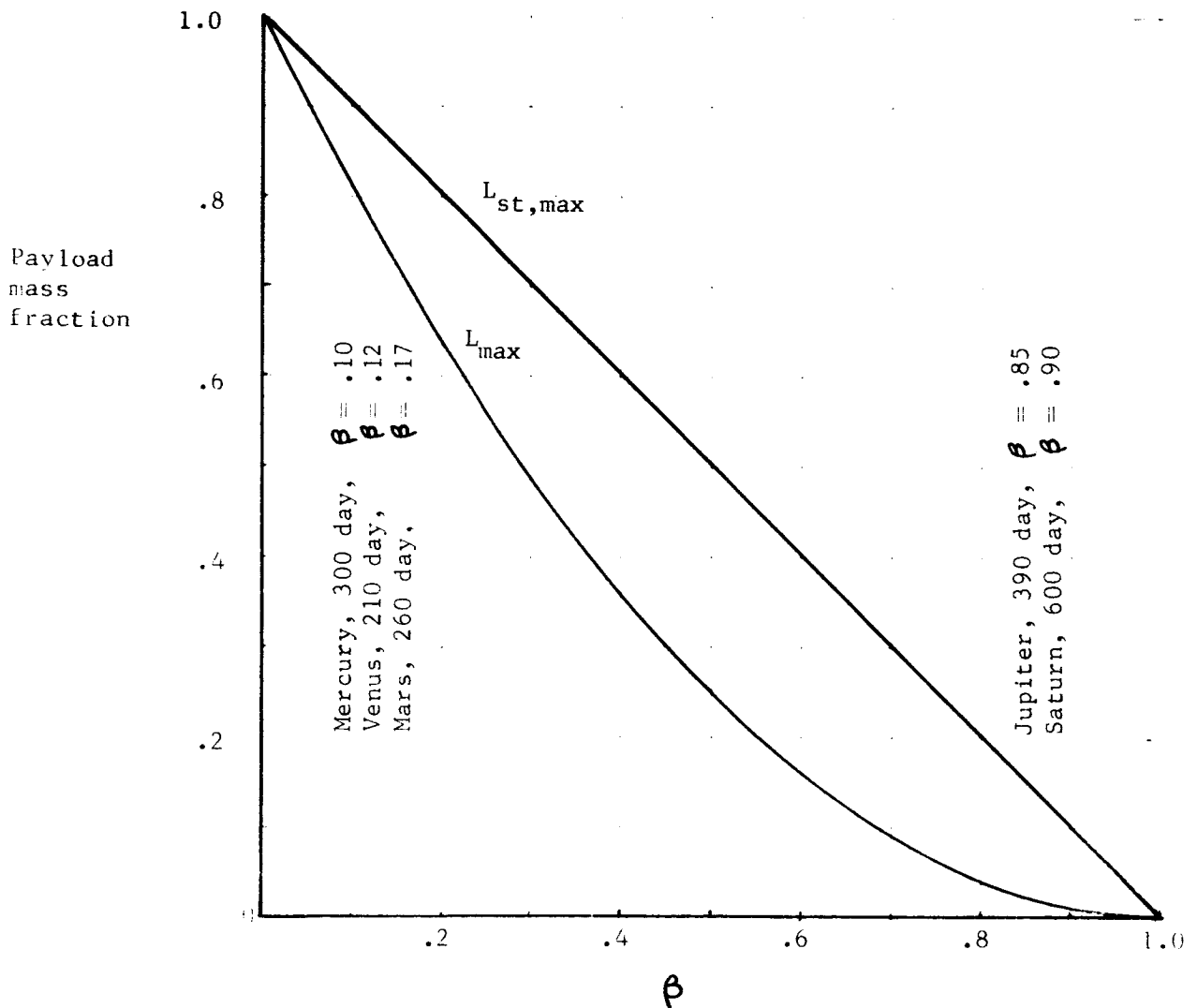
Included in Figure 2 are the approximate locations of β for various heliocentric transfer missions for planetary orbiters with $\alpha_{ps} = 15$ kg/kwj. From this figure it is also evident that the greatest payload gains by use of spent tankage will be for the more ambitious missions.

REFERENCES

1. Mickelsen, W.R.: "Future Trends in Electric Propulsion". AIAA Paper No. 66-595. June, 1966.

2. Johnsen, I.A., and Smith, G.: private communication. NASA Lewis Research Center. April 22, 1966.

3. Melbourne, W.G.: "Interplanetary Trajectories and Payload Capabilities of Advanced Propulsion Vehicles". JPL Technical Report No. 32-68. March, 1961.

ALUMINUM COLLOIDS FROM VAPOR CONDENSATION

A modified version of the Griffin[1] computer program has been developed for the analysis of homogeneous condensation. This program will calculate theoretical values of vapor condensed into colloid droplets, and the size of droplets. The program includes corrections for variation of surface tension with deoplet size and for the change in latent heat of vaporization with temperature. The program is still being de-bugged.

Future work will include an examination of radiative heat transfer, and the definition of a nozzle design for aluminum vapor homogeneous condensation.

COLLOIDS FROM CHEMICAL REACTIONS

by Dr. G.W. Tompkin Jr.

The consideration of preparation of colloid particles by the reaction of vapors is presented here in four parts and appendixes A through D.

Particles having masses between 10^4 and 10^5 amu and having a reasonably narrow size distribution are sought. A particle flux of about 10^{15} particle per square centimeter per second is needed. Both dispersion and condensation methods have been considered. Condensation techniques have been applied to both chemically reacting and non reacting systems. A discussion of studies of others in relation to mission parameters is found in Appendix A.

The study of collimated beams and reactions in collimated beams, which has been enthusiastically revived since World War II, provides enough exper- ience that it has been possible to consider whether such a system can be used to bring fuel to a reaction zone and yield particles. Unfortunately, fluxes that are available in collimated beams are low by a factor of 10^2 to 10^6 and have little likelihood of being increased without a devastating loss in mater- ial transport efficiency. This, coupled with a very low attenuation of one beam as it passes through the other has caused us to abandon this as a possibil- ity.

Discussion of reactive interaction of hydrogen halides and alkali metals is contained in Appendix B. The reactions studied were those which had reaction cross sections among the highest known in molecular beam studies.

Work with modified Sinclair-La Mer generators has demonstrated that silver and alkali halides have been condensed homogeneously and heterogeneously to form solid particles with a narrow size distribution in a particle size range analyzed to be just larger than that desired in this program. The work further suggests

that particles even smaller were produced under certain reaction conditions, but the investigators did not have at hand techniques for the determination of particle size in the smaller size range and therefore did not work extensively to prepare particles in the size range most interesting to us. This experience reported in Appendix C is interpreted as a strong indication that suitable particles can be prepared.

Appendix D begins the study of aluminum as one of the reacting fuels for the production of colloid particles. The choice of oxidizing reactant and reaction conditions will be made from consideration of existing experience. With oxygen as the second fuel component adiabatic temperature rises of about 10,000°C are indicated. Smaller adiabatic temperature rises would be experienced with water or mixtures of water and oxygen. Among the differences between reactive interaction to produce Al_2O_3 and nonreactive condensation of other materials, the following are considered to significantly favor the prospects of producing the desired particles by reactive interaction. (1) The degree of supersaturation achievable by reaction between vapors is orders of magnitude greater than that achieved by adiabatic cooling to induce condensation. (2) The higher temperature particles of small size (50 Å) nucleating at 3000°K will lose heat by radiation at a rate greater than 10^6 cal/g sec. even in a reasonably hot reaction chamber. (3) Both aluminum and water are to some extent waste materials in some orbital situations and might not have to be converted to particles with a mass efficiency as great as required for other fuels. (4) Adjustment of the reacting system to leave only aluminum vapor and aluminum oxide in the product stream facilitates the reduction of residual pressure by condensation.

Program Goals for the Last Half of 1966

The experimental conditions favorable to producing suitable particles by reacting aluminum vapor with oxygen (and water vapor) will be designed.

Appendix A

CHEMICAL FORMATION OF COLLOID-PARTICLES

Introduction

Systems analyses have shown that for certain types of missions (e.g. lunar ferries) a thrustor with a specific impulse in the range of 1000-5000 sec. is needed. Colloid-particle thrustors have promise of high efficiency throughout this range. The development of such thrustors is dependent on the development of adequate techniques for the production of beams of colloid-particles possessing the necessary characteristics. The desired beam would involve particles of about 10-100 Å in diameter (10,000-30,000 amu/e) with narrow charge/mass distribution. Typically the beam should be about 1 inch in diameter, have a particle concentration of 10^{10}-10^{15} particles/cc (producing a beam flux of 10^{17} particles/cm^2-min with the particles possessing a velocity of 10^2-10^7 cm/min), and contain less than about 10^{-6} torr of residual vapor.[1]

In general, techniques of colloid generation fall into two classes: dispersion and condensation. Dispersion techniques include the use of pre-formed particles and electrical spraying of liquids. Condensation techniques include heterogeneous condensation on a cold surface, homogeneous condensation by cooling a condensible vapor in an expansion nozzle, and, most recently, homogeneous condensation by a mixing reaction. In the cooling-condensation approach particles may be charged by electron bombardment or by direct condensation on ions.

W.R. Mickelsen[2] has presented an analysis of the present status of the above mentioned methods of particle formation. The liquid-spray thrustor has the most developed status. Laboratory versions of this thrustor have been operated which achieved thrustor efficiency of 75%. Present techniques, however, are not capable of providing adequately high exhaust-jet power density. Experiments

with pre-formed particles indicate that considerable agglomeration of particles takes place, resulting in particles whose mass/charge ratio is much too high for use in the colloid-thrustor, since exceedingly high acceleration voltages would be required to obtain even the minimum desired specific impulse. As for the expansion-condensation technique, recent theoretical analysis[3] has indicated that less than 50% of the vapor propellant can be condensed into colloid-particles. Information on colloid-particle formation by mixing-reaction was not available for inclusion in the survey.

Methods

Although chemical reaction methods have been used previously for the preparation of sub-micron aerosols, W.G. Courtney and C. Budnik[1] seem to have been the first to apply this method to the preparation of colloid-particles for an electrostatic thrustor engine. Several techniques may be used to produce chemically formed colloid-particles, however, the feasibility of some of these methods for the present application is questionable.

Diffusion burner:[1] The initial work by Courtney and Budnik used a diffusion-flame technique. Mg metal was vaporized in a boiler and passed through a small orifice. Typical propellant flow was 0.54 g/min, consisting of 0.3 g Mg/min and 0.24 g O_2/min, producing a slightly oxygen rich mixture. Chamber operating pressures ranged from 0.1-10 torr. The low pressures produced a large flame (4 inches long and 1-3 inches in diameter at 0.2 torr). At the higher pressures the flame was very close to the burner and a deposit tended to build up. As a compromise, most work was done at 0.2 torr. The diffusion-flame burner used in this investigation is shown in figure 1.

This entire investigation was tentative and no attempt at a detailed analysis of beam characteristics was made, however, the following tentative observations were made. The white color of the MgO deposit was taken as an indication of 100%

utilization of Mg. Total mass utilization efficiency was estimated as 90!% on on the basis of measurements of the pressure drop on the introduction of Mg vapor while O_2 passed through the burner at a constant rate. Electron microscopy indicated particles of less than 100 Å diameter. Actual exhaust velocities were unknown, but nominal velocities were of the order of magnitude of a few times 10^6 cm/min.

For the present application it is necessary to produce charged particles. Of the three techniques available for the ionization of a portion of the Mg vapor stream (electron-bombardment, capillary arc, and duoplasmatron) the duoplasmatron technique in which the Mg vapor is passed through a concentrated arc and an auxiliary negative potential used to extract the positive Mg ions and to repel electrons and negative ions was chosen. On the assumption that all the Mg vapor must condense, the duoplasmatron method possesses a potential for control of the mass/charge ratio of the MgO particles by controlling the per cent of ionization through control of the extractor voltage and Mg mass flow rate. A diagram of the charged colloid-particle generator used by Courtney and Budnik in this investigation is shown in figure 2.

The study indicates the use of a two stage thrustor: a high pressure stage (about 0.2 torr) for the production of the particles and a low pressure stage for their electrostatic acceleration. Problems of beam focusing and removal of residual O_2 received only preliminary examination. Another potential drawback is the considerable power required to vaporize the Mg metal.

Mg wire:[1] As a possible alternative to the diffusion-burner technique discussed above, Courtney and Budnik undertook a study of the feasibility of establishing a particle formation zone at the end of a Mg wire.

The Mg wire was fed continuously into the vacuum chamber by a friction

feed mechanism. The wire was surrounded by an O_2 sheath and ignited by a low voltage discharge between the wire and an anode. An environmental pressure of 0.2 torr and a Mg mass feed rate of about 1.5 g/min provided steady combustion, producing a flame approximately ½ inch long and ½ inch wide.

Possible advantages of this method include: 1) continuous, long-duration propellant feed, 2) elimination of the Mg vaporizer heating requirements, and 3) possible auto-ionization of the Mg by migration of electrons from the wire to the anode--this would eliminate the need for an external ionizer and the attendant power requirement.

At the time of the publication cited, no attempt at an examination of the characteristics of a beam thus produced had been made.

High-intensity arc: The Mg wire technique described above suggests the possible applicability of a high-intensity arc technique. Use of high-intensity arcs to produce submicron particles has been described by J.D. Holmgren, J.O. Gibson, and C. Sheer[4] (See also: Secondary reference 11).

The high-intensity arc is characterized by the fact that most of the arc input energy is transferred to the anode. This results in heating of the anode to temperatures in the range of 7000°K and rapid vaporization of the anode material. The tail flame which is formed issues as a well defined, unidirectional plasma jet.

As described in the reference cited, the arc was operated at an ambient pressure of 1 atmosphere, however, it is indicated (See also: Secondary reference 11) that the method would be applicable at reduced pressures. At present, particles of metals, oxides, and carbides have been produced. Typical particle sizes obtained were in the range of 100-1000 Å in diameter, but it is suggested, and some experimental evidence is given, that increasing the quenching rate by injecting cold gas into the flame will significantly reduce particle size.

Operation would be similar to the above described Mg wire technique, except that the metallic propellant to be particulated would form the anode. Another possible modification is the introduction of the O_2 at right angles to the flame rather than coaxially.

<div align="center">BIBLIOGRAPHY</div>

Primary References:

1. Courtney, W.G. and C. Budnik: "Colloid Propulsion Using Chemically-Formed Particles." AIAA Paper No. 66-254. March, 1966.

2. Mickelsen, W.R.: "Colloid-Particle Electrostatic Thrustors." Paper presented at the DGRR Sonnenberg Symposium on Electric Propulsion, Braunschweig, West Germany. February 24, 1966.

3. Goldin, D.S. and G.L. Kvitek: "An Analysis of Particle-Formation Efficiency in a Colloid Thrustor." AIAA Paper No. 66-253. March, 1966.

4. Holmgren, J.D., J.O. Gibson, and C. Sheer: "Some Characteristics of Arc Vaporized Submicron Particulates." in Ultrafine Particles, W.E. Kuhn ed.-in-chief, John Wiley and Sons, Inc., New York, (1963) pp. 129-145.

Secondary References (pertinent references not directly cited in the paper)

1. Mickelsen, W.R. and H.R. Kaufman: "Status of Electrostatic Thrustors for Space Propulsion." NASA TN D-2 72. May, 1964. (Indicates comparative advantages and disadvantages of methods of particle formation on basis of experiments to that date)

2. Singer, S., N.G. Kim, and M. Farber: "An Experimental Study of Colloidal Propulsion Using Submicron Solid Particles." AIAA Paper No. 63-052, 1963. (Pre-formed Particles)

3. Norgren, C.T.: "Onboard Colloidal Particle Generator for Electro-static Engines." ARS Paper No. 2380-62, 1962. (Homogeneous conden-sation in an expansion nozzle)

4. Goldin, D.S. and C.T. Nogren: "Thrust Measurements of Colloidal Par-ticles as an Indication of Particle Size and Thrustor Operation." AIAA Paper No. 63-050. 1963.

5. Norgren, C.T. and D.S. Goldin: "Experimental Analysis of the Exhaust Beam from a Colloidal Thrustor." AIAA Paper No. 64-674. August, 1964. (Use of quadrupole mass spectrometer to analyze exhaust for beam char-acteristics)

6. Cohen, E., C.J. Somol, and D.A. Gordon: "A 100-kv, 10-w Heavy-Particle Thrustor." AIAA Paper No. 65-377. July, 1965. (Liquid-spray colloid thrustor)

7. Gignoux D., et. al., Cosmic, Inc., Rept. No. 82. October 1964. (Liquid-spray thrustor)

8. TRW, Space Technology Laboratory: "Research on Charged Colloid Generation." APL TDR 64-75. June, 1964. (Liquid-spray thrustor)

9. Hornstein, B.: "The Generation of Charged Colloids...." Thiokol Chemical Corporation, Reaction Motors Division, 2049-F. March, 1964. (Condensa-tion onto a cold surface)

10. Cox, A.L.: "Toward Colloid Propulsion." Astronautics, June, 1962. p.56.

11. Sheer, C. and S. Korman: Arcs in Inert Atmospheres and Vacuum, W.E. Kuhn, ed., John Wiley and Sons, Inc., New York, (1956) pp. 169-183.
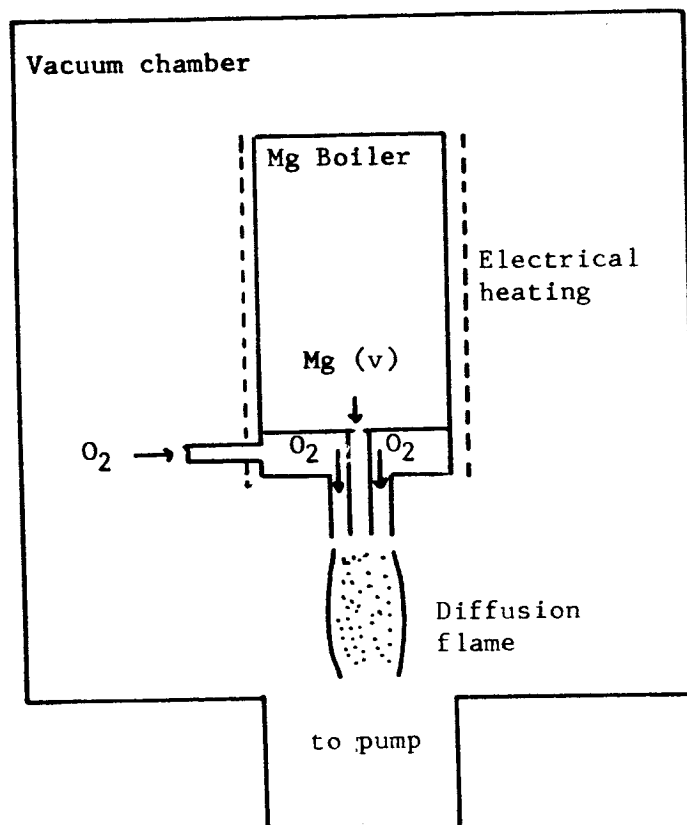
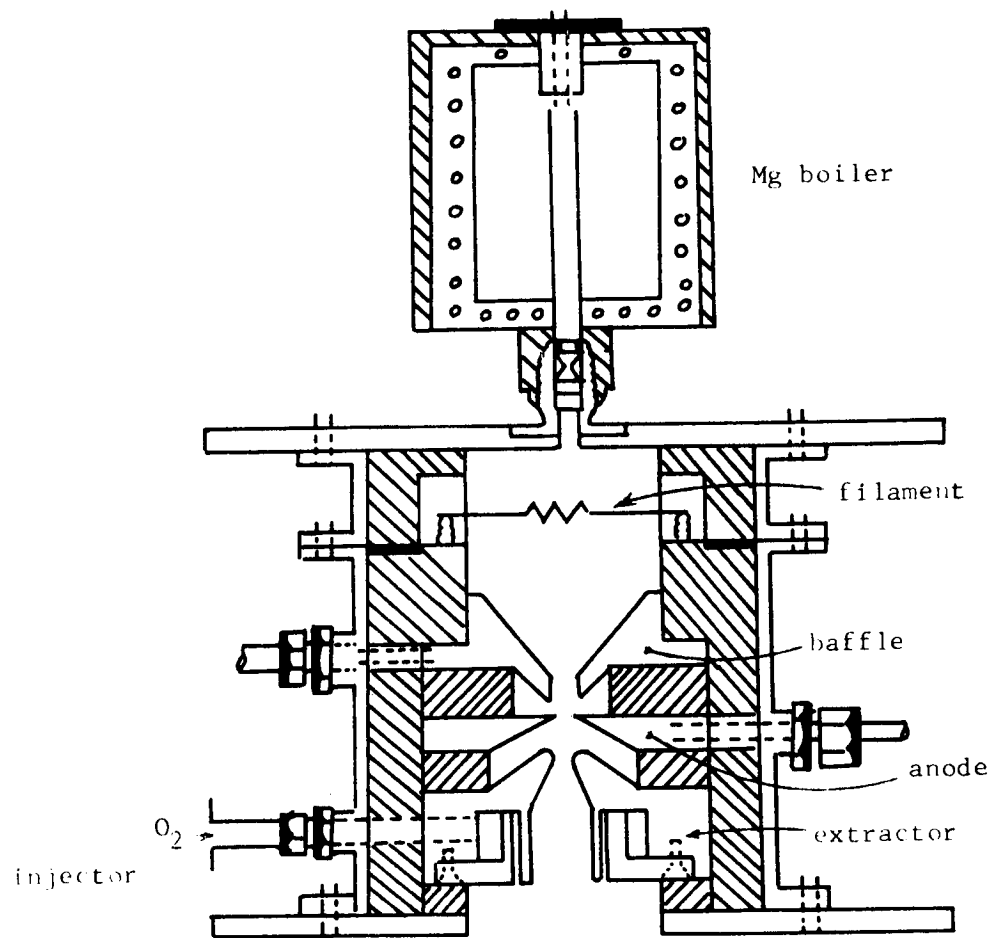Fig. 1. Mg(v)-O_2 Diffusion-Flame Burner.

Fig. 2. Charged-Particle Generator.

Appendix B

CHEMICAL REACTION IN CROSSED MOLECULAR BEAMS

Beginning with the work of Taylor and Datz[1] in 1955, considerable study has been done on chemical reaction kinetics using molecular beam techniques. With the technological background available and with the similarity of conditions in which molecular beam studies are carried out to the vacuum of space, the molecular beam technique seemed promising as a source of colloid particles for an electrostatic thrustor.

The class of reactions which has been most widely studied is that of the alkali metals with halogen compounds. Two major factors have contributed to the interest shown in this type of reaction: 1) large reaction cross sections and 2) availability of suitable detection devices. Even prior to the application of the molecular beam technique, the flame studies of Polanyi[2] had demonstrated that these reactions had very large cross sections, even larger than "hard sphere" values. Recent work by Wilson et. al.[3] has indicated a cross section > 100 Å^2. The Langmuir surface ionization gauge with a tungsten filament has been widely used for the detection of beams of alkali metals and their halides. However in most cases ionization efficiencies of tungsten for the metals and their halides are too nearly equal to permit differentiation. In contrast it has been found that platinum or an alloy of 92% platinum and 8% tungsten will ionize the metals quite well while having a poor efficiency for the halides. Taylor and Datz have used this characteristic to develop a sensitive differential ionization gauge detector[1,4,5].

The standard molecular beam source is an effusive oven. The maximum beam flux realizable from such a source is limited by the effusion rate through the oven slit which is governed by the necessity of keeping the mean free path of the

molecules in the oven larger than the smallest dimension of the slit, and by geometrical considerations involved in collimation of a beam from random initial velocities. Thus the only feasible way to increase beam flux is to increase the oven temperature and this gain is limited by the fact that the gain in intensity is proportional only to the one-half power of absolute temperature. Herschbach[6] has reported that "even for alkali atom reactions, in a typical crossed beam experiment the yield at the peak of the angular distribution corresponds to only a monolayer of product molecules per month."

In 1951 Kantrowitz and Grey[7] proposed the use of supersonic rather than effusive flow into the first defining orifice. The original Kantrowitz and Grey proposal was to replace the oven slit with a miniature De Laval nozzle. Subsequent work by Becker and Bier[8] and others has shown that a simple converging nozzle accomplishes the same ends. The gain in intensity arises from two considerations. In passing through the nozzle the kinetic energy of random motion of the molecules or atoms is transformed, at least in part, into kinetic energy of ordered motion, resulting in a larger molecular flux passing through a unit area of the first aperture than for the corresponding oven source. This gain, however, can never be large. More importantly, because of the larger ordered motion and smaller random thermal motion, the spatial intensity distribution of the beam is elongated along the direction of mean motion rather than in a cosine distribution as is the case with the oven source, and consequently a larger fraction of the molecules passing through the first aperture pass through the collimating aperture than with a conventional source. In addition, the use of a nozzle source results in a narrower velocity distribution.

Later evaluation of the theory in the light of experimental studies has led Zapata et. al.[9] to predict that beam fluxes of 10^{18} molecules/cm^2-sec are possible. Indeed, Scott and Drewry[10] report having attained a flux of 10^{17} molecules/cm^2-sec

with nitrogen, while Campargue[11] has reportedly obtained a flux of 10^{19} molecules/cm^2-sec at the collimating orifice using hydrogen, but most workers report maximum fluxes of 10^{14}-10^{16} molecules/cm^2-sec.

In order to satisfy mission parameters for the electrostatic thrustor, a usable flux of 10^{17} particles/cm^2-sec of diameter 10-100 Å is required. This beam must be sufficiently well defined that uniform particle acceleration be possible. The fluxes discussed above are for uniform, unscattered beams. Taylor and Datz[1] have shown that in spite of the high reaction cross section for alkali metal-halogen compound reactions, the collision yield for the reaction K + HBr$\rightarrow$KBr + H in a molecular beam is 1-3 X 10^{-3}, and Herschbach[6], studying the reaction CH_3I + K$\rightarrow$KI + CH_3 finds a collision yield of 5 X 10^{-4}. Attenuation due to other factors, e.g. failure to react upon collision (Herschbach's studies indicate that for K + HBr$\rightarrow$KBr + H about 10% of the collisions will not produce reactions.) and losses in collimation and through beam expansion after collimation could very possibly reduce the realized product intensity by another factor of 10. Thus starting with a reactant flux of 10^{18} molecules/cm^2-sec, the realized product flux would probably be of the order of 10^{14} molecules/cm^2-sec. This value does not appear unreasonable since nozzle sources in general are capable of producing fluxes 100-1000 times greater than comparable oven sources and Taylor and Datz[1] report a peak KBr flux of about 10^{10} molecules/cm^2-sec using a conventional source. Nevertheless, this flux is too low to satisfy mission parameters.

BIBLIOGRAPHY

1. Taylor, E.H. and S. Datz: "Study of Chemical Reaction Mechanisms with Molecular Beams. The Reaction of K with HBr." Journal of Chemical Physics, 23, September, 1955. pp. 1711-1718.

2. Polanyi, M.: Atomic Reactions, Williams and Norgate, London. 1932.

3. Wilson, K.R., G.H. Kwei, J.A. Norris, R.R. Herm, J.H. Birely, and D.R. Herschbach: "Reactive Scattering in Molecular Beams: Evidence for a Stripping Mechanism in Reactions of Alkali Atoms with Halogens." Journal of Chemical Physics, 41, August 1964. pp. 1154-1156.

4. Datz, S. and E.H. Taylor: "Ionization on Platinum and Tungsten Surfaces. 1. The Alkali Metals." Journal of Chemical Physics, 25, September, 1956. pp. 389-394.

5. Datz, S. and E.H. Taylor: "Ionization on Platinum and Tungsten Surfaces. 11. The Potassium Halides." Journal of Chemical Physics, 25, September, 1956. pp. 395-397.

6. Herschbach, D.R.: "Reactive Collisions in Crossed Molecular Beams." Discussions of the Faraday Society, 33, 1962. pp. 149-161.

7. Kantrowitz, A. and J. Grey: "High Intensity Source for the Molecular Beam, Part I, Theoretical." Review of Scientific Instruments, 22, May, 1951. pp. 328-332.

8. Becker, E.W. and K. Bier: "Die Erzeugung eines intensiven, teilweise monochromatisierten Molekularstrahles mit einer Laval-Düse." Zeitschrift für Naturforschung, 9a, 1954. pp. 975-986.

9. Zapata, R.N., H.M. Parker, and J.H. Bodine: "Performance of a Supersonic Molecular Beam." Rarefied Gas Dynamics (Proceedings of the Second International Symposium) L. Talbot, ed., Academic Press, New York. (1961) pp. 67-81.

10. Scott, J.E. Jr. and J.E. Drewry: "Characteristics of Aerodynamic Molecular Beams." Rarefied Gas Dynamics (Proceedings of the Third International Symposium, Volume I) J.A. Laurmann, ed., Academic Press, New York (1963) pp. 516-538.

11. Campargue, R.: "High Intensity Supersonic Molecular Beam Apparatus." Rarefied Gas Dynamics (Proceedings of the Fourth International Symposium, Volume II) J.H. de Leeuw, ed., Academic Press, New York (1966) pp. 279-298.

Appendix C

PRODUCTION OF ALKALI-HALIDE AEROSOLS

IN MODIFIED SINCLAIR-LA MER GENERATORS

Both Matijevic' et. al.[1,2,3] at Clarkson College and Fuchs and Sutugin[4]
at the Karpov-Institute of Physical Chemistry report the preduction of aero-
sols of alkali halides of narrow size distribution using modifications of the
Sinclair-La Mer generator.[5]

In June of 1960 Matijevic', Kerker, and Schulz[1] reported a study of the pro-
duction of aerosols of AgCl consisting of spherical particles of relatively
narrow size distribution (standard deviation from mean radius of 20-25%).
The generator is shown schematically in figure 1. AgCl was evaporated from
the combustion boat (4) in the boiler furnace (1) and then allowed to condense
in the reheater (2), the temperature of which regulated the cooling rate and
hence particle size. Temperatures used were in the range of 850-1100°C and
were controlled to $\pm$ 1°C by Variac resistors and monitored by a chromel-alumel
thermocouple in connection with a portable potentiometer. Helium gas from a
cylinder was used as the aerosol carried. When producing the smallest particles
studied, it was necessary to dilute the aerosol using helium from the dilution
line (9) to prevent agglomeration. Collection for particle size distribution
counts was made either by direct impingement on cooled microscope slides to
which electron microscope grids had been affixed or by thermal precipitation
Both methods gave comparable size distributions (see figure 2a) nor was the dis-
tribution affected by the length of time of collection (see figure 2b). If con-
stant experimental conditions were maintained, reproducibility of distribution
was good. The particles studied here ranged from 50-10,000 Å in radius.

In 1963 Matijević, Epenscheid, and Kerker[2] prepared NaCl aerosols using the generator previously described (figure 1). Temperature ranged from 820-1000°C and carrier (He) flow rates from 0.5-5 l./min. The smallest particles had diameters at least as small as the resolving power of the electron microscope used (~30 Å) and they stated that there appeared to be no apparent reason that smaller particles could not be prepared.

In 1964 Epenscheid, Matijević, and Kerker[3] prepared NaCl aerosols by vapor condensation of NaF nuclei. The apparatus is shown schematically in figure 3. Sublimation of the NaF in 1/a produces the nuclei for condensation which takes place above the combustion boats 4b and 4c containing NaCl. Under some conditions aerosols could be produced using only 4a and 4b. Particles formed when two NaCl furnaces were used were larger than those formed using only one furnace, but were generally of narrower size distribution. The NaF nuclei were too small to show a detectable Tyndall cone at 6a or to be observed in an electron microscope (resolving power 35 Å). Reproducibility was good after two precautions had been taken. The thermocouple tended to corrode and provide undesired condensation nuclei. As a remedy the temperature was calibrated against a power stat and then the generator operated without the thermocouple. The calibration was checked periodically. Recharging of the NaF produced fluctuations in particle size which disappeared after several days of continuous operation. As a result the NaF furnace was run continuously. Evaporation loss was low since the temperature was 150° below the melting point. Particle size distribution was determined by the polarization ratio method[6,7,8]. Results agreed well with electron microscopy. Figure 4a shows a typical frequency distribution while 4b shows the distribution of the two most divergent sets of data from 13 experiments run under the same conditions. Three factors govern particle size: 1) temperature (increasing temperature increases particle size) 2) flow rate (increasing flow rate

decreases particle size) and 3) nuclei dilution (particle size increases with dilution of nuclei). Thus particle size can be closely controlled. An explanation is given for the narrow distribution as a result of the presence of foreign nuclei. Provided the role of cooling is not too great, the vapor condenses uniformly in the presence of foreign nuclei. Without the foreign nuclei, a degree of supersaturation builds up which is so high that it cannot be relieved by growth to the existing nuclei, and as cooling proceeds fresh nucleation takes place resulting in a broad distribution of the final size spectrum.

The aerosols prepared by Fuchs[4] were of somewhat smaller particle size (7Å, 9.7Å, 1.18Å). His apparatus is shown in figure 5. The aerosols were monodisperse and exhibited a standard geometric deviation of less than 1.26.

The NaF-NaCl aerosols of Epenscheid et. al.[3] had a particle concentration of 10^4-10^5 particles/ml at a flow rate of 1 l./min.

BIBLIOGRAPHY

1. Matijevic', E., M. Kerker, and K.F. Schulz: "Light Scattering of Coated Aerosols:1 scattering by the AgCl cores." Discussions of the Faraday Society, 30, 1960. pp. 178-184.

2. Matijevic', E., W.F. Epenscheid, and M. Kerker: "Aerosols Consisting of Spherical Particles of Sodium Chloride." Journal of Colloid Science, 18, January, 1963. pp. 91-94.

3. Epenscheid, W.F., E. Matijevic', and M. Kerker: "Aerosol Studies by Light Scattering:III Preparation and Particle Size Analysis of Sodium Chloride Aerosols of Narrow Size Distribution." Journal of Physical Chemistry, 68, October, 1964. pp. 2831-2842.

4. Fuchs, N.A. and A.G. Sutugin: "Generation and Investigation of High-

dispersed Sodium Chloride Aerosols." <u>British Journal of Applied Physics,</u> 14, 1963, pp. 39-42.

5. Sinclair, D. and V.K. La Mer: "The Production of Monodisperse Aerosols." <u>Chemical Reviews</u>. April, 1949. p. 261.

6. Kerker, M., E. Daby, G.L. Cohen, J.P. Kratohvil, and E. Matijević: "Particle Size Distribution in La Mer Sulfur Sols." <u>Journal of Physical Chemistry</u>. 67, 1963. p. 2105.

7. Kerker, M., E. Matijević, W.F. Epenscheid, W.A. Farone, and S. Kitani: "Aerosol Studies by Light Scattering: I. Particle Size Distribution by Polarization Ratio Methods." <u>Journal of Colloid Science</u>. 19, 1964. p. 213.

8. Matijević, E., S. Kitani, and M. Kerker: "Aerosol Studies by Light Scattering: II. Preparation of Octanoic Acid Aerosols of Narrow and Reproducible Size Distribution." <u>Journal of Colloid Science</u>. 19, 1964. p. 223.

1. Boiler furnace

    heavy duty hinge type combustion furnaces
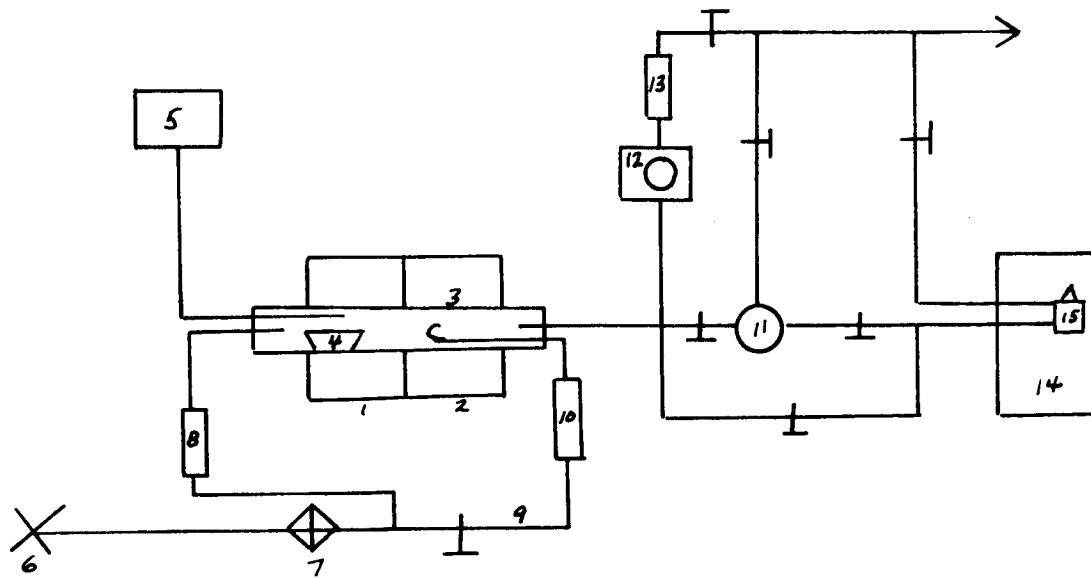
2. Reheater furnace

3. Silica combustion chamber

4. Silica combustion boat

5. Thermocouple and potentiometer

6. Helium source

7. Fritted Pyrex disc filter

8,10,13. Flowmeters

9. Dilution line

11. Viewing chamber (three-necked flask)

12. Thermopositor collector

14. Light scattering equipment

15. Light scattering cell

Figure 1

2A

2B
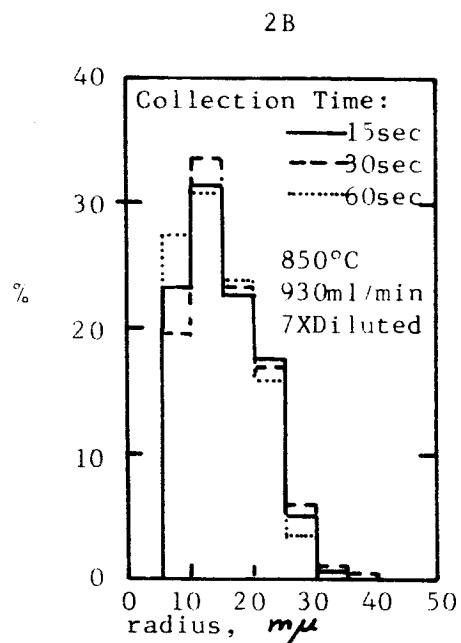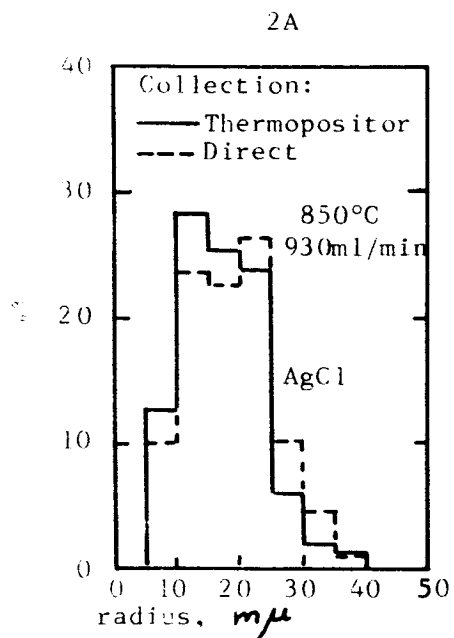
Fig. 2. Effect of the type of the aerosol collection (left)
and the collection time in thermopositor (right) on
the particle size distribution of silver chloride
aerosols.
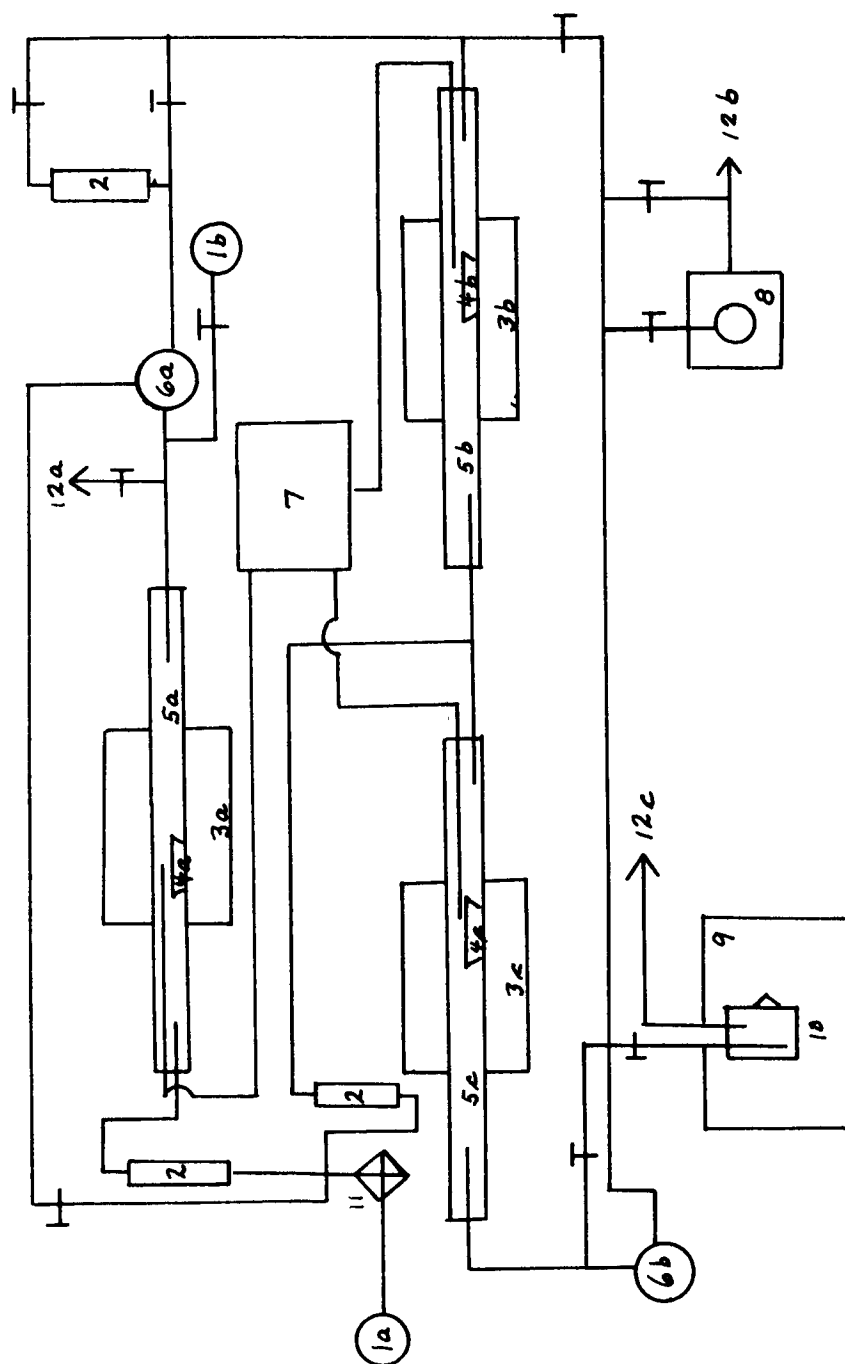
Figure 3.

1. a,b. He sources
2.   Flowmeters
3. a,b,c. Combustion furnaces
4. a,b,c. Combustion boats
5. a,b,c. Combustion tubes
6. a,b.   Viewing chambers (three-necked flasks)

7.   Potentiometer
8.   Thermopositor
9.   Light scattering photometer
10.   Light scattering cell
11.   Gas filter (fritted Pyrex glass, grade F)
12. a,b,c. Exhausts

Fig. 4a

Fig. 4b

Insulating asbestos layer
Nichrome heating coil
Clay layer
       (to increase thermal inertia)
Thick-walled stainless steel tube
Filtered N_2 (100-200 cc/min)

Ceramic rings, wetted
with NaCl solution and dried

Filtered air
(10-18 l/min)   Superheater,
Nichrome coil
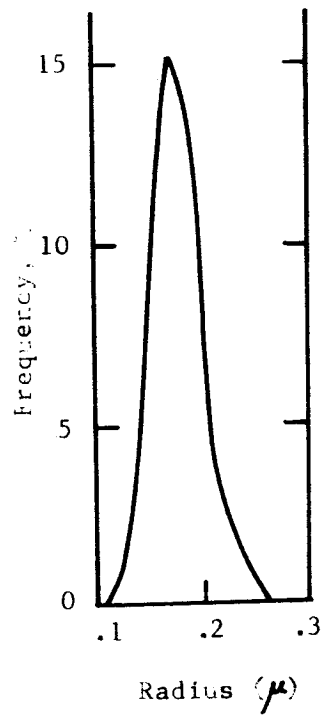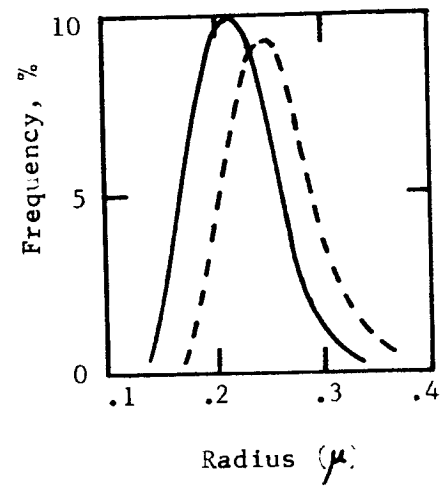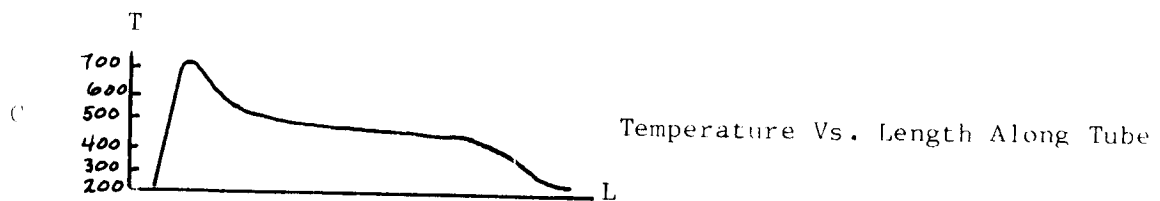
T

700
600
500
400
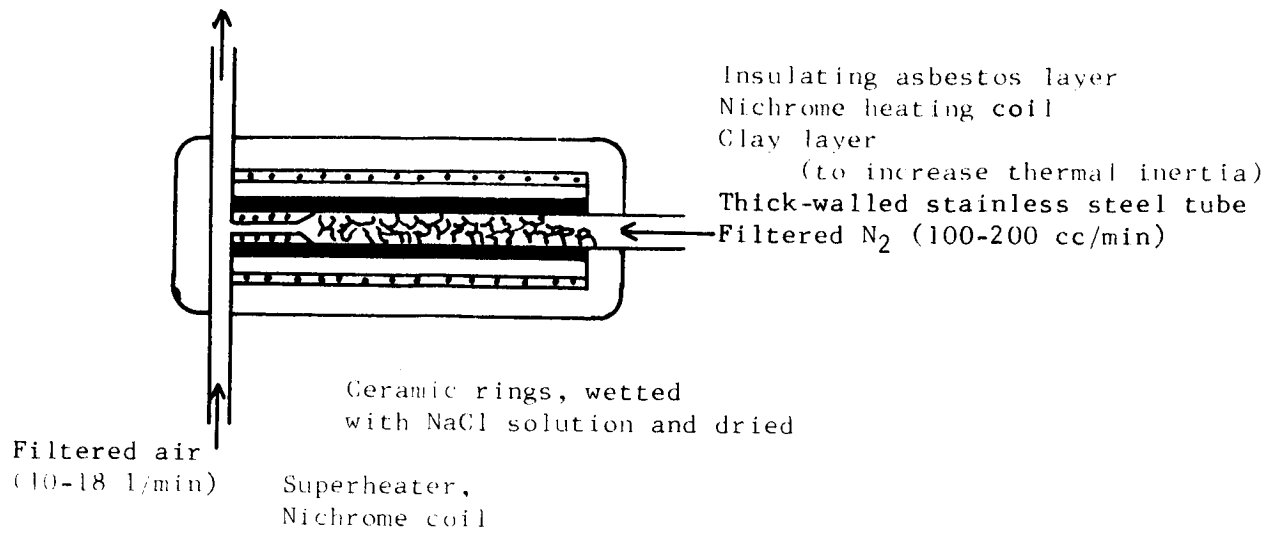300
200

C

L

Temperature Vs. Length Along Tube

Figure 5

Appendix D

HOMOGENEOUS CONDENSATION BY CHEMICAL REACTION TECHNIQUES

by Seong Woo Shin

1. INTRODUCTION

Past approaches to the particle formation can be divided into two general techniques, dispersion and condensation. Dispersion techniques include using preformed particles and electrical spraying of liquid. Condensation techniques include heterogeneous condensation onto a massive cold surface and homogeneous condensation by cooling a condensible vapor in an expansion nozzle.

Presently research on colloid particle formation is being done by W.G. Courtney, Thiokol Chemical Corporation[1], utilizing a chemical reaction between Mg and O_2 vapors in an evacuated system (about 1 Torr pressure). It has been shown in these experiments that a colloid particle formation efficiency of 90% can be obtained in the Mg-O_2 system. This new technique has several features which appear attractive in the application to colloid thrustors, including flexibility, a high mass utilization (particle formation efficiency), and the ability to use a variety of chemical reactions. The study of this new field seems to be very promising for the future use of colloid thrustors in the area of space propulsion.

This report is concerned with the theoretical analysis of homogeneous condensation in Al-O_2 and Al-Cl_2 systems. In the development of the theory, the physical apparatus used is similar to that of reference 1.

2. SELECTION OF CHEMICAL REACTIONS

This new approach involves three steps: (1) high velocity vapor streams of two materials are formed, (2) part of the material in one of the streams is

ionized, (3) the two streams are then mixed and allowed to chemically react to form charged colloid particles. High accelerating voltages require stable charged colloid particles in order to avoid, (1) field emission from the particles, and (2) particle fragmentation due to electrical stresses. Polarization of a particle by the external field will lead to a high local concentration of charge on the surface of the particle, which in turn will tend to give field emission of electrons, unless the ionic work function of material is high. Fragmentation due to polarization can be minimized if the particles are held together with strong intermolecular forces. Finally, it is important to select a chemical reaction that goes quickly to completion. Otherwise, the utilization efficiency will be lowered because of the uncondensed gas. The desired properties of end-product particles are; (1) a low polarizability,(2) strong intermolecular forces, (3) high ionic work function. The chemical reaction must also have a high negative value of Gibbs free energy change $(-\Delta G)$ to meet the spontaneity of the reaction.

Evaluation of the following properties is necessary for the proper selection of chemical reactions: (1) Polarizability, (α), which is a constant characteristic of a particle and defined as the dipole moment produced by an applied field of unit strength. That is:

$$m \quad \alpha E_o \tag{1}$$

where $m =$ dipole moment

$\alpha =$ polarizability

$E_o =$ electric field applied

The dipole moment is also related to the electronegativity[2] difference between the two atoms in the particle.

atoms	electronegativity difference
Al-O	2.0
Al-Cl	1.65

Therefore, Al_2O_3 and $AlCl_3$ have comparatively low polarizabilities.

(2) Intermolecular forces. The energy of vaporization of a liquid provides a convenient measure of the strength of these forces. The energy of vaporization is simply related to the heat of vaporization of liquid at constant pressure:

$$Q_{vap} = \Delta H_{vap} = \Delta E_{vap} + P\,(\overline{V}_{gas} - \overline{V}_{liq})$$

Approximately $\overline{V}_{gas} - \overline{V}_{liq} \cong \overline{V}_{gas} = \dfrac{RT}{P}$

$$\Delta H_{vap} = \Delta E_{vap} + RT_b$$

By the Trouton's Rule $\Delta H_{vap} = T_b \Delta S_{vap} = 21\, T_b$ for normal liquids; hence

$$\Delta E_{vap} \approx 19\, T_b \quad cal/mole \tag{2}$$

In view of equation 2, the boiling point of a liquid may be taken as a convenient measure of the cohesive energy which in turn depends upon the strength of the intermolecular forces. The Al_2O_3 has a high boiling point, approximately 3300°C[3]. However, this temperature is uncertain due to the tendency of Al_2O_3 to decompose at high temperatures. The boiling point of $AlCl_3$ is very low, 180°C. Therefore, Al_2O_3 has strong intermolecular forces. (3) Ionic work function. An electron may be extracted from the surface of a particle by any electric field which is sufficiently strong to overcome the potential barrier. The ionic work function is generally determined experimentally using the following equation:

$$I = AT^2 \exp(-e\,\varphi/kT) \tag{3}$$

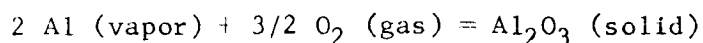where k = Boltzmann constant φ = work function

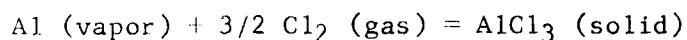 A = numerical constant I = electric current

From the experimental data, ($\ln I - 2\ln T$) is plotted as a function of $1/T$ to obtain a straight line. The quantity $e\varphi$ is determined from the slope of this curve. A literature survey on this subject shows that as yet, no theoretical method is available to determine the φ. (4) Spontaneity and ΔG-

For the reaction:

$$2 \text{ Al (vapor)} + 3/2 \text{ O}_2 \text{ (gas)} = \text{Al}_2\text{O}_3 \text{ (solid)}$$

$$\Delta G_1 = 189.67 \text{ T} - 15.4 \text{ T log T} - 0.79 \text{ X } 10^{-3} \text{ T}^2 + 3.92 \text{ X } 10^5 \text{ T}^{-1} - 557,100$$

and for the reaction:

$$\text{Al (vapor)} + 3/2 \text{ Cl}_2 \text{ (gas)} = \text{AlCl}_3 \text{ (solid)}$$

$$\Delta G_2 = 68.57 \text{ T} + 11.4 \text{ T log T} - 13.96 \text{ X } 10^{-3} \text{ T}^2 - 0.45 \text{ X } 10^5 \text{ T}^{-1} - 242,460$$

Both reactions proceed to the right spontaneously because of the high negative values of ΔG. For example, the values of ΔG at 1000°K are,
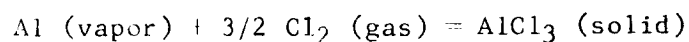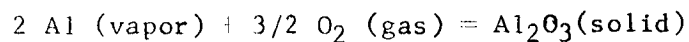
$$\Delta G_1 = -413,030 \text{ cal} \quad \text{for the formation of Al}_2\text{O}_3$$

$$\Delta G_2 = -153,700 \text{ cal} \quad \text{for the formation of AlCl}_3$$

The thermodynamic data used is taken from references 3 and 4.

As a result of the above considerations, the following chemical reactions are selected for further analysis and perhaps reduction to experiment.

3. CHEMICAL REACTIONS

$$2 \text{ Al (vapor)} + 3/2 \text{ O}_2 \text{ (gas)} = \text{Al}_2\text{O}_3 \text{(solid)}$$

$$\text{Al (vapor)} + 3/2 \text{ Cl}_2 \text{ (gas)} = \text{AlCl}_3 \text{ (solid)}$$
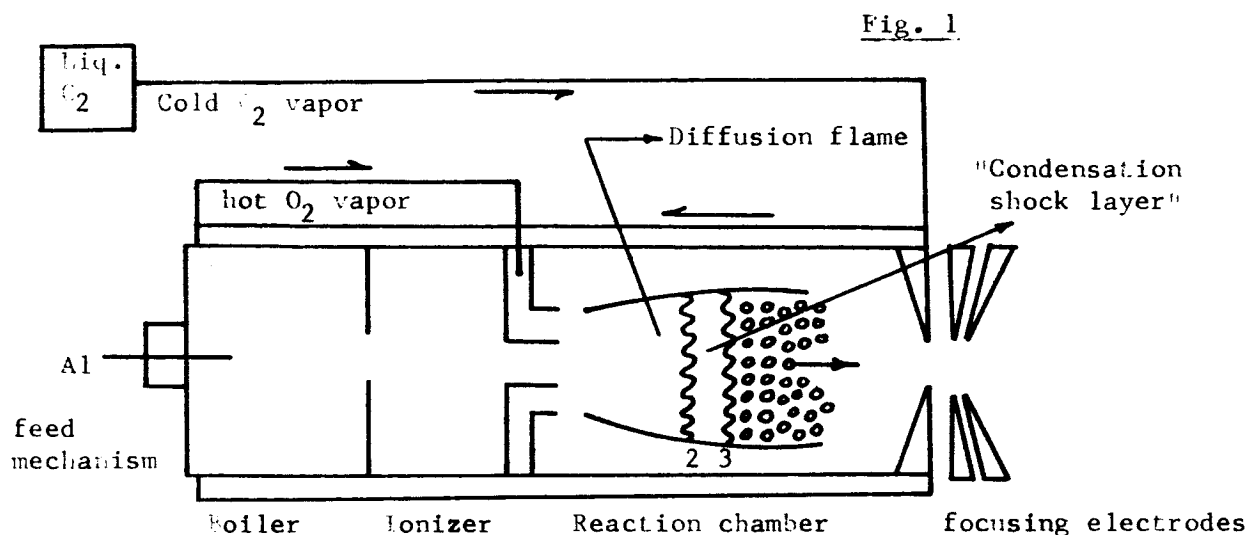
4. PHYSICAL MODEL OF PARTICLE GENERATOR

Fig. 1. Conceptual picture of particle generator.

5. THERMODYNAMICS AND FLOW EQUATIONS

(A) Thermodynamic theory of the equilibrium between a supersaturated vapor and a drop of liquid:

Surface phenomena plan an important role in processes connected with phase changes, i.e. from vapor phase to liquid phase. The Gibbs free energy of formation from the vapor of a spherical nucleus of radius r is the sum of a bulk and a surface term-

$$\Delta G = -4/3 \, \pi r^3 \frac{\rho}{M} \, RT \, \log_e \frac{Pr}{P_\infty} + 4r^2 \sigma(r) \tag{4}$$

ΔG, when plotted as a function of radius r, passes through a maximum, as seen in figure 2. The radius corresponding to ΔG maximum equals the critical radius.

Fig. 2
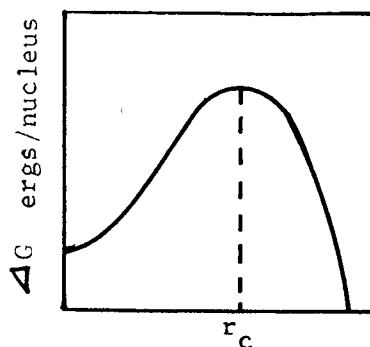
Fig. 2. Radius of Nucleus, r Å.

maximum ΔG requires: $\dfrac{d\,(\Delta G)}{dr} = 0$

At this point, it is necessary to consider the dependence of surface tension on the curvature of the droplet. For the liquid drops of large size, the surface tension is practically the same as that of flat surface. However, for small size drops of which dimensions are comparable to the thickness of the surface layer, the surface tension differs appreciably from that of the surface with infinite radius. Tolman[5] showed the following:

$$(r) \quad \frac{\sigma_\infty}{1 + \dfrac{2\delta}{r}} \tag{5}$$

where σ_∞ refers to the infinite radius of a drop and δ can be interpreted as a fraction of the intermolecular distance in liquid state. Surface tension decreases with increasing temperature. An experimental law established by Eötvös relates the surface tension with temperature:

$$\sigma(T) \quad K\,(T_c - T)$$

where T_c is the critical temperature of the material and K constant can be determined for different liquids by Ramsay-Shields formula:

$$K \quad \frac{2.12}{(M\,V_1)^{2/3}}$$

where M = molecular weight

V_1 volume occupied by a particle

The pressure dependence is very small compared to temperature or curvature dependencies.

Substituting Equation 5 into Equation 4 and setting $\dfrac{d\,(\Delta G)}{dr} = 0$

$$\log_e \frac{P_r}{P_\infty} = \frac{2M\,\sigma_\infty}{RT\rho} \times \frac{(r_c + 3\delta)}{(r_c + 2\delta)^2} \tag{6}$$

For Al_2O_3,

  $R = 8.317 \times 10^7$ ergs/mole deg

  $\rho = 3.97$ g/cm^3

  $M = 102$ g/mole

  $\sigma_\infty = 560$ ergs/cm^2 at the m.p. of Al_2O_3 (2030°C)

  $\delta = 4.34 \times 10^{-8}$ cm

The volume occupied by a single molecule of Al_2O_3 is:

$$= \frac{M}{\rho\,N_o}$$

$$= \frac{102}{3.97 \times 6.025 \times 10^{23}}$$

$$= 4/3\,\pi r_o^3$$

And:

  $r_o = 2.17 \times 10^{-8}$

  $= 2r_o = 4.34 \times 10^{-8}$ cm

Substitution of the above constants:

$$\ln \frac{P_r}{P_\infty} = \frac{3460 \times 10^{-7}}{T} \times \frac{(r_c + 13.02 \times 10^{-8})}{(r_c + 8.68 \times 10^{-8})^2} \tag{7}$$

This equation shows how the supersaturated vapor pressure over a spherical nucleus changes with the radius of nucleus under the isothermal condition. P_r/P_∞ is plotted as a function of critical radius of a nucleus r_c at the constant temperature in Figure 3. When T is 2000°K, the maximum supersaturation of Al_2O_3 vapor (from fig. 3) is $P_r/P_\infty = 7.7$ corresponding to $r_c = 2.74 \times 10^{-8}$ cm (two molecules in a nucleus). If the above derivations

are correct, this low supersaturation may not be of practical use in colloid thrustors. From the thermodynamics, it is possible to correlate the temperature with surface tension of the material, i.e. supersaturation can be achieved by cooling from T_o to T providing that volume is constant. If T_o is the temperature at which the vapor is saturated for a vapor pressure P_r, and T is the temperature at which vapor is saturated for a vapor pressure P, then:

$$dG = SdT + VdP$$

Equilibrium condition is dG = 0, $Sv = L_v/T_b$, and $V = RT/P$, where L_v is latent heat of vaporization per mole.

Integrating between the two limits, $T_o \rightarrow T$ and $P_r \rightarrow P_\infty$:

$$\frac{Lv}{R} \left[\frac{1}{T} - \frac{1}{To} \right] = \ln \frac{Pr}{P_\infty} \tag{8}$$

From equation 6 and equation 8:

$$To - T = \frac{2M\sigma_\infty}{\rho Lv} \times \frac{(rc + 3\delta)}{(rc + 2\delta)^2} \tag{9}$$

The above equation is very useful in determining the change of nucleus size with temperature.

(B) Analysis of supersaturated condensation and flow equations. To solve these problems initially, it is expedient to make several assumptions which will need reexamination in subsequent treatments.

The assumptions are:

(1) There is a condensation shock (figure 1) between the onset and the conclusion of condensation. In this region, there is an increase in stream temperature and pressure as the metastable supersaturation is relieved.

(2) The heat capacities of both liquid and vapor phases do not change in the temperature range.

(3) The noncondensed vapor behaves like an ideal gas due to the low operating pressure inside the reaction chamber ($10-10^{-2}$ Torr)

(4) The directed velocity of condensed particles is equal to the directed velocity of vapor

(5) Stream heating effects due to the friction losses between the vapor and the vapor or the particles are negligible

A pertinent paper was presented by Daniel S. Goldin[7] on the subject, "An Analysis of Particle Formation Efficiency in a Colloid Thrustor". He analyzed the nozzle-expansion system and obtained five equations of parameters from a thermodynamical approach. The basic concepts he used are followed throughout this report, except that there is no isentropic expansion in this mixing-reaction type of condensation. The energy balance equation and flow equations can be derived from the conservations of energy, mass, and momentum between the onset and conclusion of condensation. The energy balance from Bernoulli equation can be expressed as:

$$h_2' + \frac{(u_2')^2}{2} = (1 - g_3)\left[h_3' + \frac{(u_3')^2}{2}\right] + g_3\left[h_3'' + \frac{(u_3')}{2} + U_r''\right] \qquad (10)$$

$$h' = C_p' T' = \frac{\gamma R}{\gamma - 1} T' \qquad (11)$$

$$h'' = h_v'' + U_t'' + U_r'' + U_s'' + U_R'' + U_v'' \qquad (12)$$

$$h_v'' = h' - L_\infty \qquad (13)$$

Evaluations of U_t'', U_r'', U_v'', U_s'', U_R'':

(a) U_t''

From the statistical thermodynamics-

$$q_t = \left(\frac{2\pi mkT}{h^2}\right)^{3/2} V$$

$$\bar{\epsilon}_t = kT^2\left[\frac{\partial \ln q_t}{\partial T}\right]_{N,v}$$

$$= 3/2 \, kT \quad \text{ergs/particle}$$

$$\therefore U_t'' = \frac{3kT}{2m} \quad \text{ergs/g}$$

(b) U_v''

Contributions from vibrational motion are generally neglibible compared to translational or rotational motions.

(c) U_R''

For nonlinear polyatomic molecules like Al_2O_3,

$$q_R = \frac{8\pi^2 \sqrt{8\pi^2 \, I_A I_B I_C} \, (kT)^{3/2}}{\sigma \, h^3}$$

$$\bar{\epsilon}_R = kT^2\left[\frac{\partial \ln q_R}{\partial T}\right]_{N,v} = \frac{3kT}{2}$$

$$\therefore U_R'' = \frac{3kT}{2m} \text{ ergs/g}$$

The sum of U_t'', U_R'', and U_v'' is $3kT/m$. These energy terms of condensed particles per gram are neglibible compared to the volume enthalpy, $h_v'' = C_p T$.

Neglecting these three terms in equation 12 and combining equation 12 and equation 13:

$$h'' = h' - L_\infty + U_s'' \tag{14}$$

From equation 14, equation 10, and equation 11:

$$\left(\frac{\gamma R}{\gamma-1}\right)T_2' + \frac{(u_2')^2}{2} = \left(\frac{\gamma R}{\gamma-1}\right)T_3' + \frac{(u_3')^2}{2} - g_3 L_\infty\left[1 - \frac{U_s''}{L_\infty} - \frac{U_r''}{L_\infty}\right] \tag{15}$$

Equation 15 shows that the amount of latent heat that is released upon condensation ($g_3 L_\infty$) is reduced by the surface and radiation energy terms, i.e. part of latent heat goes into the particle as a form of surface tension and part of it is lost by radiation to the free space. Such reductions of latent heat are called "energy sinks" for latent heat of condensation. Energy sinks include

$$U_v'', \; U_r'', \; U_R'', \; U_s'', \; U_T''.$$

(d) U_s''

The surface energy term arises, as the drop grows, and work is done against the pressure produced by surface tension.

$$\left(\frac{U_s''}{L_\infty}\right) \cong \frac{A_p \, \sigma_\infty}{m_3 \, L_\infty} = \frac{(5.23 \times 10^{-9}) \, \sigma_\infty \, M}{\beta \, (m_3)^{1/3} (\rho_\infty)^{2/3} T_b} \tag{16}$$

where

$$L_\infty = \frac{9.24 \times 10^8 \, \beta \, T_b}{M} \quad \text{ergs/g} \tag{17}$$

From Trouton's Rule and

$$A_p = \left(\frac{m_3}{\rho_\infty}\right)^{2/3} \left(\frac{3}{4\pi}\right)^{2/3} (4\pi)$$

For the particles of Al_2O_3

$$\left(\frac{U_s''}{L_\infty}\right) \cong 0.0283,$$

assuming that Al_2O_3 liquid does not deviate from Trouton's Rule, i.e. $\beta = 1$

(e) U_r''

To approximate this term, the somewhat optimistic assumption is made that the particle radiates energy at a constant surface area equal to the final particle surface area and at the constant temperature of the diffusion flame, T_l'. It is also assumed that the particle radiates energy at a single average wavelength corresponding the flame temperature. The total emissive power e_t which is the rate of emission of energy from a cavity can be written as:

$$e_t = \sigma \, (T_l')^4 \tag{18}$$

where σ = Stefan-Boltzmann constant

$$= 5.672 \times 10^{-5} \quad \text{ergs/cm}^2 \, \text{sec:deg}^4$$

The energy radiated per gram of particles is

$$\left(\frac{U_r''}{L_\infty}\right) \approx \frac{\epsilon \, A_p \, e_t \, \tau}{m_3 \, L_\infty} \tag{19}$$

From equation 18 and equation 19 using equation 17:

$$\left(\frac{U_r''}{I_\infty}\right) \approx 2.99 \times 10^{-13}\left(\frac{T_1'}{T_b\beta}\right)\left[\frac{(T_1')^3 \tau M \epsilon}{(\rho_\infty)^{2/3}(m_3)^{1/3}}\right] \tag{20}$$

To find the radiation loss of the particles of Al_2O_3, it is important to have correct data on the emittance ϵ and flame temperature, T_1'. It is noteworthy that U_r'' is greatly influenced by T_1' due to the fourth power term. Due to the lack of this information for Al_2O_3 at the present time, the calculation of these terms are left for the time being. The state function of the uncondensed vapor at location 3 (see figure 1) is

$$KP_3 = (1 - g_3)\rho_3 RT_3' \tag{21}$$

where K is a conversion factor from Torr to dynes/cm^2.

The conservation momentum is

$$AKP_2 + \dot{m}u_2 = AKP_3 + \dot{m}u_3$$

Rearranging, we get

$$K(P_2 - P_3) = \frac{\dot{m}}{A}(u_3 - u_2) \tag{22}$$

And the equation for continuity of flow is

$$\frac{\dot{m}}{A} = \rho_2 u_2 = \rho_3 u_3 \tag{23}$$

The five essential equations for the solution of this system are equations 7, 15, 21, 22, and 23. Prior to the actual calculation, the evaluations of critical size of nucleus r_c, supersaturation P_r/P_∞, the flame temperature T_1', and u_2 should be made for the specific propellant material. Then five of the six unknown variables, g_3, u_3, T_3', P_2, u_2, can be solved in terms of one remaining unknown variable. The use of IBM computor would be necessary to execute the complicated calculations.

6. VAPOR PRESSURE CHANGE WITH TEMPERATURE

Vapor pressure curves are plotted in figure 4 according to equations 24, 25, and 26. Al liquid (1200 - 2800°K)

$$\log_{10} P \text{ (mmHg)} = -16,450/T - 1.023 \log_{10} T - 12.36 \tag{24}$$

Al_2O_3

$$\log_{10} P \text{ (mmHg)} = 7.38 - 17,200/T \tag{25}$$

obtained using Clausius-Clapeyron Equation based upon the assumption that the vaporization of molten Al_2O_3 obeys Trouton's Rule.

Al_2Cl_6

$$\log_{10} P \text{ (mmHg)} = -6.360/T - 3.77 \log_{10} T - 6.12 \times 10^{-3} T - 9.66 \tag{26}$$

NOTE

The study on the particle size distribution, and nucleation and condensation kinetics will be followed after this report.

The references cited and the symbols used in this report are explained in the attached sheets.

SYMBOLS

A   Surface Area, Cm^2

C_p Specific heat at constant pressure, ergs/g

g_3 particle formation efficiency

h   specific enthalpy, ergs/g

k   Boltzmann constant, 1.38×10^{-16} ergs/deg

K   conversion factor from Torr to dynes/cm^2

L   latent heat, ergs/g

M   molecular weight, g/mole

m   particle mass, g

P   pressure, Torr

R   gas constant, 8.317×10^7 ergs/mole-deg

U   specific energy, ergs/g

u   linear velocity of the stream, cm/sec

β ratio of actual latent heat to that predicted by Trouton's Rule

γ gaseous specific heat ratio, C_p/C_v

ϵ single particle emittance

ρ density, g/cm^3

σ surface tension, ergs/cm^2

τ residence time, sec

δ intermolecular distance, cm

q_t translational partition function for a particle

q_R rotational partition function for a particle

$\bar{\epsilon}$ average energy per particle

$\dot{m}$ mass flow rate, g/sec

SUBSCRIPTS

1	location 1 in figure 1
2	location 2 in figure 1
3	location 3 in figure 1
b	boiling point
p	particle
R	rotation
v	vibration, or volume
r	radiation
s	surface
t	translation
i	infinite bulk

SUPERSCRIPTS

'	vapor phase
"	condensed phase

REFERENCES

1. W.G. Courtney and C. Buûnik: "Colloid Propulsion Using Chemically-formed Particles". AIAA Paper No. 66-254.

2. Cotton and Wilkinson: "Advanced Inorganic Chemistry." Interscience Publishers. 1962. pp. 92.

3. Kubaschewski and Evans: "Metallurgical Thermochemistry".

4. K.K. Kelly: "Contributions to the Thermodynamic Data." National Bureau of Mines Bulletin. 592.

5. A.W. Adamson: "Physical Chemistry of Surfaces". Interscience Publishers. 1960. pp. 58.

6. C.A. Nergebauer: "Structural Disorder Phenomena In Thin Metal Films". Physics of Thin Films. Vol. 2. 1964.

7. D.S. Goldin: "An Analysis of Particle Formation Efficiency in a Colloid Thrustor". AIAA Paper No. 66-253.
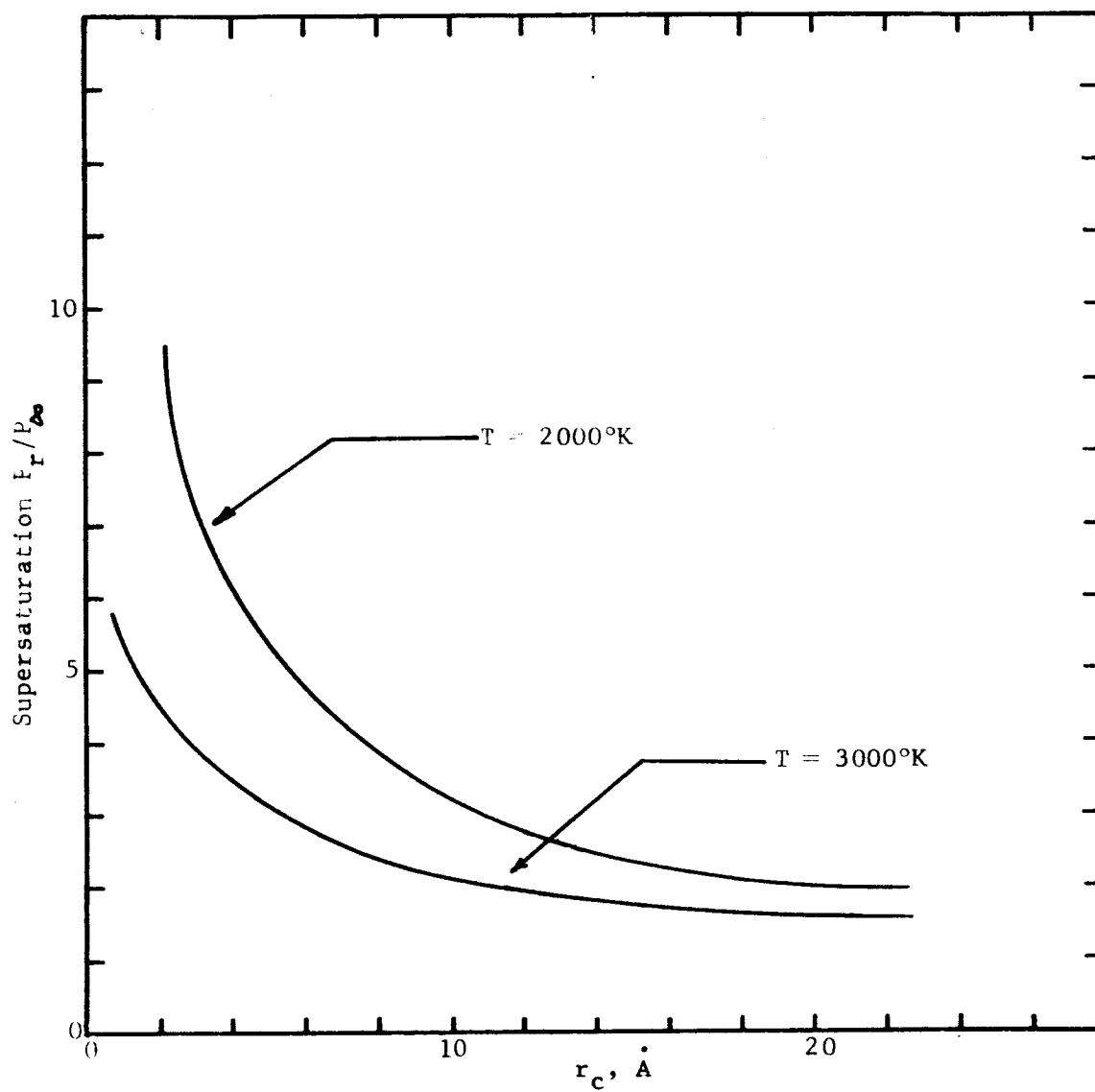
Fig. 3. Supersaturation P_r/P_∞ vs. Critical Radius of Nucleus r_c.
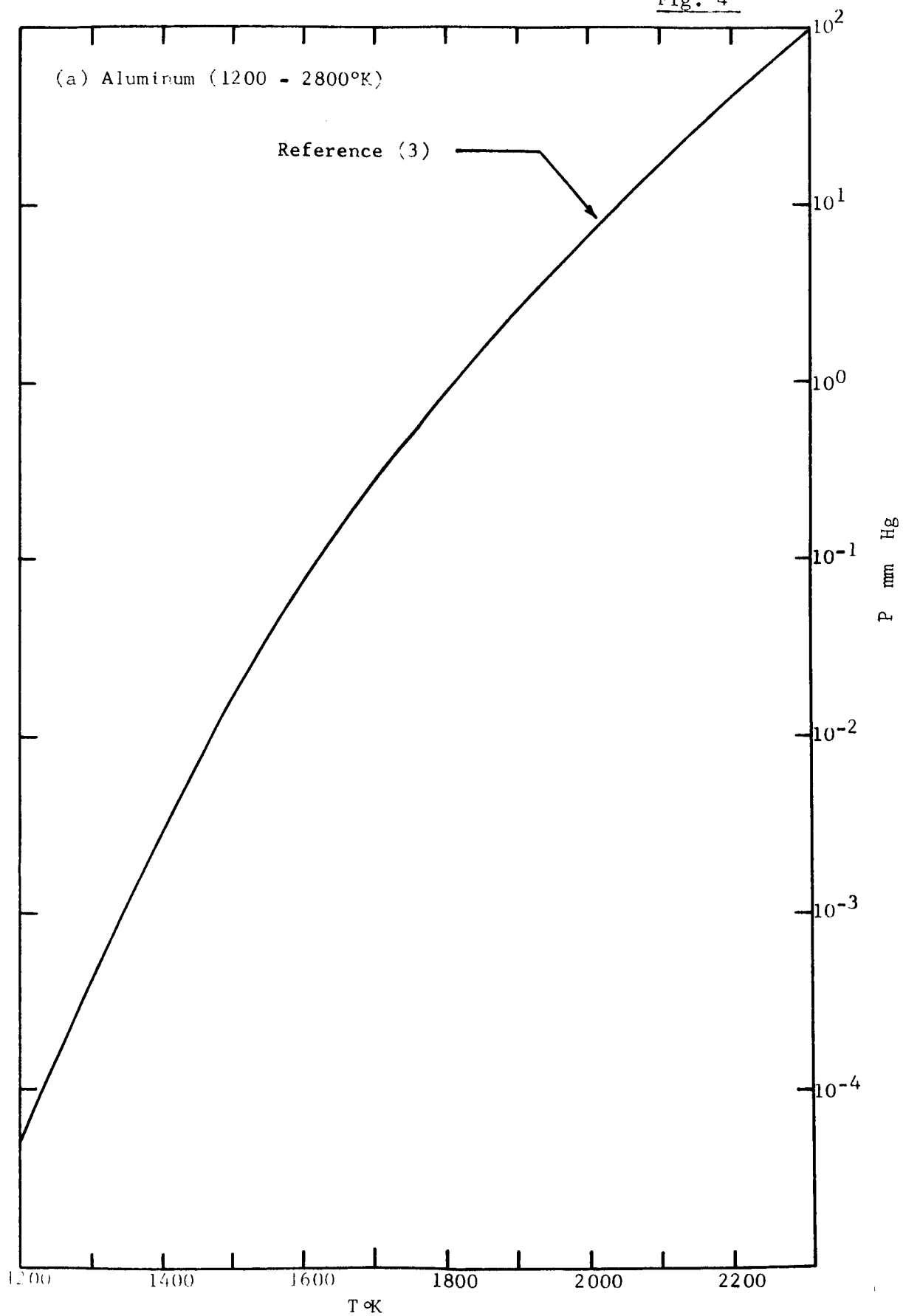
Fig. 4

(a) Aluminum (1200 - 2800°K)

Reference (3)

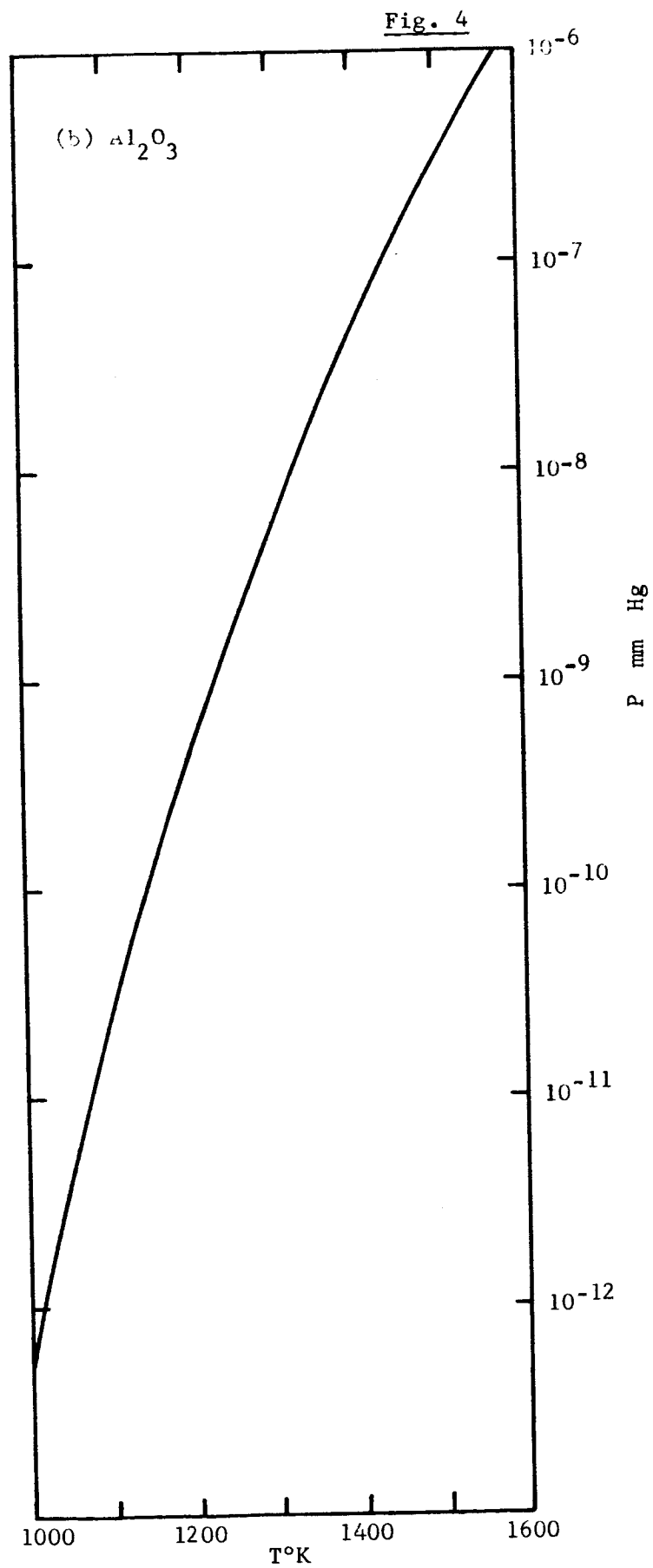Fig. 4

Fig. 4

(c) Al_2Cl_3

Reference (3)

P mm Hg

T °K

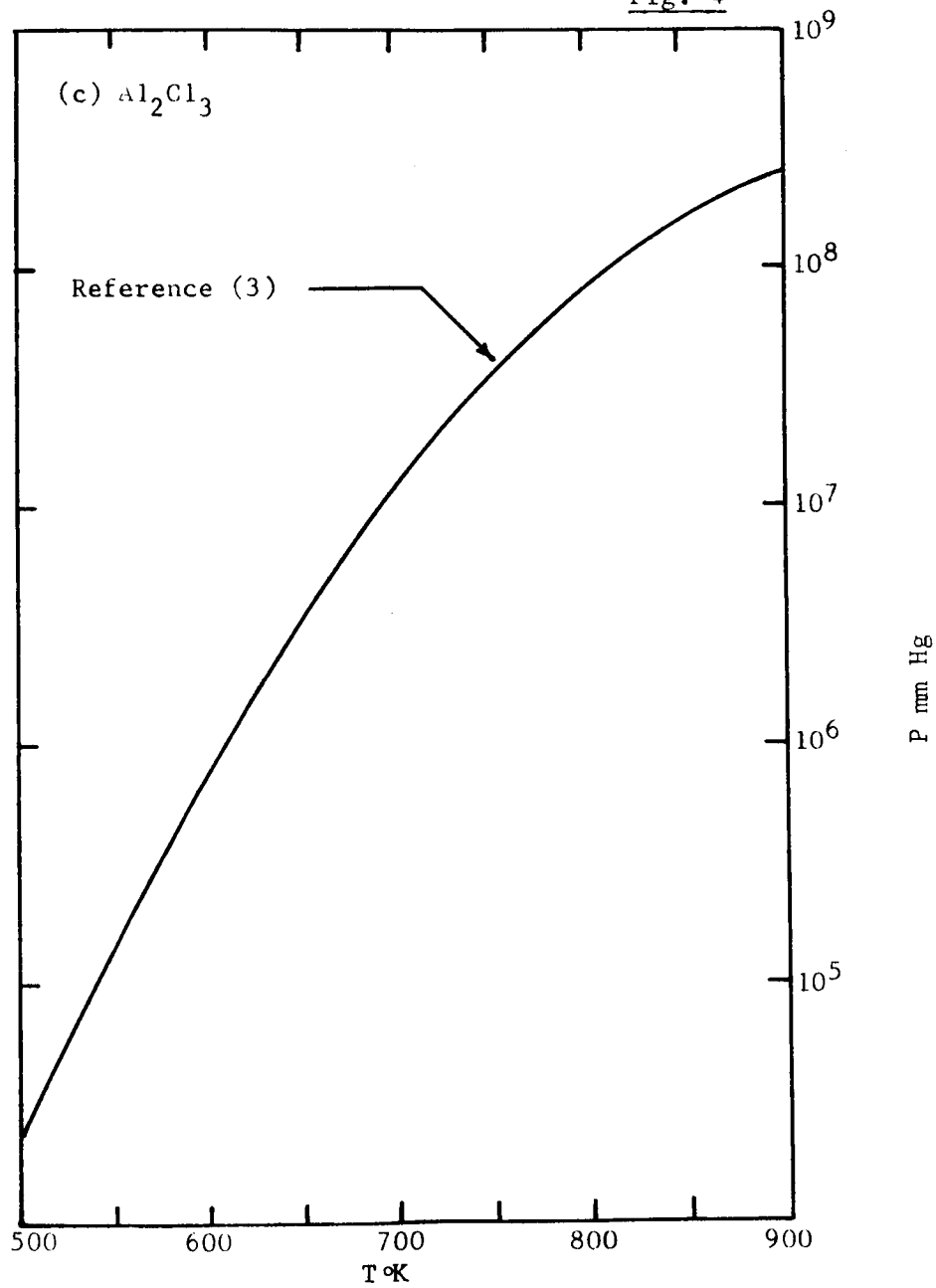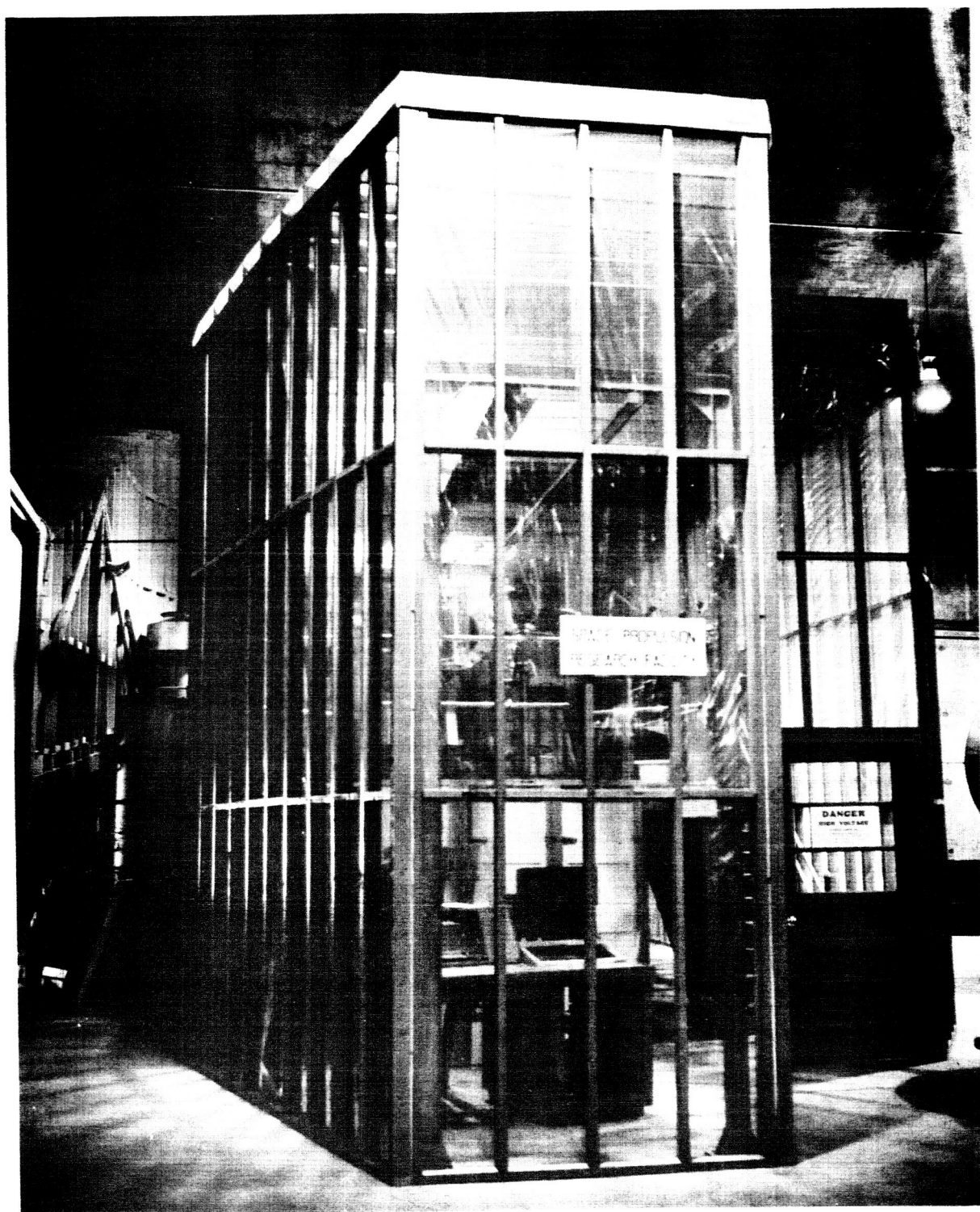## VACUUM FACILITY IMPROVEMENTS

A dust-preventive enclosure has been installed around the vacuum chamber and power-supply areas. It is expected that this enclosure will provide a relatively dust-free environment for carrying out experiments with high-voltage electrostatic thrusters. The installation is shown in Figure 1.

Two power supplies have been installed. These are 150 kilovolt, 5 milliampere, d.c. supplies. Preliminary operation has indicated satisfactory operation. Cabling and vacuum feed-throughs will be installed in the near future.

A surplus liquid-nitrogen plant has been installed and is being adapted for use with the vacuum facility.

PERSONNEL

For the grant period to June 30, 1966, the following personnel contributed to the research:

<u>principal investigator</u>

 Mr. W.R. Mickelsen, Professor of Mechanical

 and Electrical Engineering   1.67 mo.

<u>associate investigators</u>

 Dr. K.W. Arnold, Assistant Professor of

 Electrical Engineering   2.67 mo.

 Dr. G.W. Tompkin, Jr., Associate Professor

 of Chemistry   1.50 mo.

 Miss S.M. Keller, Jr. Mathematician   3.00 mo.

<u>graduate research assistants</u>

 Mr. Seong Woo Shin (M.S. candidate, Chemistry)   2.00 mo.

 Mr. Timothy D. Fehr (M.S. candidate, E.E.)   0.67 mo.

 Mr. Richard L. Moore (M.S. candidate, C.E.)   0.67 mo.

<u>engineering, secretarial, and technical support staff</u>   9.30 mo.

FUTURE RESEARCH PROGRAM

Investigations of homogeneous-condensation colloid thrusters will continue. Heat rejection from colloid particles by thermal radiation, and by vapor condensation on expansion-cone walls, will be incorporated into the digital computer program. Stagnation conditions will be varied to find the maximum particle-formation efficiency. If this information indicates a reasonably high formation efficiency, then a laboratory thruster will be designed. An appreciable amount of vapor will probably remain after the condensation region, so wall condensation will be used to recover most of this remaining vapor. The laboratory thruster will include a chamber for particle charging. Means will be provided for making large variations in the electron discharge operating conditions, so that the particle-charging mechanism can be studied in detail. Conventional electrostatic accelerator design will be used. Particle mass/charge will be measured with time-of-flight instrumentation and with a quadrupole mass spectrometer.

Colloid particle generation by chemical reaction will be a continuing investigation. When theoretical examination of this method provides enough information to establish feasibility, a laboratory thruster will be designed to continue the investigation by direct experiment. It is expected that a minimum of additional components will be required for these experiments, because the charging chamber, accelerator, etc. used for the homogeneous condensation thruster will be adapted for use in the chemical-reaction colloid thruster experiments also.

The graduate research assistant roster will be increased greatly, as shown by the following list:

name	candidate for	starting date
1. S.W. Shin	Ph.D. Chemistry	February, 1966
2. T.D. Fehr	M.S. Electrical Engineering	June, 1966
3. R.L. Moore	M.S. Civil Engineering	June, 1966
4. D.C. Garvey	Ph.D. Electrical Engineering	July, 1966
5. H.I. Leon	Ph.D. Mechanical Engineering	July, 1966
6. J.P. Rybak	Ph.D. Electrical Engineering	August, 1966
7. R.M. Roberge	Ph.D. Electrical Engineering	September, 1966
8. D.J. Fitzgerald	M.S. Mechanical Engineering	September, 1966
9. J.W. Hunt	M.S. Mechanical Engineering	September, 1966
10. F.P. Saheli	Ph.D. Mechanical Engineering	September, 1966

With this additional staff, it will be possible to investigate a number of advanced thruster concepts. These concepts will be conceived and analyzed with a strong view towards direct coupling of the thruster with the electric power-plant and with the prime power source.